SCALABILITY OF CONE CALORIMETER TEST RESULTS FOR THE PREDICTION OF FULL SCALE FIRE BEHAVIOR OF POLYURETHANE FOAM

A Thesis Submitted to the College of

Graduate Studies and Research

In Partial Fulfillment of the Requirements

For the Master of Science Degree

in the Department of Mechanical Engineering

in the College of Engineering at the

University of Saskatchewan

Saskatoon

by

LUKE DOUGLAS ROBSON

PERMISSION TO USE

In presenting this thesis in partial fulfilment of the requirements for a Postgraduate degree from the University of Saskatchewan, I agree that the Libraries of this University may make it freely available for inspection. I further agree that permission for copying of this thesis in any manner, in whole or in part, for scholarly purposes may be granted by the professor who supervised my thesis work or, in his absence, by the Head of the Department or the Dean of the College in which my thesis work was done. It is understood that any copying or publication or use of this thesis or parts thereof for financial gain shall not be allowed without my written permission. It is also understood that due recognition shall be given to me and to the University of Saskatchewan in any scholarly use which may be made of any material in my thesis.

Requests for permission to copy or to make other use of material in this thesis in whole or part should be addressed to:

Head of the Department of Mechanical Engineering

College of Engineering

University of Saskatchewan

57 Campus Drive,

Saskatoon, Saskatchewan S7N 5A9

DISCLAIMER

The names of certain commercial products were exclusively used to meet the dissertation and/or exhibition requirements for the degree of Master of Science at the University of Saskatchewan. Reference in this dissertation to any specific commercial products, process, or service by trade name, trademark, manufacturer, or otherwise, does not constitute or imply its endorsement, recommendation, or favoring by the University of Saskatchewan. The views and opinions of the author expressed herein do not state or reflect those of the University of Saskatchewan, and shall not be used for advertising or product endorsement purposes.

ABSTRACT

The ignition and subsequent burning of polyurethane foam based mattresses poses a significant danger to life and safety in North American homes. The development of fire models which can predict the full scale fire behavior of these mattresses using bench scale data would assist manufacturers and regulators to manage this danger in a cost effective manner. This thesis builds on previous work by the University of Saskatchewan and University of Waterloo fire research groups and focuses on the evaluation of one such scaling model, which was originally developed during the Combustion Behavior of Upholstered Furniture (CBUF) project. The evaluation of the CBUF model conducted in this thesis isolates the heat release rate (HRR) density sub-model and explores the effects of 1) cone calorimeter incident heat flux setting, 2) specimen thickness and 3) ignition location on the predictive capability of the CBUF model.

To provide input for the CBUF model cone and furniture calorimeter tests were conducted. Cone calorimeter tests were conducted on foam specimen thicknesses of 2.5, 5.0, 7.5 and 10.0 cm at incident heat flux settings of 25, 35, 50 and 75 kW/m^2. Furniture calorimeter tests were conducted on foam specimen thicknesses of 2.5, 5.0, 7.5 and 10.0 cm in both edge and center ignition configuration. Flame area spread rates were measured from infrared video of the furniture calorimeter tests using an automated algorithm.

It was found that HRR curves predicted by the CBUF model showed good agreement with experimental results. Experimental results from tests of thinner foams were predicted with greater success than results from thicker foams, and results from edge ignition tests were predicted with greater success than results of center ignition tests. The results of this study indicated that specimen thickness and ignition location need to be considered when selecting an appropriate incident heat flux setting for producing input data for the CBUF model.

ACKNOWLEDGMENTS

The author gratefully acknowledges the guidance and contributions provided by the following:

- Dr. D.A. Torvi for his valuable guidance and supervision during the course of this research and composition of this thesis.
- Dr. D.J. Bergstrom and Dr. D. Sumner for serving on my advisory committee.
- Dr. E.J. Weckman for providing guidance and assistance during the furniture calorimeter testing at the University of Waterloo.
- Department assistant Gord Hitchman and summer student Charles Lin for assistance during the furniture calorimeter testing.
- Matt Obach for the contribution of furniture calorimeter test data to this thesis and for assistance during other furniture calorimeter tests.
- Matt DiDomizio for contributing tests data on ignition source heat release rates.
- Melanie Fauchoux for providing guidance with humidity measurement equipment.
- Department assistants Rick Retzlaff and Dave Deutscher for providing technical assistance during the cone calorimeter testing at the University of Saskatchewan.
- Dr. Robson-MacKay for assistance during the analysis of the CBUF model results.
- The Natural Sciences and Engineering Research Council of Canada (NSERC), University of Saskatchewan College of Graduate Studies and Research (CGSR) and the University of Saskatchewan Department of Mechanical Engineering for support and funding during this research.

DEDICATION

This thesis is dedicated to my loving wife whose patience, dedication and encouragement made the completion of this thesis possible.

TABLE OF CONTENTS

PERMISSION TO USE i

DISCLAIMER ii

ABSTRACT iii

ACKNOWLEDGMENTS iv

DEDICATION v

TABLE OF CONTENTS vi

LIST OF TABLES ix

LIST OF FIGURES x

NOMENCLATURE xxiii

CHAPTER 1 : INTRODUCTION 1
- 1.1. Background 4
  - 1.1.1. Oxygen Consumption Calorimetry 4
- 1.2. Previous Research 7
  - 1.2.1. Detailed Computational Fire Models of Foam 7
  - 1.2.2. Modeling Mattress and Furniture Combustion: The CBUF Report 7
  - 1.2.3. Previous Research at the University of Saskatchewan 12
- 1.3. Objectives 16
- 1.4. Thesis Overview 19

CHAPTER 2 : EXPERIMENTAL APPARATUS AND PROCEDURE 20
- 2.1. Materials 20
- 2.2. Bench Scale Testing: the Cone Calorimeter 20
  - 2.2.1. Preparation and Conditioning of Cone Calorimeter Specimens 23
  - 2.2.2. Heat Flux Testing 27
  - 2.2.3. Foam Aging Test Series 28
- 2.3. Full Scale Testing: The Furniture Calorimeter 30
  - 2.3.1. Materials Preparation and Conditioning of Furniture Calorimeter Specimens 31
  - 2.3.2. Furniture Calorimeter Test Procedure 34
- 2.4. Full Scale Experimental Flame Spread Methodology 37
  - 2.4.1. Projective Transformation 38
  - 2.4.2. Elliptical Mask Correction for Plume Obscuration 41
  - 2.4.3. Binary Front Definition 42
  - 2.4.4. Burning Area and Flame Front Trace along Paths of Interest 43
  - 2.4.5. Manual Verification Technique 44

2.4.6. Results of Manual Verification of the Area Spread Data 45

CHAPTER 3 : EXPERIMENTAL RESULTS 49
3.1. Cone Calorimeter Test Results 49
3.1.1. General Observations 51
3.1.2. Repeatability of Cone Calorimeter Test Results 52
3.1.3. Effect of Incident Heat Flux on Cone Calorimeter Tests 54
3.1.4. Effects of Foam Aging on HRR Density 59
3.2. Furniture Calorimeter HRR Test Results 66
3.2.1. Repeatability of Furniture Calorimeter Test Results 66
3.2.2. Effect of Foam Thickness on Full Scale Test Results 70
3.2.3. Effect of Ignition Location on Full Scale Results 73
3.2.4. General Observations 79
3.3. Full Scale Flame Spread Test Results 80
3.3.1. Repeatability of Flame Spread Rates for Center Ignition Specimens 81
3.3.2. Effect of Foam Thickness on Flame Spread for Center Ignition Specimens 83
3.3.3. Repeatability of Flame Spread Rates for Edge Ignition Specimens 87
3.3.4. Effect of Foam Thickness on Flame Spread for Edge Ingition Specimens 89
3.3.5. Full Scale Area Spread Rate Curves 92
3.4. Summary 97

CHAPTER 4 : CONVOLUTION MODEL CODING AND VALIDATION METHOD 99
4.1. Coding of the Model 101
4.2. Validation of the Convolution Model Code 102
4.3. Sensitivity Study 108

CHAPTER 5 : EVALUATION OF THE CONVOLUTION MODEL 109
5.1. The Effect of Incident Heat Flux on Convolution Model Results 110
5.2. Evaluation of the Convolution Model for Center Ignition Test Configurations 114
5.3. Evaluation of the Convolution Model for Edge Ignition Test Configurations 125
5.4. Discussion of Convolution Model Evaluation 136
5.5. Variable Heat Flux Convolution Model 144

CHAPTER 6 : CONCLUSIONS AND FUTURE WORK 149
6.1. Conclusions 149
6.2. Future Work 151

REFERENCES 155

APPENDIX A: MANUAL AREA SPREAD RATE VERIFICATIONS 158

APPENDIX B: CONE CALORIMETER HRR DENSITY DATA 160

APPENDIX C: FURNITURE CALORIMETER HRR DATA 164

APPENDIX D: LINEAR FLAME SPREAD IN FULL SCALE TESTS 167

APPENDIX E: CONTOUR PLOTS OF FLAME SPREAD ON FULL SCALE TESTS 170

APPENDIX F: AREA FLAME SPREAD IN FULL SCALE TESTS 182

APPENDIX G: CBUF MODEL RESULTS 185

LIST OF TABLES

Table page

Table 2-1: Average mass and thickness information for test sets in the heat flux test series. 28

Table 2-2: Average mass and thickness information for test sets in the foam aging test series. 29

Table 2-3: Furniture calorimeter test specimens and test dates/environmental conditions. 32

Table 3-1: Summary of cone calorimeter test results. 50

Table 3-2: Summary of foam aging cone calorimeter test results. 62

Table 3-3: Summary of HRR density averages for foam aging test data. 62

Table 3-4: Summary of full scale furniture calorimeter test results. 69

Table 5-1: Summary of convolution model results for center ignition tests..... 116

Table 5-2: Summary of convolution model results for edge ignition tests..... 128

LIST OF FIGURES

Figure page

Figure 1-1: Photograph of a furniture calorimeter. 2

Figure 1-2: Photograph of a CAN-CGSB-4.2 No.27.7 bench scale cigarette test apparatus. 3

Figure 1-3: Flow chart illustrating the use of the CBUF model where Ȧ (t) is the flame spread rate, q”(t) is heat release rate density and Q(t) is the full scale HRR. 4

Figure 1-4: Simplified cylindrical model of a flame at the center of the mattress 10

Figure 1-5: Comparison of furniture calorimeter test results with the t-squared fire model and the flame spread model [21]. 13

Figure 1-6: Comparison of the convolution model with experimental heat release rate data for a center ignition test [22]. 15

Figure 2-2: FTT cone calorimeter apparatus. 21

Figure 2-3: Schematic view of the cone calorimeter (based on [26]). 22

Figure 2-4: Specimen preparation for cone calorimeter test. 24

Figure 2-5: Cone calorimeter sample conditioner. 25

Figure 2-6: Photographs taken during cone calorimeter test of 10 cm thick polyurethane foam specimen (left – just before start of test, right – 8 s after ignition) 26

Figure 2-7: Test configuration for full scale heat release measurement in the furniture calorimeter. 30

Figure 2-8: Photographs taken during centre ignition test of 1.2 by 1.2 m by 10 cm polyurethane foam specimen (left – just after ignition, right – approximately 120 s after ignition). 36

Figure 2-9: Photographs taken during edge ignition test of 1.2 by 1.2 m by 10 cm polyurethane foam specimen (left – just after ignition, right – approximately 135 s after ignition). 36

Figure 2-10: Overview of method used to extract flame spread 37

Figure 2-11: Locating the corners of the foam specimen CC4-3 prior to performing perspective transform. 39

Figure 2-12: Transformed image showing “top view” of the specimen CC4-3. 40

Figure 2-13: The transformed image of specimen CC4-3 showing the applied attenuation filter to adjust the area obscured by the plume..... 42

Figure 2-14: The binary image created for specimen CC4-3 using 300°C as the definition of the flame front. 43

Figure 2-15: Location of flame spread rate measurement on center ignition specimens. 44

Figure 2-16: Location of flame spread rate measurement on edge ignition specimens. 44

Figure 2-17: Front view of CC4-2 used for verification at t = 90 s. 45

Figure 2-18: Back view of CC4-2 used for verification at t = 90 s. 45

Figure 2-19 Comparison of flame area measurements recorded using the automated code and measurements recorded manually for test EE4-3. 46

Figure 2-20 Comparison of flame area measurements taken using the automated code and measurements recorded manually for test C1-3. 47

Figure 2-21 Comparison of flame area measurements taken using the automated code and measurements recorded manually for test E3-1..... 47

Figure 3-1 Heat release rate density measurements in tests of 5.0 cm thick foam specimens exposed to incident heat flux of 25 kW/m². “A” indicates the HRR density peak during the foam collapse. “B” indicates the HRR density peak while the foam is in liquid state. 53

Figure 3-2 Heat release rate density measurements in tests of 10.0 cm thick foam specimens exposed to incident heat flux of 50 kW/m^2. “A” indicates the HRR density peak during the foam collapse. “B” indicates the HRR density peak while the foam is in liquid state. 53

Figure 3-3 Heat release rate density measurements in tests of 2.5 cm thick foam specimens exposed to incident heat fluxes of 25 kW/m^2, 35 kW/m^2, 50 kW/m^2 and 75 kW/m^2.”A” indicates test 1-75-3 which exhibited a single peak..... 55

Figure 3-4 Heat release rate density measurements in tests of 5.0 cm thick foam specimens exposed to incident heat fluxes of 25 kW/m^2, 35 kW/m^2, 50 kW/m^2 and 75 kW/m^2. 55

Figure 3-5 Heat release rate density measurements in tests of 7.5 cm thick foam specimens exposed to incident heat fluxes of 25 kW/m^2, 35 kW/m^2, 50 kW/m^2 and 75 kW/m^2. 56

Figure 3-6 Heat release rate density measurements in tests of 10.0 cm thick foam specimens exposed to incident heat fluxes of 25 kW/m^2, 35 kW/m^2, 50 kW/m^2 and 75 kW/m^2. 56

Figure 3-7 HRR Densities measured in November 2010 of 10.0 cm thick polyurethane foam exposed to 35 kW/m^2. 60

Figure 3-8 HRR Densities measured in January 2011 of 10.0 cm thick polyurethane foam exposed to 35 kW/m^2. 60

Figure 3-9 HRR Densities measured in July 2011 of 10.0 cm thick polyurethane foam exposed to 35 kW/m^2. 61

Figure 3-10 Comparison of all HRR density curves that were collected in the foam aging test series. 63

Figure 3-11 Repeatability of furniture calorimeter heat release rate measurements (10 cm thick specimens, centre ignition). 67

Figure 3-12 Repeatability of furniture calorimeter heat release rate measurements (10 cm thick specimens, edge ignition). 67

Figure 3-13 heat release rates measured during centre ignition tests of foam with nominal thicknesses of 2.5 cm (C1-3), 5 cm (C2-2), 7.5 cm (C3-3) and 10 cm (C4-2). 71

Figure 3-14 Heat release rates measured during edge ignition tests of foam with nominal thicknesses of 2.5 cm (E1-3), 5 cm (E2-3), 7.5 cm (E3-3) and 10 cm (E4-1). 72

Figure 3-15 Comparison of HRRs measured for center (CC4) and edge (EE4) ignition locations of 1.2 m by 1.2 m by 10 cm specimens with fast and ultrafast t^2 HRR curves. 74

Figure 3-16 Comparison of HRRs measured for center (C4) and edge ignition (E4) specimens with fast and medium t^2 HRR curves. 75

Figure 3-17 Comparison of HRRs measured for center (C3) and edge ignition (E3) specimens with fast and medium t^2 HRR curves. 76

Figure 3-18 Comparison of HRRs measured for edge (E2) and center (C2) ignition specimens with medium and slow t^2 HRR curves. 76

Figure 3-19 Comparison of HRRs measured for edge (E1) and center ignition (C1) specimens with medium and slow t^2 HRR curves. 77

Figure 3-21 Flame front position in full scale center ignition tests of 2.5 cm thick polyurethane foam..... 82

Figure 3-22 Flame front position in full scale center ignition tests of 10 cm thick polyurethane foam..... 82

Figure 3-23 Flame front position in full scale center ignition tests of 2.5 cm (C1), 5 cm (C2), 7.5 cm (C3) and 10 cm thick (C4) polyurethane foam. 84

Figure 3-24 Infrared video of test E1-1 at 120 s, 180 s and 240 s after ignition (left to right)..... 85

Figure 3-25 Infrared video of test E4-3 at 120 s, 180 s and 240 s after ignition (left to right)..... 86

Figure 3-26 Flame front position in full scale edge ignition tests of 2.5 cm thick polyurethane foam. specimens E1-1, E1-2 and E1-3..... 88

Figure 3-27 Flame front position in full scale edge ignition tests of 7.5 cm thick polyurethane foam. specimens E3-1, E3-2 and E3-3..... 88

Figure 3-28 Flame front position in full scale edge ignition tests of 2.5cm (E1), 5 cm (E2), 7.5cm (E3) and 10 cm thick (E4) polyurethane foam..... 89

Figure 3-29 Flame front position contours in 10 s increments for test C4-1..... 91

Figure 3-30 Flame front position contours in 10 s increments for test E4-1. 91

Figure 3-31 Flame spread area in full scale center ignition tests of 2.5 cm thick polyurethane foam..... 93

Figure 3-32 Flame spread area in full scale edge ignition tests of 7.5 cm thick polyurethane foam..... 94

Figure 3-33 Flame spread area in full scale center ignition tests of 2.5 cm (C1), 5 cm, 7.5 cm (C2) and 10 cm thick (C4) polyurethane foam. 95

Figure 3-34 Flame spread area in full scale edge ignition tests of 2.5 cm(E1), 5 cm (E2), 7.5 cm (E3) and10 cm thick (E4) polyurethane foam..... 95

Figure 4-1 A screen capture of the spreadsheet that is used to calculate the predicted full scale heat release rate. 102

Figure 4-2 Plot of Wickstrom and Goransson's time dependent flame area [19]. 104

Figure 4-3 Plot of single gaussian distribution used to simulate input HRR density. 105

Figure 4-4 Comparison of exact solution and numerical solution for convolution integral. 106

Figure 4-5 Magnitude of error between exact and numerical solutions. 107

Figure 5-1 Cone calorimeter test results for 2.5 cm foam at 25, 35, 50 and 75 kW/m^2 incident heat flux. A – HRR density curve with highest peak and shortest duration. B – HRR density curve with lowest peak and longest duration. 111

Figure 5-2 Convolution model results for test C1-4 when the cone calorimeter test at each incident heat flux is used as input. A – HRR curve with highest peak and shortest duration. B – HRR curve with lowest peak and longest duration. 111

Figure 5-3 Cone calorimeter test results for 5 cm foam at 25, 35, 50 and 75 kW/m^2 incident heat flux. 112

Figure 5-4 Convolution model results for test C2-3 when the cone calorimeter test at each incident heat flux is used as input. 112

Figure 5-5 Cone calorimeter test results for 7.5 cm foam at 25, 35, 50 and 75 kW/m^2 incident heat flux. 112

Figure 5-6 Convolution model results for test C3-2 when the cone calorimeter test at each incident heat flux is used as input. 112

Figure 5-7 Cone calorimeter test results for 10 cm foam at 25, 35, 50 and 75 kW/m^2 incident heat flux. 113

Figure 5-8 Convolution model results for test C4-1 when the cone calorimeter test at each incident heat flux is used as input. 113

Figure 5-9 Comparison of experimental heat release rate with convolution model results for test C1-4. A – growth phase of fire. B – experimental peak HRR. C – decay phase of fire. 114

Figure 5-10 Comparison of measured peak HRR values with predicted peak HRR values using various incident heat fluxes for center ignition tests. 117

Figure 5-11 Comparison of measured time to peak HRR values with predicted time to peak HRR values using various incident heat fluxes for center ignition tests. 117

Figure 5-12 Comparison of measured THR values with predicted THR values using various incident heat fluxes for center ignition tests. 118

Figure 5-13 Comparison of experimental heat release rate with convolution model results for test C2-2. A – growth phase of fire. B – experimental peak HRR. C – rapid decay phase. D – experimental curve crosses all predictions. 119

Figure 5-14 Comparison of experimental heat release rate with convolution model results for test C3-2. A – growth phase of fire. B – experimental peak HRR. C – end of rapid decay phase. 121

Figure 5-15 Comparison of experimental heat release rate with convolution model results for test C4-2. A – growth phase of fire. 123

Figure 5-16 Comparison of experimental heat release rate with convolution model results for test CC4-2. A – growth phase of fire under predicted model. B – decay phase of fire. 124

Figure 5-17 Comparison of experimental heat release rate with convolution model results for test E1-1. 125

Figure 5-18 Comparison of flame spread area and flame spread rate for test E1-1. 127

Figure 5-19 Comparison of measured peak HRR values with predicted peak HRR values using various incident heat fluxes for edge ignition tests. 129

Figure 5-20 Comparison of measured time to peak HRR values with predicted time to peak HRR values using various incident heat fluxes for edge ignition tests. 129

Figure 5-21 Comparison of measured THR values with predicted THR values using various incident heat fluxes for edge ignition tests. 130

Figure 5-22 Comparison of experimental heat release rate with convolution model results for test E2-1. A – early stages of the fire growth. B – experimental peak HRR. C – beginning of rapid decay phase. 131

Figure 5-23 Comparison of experimental heat release rate with convolution model results for test E3-1. A – rapid decay in fire not captured by CBUF model. B – brief plateau in HRR curve. C – beginning of rapid decay phase. 132

Figure 5-24 Comparison of experimental heat release rate with convolution model results for test E4-1. A – growth phase of fire. B – experimental peak HRR. C – divergence of experimental HRR curve from CBUF model prediction. 133

Figure 5-25 Comparison of experimental heat release rate with convolution model results for test EE4-1. 135

Figure 5-27 Comparison of experimental heat release rate with convolution model results for test CC4-3. A – experimental peak HRR. B – rapid extinction behavior. 138

Figure 5-28 Flame spread contours for test E4-3 in 10 s increments. 139

Figure 5-29 Flame spread contours for test EE4-3 in 10 s increments. 139

Figure 5-30 Comparison of experimental heat release rate and single heat flux convolution results with variable heat flux convolution model results for test C4-2. A – sustained decay behavior. 145

Figure 5-31 Comparison of experimental heat release rate and single heat flux convolution results with variable heat flux convolution model results for test CC4-2. 146

Figure A-1 Comparison of flame area measurements recorded using the automated code and measurements recorded manually for test C1-3. 158

Figure A-2 Comparison of flame area measurements recorded using the automated code and measurements recorded manually for test C2-2. 158

Figure A-3 Comparison of flame area measurements recorded using the automated code and measurements recorded manually for test C3-2. 158

Figure A-4 Comparison of flame area measurements recorded using the automated code and measurements recorded manually for test C4-3. 158

Figure A-5 Comparison of flame area measurements recorded using the automated code and measurements recorded manually for test CC4-2. 159

Figure A-6 Comparison of flame area measurements recorded using the automated code and measurements recorded manually for test E2-1. 159

Figure A-7 Comparison of flame area measurements recorded using the automated code and measurements recorded manually for test E3-1. 159

Figure A-8 comparison of flame area measurements recorded using the automated code and measurements recorded manually for test EE4-3. 159

Figure B-1 Heat release rate density measurements in tests of 2.5 cm thick foam specimens exposed to incident heat flux of 25 kW/m^2. 160

Figure B-2 Heat release rate density measurements in tests of 2.5 cm thick foam specimens exposed to incident heat flux of 35 kW/m^2. 160

Figure B-3 Heat release rate density measurements in tests of 2.5 cm thick foam specimens exposed to incident heat flux of 50 kW/m^2. 160

Figure B-4 Heat release rate density measurements in tests of 2.5 cm thick foam specimens exposed to incident heat flux of 75 kW/m^2. 160

Figure B-5 Heat release rate density measurements in tests of 5.0 cm thick foam specimens exposed to incident heat flux of 25 kW/m^2. 161

Figure B-6 Heat release rate density measurements in tests of 5.0 cm thick foam specimens exposed to incident heat flux of 35 kW/m^2. 161

Figure B-7 Heat release rate density measurements in tests of 5.0 cm thick foam specimens exposed to incident heat flux of 50 kW/m^2. 161

Figure B-8 Heat release rate density measurements in tests of 5.0 cm thick foam specimens exposed to incident heat flux of 75 kW/m^2. 161

Figure B-9 Heat release rate density measurements in tests of 7.5 cm thick foam specimens exposed to incident heat flux of 25 kW/m^2. 162

Figure B-10 Heat release rate density measurements in tests of 7.5 cm thick foam specimens exposed to incident heat flux of 35 kW/m^2. 162

Figure B-11 Heat release rate density measurements in tests of 7.5 cm thick foam specimens exposed to incident heat flux of 50 kW/m^2. 162

Figure B-12 Heat release rate density measurements in tests of 7.5 cm thick foam specimens exposed to incident heat flux of 75 kW/m^2. 162

Figure B-13 Heat release rate density measurements in tests of 10.0 cm thick foam specimens exposed to incident heat flux of 25 kW/m^2. 163

Figure B-14 Heat release rate density measurements in tests of 10.0 cm thick foam specimens exposed to incident heat flux of 35 kW/m^2. 163

Figure B-15 Heat release rate density measurements in tests of 10.0 cm thick foam specimens exposed to incident heat flux of 50 kW/m^2. 163

Figure B-16 Heat release rate density measurements in tests of 10.0 cm thick foam specimens exposed to incident heat flux of 75 kW/m^2. 163

Figure C-1 Heat release rate measurements in center ignition tests of 60 cm x 50cm x 2.5 cm thick foam specimens. 164

Figure C-2 Heat release rate measurements in center ignition tests of 60 cm x 60cm x 5.0 cm thick foam specimens. 164

Figure C-3 Heat release rate measurements in center ignition tests of 60 cm x 60 cm x 7.5 cm thick foam specimens. 164

Figure C-4 Heat release rate measurements in center ignition tests of 60 cm x 60 cm x 10.0 cm thick foam specimens. 164

Figure C-5 Heat release rate measurements in edge ignition tests of 50 cm x 140 cm x 2.5 cm thick foam specimens. 165

Figure C-6 Heat release rate measurements in edge ignition tests of 60 cm x 120 cm x 5.0 cm thick foam specimens. 165

Figure C-7 Heat release rate measurements in edge ignition tests of 60 cm x 120 cm x 7.5 cm thick foam specimens. 165

Figure C-8 Heat release rate measurements in edge ignition tests of 60 cm x 120 cm x 10.0 cm thick foam specimens. 165

Figure C-9 Heat release rate measurements in center ignition tests of 120 cm x 120 cm x 10.0 cm thick foam specimens. 166

Figure C-10 Heat release rate measurements in edge ignition tests of 120 cm x 120cm x 10.0 cm thick foam specimens. 166

Figure D-1 Flame front position in full scale center ignition tests of 2.5 cm thick polyurethane foam specimens. 167

Figure D-2 Flame front position in full scale center ignition tests of 5.0 cm thick polyurethane foam. specimens. 167

Figure D-3 Flame front position in full scale center ignition tests of 7.5 cm thick polyurethane foam specimens. 167

Figure D-4 Flame front position in full scale center ignition tests of 10.0 cm thick polyurethane foam specimens. 167

Figure D-5 Flame front position in full scale edge ignition tests of 2.5 cm thick polyurethane foam specimen. 168

Figure D-6 Flame front position in full scale edge ignition tests of 5.0 cm thick polyurethane foam specimens. 168

Figure D-7 Flame front position in full scale edge ignition tests of 7.5 cm thick polyurethane foam specimens. 168

Figure D-8 Flame front position in full scale edge ignition tests of 10 cm thick polyurethane foam specimens. 168

Figure D-9 Flame front position in full scale center ignition tests of 10.0 cm thick polyurethane foam specimens. 169

Figure D-10 Flame front position in full scale edge ignition tests of 10 cm thick polyurethane foam specimens. 169

Figure E-1 flame spread contours for test E1-1 in 10 s increments. 170

Figure E-2 Flame spread contours for test E1-2 in 10 s increments. 170

Figure E-3 Flame spread contours for test E1-3 in 10 s increments. 170

Figure E-4 Flame spread contours for test E2-1 in 10 s increments. 171

Figure E-5 Flame spread contours for test E2-2 in 10 s increments. 171

Figure E-6 Flame spread contours for test E2-3 in 10 s increments. 171

Figure E-7 Flame spread contours for test E3-1 in 10 s increments. 172

Figure E-8 Flame spread contours for test E3-2 in 10 s increments. 172

Figure E-9 Flame spread contours for test E3-3 in 10 s increments. 172

Figure E-10 Flame spread contours for test E4-1 in 10 s increments. 173

Figure E-11 Flame spread contours for test E4-2 in 10 s increments. 173

Figure E-12 Flame spread contours for test E4-3 in 10 s increments. 173

Figure E-13 Flame spread contours for test EE4-1 in 10 s increments. 174

Figure E-14 Flame spread contours for test EE4-2 in 10 s increments. 174

Figure E-15 Flame spread contours for test EE4-3 in 10 s increments. 175

Figure E-16 Flame spread contours for test C1-2 in 10 s increments. 176

Figure E-17 Flame spread contours for test C1-3 in 10 s increments. 176

Figure E-18 Flame spread contours for test C1-4 in 10 s increments. 176

Figure E-19 Flame spread contours for test C2-1 in 10 s increments. 177

Figure E-20 Flame spread contours for test C2-2 in 10 s increments. 177

Figure E-21 Flame spread contours for test C2-3 in 10 s increments. 177

Figure E-22 Flame spread contours for test C3-1 in 10 s increments. 178

Figure E-23 Flame spread contours for test C3-2 in 10 s increments. 178

Figure E-24 Flame spread contours for test C3-3 in 10 s increments. 178

Figure E-25 Flame spread contours for test C4-1 in 10 s increments. 179

Figure E-26 Flame spread contours for test C4-2 in 10 s increments. 179

Figure E-27 Flame spread contours for test C4-3 in 10 s increments. 179

Figure E-28 Flame spread contours for test CC4-1 in 10 s increments. 180

Figure E-29 Flame spread contours for test CC4-2 in 10 s increments. 180

Figure E-30 Flame spread contours for test CC4-3 in 10 s increments. 181

Figure F-1 flame spread area in full scale center ignition tests of 2.5 cm thick polyurethane foam specimens. 182

Figure F-2 Flame spread area in full scale center ignition tests of 5.0 cm thick polyurethane foam specimens. 182

Figure F-3 Flame spread area in full scale center ignition tests of 7.5 cm thick polyurethane foam specimens. 182

Figure F-4 flame spread area in full scale center ignition tests of 10.0 cm thick polyurethane foam specimen. 182

Figure F-5 Flame spread area in full scale edge ignition tests of 2.5 cm thick polyurethane foam specimens. 183

Figure F-6 Flame spread area in full scale edge ignition tests of 5.0 cm thick polyurethane foam specimens. 183

Figure F-7 Flame spread area in full scale edge ignition tests of 7.5 cm thick polyurethane foam specimens. 183

Figure F-8 Flame spread area in full scale edge ignition tests of 10.0 cm thick polyurethane foam specimens. 183

Figure F-9 Flame spread area in full scale edge ignition tests of 7.5 cm thick polyurethane foam specimens. 184

Figure F-10 Flame spread area in full scale edge ignition tests of 10.0 cm thick polyurethane foam specimens. 184

Figure G-1 Comparison of experimental heat release rate with convolution model results for test E1-1. 185

Figure G-2 Comparison of experimental heat release rate with convolution model results for test E1-2. 185

Figure G-3 Comparison of experimental heat release rate with convolution model results for test E1-3. 185

Figure G-4 Comparison of experimental heat release rate with convolution model results for test E2-1. 185

Figure G-5 Comparison of experimental heat release rate with convolution model results for test E2-2. 186

Figure G-6 Comparison of experimental heat release rate with convolution model results for test E2-3. 186

Figure G-7 Comparison of experimental heat release rate with convolution model results for test E3-1. 186

Figure G-8 Comparison of experimental heat release rate with convolution model results for test E3-2. 186

Figure G-9 Comparison of experimental heat release rate with convolution model results for test E3-3. 187

Figure G-10 Comparison of experimental heat release rate with convolution model results for test E4-1. 187

Figure G-11 Comparison of experimental heat release rate with convolution model results for test E4-2. 187

Figure G-12 Comparison of experimental heat release rate with convolution model results for test E4-3. 187

Figure G-13 Comparison of experimental heat release rate with convolution model results for test C1-2. 188

Figure G-14 Comparison of experimental heat release rate with convolution model results for test C1-3. 188

Figure G-15 Comparison of experimental heat release rate with convolution model results for test C1-4. 188

Figure G-16 Comparison of experimental heat release rate with convolution model results for test C2-1. 188

Figure G-17 Comparison of experimental heat release rate with convolution model results for test C2-2. 189

Figure G-18 Comparison of experimental heat release rate with convolution model results for test C2-3. 189

Figure G-19 Comparison of experimental heat release rate with convolution model results for test C3-1. 189

Figure G-20 Comparison of experimental heat release rate with convolution model results for test C3-2. 189

Figure G-21 Comparison of experimental heat release rate with convolution model results for test C3-3. 190

Figure G-22 Comparison of experimental heat release rate with convolution model results for test C4-1. 190

Figure G-23 Comparison of experimental heat release rate with convolution model results for test C4-2. 190

Figure G-24 Comparison of experimental heat release rate with convolution model results for test C4-3. 190

Figure G-25 Comparison of experimental heat release rate with convolution model results for test EE4-1. 191

Figure G-26 Comparison of experimental heat release rate with convolution model results for test EE4-2. 191

Figure G-27 Comparison of experimental heat release rate with convolution model results for test EE4-3. 191

Figure G-28 Comparison of experimental heat release rate with convolution model results for test CC4-1. 191

Figure G-29 Comparison of experimental heat release rate with convolution model results for test CC4-2. 192

Figure G-30 Comparison of experimental heat release rate with convolution model results for test CC4-3. 192

NOMENCLATURE

English Letters

A	Cross-sectional area (m^2)
$\dot{A}$	Area burning rate (m^2/s)
A_f	Burning area (m^2)
A_p	Area of the base of a fire plume (m)
A_0	Initial burning area due to ignition (m^2)
a	Empirically determined constant describing HRR density peak (kW/m^2)
b	Empirically determined constant describing width of HRR density peak (s^{-2})
CO_2^i	Initial carbon dioxide content of air (mole fraction)
CO_2^i	Initial carbon dioxide content of air (mole fraction)
CO_2	Carbon dioxide content of air during a test (mole fraction)
c	Empirically determined constant describing time to peak HRR density (s)
d	Mattress thickness (m)
E	Heat release per unit volume of oxygen consumed (kJ/m^3)
$f(Re)$	Reynolds number correction for bidirectional pressure probe (Pa)
k	Duct calibration factor ($m^2/s^{3/2}N^{1/2}$)
L	Mattress length (m)
O_2^i	Initial oxygen content of air (mole fraction)
O_2	Oxygen content of air during a test (mole fraction)
P	Pressure (Pa)
Q	Heat release rate (kW)
$q"$	Heat release rate per unit area (heat release rate density) (kW/m^2)

R	Mattress width (m)
r_p	Radius of fire plume (m)
T	Temperature (ºC)
t	Time (s)
t_{ign}	Time to ignition (s)
t_0	Incubation time (s)
t_x	Empirically determined time constant (s)
V	Volumetric flow rate (m^3/s)
Z_f	Fire height (m)

Greek Letters

α	Fire growth coefficient (kW/s^2),
α_c	Combustion expansion factor (dimensionless)
ϑ	Empirical constant describing the rate of fire growth (s^{-1})
ρ_{298}	Density of air at 25ºC (kg/m^3)
σ	Standard Deviation
τ	Dummy variable (s)
φ	Oxygen depletion factor (dimensionless)

Abbreviations

ASTM	American Society for Testing and Materials
CBUF	Combustion Behavior of Upholstered Furniture
CFR	Code of Federal Regulation
CGSB	Canadian General Standards Board
HRR	Heat Release Rate
NBS	National Bureau of Standards
TDI	Toluene Diisocyanate
THR	Total Heat Release

CHAPTER 1 : INTRODUCTION

On average there are approximately 60,000 unintentional fires in Canada every year, resulting in over 1.2 billion dollars in capital losses [1]. In these fires, an average of 374 Canadians lose their lives every year and over 3000 Canadians are injured. It is difficult to quantify the cost of human suffering and tragedy; however these fire statistics provide a sense of scale of threat to life and safety posed by residential fires. A report published by the National Fire Protection Association in 2005 ranks mattress and bedding fires as the leading cause of home fire deaths [2]. In light of this, fires related to the ignition and subsequent burning of mattresses is a significant concern in North America.

A key tool in the mitigation of this type of fire risk is experimental fire testing. Recent progress in the prevention of mattress fires includes the adoption of new full-scale fire test standards for mattresses in Canada (CAN/ULC-S137) [3] and the United States (16 CFR Part 1633) [4]**.**These tests measure the performance of a mattress by exposing it to propane burners located on the top and side of the mattress, allowing it to burn freely and measuring parameters such as the heat release rate (HRR) using a furniture calorimeter (see Figure 1-1). These tests are designed to simulate the exposure of a mattress to open flame ignition sources such as a candle or pre-ignited bedclothes. The goal of these test standards is to limit the mattresses on the market to those that generate a smaller fire size with a slower growth rate, thereby reducing the possibility of flashover occurring. Other open flame full scale tests include ASTM E 1590 [5] which is used to regulate mattresses for special occupancies such as prisons and CFR 1632 [6] which uses a cigarette as an ignition source instead of an open flame.

Figure 1-1: Photograph of a furniture calorimeter.

In addition to full scale fire testing, there are a variety of bench scale fire tests which are used to assess the fire safety of mattresses. An example of this is standard CAN-CGSB-4.2 No.27.7 [7] which uses a cigarette as the ignition source (see Figure 1-2). Some other examples include ASTM E 622 [8] which measures smoke density, ASTE 162 [9] which measures flame spread and ASTM E 1474 [10] which uses a cone calorimeter to test small mattress mock-ups and individual mattress components.

Figure 1-2: Photograph of a CAN-CGSB-4.2 No.27.7 bench scale cigarette test apparatus.

Bench scale testing is a cost effective tool, however much of the realism of a full size fire is lost when only a portion of a mattress is burned. This research is working toward bridging the gap between tests conducted using the bench scale cone calorimeter and full scale open flame mattress tests. The ultimate trajectory of this research is developing a model that will take bench scale test data and information about the mattress geometry as input, and will output a prediction of full scale fire behavior. The model that was selected for evaluation in this thesis is known as the convolution integral and is illustrated in Figure 1-3. Some of the seminal work on the convolution integral model was conducted by the European CBUF (Combustion Behavior of Upholstered Furniture) Research Program; in this research program the convolution integral model was known as the CBUF II model. For the remainder of this thesis the CBUF II model, or the convolution integral will be referred to at the CBUF model. The CBUF program will be discussed in more detail in Section 1.2.2.

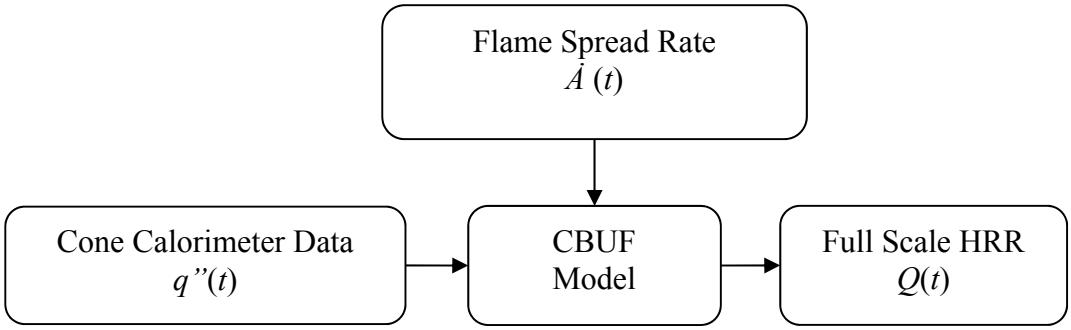

Figure 1-3: Flow chart illustrating the use of the CBUF model where $\dot{A}$ (t) is the flame spread rate, q"(t) is heat release rate density and Q(t) is the full scale HRR.

One of the challenges involved with the evaluation and development of this model is that, as illustrated in Figure 1-3, it requires the input of two sub-models: a time dependent flame spread, and a time-dependent heat release rate density. If this model were to be assembled, complete with both sub-models, and evaluated against experimental data, it would be difficult to discern which part of the model was the cause of a discrepancy. To properly develop this model, intermediate evaluations must be undertaken that can isolate the behavior of the sub-models.

1.1. Background

1.1.1. Oxygen Consumption Calorimetry

One of the fundamental techniques used in this thesis is oxygen consumption calorimetry. Oxygen consumption calorimetry was pioneered in the 1970s by researchers at the United States National Bureau of Standards (NBS), and gained traction as a scientifically sound and accurate experimental technique in the greater fire science community during the 1980s [11]. Oxygen consumption calorimetry is based on the physical principle that for most common fuels, the amount of energy released during the combustion process is constant if expressed in terms of the amount of oxygen consumed [12]. Later refinement of this technique involved the measurement

of carbon monoxide and carbon dioxide to correct for effects such as incomplete combustion [11].

In practice, oxygen consumption calorimetry is implemented by capturing the products of combustion in a hood and exhaust fan assembly and measuring the concentrations of oxygen and sometimes carbon monoxide and carbon dioxide. The cone calorimeter and the furniture calorimeter are the oxygen consumption calorimetery devices that were used in this research, the specifics of these devices will be discussed in Chapter 2.

The key parameter that oxygen consumption calorimetry is estimating is heat release rate or HRR. The HRR of a fire is the rate at which a given fire is releasing heat to its surroundings in the form of convection, conduction and radiation. The following are examples of oxygen consumption calorimetry equations and are adapted from ASTM E 1590 [5], and ISO 9705 [13]. In this case, heat release rate is calculated as

$$Q = EVO_2^i \left(\frac{\varphi}{\varphi(\alpha_c - 1) + 1} \right), \tag{1.1}$$

where φ is given by (considering oxygen only)

$$\varphi = \frac{O_2^i - O_2}{O_2^i(1 - O_2)}, \tag{1.2}$$

or when considering oxygen and carbon dioxide,

$$\varphi = \frac{O_2^i(1 - CO_2) - O_2(1 - CO_2^i)}{O_2^i(1 - CO_2 - O_2)}, \tag{1.3}$$

where Q is the heat release rate (kW),

E is heat release per unit volume of oxygen consumed, 17,200 (kJ/m^3),

V is the volumetric flow rate through the exhaust duct, corrected to 25ºC (m^3/s),

φ is the oxygen depletion factor,

α_c is the combustion expansion factor (approximated as 1.105)

O_2^i is the initial reading of the oxygen analyzer (mole fraction),

O_2 is the reading of the oxygen analyzer during the test (mole fraction),

CO_2^i is the initial reading of the carbon dioxide analyzer (mole fraction) and

CO_2 is the reading of the carbon dioxide analyzer during the test (mole fraction).

The corrected volumetric flow rate through the exhaust duct, V, for equation (1.1) is calculated as

$$V = \frac{26.54}{\rho_{298}} \frac{A\,k}{f(Re)} \sqrt{\frac{\Delta P}{T}} = 2.69k \sqrt{\frac{\Delta P}{T}}, \tag{1.4}$$

where ρ_{298} is the density of air at 25ºC, 1.18 (kg/m^3),

A is the cross-sectional area of the exhaust duct (m^2),

k is the duct calibration factor (m^2/s$^{3/2}$N$^{1/2}$),

$f(Re)$ is the Reynolds number correction for bidirectional probe (Pa),

ΔP is the pressure difference recorded by the bidirectional probe (Pa) and

T is the temperature of the gases in the exhaust duct (K).

It should be noted that A, k and $f(Re)$ are parameters that are specific to a given apparatus.

1.2. Previous Research

1.2.1. Detailed Computational Fire Models of Foam

An area of active research in the field of fire behavior of foam mattresses is the development of detailed computational models. These models take into account heat transfer, chemical reactions, changes in thermal characteristics and other phenomena related to the ignition and burning of foams. One of the outcomes of these studies has been the identification of two distinct stages of combustion for polyurethane foams. The first stage occurs during the collapse of the foam structure, and the second stage of combustion takes place while the foam is in a liquid state. These two stages are discussed in detail by Kramer et al. [14], who using results from thermal gravimetric analysis as well as microscale calorimetry, developed a detailed fire model of the combustion of polyurethane foam. In recent years, other researchers have put forward similarly detailed fire models [15-17].

Although this type of model shows promise, and certainly has significant merit in the pursuit of a more thorough understanding of the fire behavior of foams, these models require a significant amount of input data regarding the thermal and chemical kinetic properties of the materials being tested. In the context of consumer product regulation or the modeling of full scale mattress fires for the design of fire safety systems, this significant initial outlay to obtain material properties may pose a significant barrier, particularly in the rapidly changing and often secretive field of polymer foams.

1.2.2. Modeling Mattress and Furniture Combustion: The CBUF Report

A significant contribution to the area of mattress and furniture combustion research is the European Commission Measurements and Testing Report EUR 16477 [18]. This document is the final report detailing the findings of the European CBUF (Combustion Behavior of Upholstered

Furniture) research program. The work in this report represents the contributions of over 50 scientists located in Denmark, the U.K., Germany, Italy, France, Finland, Sweden and Belgium. The research program was sponsored by the European Commission as a means to prepare for issuing a fire performance directive targeting the fire safety of upholstered furniture. The scope of the research program was large, encompassing full and bench scale testing as well as well as the development of various fire models.

Among of the most significant contributions of the CBUF program were three fire models commonly referred to as models I, II and III. The intent of these models was to predict full scale fire behavior of upholstered furniture based on cone calorimeter test results. Model I uses a set of statistically correlated factors to predict the peak HRR, as well as the time to peak HRR and the time until conditions in a standardized room would be considered untenable. The development of this model was limited to the application of upholstered chairs and sofas.

Model II, the model that will be referred to as the CBUF model in this thesis, takes the same input as model I, cone calorimeter data, however it predicts a heat release rate history for the full scale specimen. Model II is based on an area convolution technique which was originally developed to predict the heat release rate (HRR) due to flame spread along walls and ceilings [19]. The underlying concept of the convolution integral formulation is simple: a surface does not contribute to heat release rate until it is ignited. Once a given area is ignited, it will contribute the same HRR time-history as a sample that is burned in the cone calorimeter. This concept is expressed in mathematical terms as

$$Q(t) = \int_0^t q''(t-\tau)\dot{A}(\tau)d\tau, \tag{1.5}$$

where $Q(t)$ is the predicted full scale heat release rate (kW),

$q"(t-\tau)$ is the heat release rate per unit area (heat release rate density) history as measured in the cone calorimeter (kW/m^2),

$\dot{A}(\tau)$ is the area burning rate at time t (m^2/s),

τ is a dummy variable (s).

When Equation (1.5) is applied to lining materials for walls and ceilings (e.g., wood paneling),$\dot{A}(\tau)$, the area burning rate at time t, may be obtained from standard flame spread tests of the given material. The CBUF researchers applied this method to furniture's more complex burning behavior by replacing the area burning rate with an empirically determined effective burning rate. This effective burning rate was to be equal to such a value that when it is convolved with the cone calorimeter HRR density curve, the resulting prediction of the full-scale HRR curve exactly matches the experimentally determined curve. Thus, the effective area was determined through a mathematical process known as deconvolution. The intent behind Model II is that once an effective area burning rate is obtained for a specific furniture design, predictions can be made for different materials for which cone calorimeter data exist. In the CBUF report this method was applied to 20 different pieces of furniture limited to only armchairs and three-cushion sofas. The resulting model showed good agreement with test results for armchairs, however the model did not exhibit the same degree of agreement for the sofas. This was attributed to the fact that the effective area function used in the model was developed using predominantly data from tests of armchairs.

Model III is similar to model II in that it predicts a HRR curve given cone calorimeter data, however it uses a more sophisticated physics based method for predicting the flame spread rates as well. Out of the three models it was also the only one to be applied to mattresses. The CBUF model III used a thermal flame spread theory to predict the flame spread rate across a

mattress. This model is based on previous work by CBUF scientists D. Baroudi and M. Kokkala on upward and concurrent flame spread [19]. The model makes several simplifying assumptions to ease the numerical complexity of the fire scenario including treating the fire plume as a cylinder for radiation purposes, assuming that the area outside of the plume is exposed only to radiative heat flux and simplifying the radiation exposure of the unburned foam to a uniform heat flux to an annulus immediately surrounding the fire plume. CBUF model III is schematically shown in Figure 1-4.

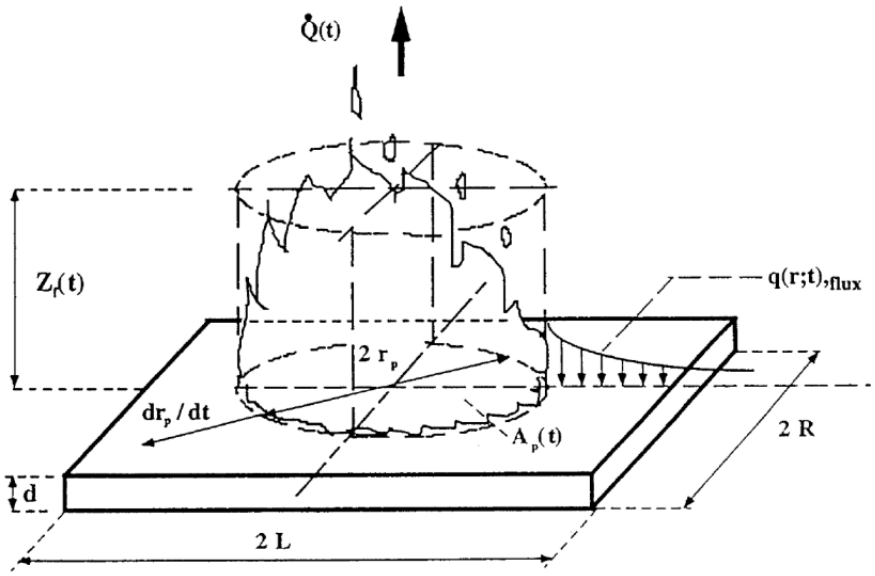

Figure 1-4: Simplified cylindrical model of a flame at the center of the mattress[*] *(CBUF Model III) [18].*

In this figure the symbols refer to the following:

$\dot{Q}$ is the predicted full scale heat release rate (kW),

q is heat release rate density (kW/m^2),

[*] Reprinted from section 8.4 Fire spread model - model III pp. 200, CBUF : fire safety of upholstered furniture : the final report on the CBUF research programme" 1996, Edited by Bjorn Sundstrom. Published Interscience Communications Ltd, 1996 with permission from Interscience Communications Ltd.

Z_f is the fire height (m),

r_p is the radius of the plume (m),

A_p is the area of the base of the plume (m),

d is the thickness of the mattress (m),

L is the length of the mattress (m) and

R is the width of the mattress (m).

As shown in Figure 1-4 the burning area is assumed to be a circle spreading radially outward until it reaches the edge of the mattress. The propagation rate of this circle is calculated based on how quickly the surrounding material is preheated to its ignition temperature due to the radiative heat flux exposure from the flame plume. Once the flame spread rate is obtained, CBUF model III uses the same area convolution technique that is used in model II to produce a prediction of the HRR time history.

CBUF model III was applied to a total of five full scale fire tests of mattresses including four solid foam core mattresses and one inner spring mattress. The foam core mattress constructions were as follows: Polyether foam with a FR polyester wrap and a cotton cover, latex foam with a cotton cover, CMHR foam with polyester cover and HR urethane foam with a FR treated cotton cover. The inner spring mattress that was used to evaluate the model contained CMHR foam and had a polyester cover. Predictions from the CBUF III model showed reasonable agreement with experimental results, particularly early in the growth phase and at peak HRR.

1.2.3. Previous Research at the University of Saskatchewan

The fire research group at the University of Saskatchewan began its focus on mattress combustion in September of 2004 when Threlfall [20] conducted full scale fire tests of mattresses in an abandoned office building. Three mattresses were tested including two inner spring mattresses containing polyurethane foam which burned completely and one rayon and fiber filled mattress that only smoldered. The temperatures recorded during the fires were compared to several fire protection engineering correlations including the Alpert ceiling temperature correlation [12]. One of the difficulties in completing this analysis was a lack of any experimental heat release rate data to use as input for Alpert's correlation.

In cooperation with the fire research group at the University of Waterloo, this work was continued when cone and furniture calorimeter tests of polyurethane foam were conducted in July and November of 2006. This study was aimed at obtaining fire response data from specimens that would be useful for correlating full and small scale fire tests and ultimately predict real life fire scenarios. In addition to the oxygen consumption calorimetry data that were collected, conventional and infra-red cameras were used to collect a video record of the flame spread. Utilizing the experimental data two models were used to predict the full scale behavior using the cone calorimeter test data. The first model was a classical t-squared model that is expressed mathematically as

$$Q(t) = \alpha(t - t_0)^2, \tag{1.6}$$

where $Q(t)$ is the full scale heat release rate (kW),

α is a fire growth coefficient that is dependent on the fuel type (kW/s^2),

t is the time (s) and

t_0 is an incubation time (s).

The second model was a time dependent area model which multiplies a time dependent burning area with a constant heat release rate density. This model is expressed as

$$Q(t) = A(t)Q'', \tag{1.7}$$

where $Q(t)$ is the full scale heat release rate (kW),

$A(t)$ is a time-dependent burning area (m^2) and

Q'' is a constant heat release density (kW/m^2).

Figure 1-5 is a plot comparing these two fire models with full scale test results.

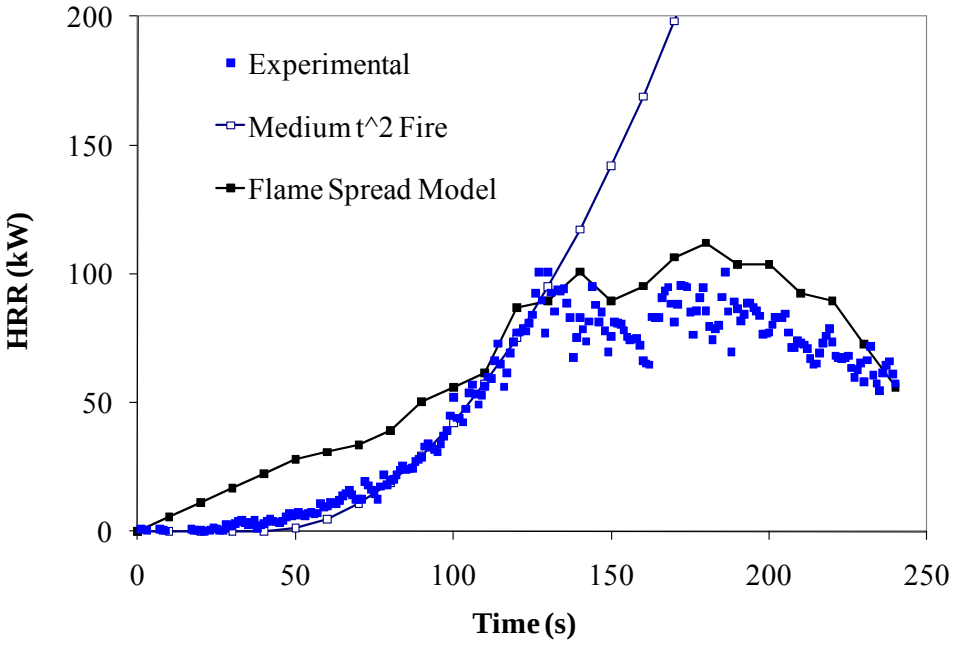

Figure 1-5: Comparison of furniture calorimeter test results with the t-squared fire model and the flame spread model [21].

As seen in Figure 1-5 the resulting predictions were similar to full scale test results, however the t-squared model lacked a decay phase prediction and the time-dependent area model

tended to over-predict the heat release rate early in the fire. The over-prediction of the time-dependent area model was attributed to the use of the averaged heat release rate density from the cone calorimeter results as input for the fire models; by using an averaged heat release density the model attributes a fully developed heat release density to areas of the specimen that are in early stages of combustion.

Again in May of 2008 testing commenced with the cooperation of the University of Waterloo (UW) with the intention of collecting more experimental data for use in correlating small and full scale fire tests of polyurethane foam [22]. The tests this time included ignition at both the edge and the center of the specimen to explore the effect of ignition location on fire behavior. From this set of tests it was found that flame spread and heat release rates were similar for the early portion of the tests, however as the fires developed the flame spread and heat release rates increased at a higher rate for the center ignition tests than the edge ignition tests. For similarly sized foam specimens, peak flame areas were approximately 10% higher and heat release rates were approximately 20% higher in center ignition tests.

Upon completion of the May 2008 fire tests, the modeling work was furthered by Ezinwa who utilized a version of Equation (1.5), the CBUF model, to predict furniture calorimeter results from cone calorimeter data [22]. In Ezinwa's version of the CBUF model, the input for the time dependent heat release rate density ($\dot{q}''$) consisted of a Gaussian curve fitted to a cone calorimeter data set. The cone calorimeter data were obtained using an incident heat flux setting of 35 kW/m^2 as was done in the CBUF project. To supply the time-dependent area spread rate ($\dot{A}(\tau)$) input for the model, flame area spread data were collected from the video record of the furniture calorimeter tests. This allowed Ezinwa to test the basic assumption of the CBUF method that in a full scale fire each differential area, once ignited, will exhibit the same heat

release rate density history as is produced in a cone calorimeter test. Figure 1-6 is a comparison of the CBUF model with experimental heat release data from a center ignition test.

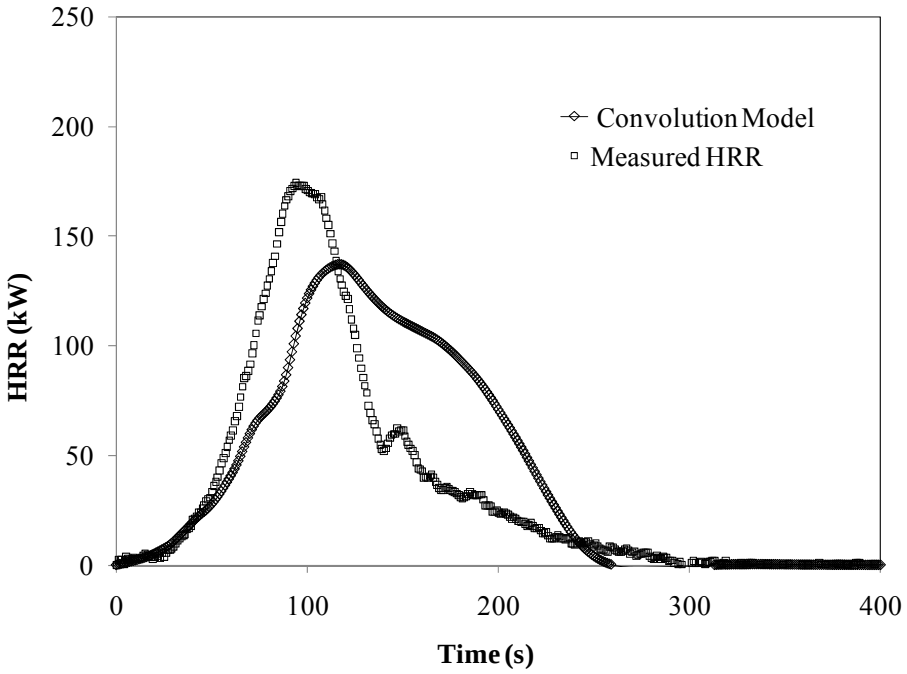

Figure 1-6: Comparison of the convolution model with experimental heat release rate data for a center ignition test [22].

As seen in Figure 1-6 the results of this modeling technique showed reasonable agreement during the growth phase of the fire between 0 and 50 s, however the model tended to over-predict heat release rates in late stages of the fire. The difference was attributed to the complex burning behavior exhibited in a full scale test of a thick foam specimen such as the three-dimensional transient heat transfer and pool fire behavior.

Two main issues were identified in this stage of the research. The first was that the incident heat flux setting for the cone calorimeter will likely have an effect on the outcome of the CBUF model. The incident heat flux setting of the cone calorimeter can have a significant effect on cone calorimeter results altering the peak HRR density as well as how long the heat release is sustained. Many of the cone calorimeter test standards such as ASTM E 1474 [10] specify

incident heat setting of 35 kW/m^2; however others specify higher and lower heat fluxes. Babrauskas [23] provides an overview of the many factors involved in selecting an appropriate incident heat flux setting. Ultimately the selection of an incident heat flux setting cannot be determined apriori, or be broadly standardized, rather the selection of an appropriate incident heat flux setting must be determined in the context of the material being tested and the application in which the data are to be used. In light of this, a larger cone calorimeter data set is required with which to begin to explore which incident heat flux setting should be used in conjunction with the CBUF model.

The second issue that was identified is that the CBUF model may not adequately model some of the complexities related to the burning behavior of thick foam slabs. The area convolution tecnhnique used in the CBUF model was originally developed for thin room lining materials and it may be best suited for similarly thin materials. It was noted that the burning rates down through the thickness of the foams were different in the 10 cm thick full scale specimen than the cone calorimeter specimen. It was also suggested that phenomena such as pool fires may affect the ability of the CBUF model to predict the fire behavior of the thicker foams. To begin to examine the effect of foam thickness on the burning behavior of polyurethane foam, and more specifically the ability of the CBUF model to make predictions, a larger data set was required.

1.3. Objectives

The over-arching goal of this research project is to improve the understanding of the relationship between full scale and bench scale fire test behavior of polyurethane foam. To accomplish this, research is focused on filling out the experimental data set for this body of research, making observations about the fire behavior seen in these tests and continuing the

analysis of the CBUF model. The specific objectives for this thesis are listed below. The first four objectives relate specifically to the collection and analysis of experimental data.

1. The bench scale testing for this research was conducted using a cone calorimeter. One of the important settings on a cone calorimeter is the incident heat flux setting. The first objective of this research was to determine the effect that incident heat flux setting has on the bench scale burning behavior of polyurethane foam. To provide data for this evaluation, cone calorimeter tests were conducted at incident heat flux settings of 25, 35, 50 and 75 kW/m^2 and the results were compared and contrasted.
2. One of the variables in full scale fire testing of mattresses is the location at which the specimen is ignited. Past research has shown that ignition location can have a significant effect on the full scale burning behavior of polyurethane foam [24]. It has also been seen that specimen thickness can have an effect on the full scale fire behavior of polyurethane foam. The second objective of this thesis was to observe the effect of specimen thickness and ignition location on full scale fire test results of polyurethane foam. To accomplish this, furniture calorimeter tests were conducted on foam specimens with thicknesses of 2.5, 5, 7.5 and 10 cm, in both a center and an edge ignition configuration.
3. As an extension of the second objective, the third objective of this research was to observe the effect that foam thickness and specimen ignition location have on the flame spread characteristics of full scale tests of polyurethane foam. To accomplish this, flame spread rates were measured from infrared video of the full

scale tests and the resulting data were compared for various configuration of specimen thickness and ignition.

4. The fourth objective of this research was to explore the possible effect of foam aging on combustion characteristics. To accomplish this, a study was conducted to compare cone calorimeter results for polyurethane foam samples that were aged with exposure to oxygen and light for periods ranging from one week to three months.

The final three objectives of this research focus on the evaluation of the CBUF model as a tool for the prediction of full scale fire behavior of polyurethane foam.

5. The fifth objective of this research was to study the ability of the CBUF model to predict full scale heat release rates for specimens of varying thickness and ignition location. To accomplish this, the CBUF model was coded and validated in Microsoft Excel®, and the model was run to predict the heat release rate of the full scale tests that were conducted in this research
6. As was mentioned in the first objective, cone calorimeter incident heat flux setting can have a significant effect on the outcome of cone calorimeter test results. In light of this, the sixth objective of this research was to observe how the CBUF model performs when cone calorimeter data obtained using different incident heat flux settings are used as the input.
7. The seventh objective of this research was to investigate a possible improvement to the CBUF model where several cone calorimeter data sets with differing heat flux settings are used as the input.

1.4. Thesis Overview

The following is an overview of this thesis with a brief description for the content of the chapters. In Chapter 2 the material and testing procedure are introduced for the cone calorimeter and furniture calorimeter and the automated procedure used to obtain the full scale flame spread results is discussed. Chapter 3 discusses the results of the experimental testing that was done as a part of this thesis. Topics include the effects of incident heat flux and specimen thickness on cone calorimeter HRR density curves and the effect of specimen thickness and ignition location on furniture calorimeter HRR curves and experimental flame spread. Chapter 4 focuses on the modeling that was done in this thesis. The coding method for the CBUF model used in this thesis is discussed and the technique used to validate this coding of the CBUF model is introduced and the results of this validation are shown. Chapter 5 presents an evaluation of the CBUF model and explores the effect of cone calorimeter incident heat flux setting, foam thickness, and full scale specimen ignition location on the predictive ability of the CBUF model. Finally a proposal is made for the modification of the convolution model and the preliminary results from this modification are presented. Chapter 6 discusses the conclusions from this thesis and proposed future work.

CHAPTER 2 : EXPERIMENTAL APPARATUS AND PROCEDURE

The testing that was completed during the course of this research includes both large and small scale experiments. The cone calorimeter testing can be broken down into a test series varying the heat flux setting of the cone calorimeter, and a test series exploring the effect that foam age has on the combustion characteristics of polyurethane foam. The full scale testing in this research was conducted using a furniture calorimeter.

2.1. Materials

All polyurethane foam samples used in this research were obtained in Saskatoon, SK, or Kitchener-Waterloo, ON, branches of a Canadian retail chain. These foams are less dense than foams typically found in solid-core mattresses and furniture, as they are mainly intended for use as camping pads. No detailed information was available on the base chemical composition of the foam; however, they did not appear to contain a fire retardant, as past research has shown that they are easy to ignite in full-scale fire tests using small ignition sources, which result in self-propagating fires that consume practically the entire specimen [25]. The foams were sold in rolls with nominal dimensions of 0.5 m by 1.4 m by 2.5 cm thick, 0.6 m by 1.8 m by 5.0 cm thick, 0.6 m by 1.8 m by 7.5 cm thick and 1.2 m by 1.8 m by 10 cm thick.

2.2. Bench Scale Testing: the Cone Calorimeter

An important component in this research involved collecting small scale heat release data from polyurethane foam specimens. This small scale heat release testing served a number of purposes including the investigation of effects of incident heat flux setting and specimen

thickness, as well as the effect of foam aging. The small scale heat release testing apparatus for this research was the FTT dual cone calorimeter (Fire Testing Technology, West Sussex, UK). The cone calorimeter that was used in this research is located in the Thermodynamics Laboratory in the Engineering Building at the University of Saskatchewan. Figure 2-1 is a photograph of the cone calorimeter.

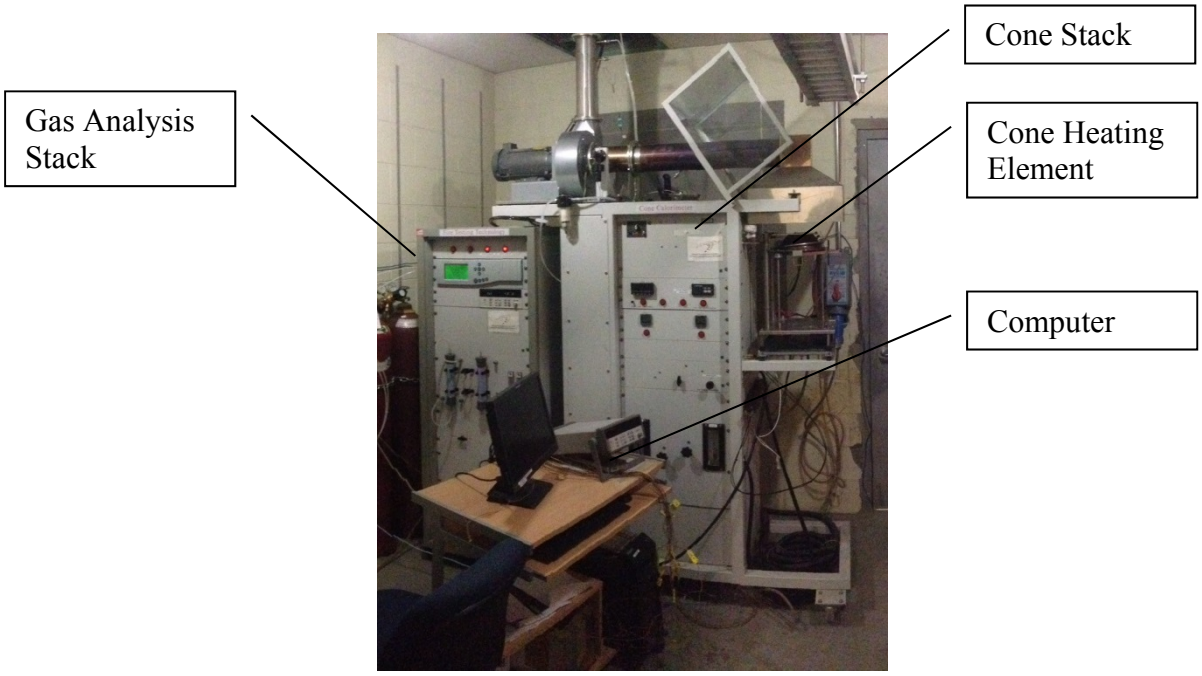

Figure 2-1: FTT cone calorimeter apparatus.

As seen in Figure 2-1 the cone calorimeter consists of three parts: the gas analysis stack, the cone stack and a computer. The gas analysis stack contains a Servomex Xentra 4100 gas analyzer (Servomex Company Inc., Boston, MA) which measures the carbon monoxide (CO), carbon dioxide (CO_2) and oxygen (O_2) concentrations in the exhaust stream. The gas analyzer measures the CO and CO_2 concentrations using an IR transducer and O_2 concentrations using a paramagnetic transducer. The gas analysis stack also contains an Agilent 34970A data acquisition system (Agilent Technologies, Mississauga, ON) that connects to the computer that

stores the data for post processing. The gas analysis stack also contains the plumbing necessary to pump, cool and dry the exhaust gas prior to analysis.

The cone stack contains the exhaust ducting, the conical heating element as well as the instrumentation which measures the specimen mass, controls the cone temperature and controls the exhaust fan speed. The operating principle of the cone calorimeter is illustrated in Figure 2-2.

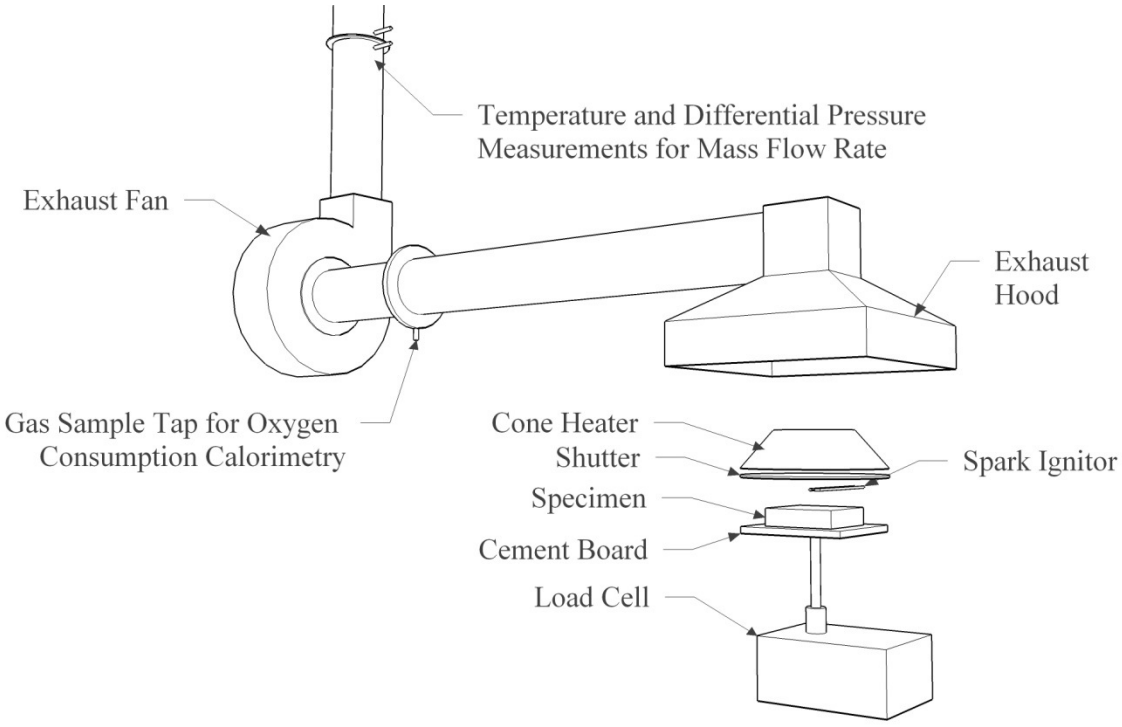

Figure 2-2: Schematic view of the cone calorimeter (based on [26]).

As seen in Figure 2-2, for this research the specimen that is to be tested in the cone calorimeter is placed on cement board on top of the load cell. To assist with cleanup, the cement board is covered with a sheet of aluminum foil. In other test methods a steel tray lined with mineral wool is used in place of the cement board. Since piloted ignition rather than auto-ignition is of interest in this research, a spark igniter is then placed over the specimen to pilot the ignition process and a shutter is opened exposing the specimen to the cone heater element. The cone heater element is maintained at a predetermined temperature as to expose the specimen to an

incident heat flux. Measurements taken by others in the U of S fire research group indicate that this conical heater provides a relatively uniform heat flux, as most of the specimen surface at the time of ignition will receive 90% of the incident heat flux that is measured at the center of the specimen [27].

The purpose of this incident heat flux is to assist with the ignition of the specimen and to simulate the additional heat flux that the surface of the foam would be exposed to in a full scale fire scenario. In a full scale fire, any given specimen area is exposed to the radiation that is emitted from the entire full scale fire plume. Without supplementing the heat flux in a small scale test with an external heat flux, the heat release rate densities would be much lower than would be expected in a full scale scenario. The combustion by-products from the burning specimen are drawn into the exhaust duct where the gas specimen stream is extracted and the temperature and flow rate are measured. The gas specimen stream is analyzed using oxygen consumption calorimetry [26].

2.2.1. Preparation and Conditioning of Cone Calorimeter Specimens

The cone calorimeter specimens were cut from the full size pad using a razor blade to ensure smooth straight edges. The specimens were cut to standard 10 cm by 10 cm surface area as per the ASTM E 1474 test standard [10]. The dimensions of the specimens were then measured using a vernier caliper and the specimens were weighed using an Ohaus Adventurer AR2140 balance (OHAUS Canada, Dundas, ON).

To contain the molten foam created during the burning process, the bottom 1 cm of the specimen was wrapped in aluminum foil (as shown in Figure 2-3).

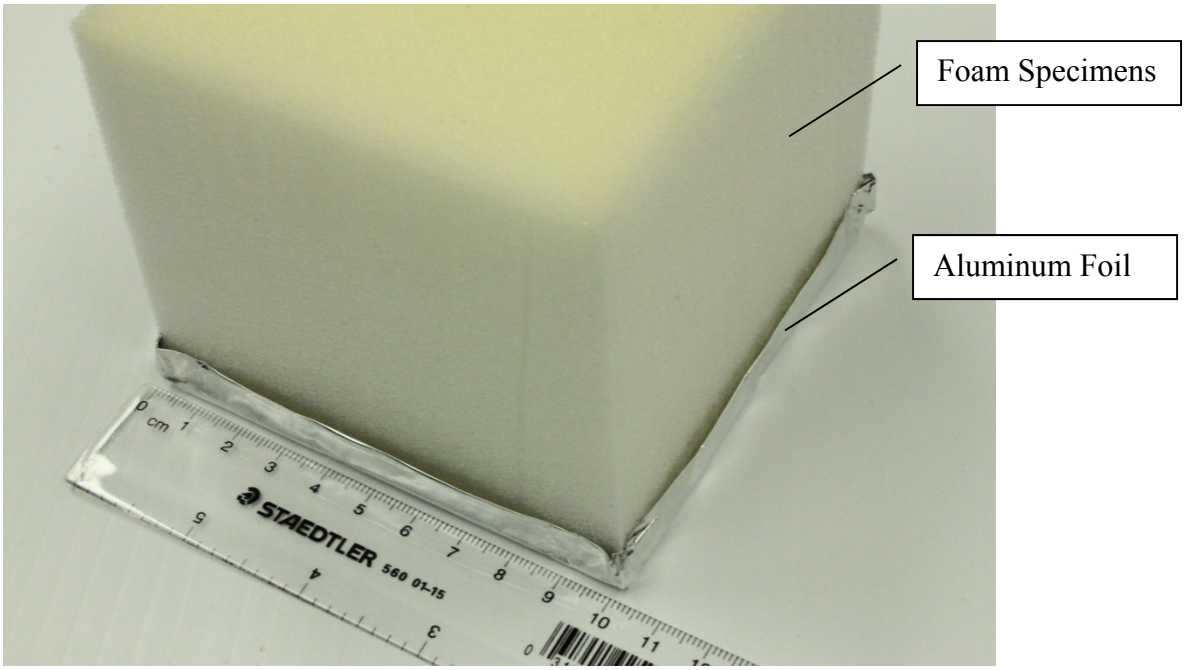

Figure 2-3: Specimen preparation for cone calorimeter test.

Prior to testing, specimens were placed in a sample conditioner for at least 24 hours that was held at 22°C ± 5°C and 50% ± 5% RH using an aqueous solution of magnesium chloride with a density of 1.27 g/cm^3 [28]. The sample conditioner used for this procedure is shown in Figure 2-4.

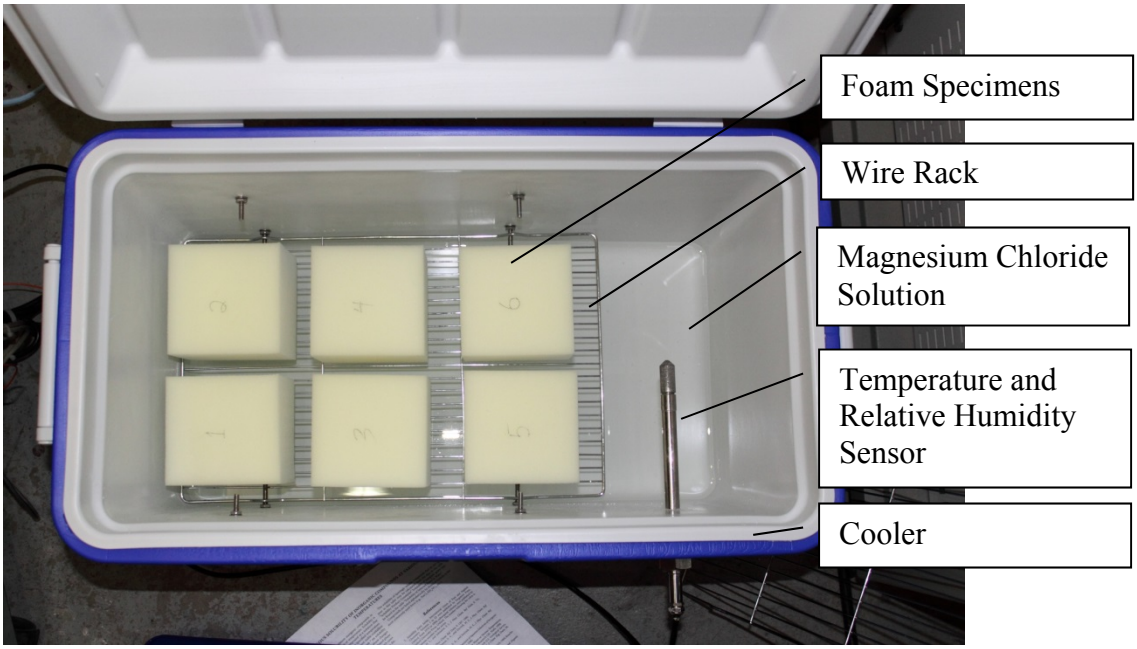

Figure 2-4: Cone calorimeter sample conditioner.

As seen in Figure 2-4 the sample conditioner was constructed using a cooler with wire racks installed for specimen storage. Four liters of magnesium chloride aqueous solution were placed at the bottom of the cooler. The density of the magnesium chloride solution was periodically measured using an Anton Paar DMA4500M density meter (Anton Paar GmbH, Graz Austria) between tests to maintain an appropriate concentration. To select the magnesium chloride solution density, a Vaisala HMP 233 hygrometer (Vaisala; Helsinki, Finland) with an Agilent 34972A data acquisition system was utilized to monitor the conditioner temperature and humidity to ensure that appropriate conditions could be maintained. For measuring conditioner humidity and temperature during sample conditioning, a Fisher Scientific Traceable™ relative temperature/humidity meter (Fisher Scientific Company, Ottawa, ON) was placed inside of the conditioner for the 24 hour conditioning period.

The ambient temperature of the U of S thermodynamics laboratory was controlled by the building air handling system and varied between 21.0 and 23.9°C during the test period. The building system does not control relative humidity; however, humidity in the laboratory was only recorded to vary from 22 to 24% RH during the November 2010 cone calorimeter testing period.

Once the 24 hour conditioning time had elapsed, the conditioner was briefly opened to retrieve the specimen being tested. Prior to the start of testing the cone calorimeter instruments were calibrated and the incident heat flux setting was adjusted using a Schmidt-Boelter gauge (Medtherm, Huntsville AL) positioned at the same elevation as the top of the foam, 2.5 cm below the cone heater element. The specimen was placed directly on the cement board under the cone calorimeter hood, and the test was initiated. Figure 2-5 shows photographs of a cone calorimeter test of a 10 cm thick polyurethane foam sample, taken just before and eight seconds after ignition.

Figure 2-5: Photographs taken during cone calorimeter test of 10 cm thick polyurethane foam specimen (left – just before start of test, right – 8 s after ignition).

During the test, gas concentrations and other oxygen consumption calorimetry measurements were recorded at 1 s intervals, and software running on the cone calorimeter computer calculated parameters such as the HRR density.

In order to provide a visual record, the tests were filmed using a Canon T1i digital SLR camera with either a Canon 18-55mm f/3.5-5.6 lens or a Canon 50mm f/1.8 lens.

2.2.2. Heat Flux Testing

One of the major purposes of the cone calorimeter testing in this research is to investigate the effect that varying the cone calorimeter incident heat flux setting has on the heat release rate measured when the specimens burn. As such, the tests in this series were conducted at four different cone calorimeter heat flux settings commonly found in the literature and test standards: 25 kW/m^2, 35 kW/m^2, 50 kW/m^2 and 75 kW/m^2. Another purpose of cone calorimeter testing in this research was to investigate the effect that specimen thickness has on heat release rate. Four nominal specimen thicknesses were selected for this series: 2.5 cm, 5.0 cm, 7.5 cm and 10.0 cm. As such, this research consisted of 16 test series: one set for each combination of thickness and heat flux. Each configuration was repeated three times, as recommended by cone calorimeter test standards (e.g., ASTM E 1474 [10]), resulting in a total of 48 individual tests

Table 2-1 provides a summary of the mass and thickness data that were collected for each of the test sets in the test series. The data are presented as an average of the three tests in a given test set. Tests in this series are labeled using the following convention: thickness-heat flux-test number (e.g., 1-35-1 is the first in the series of tests of 2.5 cm (1 in.) thick pieces of foam conducted using an incident heat flux of 35 kW/m^2).

Table 2-1: Average mass and thickness information for test sets in the heat flux test series.

Test Set	Mass (g) Ave.	(σ)	Thickness (cm) Ave.	(σ)
1-25	4.22	(0.03)	2.5	(0.00)
1-35	4.18	(0.05)	2.5	(0.06)
1-50	4.22	(0.03)	2.5	(0.06)
1-75	4.23	(0.16)	2.5	(0.00)
2-25	8.09	(0.08)	5.0	(0.06)
2-35	8.28	(0.06)	5.0	(0.06)
2-50	8.20	(0.06)	5.0	(0.00)
2-75	8.11	(0.14)	5.0	(0.00)
3-25	12.81	(0.26)	7.3	(0.00)
3-35	12.59	(0.13)	7.4	(0.06)
3-50	12.61	(0.37)	7.4	(0.06)
3-75	12.71	(0.19)	7.3	(0.06)
4-25	15.88	(0.14)	9.8	(0.15)
4-35	15.96	(0.15)	9.8	(0.00)
4-50	15.90	(0.09)	9.7	(0.06)
4-75	15.95	(0.05)	9.8	(0.00)

2.2.3. Foam Aging Test Series

It has been noted that once the polyurethane foam used in this research has been unwrapped, it gradually changes color from a bright white to a tan color. It is suspected that this discoloration is due to an oxidation process. The purpose of the foam aging series is to investigate the effect that foam aging might have on heat release rate characteristics. To accomplish this, a new roll of polyurethane foam was purchased and unwrapped. During the following months three test sets were conducted, one in November of 2010, one in January of 2011 and one in May of 2011. All tests were conducted at an incident heat flux setting of 35 kW/m^2.

Table 2-2: Average mass and thickness information for test sets in the foam aging test series.

Test Set	Mass (g) Ave.	(σ)	Thickness (cm) Ave.	(σ)
Nov 2010	15.78	(0.15)	9.3	(0.06)
Jan 2011	15.96	(0.39)	9.5	(0.10)
July 2011	15.88	(0.39)	9.8	(0.00)

2.3. Full Scale Testing: The Furniture Calorimeter

The full scale testing for this research was conducted in the furniture calorimeter located at the University of Waterloo's Live Fire Research Facility. The University of Waterloo's furniture calorimeter was constructed to the specifications listed in ASTM standard E 1590 test configuration C [5], the open calorimeter layout (Fire Testing Technology). Figure 2-6 illustrates the configuration of the furniture calorimeter.

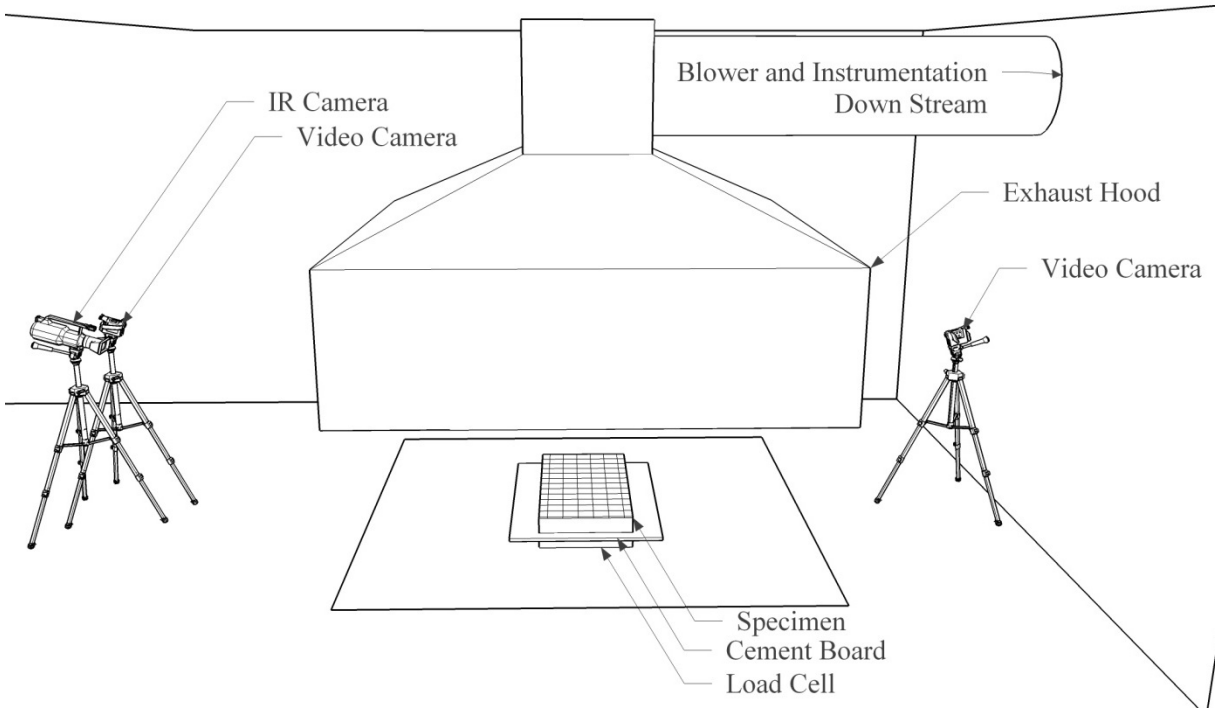

Figure 2-6: Test configuration for full scale heat release measurement in the furniture calorimeter.

As seen in Figure 2-6, the test specimen was placed on aluminum foil lined cement board located under the calorimeter exhaust hood. As the specimen burns the mass loss rate is recorded by the load cell and the combustion bi-products are collected by the hood for analysis. The exhaust system contains instrumentation to measure temperature and mass-flow rates of the exhaust stream. The exhaust ducting also includes a sample tap which leads to a gas analysis stack where oxygen, carbon dioxide and carbon monoxide levels are measured. The gas analysis

instrumentation stack used by the furniture calorimeter at the University of Waterloo is the same as the one used by the cone calorimeter at the University of Saskatchewan.

2.3.1. Materials Preparation and Conditioning of Furniture Calorimeter Specimens

Similar to the foam used in the cone calorimeter testing, the foam for these tests was purchased from Canadian retail outlets in Kitchener-Waterloo and Saskatoon between July 2006 and June 2010.

The rolls were unwrapped and the foam was allowed to expand. The foam was then cut into individual test specimens with nominal dimensions of 0.6 by 0.6 m, 0.6 by 1.2 m, 0.5 by 1.4 m or 1.2 by 1.2 m. Dimensions of individual test specimens are given in Table 2-3 along with the dates of testing and conditions in the laboratory. The author performed the tests done in July 2010, the June 2009 tests were conducted by Matt Obach from the University of Waterloo fire research group, and all other tests were conducted as a part of previous studies [24, 29, 30]. The full scale tests are labeled using three identifiers: a configuration code, the specimen thickness in inches, and an iteration number. In the furniture calorimeter testing, each configuration was tested three times as recommended by furniture calorimeter test standards (e.g., CAN/ULC-S137 [3]). The configuration codes for the full scale tests are as follows: C – smaller center ignition configuration nominally 60 by 50 cm or 60 by 60 cm, CC – larger center ignition configuration nominally 120 by 120 cm, E – smaller edge ignition configuration nominally 50 by 140 cm or 60 by 120 cm, and finally EE – larger edge ignition configuration nominally 120 by 120 cm. The average density of the test specimens was 17.1 kg/m^3 with a standard deviation of 1.2 kg/m^3. The density of individual specimens ranged between 15.8 and 20.6 kg/m^3. The main reason for the higher density values was that the foams were tightly wrapped in their packaging and some pieces did not expand as much as others, even after several

days. For example, specimen EE-4-1 was purchased in late 2006, but was not tested until May, 2008. If it had expanded to its nominal thickness of 10 cm, the density would have dropped from 20.6 to 18.1 kg/m^3. As the foams were purchased over a relatively long period of time, it is also expected that the composition of individual foam specimens may not be exactly the same.

Table 2-3: Furniture calorimeter test specimens and test dates/environmental conditions.

Test Specimens	Test Date (temperature and relative humidity)	Ignition Location	Dimensions (cm)			Mass (kg)
			Width	Length	Thickness	
C1-1	July 19, 2010 (26°C, 56%)	Centre	61	52	2.5	0.13
C1-2	July 20, 2010 (25°C, 56%)	Centre	61	53	2.5	0.13
C1-3	July 20, 2010 (29°C, 43%)	Centre	61	53	2.5	0.14
C1-4	July 21, 2010 (27°C, 60%)	Centre	61	52	2.5	0.13
C2-1	July 19, 2010 (26°C, 54%)	Centre	61	63	5.0	0.31
C2-2	July 20, 2010 (28°C, 43%)	Centre	61	62	5.0	0.32
C2-3	July 21, 2010 (27°C, 59%)	Centre	61	63	5.0	0.31
C3-1	July 20, 2010 (24°C, 66%)	Centre	62	61	7.5	0.50
C3-2	July 20, 2010 (29°C, 40%)	Centre	61	62	7.5	0.47
C3-3	July 21, 2010 (28°C, 56%)	Centre	62	61	7.5	0.47
C4-1	May 15, 2008 (17°C, 38%)	Centre	60	62	9.3	0.58
C4-2	May 15, 2008 (18°C, 36%)	Centre	60	62	9.5	0.58
C4-3	July 21, 2010 (28°C, 53%)	Centre	59	61	9.3	0.58
CC4-1	May 16, 2008 (18°C, 36%)	Centre	121	124	8.8	2.31

Table 2-3: Furniture calorimeter test specimens and test dates/environmental conditions.

Test Specimens	Test Date (temperature and relative humidity)	Ignition Location	Dimensions (cm)			Mass (kg)
			Width	Length	Thickness	
CC4-2	July 22, 2010 (25°C, 59%)	Centre	121.6	124	9.3	2.53
CC4-3	July 22, 2010 (28°C, 50%)	Centre	122	125	9.3	2.35
E1-1	June 18, 2009 (16°C, 90%)	Edge	50.8	142	2.5	0.35
E1-2	June 18, 2009 (16°C, 90%)	Edge	52	142	2.5	0.30
E1-3	June 18, 2009 (16°C, 90%)	Edge	52	142	2.5	0.30
E2-1	July 20, 2010 (26°C, 49%)	Edge	62.5	119.5	5.0	0.63
E2-2	July 21, 2010 (24°C, 82%)	Edge	61.5	121	5.0	0.63
E2-3	July 21, 2010 (28°C, 53%)	Edge	63	118.5	5.0	0.61
E3-1	July 20, 2010 (28°C, 44%)	Edge	61.5	123	7.5	1.04
E3-2	July 21, 2010 (25°C, 75%)	Edge	62	124	7.5	0.95
E3-3	July 21, 2010 (27°C, 53%)	Edge	61.5	124	7.5	0.96
E4-1	May 15, 2008 (16°C, 41%)	Edge	61	126	8.8	1.38
E4-2	July 21, 2010 (26°C, 68%)	Edge	61	125	9.3	1.19
E4-3	July 22, 2010 (23°C, 69%)	Edge	61	125	9.3	1.17
EE4-1	May 15, 2008 (18°C, 35%)	Edge	122	125	8.8	2.76
EE4-2	May 16, 2008 (14°C, 45%)	Edge	122	125	9.8	2.43
EE4-3	July 22, 2010 (27°C, 54%)	Edge	122	122	9.8	2.32

Testing was conducted in the main burn hall at the University of Waterloo Live Fire Research Facility. Specimens were conditioned for at least 24 hours in the cone calorimeter laboratory and other rooms within the facility prior to testing. Temperature and relative humidity in the rooms used for conditioning during the test period were between 14 and 29°C, and 35 and 90% respectively. Conditions in these rooms were loosely controlled using an air handling system. A dehumidifier was also run during the day, if necessary. However, this dehumidifier was not run during evenings or the weekend.

The temperature and relative humidity in the main burn hall of the facility were not controlled, as the facility has large open fan dampers and a large door which is often open to the outside. Therefore, as shown in Table 2-3, there were significant variations in the environmental conditions during some of the tests, as tests were performed in May, June and July. The humidity ratio of the air in the laboratory ranged between a low of 0.004 kg of water vapour per kg dry air for some of the tests in May and a high of 0.015 kg of water vapour per kg dry air during some of the tests in July.

2.3.2. Furniture Calorimeter Test Procedure

Specimens were placed on top of the electronic load cell under the furniture calorimeter hood. The test specimens were ignited using either a small hand-held propane torch (May, 2008 tests) or a butane barbecue lighter (June, 2009 and July, 2010 tests). The heat release rate of these ignition sources was measured using oxygen consumption calorimetry and was found to be 1.34 kW for the hand-held propane torch, and 0.10 kW for the butane barbecue lighter [31]. Once the specimen was ignited, testing followed standard test procedures for large-scale oxygen consumption calorimetry.

Two ignition locations were used for testing. For centre ignition tests, a 6.4 cm diameter hole with a depth of 1.3 cm was cut at the centre of the specimen to ensure a consistent ignition location for each test (Figure 2-7). The ignition source was positioned at this location. For edge ignition, the ignition source was placed on a mark on the top surface of the specimen at the midpoint point along the width (Figure 2-8).

In order to measure flame spread rates for input into the CBUF model, equation (1.5), the top surface of each test specimen was marked in a grid pattern of 10 cm by 10 cm squares before testing. A FLIR ThermaCAM® S60 infrared (IR) camera (FLIR Systems, Burlington, ON) with a spectral range of 7.5 to 13 μm, and one or two Sony MiniDV camcorders (Sony of Canada, Toronto, ON) were used to record each of the fire tests. Still photographs were also taken at various times during the test using an Olympus Stylus 770SW (Olympus Canada Inc., Markham, ON) or a Panasonic DMC-LZ10 (Panasonic, Canada, Inc., Mississauga, ON) digital camera.

Figure 2-7: Photographs taken during centre ignition test of 1.2 by 1.2 m by 10 cm polyurethane foam specimen (left – just after ignition, right – approximately 120 s after ignition).

Figure 2-8: Photographs taken during edge ignition test of 1.2 by 1.2 m by 10 cm polyurethane foam specimen (left – just after ignition, right – approximately 135 s after ignition).

2.4. Full Scale Experimental Flame Spread Methodology

In order to better understand the flame spread pattern that occurred during the full scale tests, and ultimately to obtain a flame spread rate, footage from the FLIR ThermaCAM® S60 infrared (IR) camera (FLIR Systems, Burlington, ON) was analyzed using MATLAB's Image Processing Toolbox. This section describes the method that was used during the processing of the infrared (IR) footage. This technique was inspired by research that Pastor et al have conducted on thermal imaging processing for computing the rate of spread of forest fires [32].

Two goals were kept in mind when processing the infrared footage. The first was to obtain flame area spread rates (m^2/s) representing the time varying ignited area of the specimen which will be used as input into the CBUF equation, and the second was to obtain linear spread rates representing the velocity (m/s) at which the flame front was progressing at a given moment. Figure 2-9 outlines the method that was used to extract flame spread information from the infrared video record.

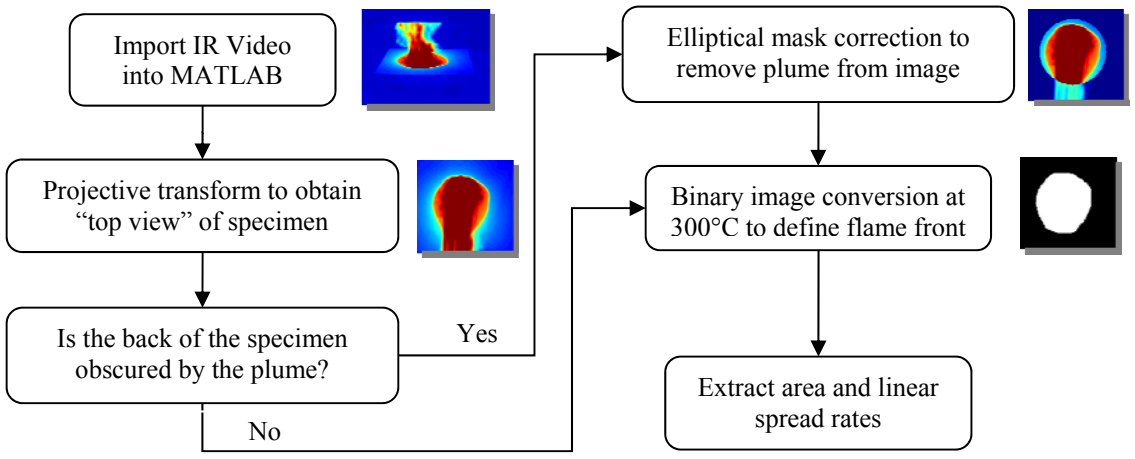

Figure 2-9: Overview of method used to extract flame spread information from infra-red video record.

The processing of the IR footage involved five key steps, namely: perform a projective transform, apply an elliptical mask correction, convert the thermal image to a binary image showing the location of the flame front and finally measure the flame area and linear flame spread rates

2.4.1. Projective Transformation

The first step in the image processing method involved applying a projective transform to the original IR images. The purpose of the projective transform was to obtain a "top view" of the specimen in which areas and distances could be directly measured. This style of transform involves identifying in the image the location of at least four known points on a single plane and assigning a coordinate system to the plane being identified [33]. For the purpose of this procedure, the plane was taken to be the top surface of the foam specimens and the four corners of the specimen were taken to be the four known points. The coordinate system was defined with its origin located at the left corner on the edge nearest the infra-red camera, camera right as the positive *x* direction, and away from the camera as the positive *y* direction. This coordinate system is illustrated in Figure 2-10.

To accomplish this transformation, a script was written where a four corner polygon is stretched over the specimen surface (as seen in Figure 2-10) and the corners are read as input to create the 2D spatial transformation matrix using MATLAB's built in function *maketform* [34]. This transformation matrix was then used as input for MATLAB's built in function *imtransform* [34] which applies a spatial transformation matrix to a specified image. The resulting transformed image is *m* x *n* pixels in size where *m* and *n* are the specimen width and length in centimeters respectively. Since centimeters were selected as the base unit for the transformation, one pixel in the transformed image corresponds to one square centimeter in the specimen. This

selection provided a close match to the pixel density in the original image while providing a simple conversion when reading distances and areas from the transformed image.

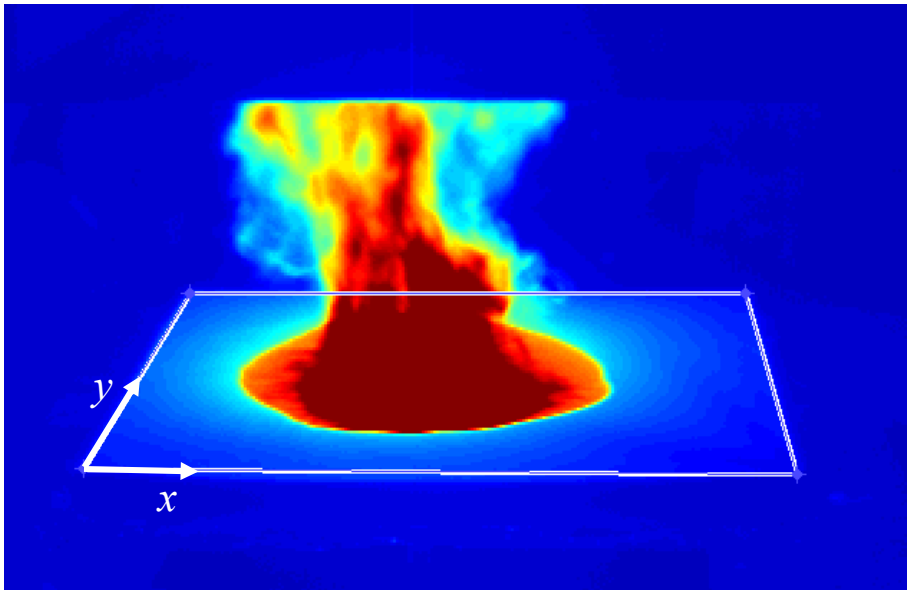

Figure 2-10: Locating the corners of the foam specimen CC4-3 prior to performing perspective transform.

Figure 2-11 shows the transformed "top view" for specimen CC4-3. Due to the coordinate convention for image pixel numbering, the origin in Figure 2-11 is located in the top left corner. This is why the image appears to be mirrored vertically.

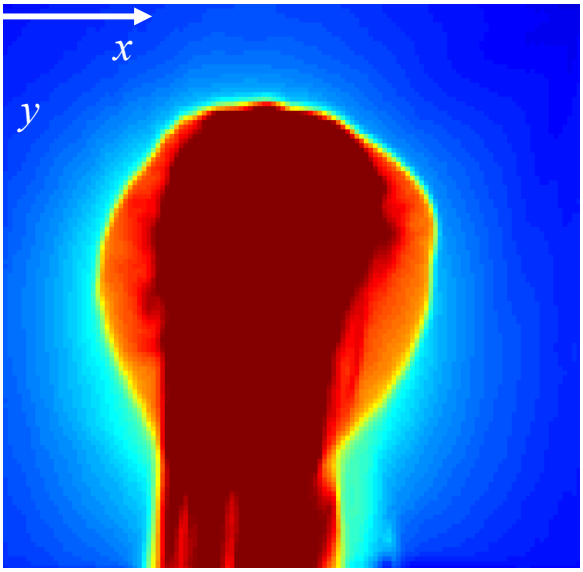

Figure 2-11: Transformed image showing "top view" of the specimen CC4-3.

It is worth noting at this point that the 2D spatial transformation described above does not correct for distortions native to the camera optics such as spherical aberration. Although this form of distortion is present to some degree in most optics it was found that the edges of the foam specimens lined up well with the defined coordinate system indicating that for this experimental apparatus the effect of spherical aberration is negligible relative to the size of the specimen.

The identification of the specimen corners is a subjective process and as such is a possible source of error. It was found that by scrolling through the footage, the corners of the specimen were fairly easily identified and as such was deemed to be negligible. Another possible source of error in this procedure was the presence of curvature in the specimen surface. Since the specimens of polyurethane foam were prepared from densely packed rolls, even after long periods of flat storage the specimens still exhibited some curvature and as a result did not sit entirely flat during the experiments. Since this procedure assumes that the top surface of the specimen is a plane, deviation from a flat surface results in some distortion of the "top view"

geometry. This distortion was observed in some of the transformed images as an apparent shift in the ignition location of the specimen. This distortion was limited to two to three centimeters and was thus deemed to be negligible.

2.4.2. Elliptical Mask Correction for Plume Obscuration

In tests where a particularly large fire was observed, the back half of the specimen tended to be obscured by the plume (this effect can be observed in the lower part of Figure 2-11). To take this into account, it was assumed that the flame front obscured by the plume, maintained approximately the same radius of curvature as the rest of the flame front. To apply this correction an elliptical mask was created approximately the same size as the flaming area and was placed in such a way as to attenuate the temperature of the plume. A simple attenuation filter of the form $f = x^{0.92}$ was used to correct the plume region. This filter was developed through trial and error to provide a level of attenuation that lowers the plume temperature below the flame front temperature. This filter also tended to attenuate the high temperature regions to a higher degree than the lower temperature regions allowing the images to retain a level of detail in the cooler regions. Figure 2-12 shows the corrected image. If in future research an infrared camera is placed on each side of the specimen, the need for the elliptical mask correction could be eliminated.

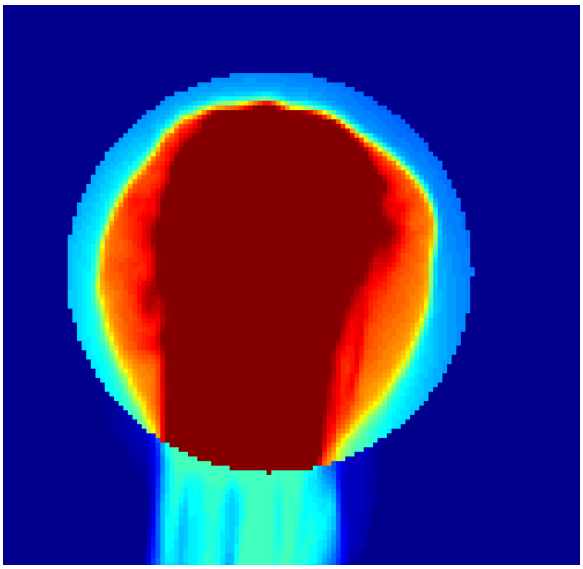

Figure 2-12: The transformed image of specimen CC4-3 showing the applied attenuation filter to adjust the area obscured by the plume.

2.4.3. Binary Front Definition

In order to extract a flame front from the IR images it was necessary to define the temperature threshold where the foam would be considered to have reached ignition. For TDI based foams, urethane bonds begin to thermally degrade and break apart at temperatures ranging from 200°C - 300°C [35]. It was found that choosing 300°C as the definition of the flame front produced a flame front that closely matched the flame front determined using manual verifications (the manual verification technique will be discussed in Section 2.4.5).

Using 300°C as the definition of the flame front a binary image was created where 0 was assigned to pixels below 300°C and 1 was assigned to pixels above 300°C. A binary image that was produced for specimen CC4-3 can be seen in Figure 2-13.

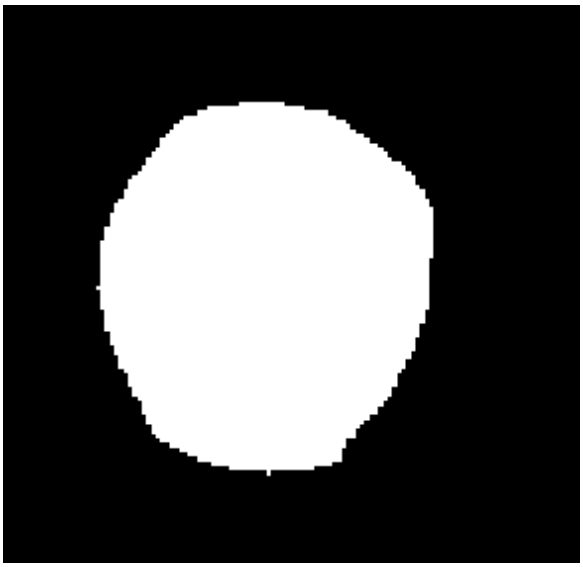

Figure 2-13: The binary image created for specimen CC4-3 using 300°C as the definition of the flame front.

2.4.4. Burning Area and Flame Front Trace along Paths of Interest

Once the IR images were converted into binary images the burning area of a specimen was calculated using MATLAB's function *bwarea* [34] which calculates the number of white pixels in a binary image. These are the data that form the experimental area spread rate data (m^2/s).

To account for asymmetrical flame spread, flame front velocity was measured at multiple locations on each specimen. Figure 2-14 and Figure 2-15 illustrate the vectors of interest for the center and edge ignition specimens, respectively.

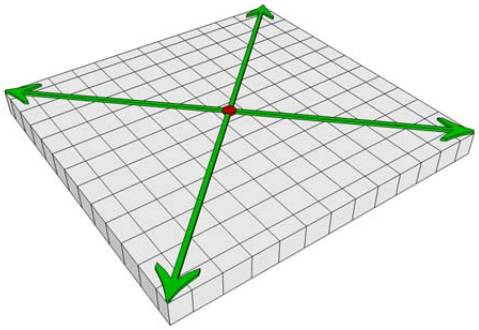

Figure 2-14: Location of flame spread rate measurement on center ignition specimens.

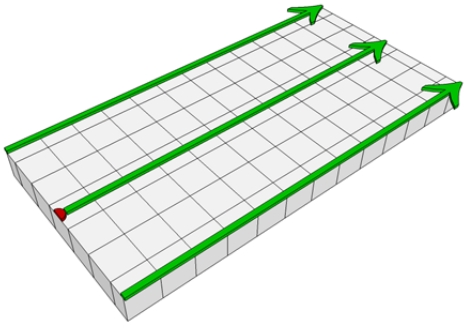

Figure 2-15: Location of flame spread rate measurement on edge ignition specimens.

For the center ignition specimens, the flame front velocity was measured along four vectors: all starting from the ignition location and moving outward to the four corners of the specimen. For the edge ignition specimens the flame front velocity was measured in three locations: one starting from the ignition location and moving toward the opposite end of the specimen and one along either edge of the specimen starting on the ignited edge and moving across the length of the specimen.

2.4.5. Manual Verification Technique

Since the flame spread rate measurement procedure was largely automated it was necessary to verify these data against some other measurement. For this verification the flame spread was manually estimated by examining frames from the video record and counting the number of 10 cm X 10 cm squares that were ignited at 30 s intervals. This verification was performed on one specimen of each geometric configuration namely, C4-3, CC4-2, E2-1 and EE4-3. In addition, since tests C1-3, C2-2, C3-2 and E3-1 were performed using a reduced range on the IR camera, this verification was run to verify the accuracy of the flame spread measurement for these tests as well.

In this verification both perspectives were examined so that all parts of the flame front could be accurately gauged. Figure 2-16 and Figure 2-17 show the front and back views used for the manual verification of test CC4-2.

Figure 2-16: Front view of CC4-2 used for verification at t = 90 s.

Figure 2-17: Back view of CC4-2 used for verification at t = 90 s.

At each time step the fraction of partially burning squares were also estimated and this was added to the burning area for each time step. The 30 second data points were then plotted with the data gathered using the automated routine and the results were compared.

2.4.6. Results of Manual Verification of the Area Spread Data

Figure 2-18 shows the result of the manual verification of test EE4-3.

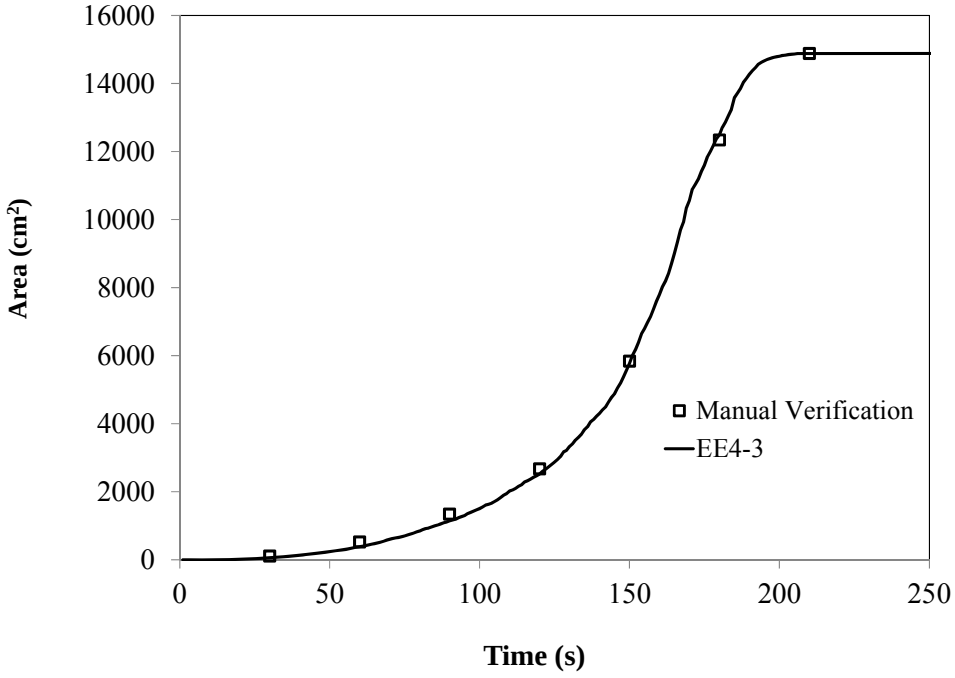

Figure 2-18 Comparison of flame area measurements recorded using the automated code and measurements recorded manually for test EE4-3.

The manual verification of test EE4-3 seen in Figure 2-18 represents one of the tests with the best degree of agreement. Throughout the test, the manually verified flame spread area closely follows the curve from the automated process. In all of the tests the difference tended to be within 150 cm^2 independent of the size of the test specimen. In some cases the manual rate was higher than the automated rate, and in some cases the automated rate was higher than the manual rate. For example in test C1-3 (shown in Figure 2-19) the manual verification shows a flame spread rate slightly higher than the automated process whereas in test E3-1 (shown in Figure 2-20) the manual verification shows a spread rate slightly lower than the rate predicted with the automated process.

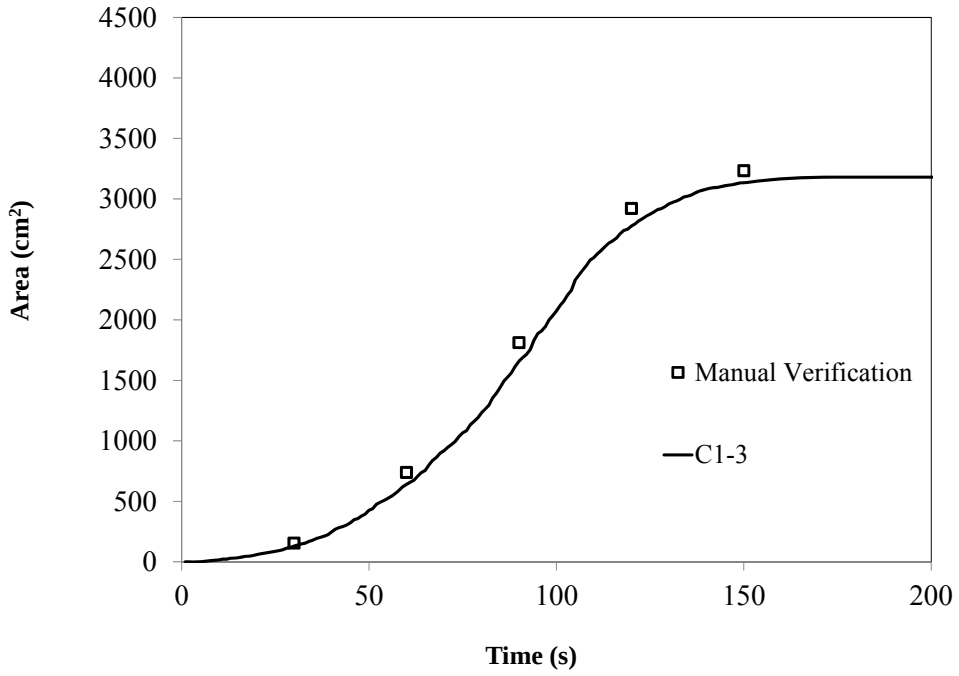

Figure 2-19 Comparison of flame area measurements taken using the automated code and measurements recorded manually for test C1-3.

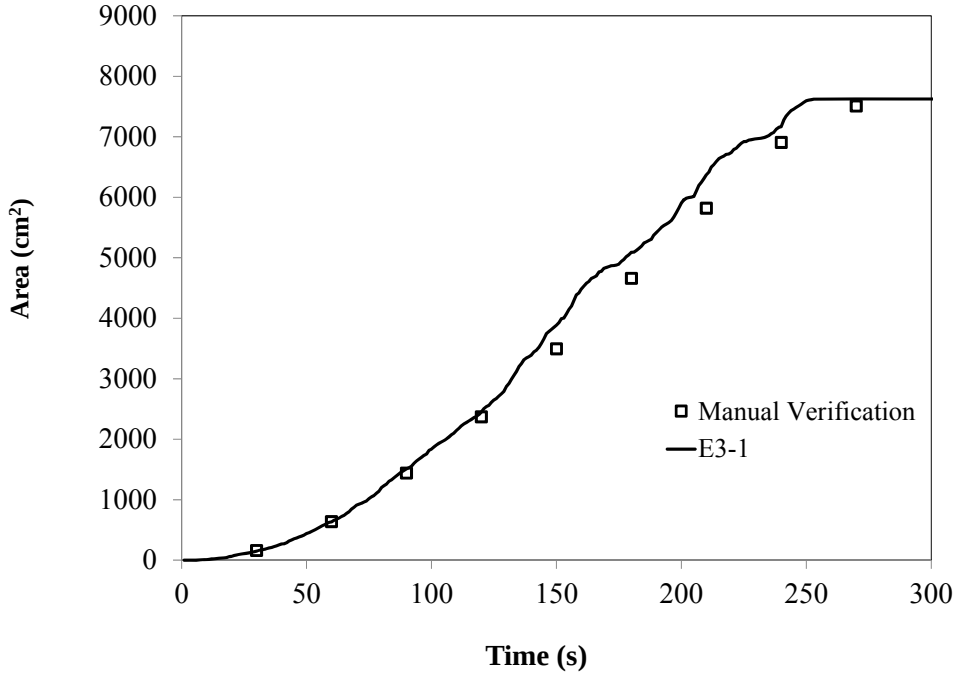

Figure 2-20 Comparison of flame area measurements taken using the automated code and measurements recorded manually for test E3-1.

The variations that are seen between the automated process and the manual verification are likely due to a couple of factors. In the case of test E3-1, the over-prediction shown by the automated technique is likely due to the flickering of the flame front that is present in some of the infra-red video footage; when a high temperature flame flickers ahead of the actual flame front, the automated algorithm can record that quick temperature variation as a progression of the flame front. For the case of test C1-3 the under-prediction of the flame front position is likely due to a slight misalignment in the identification of the specimen corners (as was described previously in Section 2.4.1) when the infra-red footage was fed into the automated algorithm.

Finally, another factor that could have played a role in the differences seen between the automated flame front measurements and the manually observed flame front measurements is the subjective nature of the manual measurement technique. When the flame front is being visually observed from a video record, the observer is required to make a judgment call as to where the foam has actually ignited. This effect has been explored in previous work by the U of S fire protection engineering research group [24]. In this previous work it was noted that although the nature of manual flame front estimation can be considered to be subjective, flame diameters measured by three individuals for a particular full scale test were within 5 to 10% of one another for much of the growth phase of the fire.

Plots of all manual area spread rate verifications can be found in Appendix A.

CHAPTER 3 : EXPERIMENTAL RESULTS

3.1. Cone Calorimeter Test Results

This section of the thesis will discuss four aspects of the cone calorimeter testing that was conducted in this research. First some general observations will be made regarding the experimental results. Next the cone calorimeter results will be discussed in the context of experimental repeatability. Next the effect of incident heat flux setting will be discussed followed by a discussion of the effects of foam aging on HRR properties.

In this section, the individual cone calorimeter tests will be referred to using the nomenclature that was discussed in Section 2.1.2. Table 3-1 summarizes the heat release rate measurements for the four thicknesses of foam that were tested in terms of commonly used parameters. The Peak HRR Density refers to the maximum value for HRR Density that was recorded during the test. The Average HRR Density is an average value taken over the duration that the specimen was burning i.e., from the start of the test until "flame out" was observed. The THR (total heat released) value is a summation of the energy released during the burning duration and can be thought of as the area under the HRR curve. Finally the THR/mass value represents the amount of energy that was released for each kilogram of material burnt and is similar in concept to the heat of combustion of the material being tested. These four parameters were calculated for each test. Table 3-1 presents an average and standard deviation of these parameters for any given configuration of incident heat flux and foam thickness. When HRR Density curves are presented in this section, the time $t = 0$ was taken as the time that was

recorded as ignition on the cone calorimeter apparatus; no adjustments were made for the alignment of the HRR Density Curves.

Table 3-1: Summary of cone calorimeter test results.

Test Set	Nom. Thick. (cm)	Incident Heat Flux (kW/m^2)	Peak HRR Density (kW/m^2)		Ave. HRR Density (kW/m^2)		THR (MJ/m^2)		THR/mass (MJ/kg)	
			Ave.	(σ)	Ave.	(σ)	Ave.	(σ)	Ave.	(σ)
1-25	2.5	25	428	(34.4)	241	(7.2)	10.5	(0.19)	24.8	(0.59)
1-35		35	556	(29.6)	225	(11.8)	10.4	(0.07)	24.8	(0.09)
1-50		50	749	(63.5)	322	(72.8)	11.1	(0.28)	26.2	(0.56)
1-75		75	950	(57.4)	370	(25.6)	11.3	(0.39)	26.7	(0.88)
2-25	5	25	419	(13.8)	245	(12.5)	19.6	(0.31)	24.3	(0.35)
2-35		35	472	(19.5)	251	(2.1)	19.5	(0.09)	23.6	(0.26)
2-50		50	670	(17.9)	382	(14.6)	19.7	(0.40)	24.0	(0.45)
2-75		75	989	(26.6)	505	(13.3)	21.0	(0.24)	25.9	(0.09)
3-25	7.5	25	424	(21.4)	260	(10.2)	31.3	(0.55)	24.4	(0.13)
3-35		35	504	(20.6)	274	(14.1)	30.5	(1.09)	24.2	(0.66)
3-50		50	603	(9.9)	367	(13.9)	30.6	(1.22)	24.2	(0.51)
3-75		75	919	(16.4)	520	(4.8)	31.5	(0.03)	24.8	(0.28)
4-25	10	25	373	(4.8)	246	(7.9)	38.9	(0.37)	24.5	(0.41)
4-35		35	420	(19.5)	273	(21.6)	38.0	(0.63)	23.8	(0.52)
4-50		50	503	(52.8)	347	(14.9)	37.6	(0.88)	23.7	(0.53)
4-75		75	723	(33.0)	449	(50.5)	39.6	(0.18)	24.9	(0.17)

The values recorded in Table 3-1 illustrate that there was a good level of consistency in peak and average values of heat release rate density within each test series. The standard deviations for the peak heat release rate density ranged from 4.8 kW/m^2 in 4-25 tests to a high of 63 kW/m^2 in the 1-50 tests with standard deviations always staying below 10% of the average experimental value. A very good level of consistency is seen in the values of total heat released, especially when total heat released is normalized using the mass of the specimen. The mass normalized total heat released standard deviations ranged from 0.09 MJ/kg in the 2-75 tests to a high of 0.88 MJ/kg in the 1-75 tests, with the standard [35] deviation always staying below 3.3% of the mean experimental value.

3.1.1. General Observations

After reviewing the test footage for the cone calorimeter tests it is apparent that there are two distinct stages of the combustion process that are exhibited for all thicknesses of foam burned in the cone calorimeter. The first stage of combustion takes place while the structure of the foam is collapsing; the second stage takes place while the foam is in a liquid state. These two stages are also observable as two distinct peaks in the heat release curves, including A and B in Figure 3-1 and Figure 3-2. The general shape of the heat release rate curve was similar in each of the individual tests within a series, with more consistency in the earlier portions of the tests and the first peak of the individual curves than in the second peak and the decay period of the individual curves.

This behavior is similar to what is described by Krasney et al. [36] when describing the smoldering behavior of polyurethane foam, however without the charring stage. It appears that with this polyurethane foam in flaming combustion, there is limited charring, and a significant portion of the total heat released takes place while the foam has become what Krasney et al. refer to as a tar.

This behavior is also consistent with Wooley as cited by Wilkie [35] who found that toluene 2,4- and 2,6-diisocyanate (TDI) based flexible polyurethane foams begin to degrade at 200°C–300°C when urethane bonds dissociate producing fairly nonvolatile polyol components and nitrogen rich volatiles which were reported to be condensed forms of TDI. At higher temperatures the polyol component of the foam begins to degrade producing small volatile organic species. This two stage decomposition may provide a physical explanation of the two peaks in the HRR density curves. When the foam is first ignited the first stage is dominantly fueled by the nitrogen rich volatiles that are released during the degradation of the urethane bonds [35]. As the thermal wave proceeds down through the foam block the foam continues to

collapse into a pool of polyol residue. When the foam has completely collapsed the nitrogen rich volatiles are no longer available for fuel and the dip after the first peak is produced. As the fire continues, the temperature of the polyol pool continues to rise accelerating the rate at which it releases small organic species into the plume producing the second HRR density peak.

This two-stage combustion process is also discussed in detail by Kramer et al [14] who used microscale calorimeter tests and thermo-gravametric analysis to analyze this physical process.

3.1.2. Repeatability of Cone Calorimeter Test Results

This section will focus on the repeatability of the cone calorimeter tests that were completed in this research. As was discussed in Section 3.1, when these data are analysed using common statistical parameters, the data exhibits a good deal of repeatability. In additional to the statistical analysis, the shapes of the HRR curves were visually assessed to find any clear divergences in burning behavior.

For any given configuration of thickness and heat flux, this cone calorimeter testing showed very good repeatability. Figure 3-1and Figure 3-2 are plots of the heat release rate density for three individual tests conducted in each of the 2-25 (5.0 cm (2 in.) foam tested at 25 kW/m^2) and 4-50 test series (10 cm (4 in.) foam tested at 50 kW/m^2), respectively, and represent the level of repeatability that was typically seen in this testing.

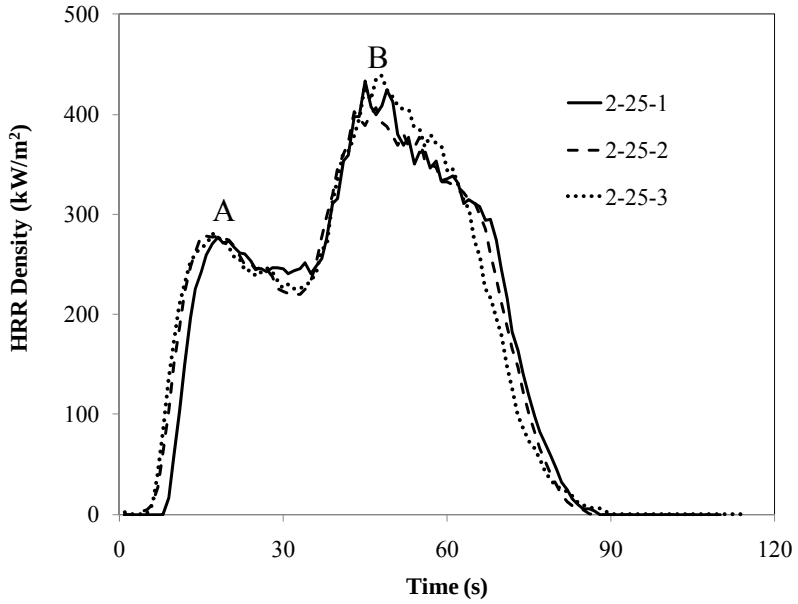

Figure 3-1 Heat release rate density measurements in tests of 5.0 cm thick foam specimens exposed to incident heat flux of 25 kW/m². "A" indicates the HRR density peak during the foam collapse. "B" indicates the HRR density peak while the foam is in liquid state.

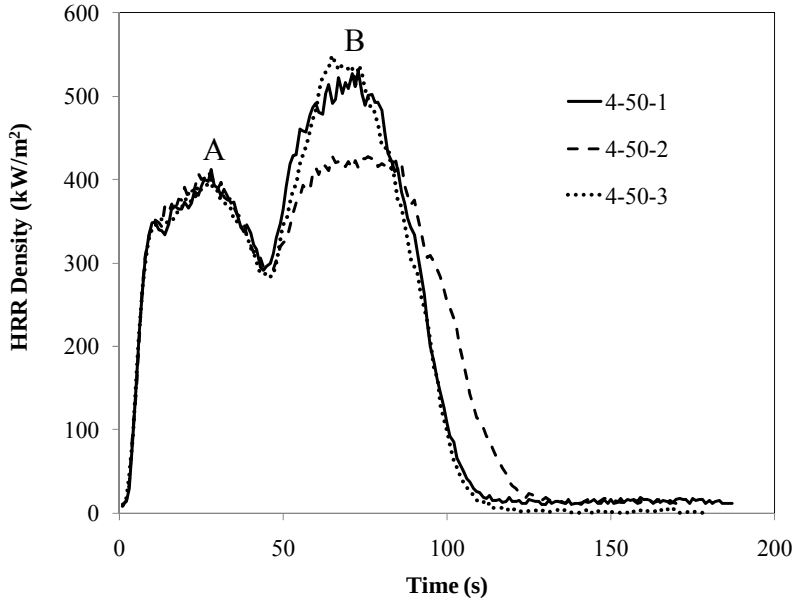

Figure 3-2 Heat release rate density measurements in tests of 10.0 cm thick foam specimens exposed to incident heat flux of 50 kW/m^2. "A" indicates the HRR density peak during the foam collapse. "B" indicates the HRR density peak while the foam is in liquid state.

As seen in Figure 3-1 and Figure 3-2, some of the test series showed better repeatability than others. Figure 3-1 represents one of the more consistent test series that was completed. In this test series the HRR density data produced similar curves. Representing one of the tests with greater variation is Figure 3-2. While the three tests shown in this figure still show a large degree of repeatability, the peak HRR of test 4-50-2 at 429 kW/m^2 is notably lower than tests 4-50-1 and 4-50-3 which had peak HRR values of 530 kW/m^2 and 549 kW/m^2 respectively.

Plots of all cone calorimeter HRR density data can be found in Appendix B.

3.1.3. Effect of Incident Heat Flux on Cone Calorimeter Tests

One of the main observations that can be made using these data is regarding the effect that incident heat flux has on the HRR density curves for cone calorimeter tests. Figure 3-3 through Figure 3-6 show a comparison between HRR density curves for the four heat flux settings for each specimen thickness.

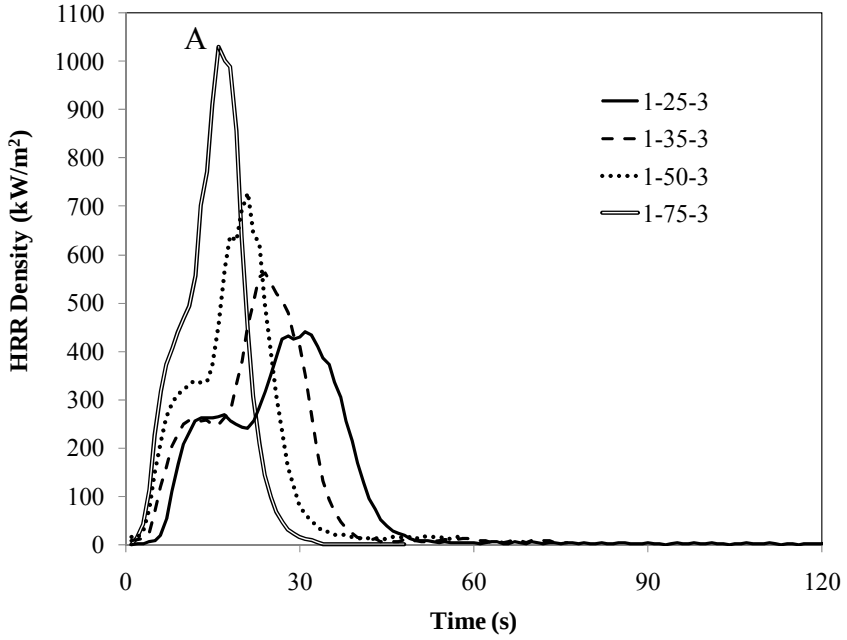

Figure 3-3 Heat release rate density measurements in tests of 2.5 cm thick foam specimens exposed to incident heat fluxes of 25 kW/m^2, 35 kW/m^2, 50 kW/m^2 and 75 kW/m^2."A" indicates test 1-75-3 which exhibited a single peak.

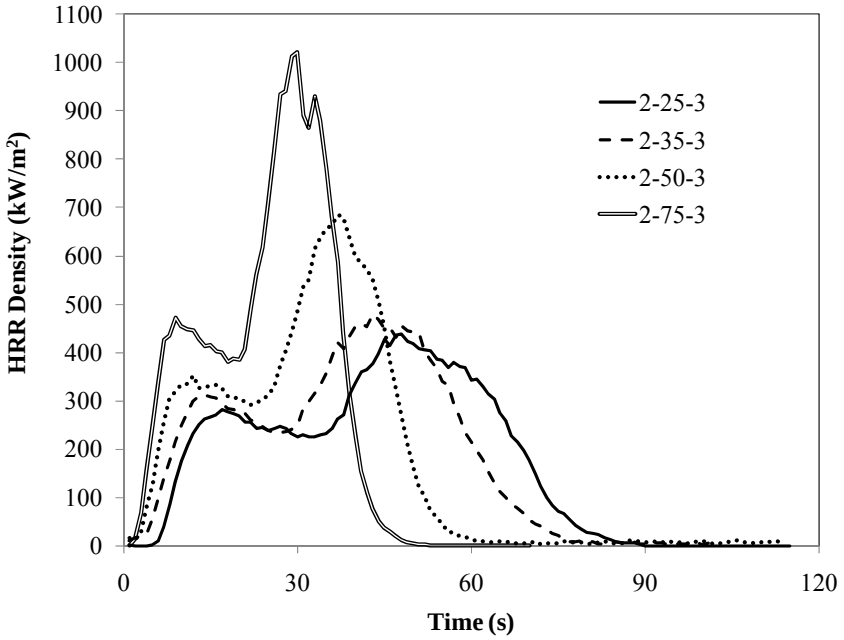

Figure 3-4 Heat release rate density measurements in tests of 5.0 cm thick foam specimens exposed to incident heat fluxes of 25 kW/m^2, 35 kW/m^2, 50 kW/m^2 and 75 kW/m^2.

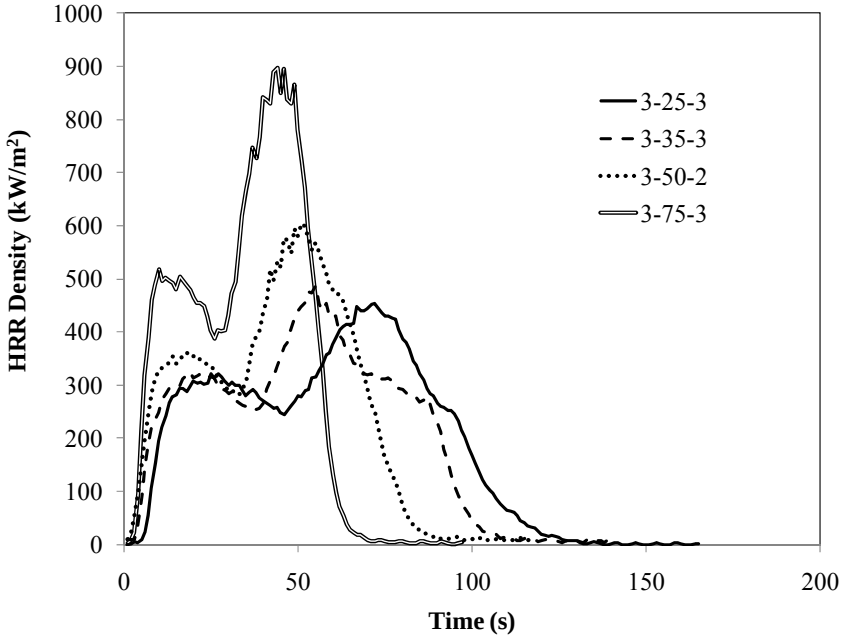

Figure 3-5 Heat release rate density measurements in tests of 7.5 cm thick foam specimens exposed to incident heat fluxes of 25 kW/m^2, 35 kW/m^2, 50 kW/m^2 and 75 kW/m^2.

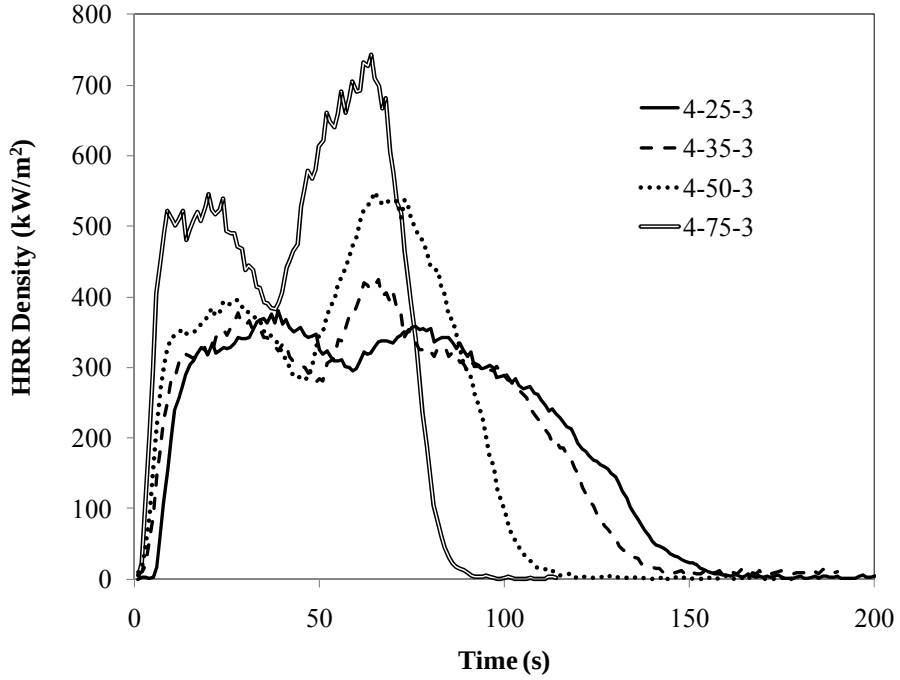

Figure 3-6 Heat release rate density measurements in tests of 10.0 cm thick foam specimens exposed to incident heat fluxes of 25 kW/m^2, 35 kW/m^2, 50 kW/m^2 and 75 kW/m^2.

Table 3-1 and Figure 3-3 through Figure 3-6 indicate that the incident heat flux had a significant effect on the heat release rate density measurements. As the incident heat flux increased, the peak values of the heat release rate density increased. While the average heat release rate densities were similar for the two lowest incident heat fluxes, the average value increased significantly as the heat flux was increased to 50 kW/m^2 and 75 kW/m^2. In general, the peak heat release rate densities measured using a 75 kW/m^2 incident heat flux were 80% to 135% higher than the values measured using a 25 kW/m^2 incident heat flux, while the average values over the period that the specimen burned were 80% to 110% percent higher in most cases when using the highest incident heat flux. The general shape of the heat release rate curve remained the same for all incident heat fluxes, but as the incident heat flux increased the second peak became sharper and the time required to burn the specimen decreased. The heat release rate curve for the 2.5 cm (1 in.) foam tested at an incident heat flux of 75 kW/m^2 was different than the rest of the heat release rate curves as it exhibited only a single peak (A in Figure 3-3). The single peak behavior seen in this test configuration is likely due to a superposition of the heat release rates from the foam collapse and the combustion of the polyol residue. At lower heat fluxes these appear as separate peaks in the HRR density curve, but as the heat flux is increased the polyol pool burning peak is moved earlier to the point that it is concurrent with the foam structure collapse. In the case of the of 75 kW/m^2 test of the 2.5 cm specimen, the foam was relatively thin resulting in a very short collapse of the foam structure. Following the collapse of the foam structure, the resulting polyol pool would have possessed a lower thermal mass than a larger polyol pool allowing the polyol residue to reach its peak fuel producing temperature much faster. The video record was reviewed for visible evidence of this phenomenon, however, aside from the collapse of the foam coinciding with the dip in HRR, no visible sign of this phenomenon was

observed. It should be noted however that much of the flame plume in the cone apparatus is obscured by the heater assembly and exhaust hood. If these tests could be repeated without the hood in place where the entire plume could be observed, perhaps this change in HRR could be noticed in a change in plume height.

The observations made in this study with regards to the effects of the incident heat flux on the shape of the heat release rate curve were similar to those made by Kramer et al., who tested 3.9 cm thick polyurethane foam specimens in the cone calorimeter using incident heat fluxes from 11 kW/m^2 to 33 kW/m^2 [14].

In summary, the choice of incident heat flux had a very strong effect on burning behavior of polyurethane foam in a cone calorimeter. This goes to show that if cone calorimeter test results are going to be meaningful careful attention must be paid to external heat flux setting. As was discussed by Babrauskas in his review paper on the topic of specimen heat fluxes in bench-scale heat release rate testing [23], it is difficult to know apriori what heat flux may be appropriate for a given material and purpose. This is particularly true for cone calorimeter tests that are to be used as input to model full scale fire behavior. Later in this thesis the effect that incident heat flux setting has on convolution model predictions will be discussed.

An issue that should be highlighted, and should be addressed in future research, is that for thicker foam specimens, as the foam burns, the surface of the foam regresses away from the cone heater element. This regression from the heating element will affect the incident heat flux that reaches the surface of the specimen from the cone heating element. Some initial testing on this effect indicates that as the foam regresses, the incident heat flux rapidly diminishes, for instance, for a 10 cm thick specimen being exposed to 35 kW/m^2, by the time that the specimen reaches a

pool fire state, the specimen surface will only be exposed to a heat flux of approximately 12 kW/m^2 [37].

3.1.4. Effects of Foam Aging on HRR Density

The fourth objective of this research is to investigate the effect that foam aging has on the heat release characteristics of polyurethane foam. This section presents the result of the foam aging testing that was completed in this research. It should be noted that at this stage the foam aging study is just being initiated. More conclusive results are anticipated upon completion of tests at a greater age interval in the future.

Figure 3-7 through Figure 3-9 are plots of HRR density for specimens of polyurethane foam that were tested in November of 2010, January of 2011, and July of 2011. As seen in Figure 3-7 though Figure 3-9 these tests showed a similar level of repeatability to those discussed in the Repeatability of Cone Calorimeter Results in Section 3.1.2.

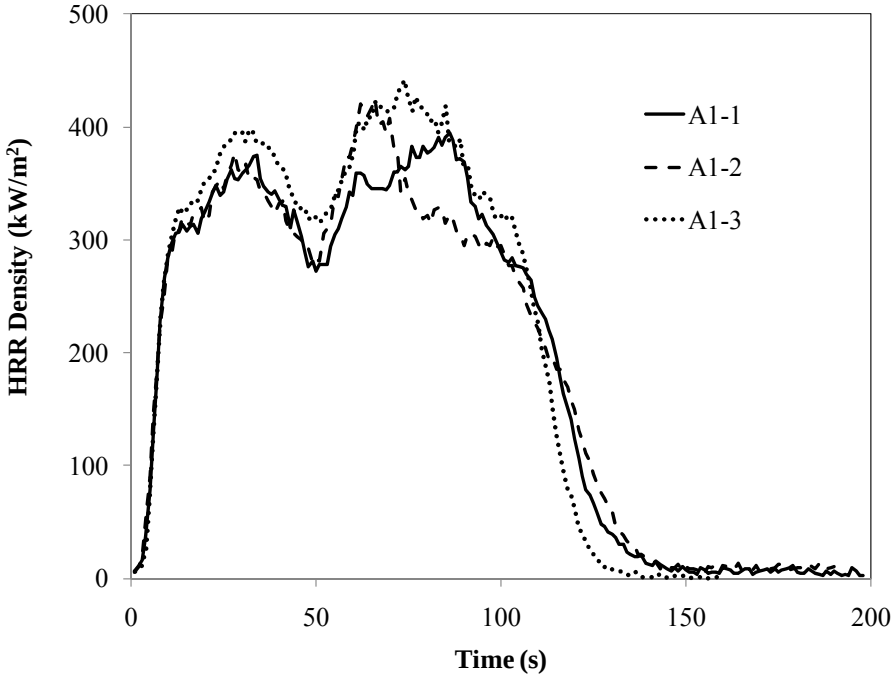

Figure 3-7 HRR Densities measured in November 2010 of 10.0 cm thick polyurethane foam exposed to 35 kW/m^2.

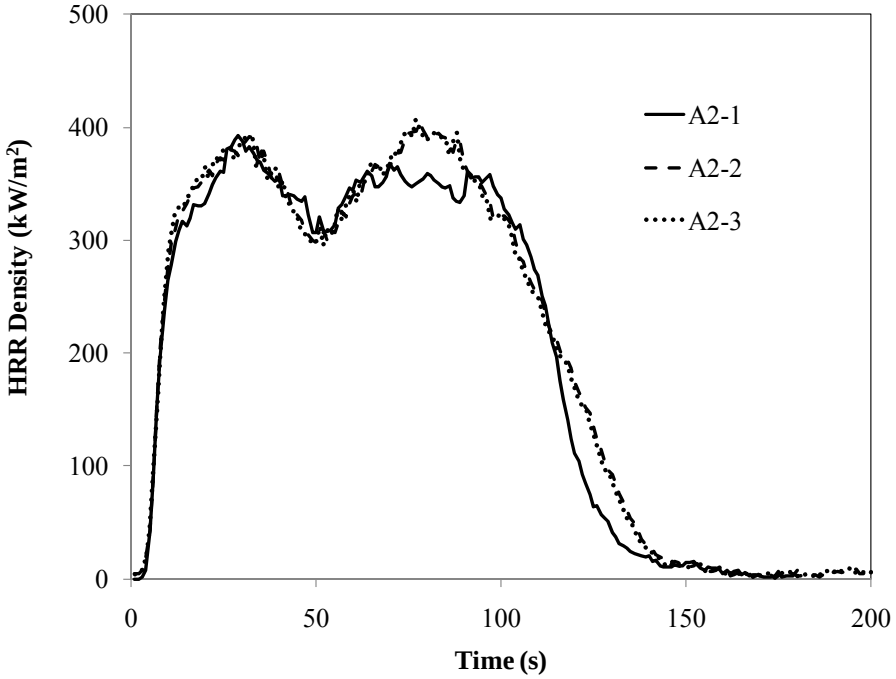

Figure 3-8 HRR Densities measured in January 2011 of 10.0 cm thick polyurethane foam exposed to 35 kW/m^2.

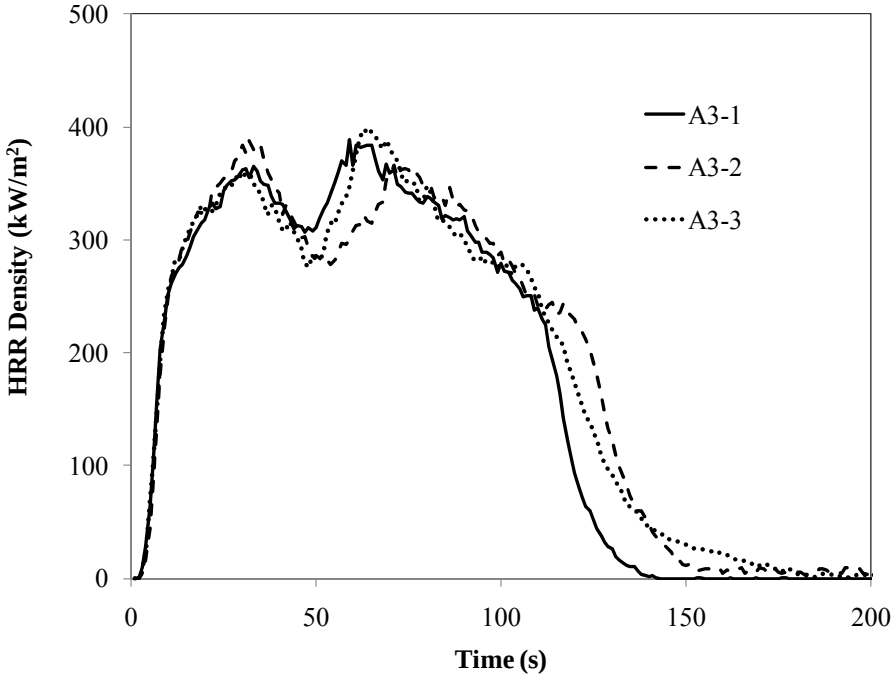

Figure 3-9 HRR Densities measured in July 2011 of 10.0 cm thick polyurethane foam exposed to 35 kW/m^2.

Although all four tests sets showed a good level of repeatability, the shapes of the curves do vary to some degree within the test set. The foams that produced the largest variation in the curve shape were the earliest tested. Table 3-2 is a summary of the test results for the foam aging cone calorimeter tests. To a large degree this table confirms the observations that were made based on the shapes of the curves shown in the above figures.

Table 3-2: Summary of foam aging cone calorimeter test results.

Test Date	Peak HRR Density (kW/m^2)		THR (MJ/m^2)		THR/mass (MJ/kg)	
	Ave.	(σ)	Ave.	(σ)	Ave.	(σ)
Nov. 2010	420	(23.9)	38.0	(0.83)	23.8	(0.63)
Jan. 2011	401	(7.5)	39.5	(1.10)	24.7	(0.27)
Jul. 2011	391	(5.7)	37.5	(1.60)	23.6	(0.68)

Table 3-3: Summary of HRR density averages for foam aging test data.

Test Date	30s Ave. HRR Density (kW/m^2)		60s Ave. HRR Density (kW/m^2)		90s Ave. HRR Density (kW/m^2)		120s Ave. HRR Density (kW/m^2)	
	Ave.	(σ)	Ave.	(σ)	Ave.	(σ)	Ave.	(σ)
Nov. 2010	273	(26.5)	307	(12.8)	330	(17.5)	308	(12.4)
Jan. 2011	253	(5.1)	309	(1.7)	329	(6.3)	314	(4.6)
Jul. 2011	243	(22.3)	294	(4.6)	311	(3.0)	295	(2.1)

As seen in Table 3-2 the tests with the largest degree of variation with regard to peak HRR density were those conducted in November of 2010. These tests showed a standard deviation of 23.9 kW/m^2 and 26.5 kW/m^2 for the peak and average HRR densities, respectively. Although higher than the other tests these standard deviations are still within 5.7% of the mean peak HRR density. With regard to total heat released and total heat released per-unit-mass, the July 2011 test set showed the greatest level of variation at 1.60 MJ/m^2 and 0.68 MJ/kg, respectively. These standard deviations were once again within reasonable levels ranging from 4.3% of the mean THR and 2.9% of the THR per-unit-mass.

Figure 3-10 compares plots of representative HRR density curves for each of the ages of foam tested.

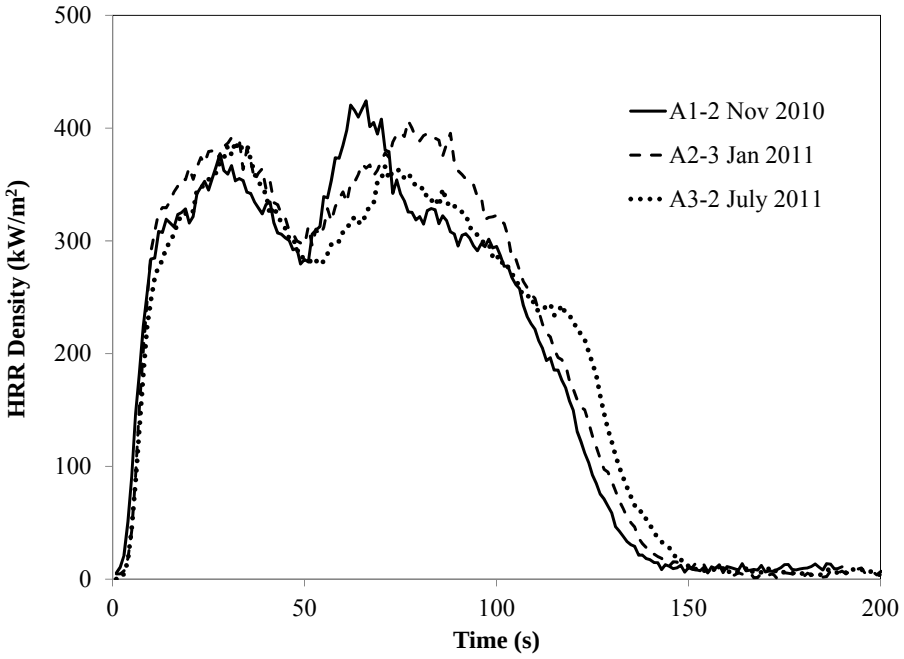

Figure 3-10 Comparison of all HRR density curves that were collected in the foam aging test series.

From observing Figure 3-10, it can be noted there are some changes in the shape of the HRR density curve as the foam ages, however these changes are small and it is difficult to draw strong conclusions from these differences.

Both the peak HRR density and the average HRR density decrease slightly with the foam age. Between November 2010 and January 2011 the peak HRR density drops by 4.5% from 420 kW/m^2 to 401 kW/m^2, and again between January and July 2011 the peak HRR density drops by 2.5% from 401 kW/m^2 to 391 kW/m^2. Similarly the average HRR density drops as the foam ages; between November of 2010 and January of 2011 the average HRR density drops by 7.3% from 273 kW/m^2 to 253 kW/m^2, and again between January and July 2011 the average HRR density drops by 3.7% from 253 kW/m^2 to 243 kW/m^2. It should be noted that these trends are small when compared to the test set standard deviations. For example the difference between

the average HRR density for November 2010 and January 2011 is 20 kW/m^2 and the standard deviation for the November 2010 test set is 26.5 kW/m^2.

The data that are presented in Table 3-3 are average HRR values which take into account data from a specific time frame. For example, the 30 s average HRR values are an average of the HRR density values that were recorded from ignition until 30 s into the test. From observing the average HRR density data that are presented in Table 3-3, the average HRR density tends to decrease slightly as the foam ages. For the 30 s average HRR density, the value makes a fairly steady decrease dropping 7.3% and 4.0% for each of the time intervals resulting in a cumulative drop of 11.3% during the course of this test series. Moving on to the 60 s average HRR density, the value actually increases by 0.7% between the November 2010 value of 307 kW/m^2 and the January 2011 value of 309 kW/m^2. Following this small increase the 60 s average HRR density then drops by 4.9% between January 2011 and July 2011. The 90 s and 120 s average HRR density values show very similar behavior to that of the 60 s average. Once again for the first aging interval, the 90 s and 120 s averages show a very small change the 90 s average HRR density value decreases by 0.3% from 330 kW/m^2 to 329 kW/m^2 and the 120 s average HRR density value increases by 1.9% from 308 kW/m^2 to 314 kW/m^2. For the second aging interval from January 2011 to July 2011 the 90 s and 120 s average HRR values once again show a larger decrease of 5.5% and 6.1% respectively.

For both the mass and area normalized THR values, there is a slight increase between November 2010 and January 2011, followed by a drop between January 2011 and July 2011. For the mass normalized THR this initial increase is 3.6% from 23.8 MJ/kg to 24.7 MJ/kg. Subsequently the drop from January 2011 to July 2011 is 4.5% from 24.7 MJ/kg to 23.6 MJ/kg. Once again it should be noted that these trends are small when compared to the test set standard

deviations which range from 1.0% to 3.9% of the mean in the January 2011 and July 2011 tests respectively.

A final observation that was made is that as the foam aged, it changed in color. When the foams were first unwrapped and prepared they were fairly white in color. Over time the specimens began to take on a more yellow or tan color which appeared to darken as time progressed.

The results that were discussed in this section should be interpreted as preliminary results of a larger study. In order to draw strong conclusions regarding the effects of foam age on it burning characteristics, further testing is required to obtain a larger sample set over a longer time period.

3.2. Furniture Calorimeter HRR Test Results

This section will focus on the results of the full scale experimental testing that was conducted during this research. It should be noted that when comparing full scale HRR, these curves were manually aligned so that they intersected at early stages of the fire (approximately 10 kW). In full scale fire testing of this sort, there is a period at the beginning of the fire when the heat release is small and the fire is susceptible to influence by environmental factors such as air currents. During this time period the growth of the fire is unpredictable [12]. This time period is sometimes referred to as the incubation time of a fire. The portion of the fire which is of interest to this research occurs once the fire is established and growing in a predictable manner. In the data collected for this research 10 kW were observed to be a HRR after which the HRR curve consistently became predictable. To allow for comparison of this interesting portion of the HRR curves, the curves were manually aligned at a HRR of 10 kW, with the apparent point of near-zero heat release at a time of 0 s.

3.2.1. Repeatability of Furniture Calorimeter Test Results

Figure 3-11 and Figure 3-12 illustrate the repeatability that was exhibited in the furniture calorimeter tests of the polyurethane foam. These examples are for center and edge ignition tests of 10 cm thick polyurethane foam specimens.

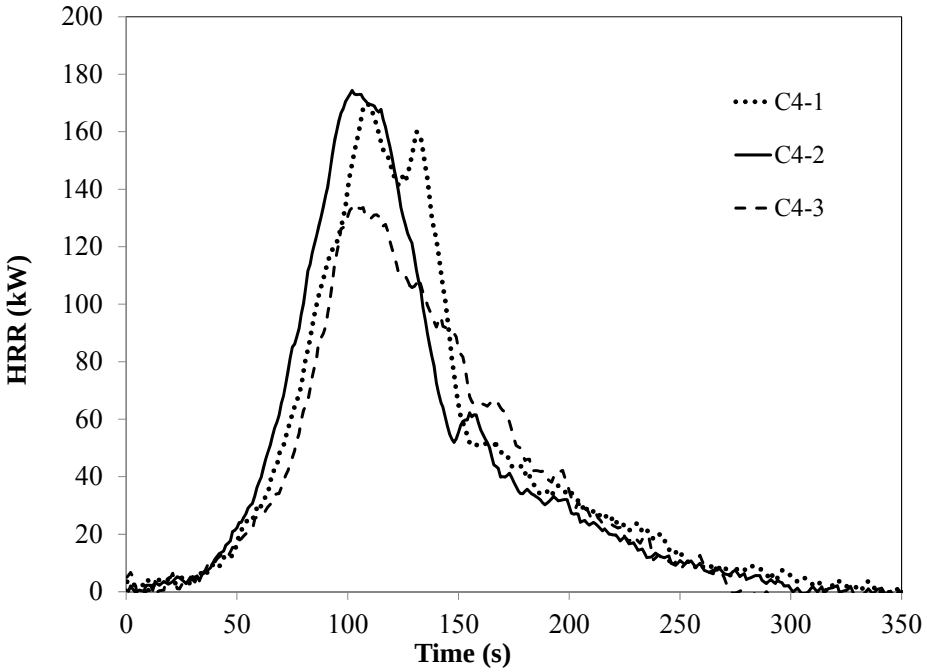

Figure 3-11 Repeatability of furniture calorimeter heat release rate measurements (10 cm thick specimens, centre ignition).

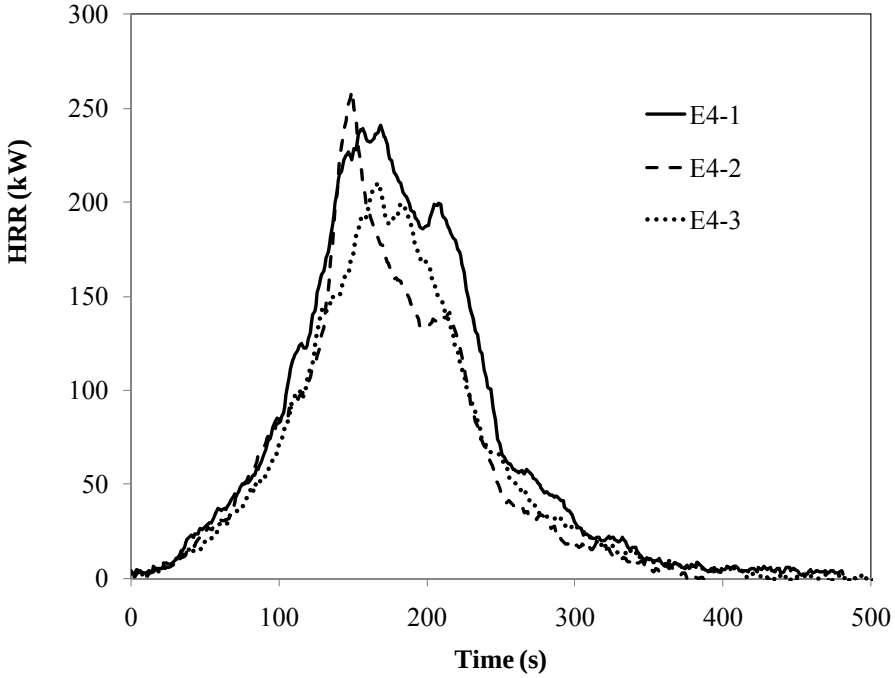

Figure 3-12 Repeatability of furniture calorimeter heat release rate measurements (10 cm thick specimens, edge ignition).

Plots of all full scale HRR data from this research can be found in Appendix C. As seen in the above two figures, the heat release curves for the full scale tests show reasonable agreement through the growth and decay phases. However, there was some variability in peak heat release values, as well as how long the peak heat release was sustained. These differences could be partially accounted for by the variations in environmental conditions. For example, specimens C4-1 and C4-2 were tested in May 2008 when the ambient air had a moisture content of 5.26 g of water per kg of dry air, while specimen C4-3 was tested in July 2010 had a moisture content of 14.39 g of water per kg of dry air**.** This would be consistent with the findings of Hurd et al. who found that the peak heat release rate of bench scale tests of polyurethane foam were reduced by 10% when the specimens were conditioned in 80% relative humidity instead of 20% relative humidity [38]. It was noted that although the change in humidity affected the peak heat release rate, it had minimal effect on the shape of the heat release rate curve. This suggests that the differences seen in these tests may also be due to changes in the exact composition of the foam over the time period it was purchased.

Table 3-4 contains total heat release and peak heat release rate data for the eight test series that are discussed in this research. Since each of the test series represents three individual tests, an average and a standard deviation is given for each test series.

Table 3-4: Summary of full scale furniture calorimeter test results.

Test Series (Nominal Thickness)	THR (MJ) Ave. (σ)	THR/Mass (MJ/kg) Ave. (σ)	Peak HRR (kW) Ave. (σ)	Time to Peak (s) Ave. (σ)	Peak/Thick (kW/cm) Ave. (σ)
C1 (2.5 cm)	3.2 (0.39)	24.1 (3.57)	36.5 (8.06)	72.0 (18.78)	14.6 (3.22)
C2 (5.0 cm)	6.9 (0.15)	22.1 (0.18)	86.0 (8.27)	85.7 (4.73)	17.2 (1.65)
C3 (7.5 cm)	10.5 (0.43)	21.7 (0.11)	137.9 (10.61)	105.7 (10.02)	18.4 (1.41)
C4 (10.0 cm)	13.9 (0.95)	24.0 (1.70)	159.7 (21.60)	104.7 (3.79)	17.0 (2.20)
CC4 (10.0 cm)	55.3 (3.45)	23.1 (1.53)	552.3 (51.9)	129.7 (2.52)	60.6 (7.73)
E1 (2.5 cm)	7.5 (1.01)	23.6 (1.37)	46.3 (10.03)	80.0 (6.24)	18.5 (4.01)
E2 (5.0 cm)	13.7 (0.30)	22.0 (0.22)	83.7 (12.09)	118.0 (5.29)	16.7 (2.42)
E3 (7.5 cm)	22.8 (1.22)	23.2 (0.36)	168.9 (13.69)	167.7 (29.30)	22.5 (1.83)
E4 (10.0 cm)	28.9 (3.94)	23.2 (1.04)	237.0 (24.75)	161.7 (11.02)	26.0 (2.91)
EE4 (10.0 cm)	58.0 (3.68)	23.2 (1.35)	485.9 (34.8)	182.0 (11.27)	51.5 (5.86)

The values recorded in Table 3-4 illustrate that there was a good level of consistency in peak and average values of heat release rate within each test series. The standard deviation for the total heat release ranged from a low of 0.15 MJ in the C2 tests to a high of 3.94 MJ in the E4 tests, always staying below 14% of the average value. As can be expected, as the size of the specimens increased the THR also increased. This behavior is perhaps best observed when normalized by the mass of the specimen as a THR/mass value, or an effective heat of combustion value.

As was also seen in the small scale tests, when the total heat release is normalized using mass, the tests demonstrate good repeatability ranging in standard deviation from 0.11 MJ/kg in the C3 tests to a high of 3.57 MJ/kg in the C1 tests. Comparing the THR/mass value for all full scale tests the average value produced is 23.1 MJ/kg with a standard deviation of 1.6 MJ/kg. It is interesting to note that this value is only 1.6 MJ/kg lower than the average THR/mass for the cone calorimeter specimens of 24.7 MJ/kg. This small difference indicates that the foam is burning in a similar fashion in the cone calorimeter and the furniture calorimeter. This similarity also suggests that the oxygen consumption calorimetry equipment in the furniture and cone

calorimeters are properly calibrated and working properly. Although this value is lower, it is within one standard deviation of the bench scale value. Similarly the average full scale THR/mass is only 1.3 MJ/kg lower than the heat of combustion (ΔH_c) for polyurethane foam of 24.4 MJ/kg that is published in Drysdale [12]. It should be noted that the heat of combustion value reported in Drysdale can be expected to be different from these experimental results since the ΔH_c was obtained by burning the material in 100% oxygen. This process results in a more complete combustion and as a result a higher heat of combustion. Variability of foam composition is likely also playing a role in the differences between the experimental data from this thesis and that published in Drysdale. This is certainly the case for the cone calorimeter data from this thesis which shows an effective heat of combustion higher than Drysdale's value of the heat of combustion from a specimen burned in 100% oxygen.

As is typically seen in tests of this type the peak heat release rate shows a greater level of variability with standard deviations ranging from 8.06 kW in the C1 tests to a high of 34.8 kW in the EE4 group of tests. The standard deviation of the time to peak value ranged from a low of 2.52 s in the CC4 test series to a high of 29 s in the E3 tests. The peak HRR and time to peak HRR values will be discussed in more detail in the following subsections within the context of the effects of specimen thickness and ignition location.

3.2.2. Effect of Foam Thickness on Full Scale Test Results

One of the objectives of this research was to examine the effect that foam thickness has on full scale fire test results. This section will compare and contrast the furniture calorimeter test results that were collected for specimens of varying thickness. For clarity, these results will be divided into center and edge ignition configurations. Figure 3-13 and Figure 3-14 are plots of heat release rate for nominal thicknesses of 2.5 cm, 5 cm, 7.5 cm and 10 cm. Figure 3-13 shows

this comparison for center ignition and Figure 3-14 shows this comparison for edge ignition tests. Tests series CC4 and EE4 have been left out of this analysis since the specimen surface area is different than the other test configurations.

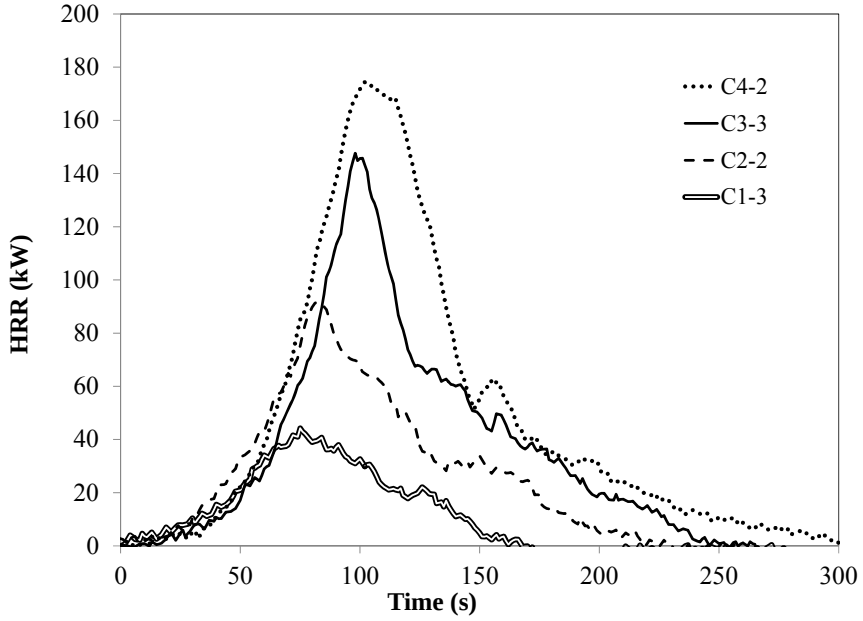

Figure 3-13 heat release rates measured during centre ignition tests of foam with nominal thicknesses of 2.5 cm (C1-3), 5 cm (C2-2), 7.5 cm (C3-3) and 10 cm (C4-2).

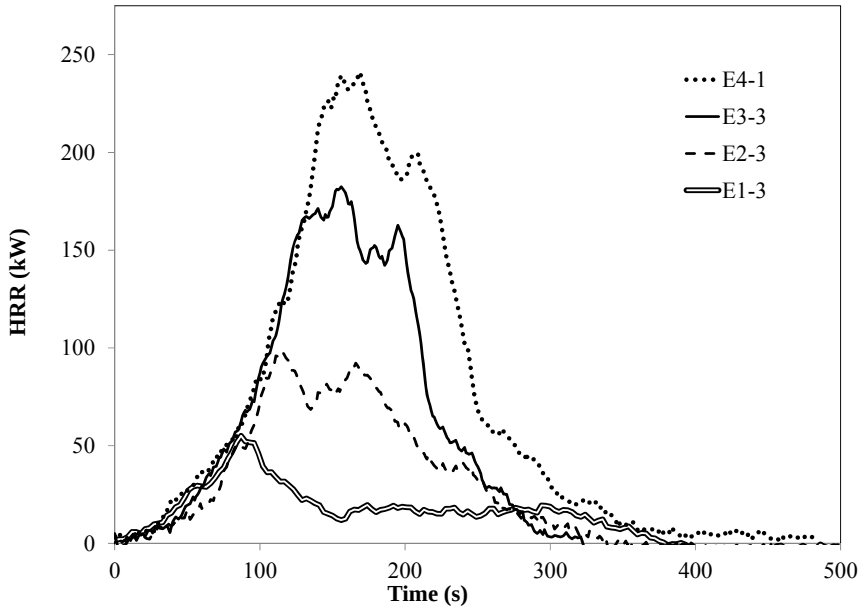

Figure 3-14 Heat release rates measured during edge ignition tests of foam with nominal thicknesses of 2.5 cm (E1-3), 5 cm (E2-3), 7.5 cm (E3-3) and 10 cm (E4-1).

In Figure 3-13 and Figure 3-14 it can be seen that the growth phases of the heat release rate curves for all thicknesses are very similar to one another for a given ignition configuration. The differentiating feature between the thicknesses during the growth phase is the peak heat release rate that is achieved prior to the decay phase in the case of the center ignition, or the plateau in the case of the edge ignition specimens. For example, in Figure 3-13 heat release rates for all four of the thicknesses follow the same growth curve up until 40 kW. From 40 kW heat release rates for the 5 cm, 7.5 cm and 10 cm thick specimens follow the same growth curve to 90 kW, where the curve for the 5 cm thick specimen levels off. From 90 kW to 145 kW the heat release rates for the 7.5 cm and 10 cm thick specimens follow similar curves until the curve for the 7.5 cm thick specimen begins to level off. A similar trend is observed in the edge ignition configuration shown in Figure 3-14.

In order to further examine the effect of thickness on peak heat release rates, the peak heat release rate per unit thickness was calculated for each test. This value was fairly consistent for the center ignition tests; average values ranged between 14.6 kW/cm and 18.4 kW/cm. There was less consistency in this value for the edge ignition tests; average values ranged between 16.7 and 26.0 kW/cm. This appears to indicate that specimen thickness has a stronger effect on the peak HRR of edge ignition specimens than center ignition specimens.

3.2.3. Effect of Ignition Location on Full Scale Results

This section will discuss the effect that ignition location has on the burning behavior of full scale specimens. For this section, most of the discussion will focus on comparing the center ignited CC4 and edge ignited EE4 test series since both of these test series share common nominal dimensions of 1.2 m by 1.2 m by 10 cm thick. The other test series will also be briefly discussed in this section, since although the differing surface area between the center and edge ignition specimens introduces another variable, some general observations can be made regarding the nature of center and edge ignition tests. Plotted along with the HRR curves in this section will be t^2 fire curves. These t^2 fire curves are used by fire protection engineers as a benchmark to characterize the rate at which fires grow. As was mentioned in section 1.2.3, the t^2 fire equation is expressed as

$$Q(t) = \alpha(t - t_0)^2 \tag{1.6}$$

where α is a fire growth coefficient. There are four standard fire growth coefficients that are commonly used. These are referred to as slow (α = 0.00293 kW/s^2), medium (α = 0.01172 kW/s^2), fast (α = 0.0469 kW/s^2) and ultrafast (α = 0.0.1876 kW/s^2) [12]. Typically a traditional inner spring mattress and box spring would be described using a medium t^2 fire and a polyurethane foam mattress would be described using fast t^2. As was discussed at the beginning

of Section 3.2, the early stages of the experimental fires can be unpredictable. For comparison of the experimental results to the t^2 fires, the values of t_0 were manually selected to align the t^2 fire curves with the growth phase of the experimental HRR curves.

Figure 3-15 is a plot of the HRR data from EE and CC test series. These two test series allow for the most direct comparison of the effect of ignition location.

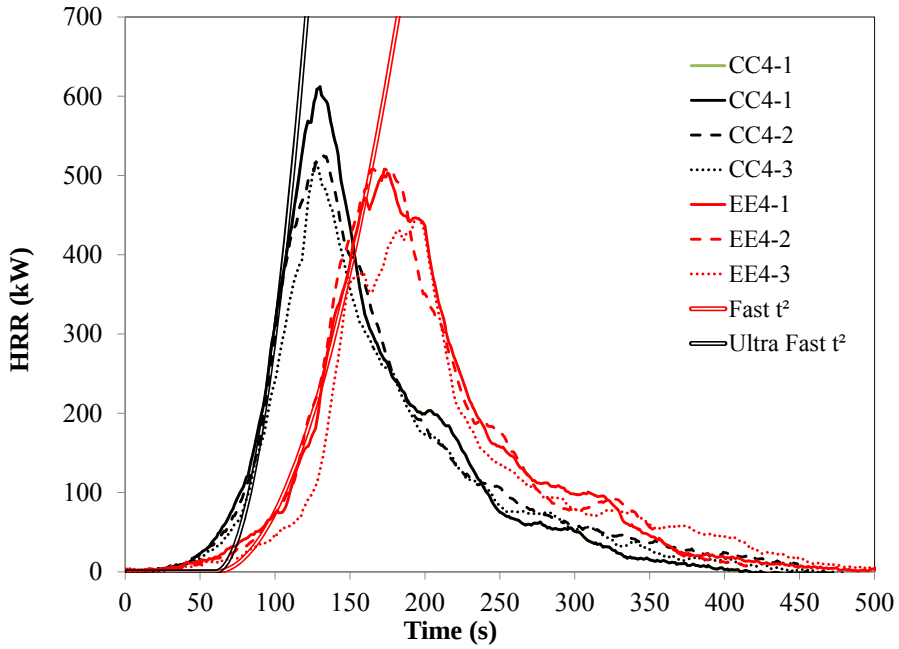

Figure 3-15 Comparison of HRRs measured for center (CC4) and edge (EE4) ignition locations of 1.2 m by 1.2 m by 10 cm specimens with fast and ultrafast t^2 HRR curves.

The first comparison that will be made between the CC4 and EE4 test series is the peak HRR. By observing Figure 3-15 it can be seen that the center ignition tests tend to reach a higher peak HRR than the edge ignition tests. The average peak HRR for the CC4 test series is 552.3 kW whereas the average peak HRR value for the EE4 tests was 485.9 kW, this constitutes a 12% difference in peak HRR.

The next comparison between the CC4 and EE4 test series is the time to peak HRR. Again, by comparing the plots shown in Figure 3-15, it can be seen that the center ignition tests

tend to be quicker to reach their peak HRR. On average the EE4 test series reached their peak HRR in 129.7 s which is 28% faster than the center ignited CC4 test series which reached their peak HRR on average after 182.0 s.

Comparing rate of fire growth for the CC4 and EE4 tests, the center ignition tests show a tendency to accelerate faster than the edge ignition tests. Using the t^2 fires as a benchmark, it can be seen that the edge ignition specimens are similar to the fast t^2 fire whereas the center ignition tests are more closely described by the ultrafast t^2 fire.

Figure 3-16 through Figure 3-19 present comparisons of the HRR curves for center and edge ignition configurations for each specimen thickness with standard t^2 fire HRR curves.

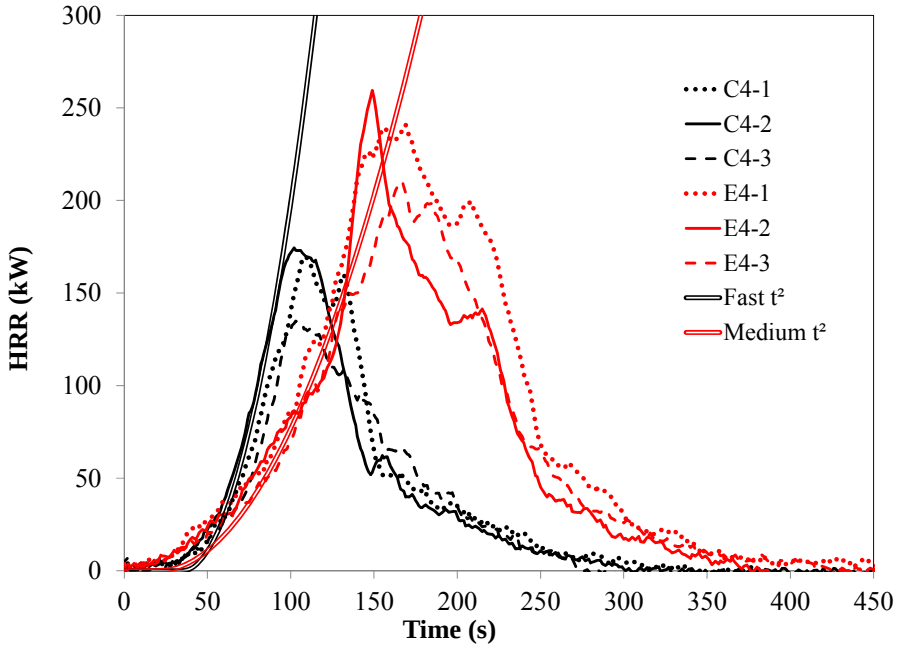

Figure 3-16 Comparison of HRRs measured for center (C4) and edge ignition (E4) specimens with fast and medium t^2 HRR curves.

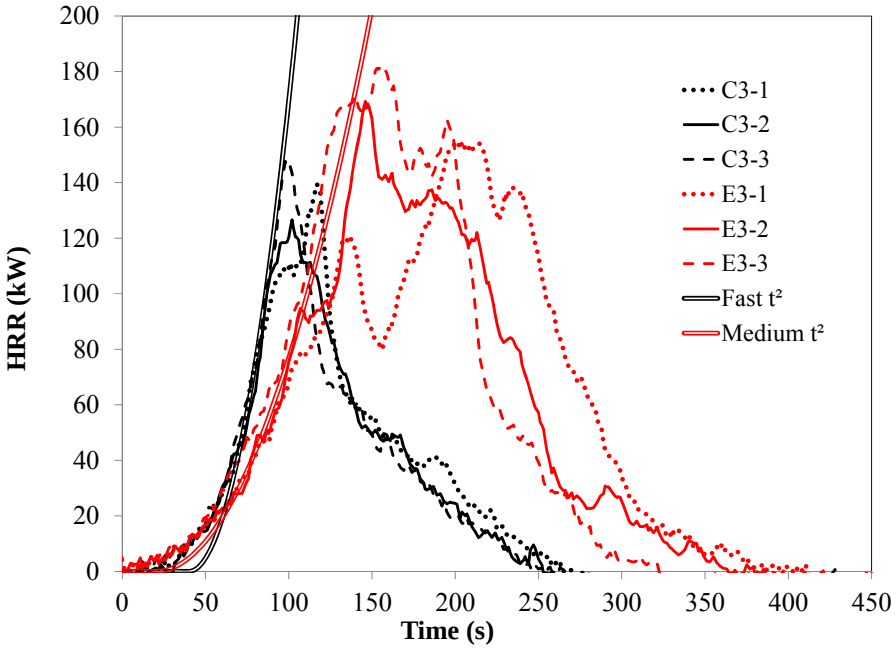

Figure 3-17 Comparison of HRRs measured for center (C3) and edge ignition (E3) specimens with fast and medium t^2 HRR curves.

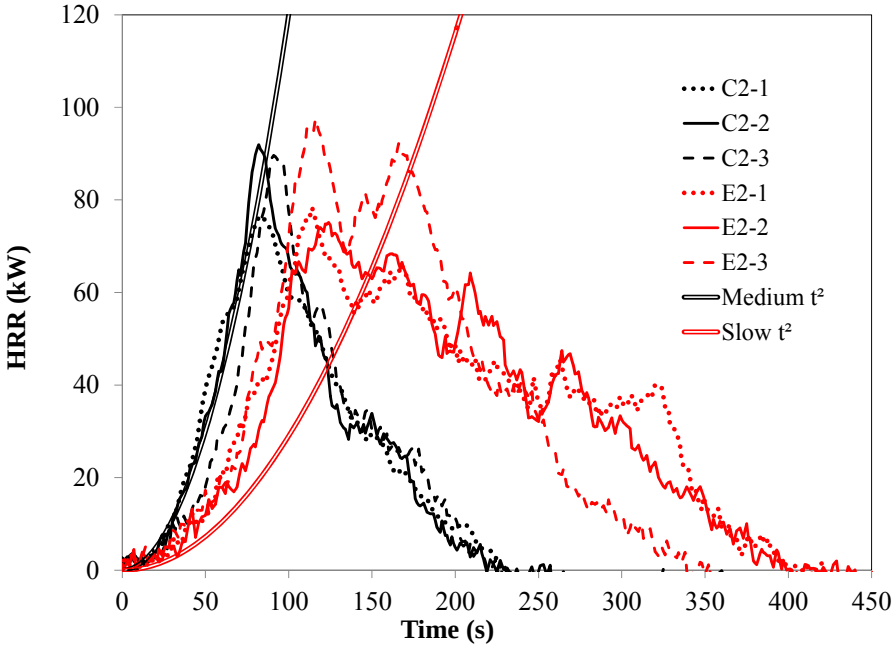

Figure 3-18 Comparison of HRRs measured for edge (E2) and center (C2) ignition specimens with medium and slow t^2 HRR curves.

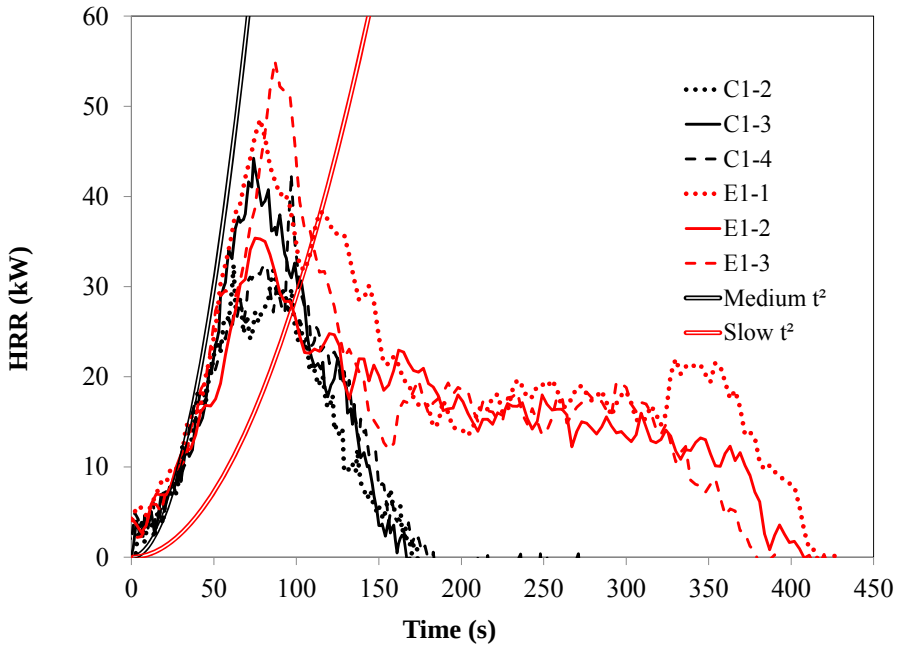

Figure 3-19 Comparison of HRRs measured for edge (E1) and center ignition (C1) specimens with medium and slow t^2 HRR curves.

Where the center ignition CC4 tests showed a higher peak HRR than the similarly sized edge ignition EE4 tests, the inverse appears to be the case for the smaller C and E tests. For instance, it was seen that the C4 tests produced an average peak HRR of 159.7 kW whereas the E4 tests on average peaked 33% higher than the C4 tests at 237.0 kW. Similarly, the E3 tests peaked on average 18% higher than the C3 tests and the E1 tests peaked on average 21% higher than the C1 tests. The exception to this is the C2 test which peaked 3% higher than the E2 test.

Although the differing surface area appears to skew the comparison of peak HRR between the E and C tests, the phenomenon of the HRR in the CC4 tests growing faster than the EE4 tests is continued in the smaller E and C test series. Plotting the E and C tests against standard t^2 fires shows that the center ignition tests still to grow faster than the edge ignition tests in spite of the larger surface area of the edge ignition specimens. In Figure 3-16 it is seen that the C4 tests show a growth rate most similar to a fast t^2 fire with a 35 s incubation time, whereas the E4 test is most similar to the slower growing medium t^2 fire with a 20 s incubation time. This is also the case for Figure 3-17 comparing the C3 and E3 tests where the C3 tests show a growth rate most similar to a fast t^2 fire with a 40 s incubation time and the E4 test being most similar to the medium t^2 fire with a 20 s incubation time. Figure 3-18 comparing the C2 and E2 tests with t^2 fires shows that for 5 cm thick foam, the center ignition tests are still growing faster than the edge ignition tests. In this case the C2 tests were most similar to a medium t^2 fire whereas the E2 tests were somewhere between the medium and slow t^2 fires.

Finally for the 2.5 cm thick E1 and C1 tests, ignition location does not appear to have an effect on the fire growth rate. As seen in Figure 3-19 the growth portion of the HRR curve for both the C1 and E1 tests appear to be most similar to the medium t^2 fire curve.

3.2.4. General Observations

An observation that was made during the review of the furniture calorimeter test data is that for the thicker foam specimens there appears to be a point of inflection on the growth phase of the HRR curve where the HRR accelerates. From reviewing the video footage, it appears that this inflection in the HRR curve coincides with flame front reaching the edges of the specimen. This observation suggests that the flame spread along the edges of the specimen may be contributing significantly to the overall heat release rate of the thicker specimens, leading to a sharper peak when the peak HRR is attained. In early stages of a full scale fire test, the flame is spreading predominantly on the top surface of the foam (see photograph A in Figure 3-20). There reaches a point when the flame front reaches the edge of the specimen. At this point the flame front is free to spread down the edge of the specimen so that the foam at the perimeter of the specimen is effectively burning from two sides, the top and the edge (see photograph B in Figure 3-20).

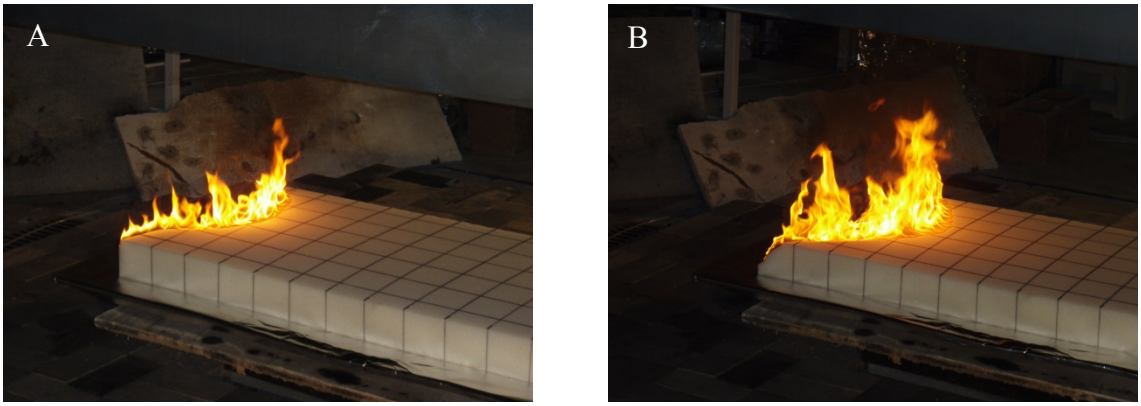

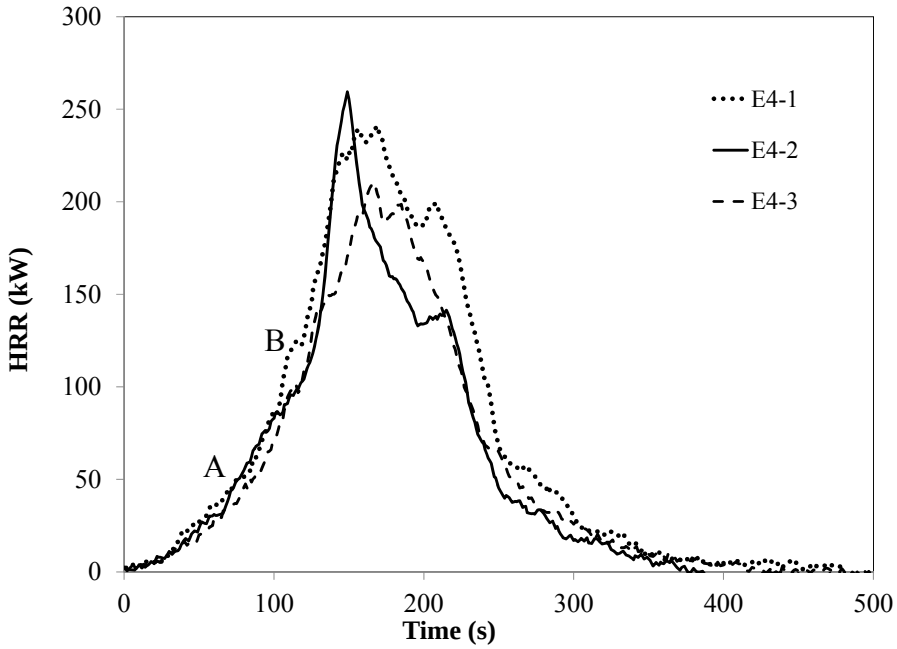

Figure 3-20: Photographs and HRR plots from edge ignition test of 0.6 by 1.2 m by 10 cm polyurethane foam specimen. A – top surface only burning at 68 s. B – flame begins spread to edge of specimen at 100 s.

3.3. Full Scale Flame Spread Test Results

This section of the thesis will focus on the flame spread rates that were measured from the infrared video record of the full scale furniture calorimeter tests. By analyzing the flame spread rates in furniture calorimeter tests, a better understanding can be obtained of the coupling of specimen properties and how quickly the flame front moves across the specimen. Understanding how flame spreads across a full scale test specimen is important to select an

appropriate flame spread model for predicting full scale fire behavior using the convolution model.

As was discussed in the Experimental Apparatus and Procedure section (2.4) of this thesis, these flame spread rates were measured from the infrared video record using an automated algorithm in MATLAB.

3.3.1. Repeatability of Flame Spread Rates for Center Ignition Specimens

This section will discuss the repeatability of flame spread measurement results for the center ignition tests. Figure 3-21 and Figure 3-22 are plots of flame front position for the full scale tests of 2.5 cm and 10 cm thick polyurethane foams, respectively, and represent the range of repeatability that was seen for this measurement. As was discussed in the Apparatus and Procedure section (2.4), the flame front for the center ignition tests was measured in four directions, starting at the ignition location and proceeding to the corners of the specimen. Since the results were similar in all directions, this section will discuss the flame front position that was measured between the ignition location and the left-near corner of the specimen. Plots of the remaining linear flame spread results can be found in Appendix D.

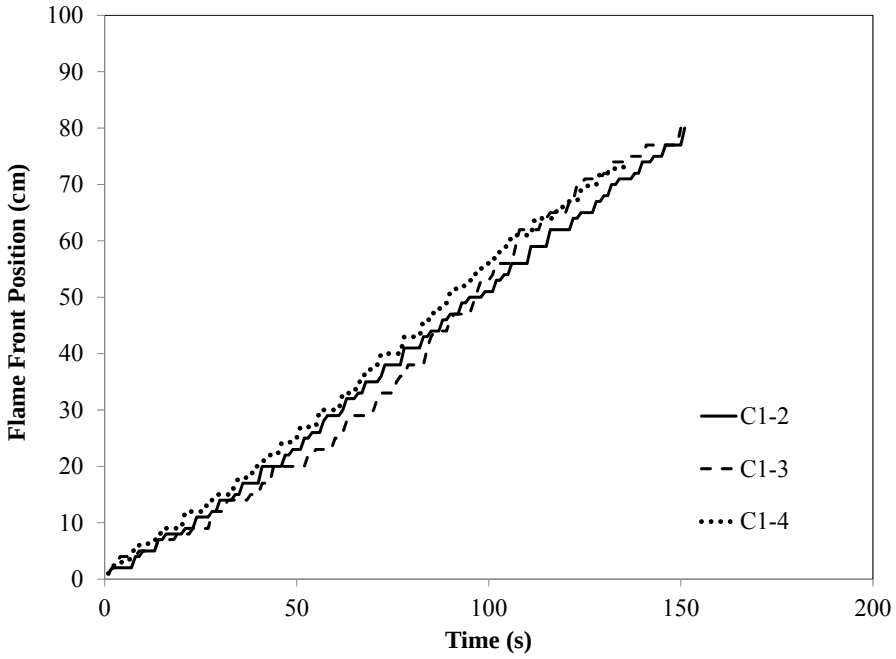

Figure 3-21 Flame front position in full scale center ignition tests of 2.5 cm thick polyurethane foam.

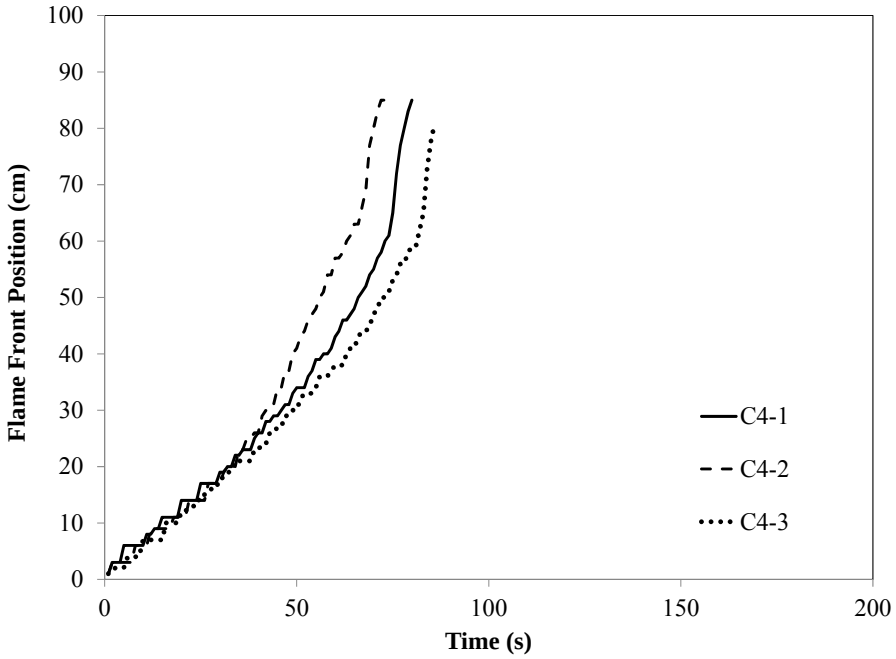

Figure 3-22 Flame front position in full scale center ignition tests of 10 cm thick polyurethane foam.

As seen in Figure 3-21 and Figure 3-22, some tests exhibited greater repeatability than others. Figure 3-21 presents the 2.5 cm thick center ignition tests and demonstrates the level of repeatability that was also seen in the 5.0 cm and 7.5 cm thick center ignition specimens. In these tests the flame fronts in each test remained within 12 cm of each other and demonstrated very similar curve shapes. Figure 3-22 however exhibits a greater level of variation, specifically in test C4-3. Test C4-3 at times lags behind the other tests as much as 40 cm. On first inspection these tests appear to be misaligned at the time of ignition, however these spread rates were coordinated at the point of ignition. A large part of the variation occurs early in the test during the fire incubation period. In Section 3.2.1, test C4-3 was also noted as being an outlier from the other tests (as seen in Figure 3-11) exhibiting a lower peak heat release rate than the other tests in its configuration. An observation that can be drawn from this deviation is that the lower heat release rate of test C4-3 is matched with a corresponding lower flame spread rate for this particular test.

3.3.2. Effect of Foam Thickness on Flame Spread for Center Ignition Specimens

Figure 3-23 is a comparison of the flame spread rates that were measured for the 2.5, 5.0, 7.5 and 10.0 cm thick center ignition tests.

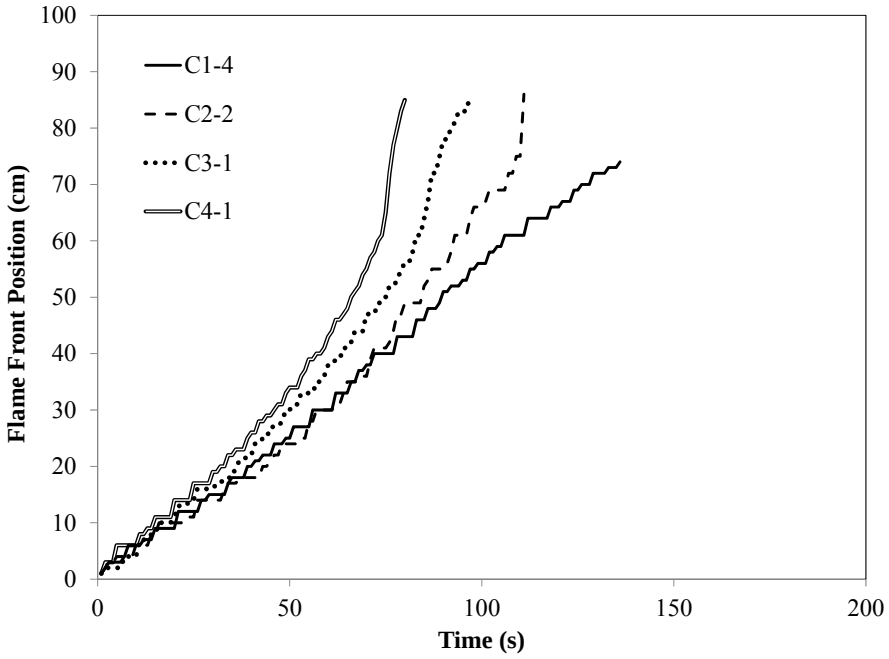

Figure 3-23 Flame front position in full scale center ignition tests of 2.5 cm (C1), 5 cm (C2), 7.5 cm (C3) and 10 cm thick (C4) polyurethane foam.

As seen in Figure 3-23, there is a distinct difference in the shape of the flame spread rate curve for each different thickness of foam. The 2.5 cm thick foams tend to follow a very linear flame spread rate; at the end of the test the flame front is moving at the same rate as at the beginning. For much of the test, the 5.0 cm thick foam also shows a linear flame spread rate, however at 80 s the flame spread rate begins to accelerate. The 7.5 cm and 10.0 cm thick specimens continue this trend each one exhibiting an increase in flame spread rate as well as a distinct acceleration as the flame front reaches the edge of the foam.

This behavior is important to note if a flame spread rate model is to be selected that can accurately model the flame spread rates that are seen in full scale tests. A possible explanation for the acceleration of the flame front with thicker specimens could be the coupling of radiative heat flux and flame spread rate. When a fuel bed is exposed to a radiant heat flux, the rate of flame spread will increase due to preheating of the fuel bed [12]. It would follow then that as the

fire plume gets larger, the emitted radiant heat flux increases. As the radiant heat flux increases the fuel bed ahead of the flame front will receive a greater level of preheating. This is consistent with observation of the infrared video which showed higher surface temperatures ahead of the flame front for the thicker foams.

Another difference that was noted from inspection of the video footage is that the thinner foam specimens tend to experience extinction of the fire at the ignition location sooner than the thick foams. This means that thicker foams are able to develop a lager actively burning area than the thinner foams. When a thin specimen such as the 2.5 cm thick foams are burnt, the combustion pattern in both the center and edge ignition configuration consists of a flame front followed by an extinction front that follows at a relatively short distance behind the flame front. Figure 5-30 shows frames from the infrared video of test E1-1 120 s, 180 s and 240 s after ignition.

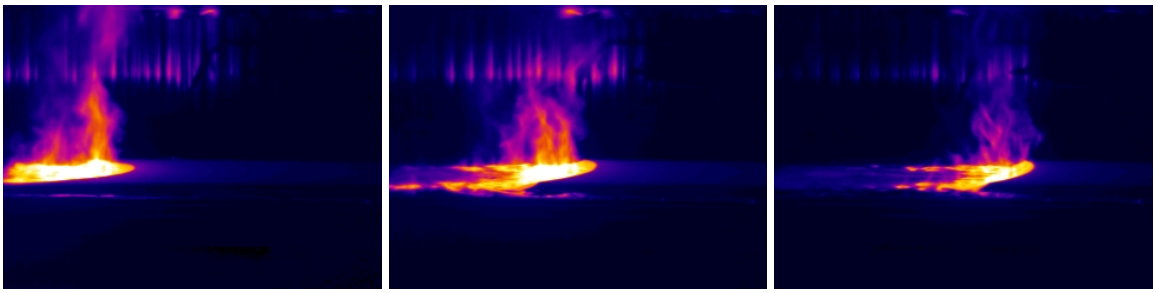

Figure 3-24 Infrared video of test E1-1 at 120 s, 180 s and 240 s after ignition (left to right).

As seen in Figure 3-24 the extinction front in test E1-1 follows fairly close after the flame front. In this way the burning area is relatively consistent throughout the burning process leading to a relatively consistent incident heat flux condition for the duration of the test.

Figure 3-28 shows frames from the infrared video of test E4-3 120 s, 180 s and 240 s after ignition.

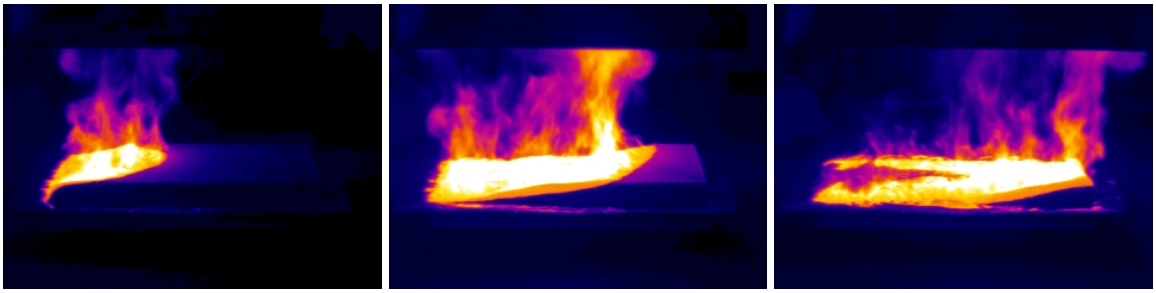

Figure 3-25 Infrared video of test E4-3 at 120 s, 180 s and 240 s after ignition (left to right).

As seen in Figure 3-25, at 180 s after ignition the ignition location is still burning. This illustrates how for thicker materials, the burning duration of any given area is longer which leads to a larger actively burning area which thereby leads to an elevated incident heat flux ahead of the flame position. In order to quantitatively measure the actively burning area of the specimens, a measure of the extinction rate of the specimen would be required. This measurement was unfortunately outside of the scope of this thesis. It is recommended that future research include the measurement of the extinguished area, and as an extension the total actively burning area as a function of time.

Looking back to Figure 3-13, it was seen that thicker foams produced higher heat release rates. Carrying this observation forward to the inspection of Figure 3-23 suggests that higher heat release rates correlate with faster flame spread rates. If flame spread rate can be correlated to heat release rate for this type of test, it would be possible to produce a flame spread model which uses the HRR at time t_n to predict the flame spread rate at time t_{n+1}.

These flame spread rates can also be compared to flame spread rates for polyurethane foam found in literature. Drysdale [12] published flame spread rates for two densities of polyurethane foam, a 15 kg/m^3 foam with a flame spread rate of 2.5 mm/s and a 22 kg/m^3 foam which had a flame spread rate of 3.7 mm/s. The foams tested in this research averaged 17 kg/m^3 with a standard deviation of 1.18 kg/m^3 placing the density of these foams between the data

published in Drysdale. When comparing the experimental flame spread rates seen in Figure 3-23 to those published by Drysdale it can be seen that the foams used in this research produced a higher flame spread rate. The most linear of the flame spread rates were the 2.5 cm foams with an average flame spread rate of 5.4 mm/s, still significantly faster than the data published in Drysdale. Since the composition of polyurethane foam can vary greatly, it is possible that the difference in flame spread rate is largely due to a difference in foam composition or manufacturing technique. Drysdale indicates that the aforementioned flame spread rates were measured in a horizontal configuration without supporting radiation. If Drysdale's rates were measured in a small fire, the absence of radiation feedback from the fire plume could partially explain the slower spread rates, however the thickness, specimen dimensions, ignition technique and measurement technique are not given, all of which will influence flame spread rate [12].

3.3.3. Repeatability of Flame Spread Rates for Edge Ignition Specimens

Figure 3-26 and Figure 3-27 are plots of flame front position for the full scale tests of 2.5 cm and 7.5 cm thick polyurethane foams and provide an indication of the range of repeatability that was seen for this measurement. These rates presented here were measured along the centerline of the specimen.

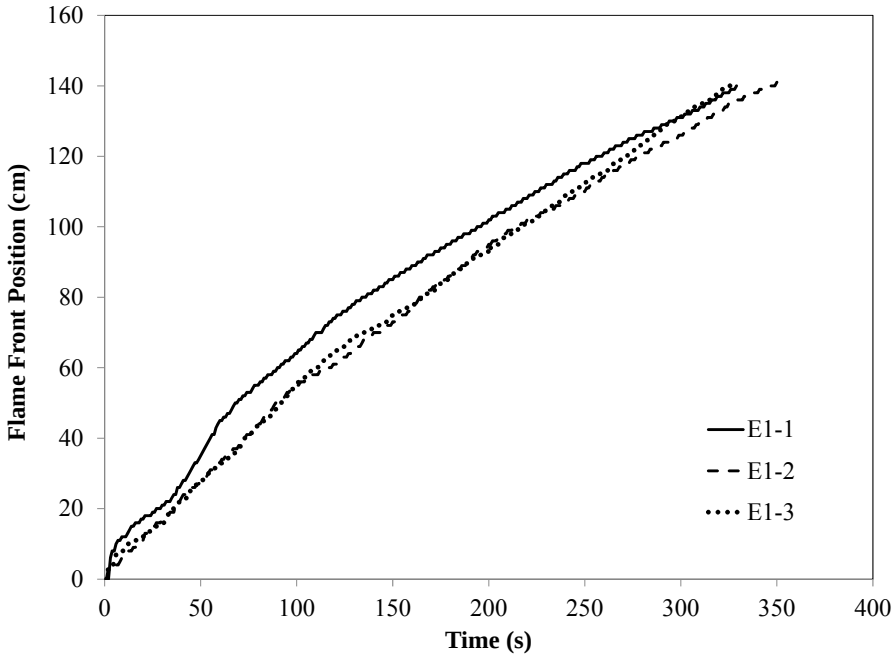

Figure 3-26 Flame front position in full scale edge ignition tests of 2.5 cm thick polyurethane foam. specimens E1-1, E1-2 and E1-3.

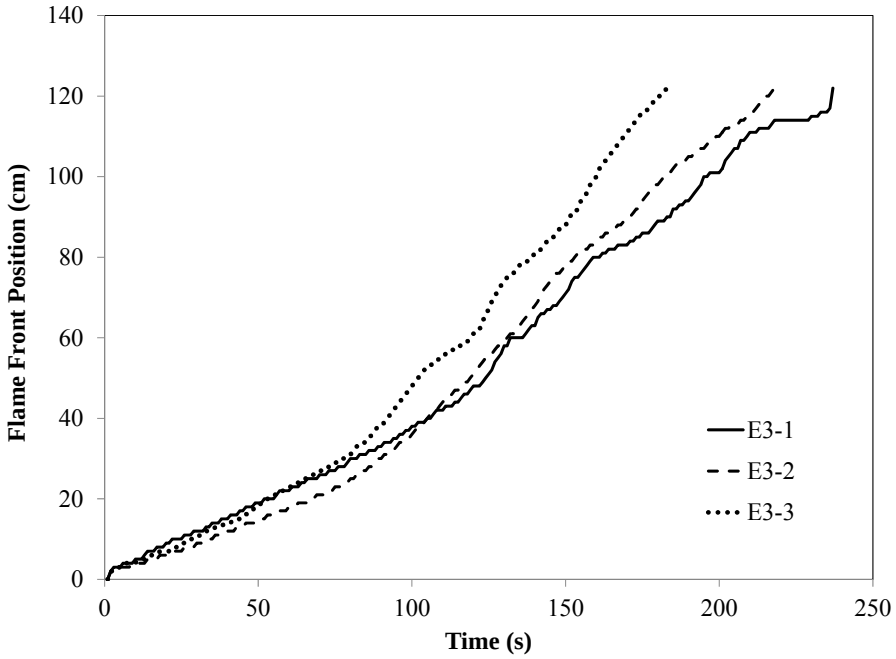

Figure 3-27 Flame front position in full scale edge ignition tests of 7.5 cm thick polyurethane foam. specimens E3-1, E3-2 and E3-3.

The E1 test series (2.5 cm thick) shown in Figure 3-26 is the edge-ignition test series with the least variation in flame front position. In test series E1 the flame fronts were within 16 cm of each other at any given moment. Figure 3-27 shows the 7.5 cm thick E3 test series which exhibited the greatest level of variation in flame front position of the edge ignition series, a maximum variation of 31 cm at 187 s after ignition.

3.3.4. Effect of Foam Thickness on Flame Spread for Edge Ingition Specimens

Figure 3-28 is a comparison of the flame front positions seen in the four thicknesses of polyurethane foam that were tested in this research.

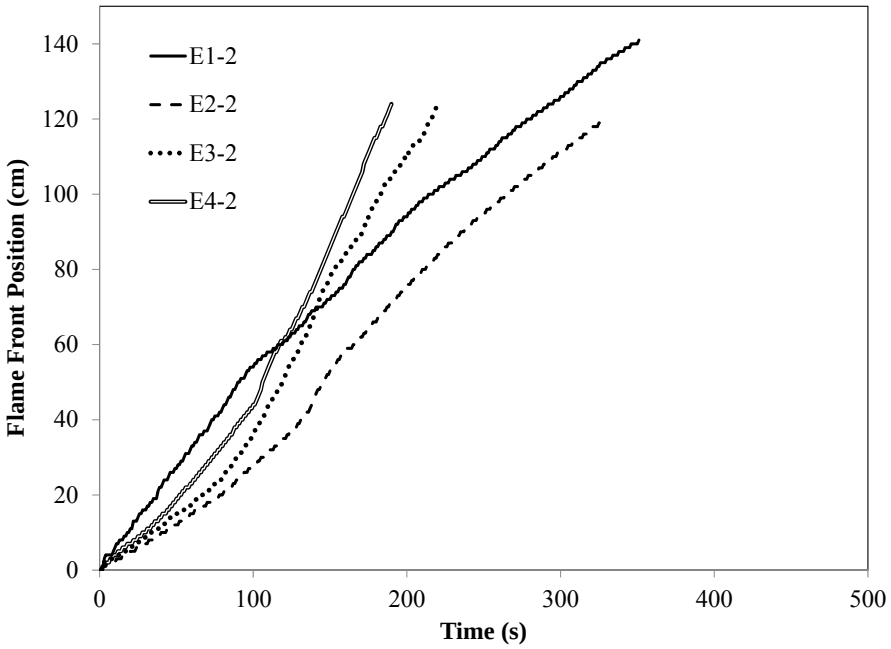

Figure 3-28 Flame front position in full scale edge ignition tests of 2.5cm (E1), 5 cm (E2), 7.5cm (E3) and 10 cm thick (E4) polyurethane foam.

The first observation that can be made about Figure 3-28 is that there is a distinct difference between the behaviors of center ignition specimens and the edge ignition specimens. In the center ignition specimens, as was observed in Figure 3-23, flame spread rates increase as

foam thickness increases. In edge ignition tests however, the thinnest foam demonstrates flame spread rates almost as fast as those seen in the 10 cm tests for the first 100 s after which point the flame spread rate begins to decelerate. With the exception of the 2.5 cm specimens, the edge ignition tests also follow the trend that as foam thickness increases flame spread rate increases.

The edge ignition specimens produce flame spread rates that are much closer to those that are published in Drysdale. In fact the E1 test series produced an average flame spread rate of 4.1 mm/s which is only 10% higher than the published data at 3.7 mm/s. This would suggest that the differences in fire behavior linked to ignition location could be having some effect on the rate at which it propagates, even in the cases where the spread rate is very linear such as the E1 and C1 test series. It is interesting to note that not only are the flame spread rates faster in the center ignition specimens, center ignition tests become non-linear and accelerate toward the end of the burn. As was discussed earlier, a possible cause for this difference in flame spread rates is the incident heat flux that the fire plume is imposing on the unburned foam providing some preheating prior to the arrival of the flame front. For discussion of the differences in shape between center and edge ignition flame fronts, Figure 3-29 and Figure 3-30 present flame front contour plots for tests C4-1 and E4-1.

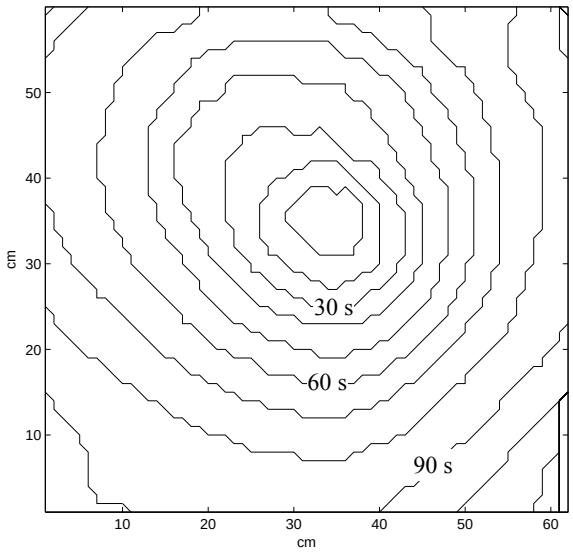

Figure 3-29 Flame front position contours in 10 s increments for test C4-1.

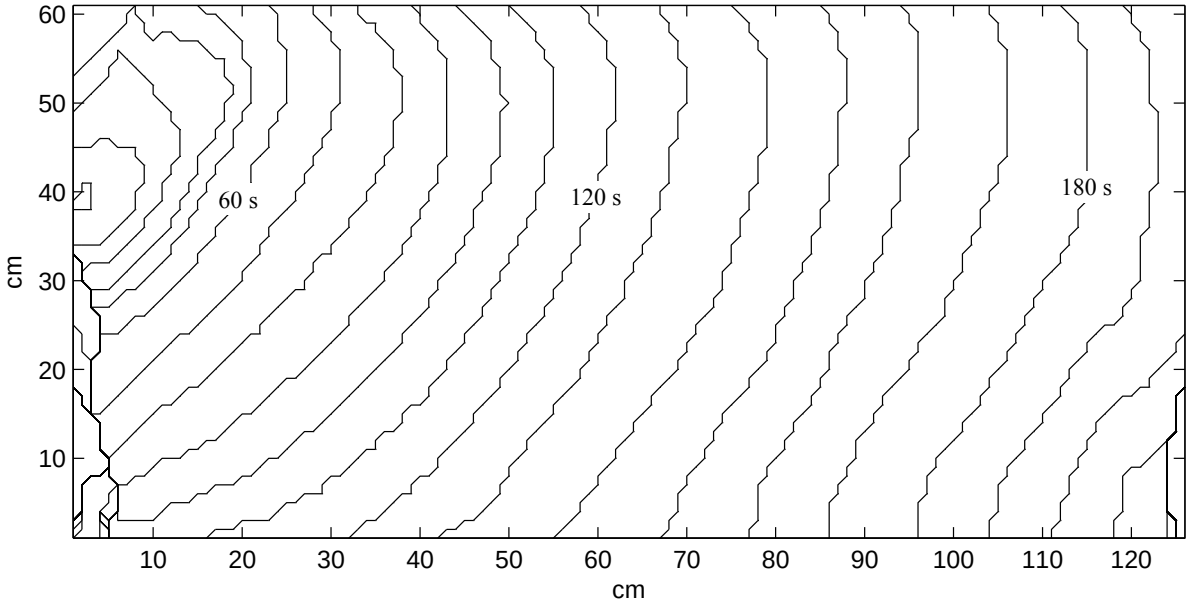

Figure 3-30 Flame front position contours in 10 s increments for test E4-1.

Plots of all contour plots from the furniture calorimeter tests can be found in Appendix E.

As seen in Figure 3-29, the flame front on center ignition specimens tends to follow a circular growth pattern, starting at the ignition location and proceeding towards the specimen edges. The flame fronts in the center ignition tests however were not perfect circles and often

grew faster in a particular direction producing a more elliptical growth pattern. In an edge ignition specimen on the other hand, the flame front starts out as a semi-circle and fairly quickly flattens out into a nearly flat flame front. Differences in boundary conditions related to the different flame spread patterns could be a contributing factor as to why the flame spread rates behave differently in the center and edge ignition specimens. In center ignition tests, the fire is surrounded by unburned foam that would act to insulate the burning area. This would reduce the heat loss from the burning area of the foam when compared to an edge ignition configuration. A reduced heat loss would increase the core temperature, which would increase the fire HRR and plume size, increasing the radiation feedback to the unburned foam and ultimately increasing the rate of flame spread.

An area for future research could be to compare the burning area shape and size from these tests with the plume height. If plume height can be predicted from total burning area, then incident heat flux exposure to the surrounding material could be calculated using either engineering correlations or radiation heat transfer calculations.

3.3.5. Full Scale Area Spread Rate Curves

The final parameter of the experimental results that will be discussed is the area spread curves that were measured from the full scale fire tests in the furniture calorimeter. The time dependent area spread rate curve, or *A(t)* curve, is one of the input parameters that was used for the convolution modeling that will be discussed in subsequent chapters. This parameter is a running total of the amount of specimen area over which the flame front has passed. It is important to note that the *A(t)* curve includes all area over which the flame front has passed regardless of whether or not it is still burning. Figure 3-31 and Figure 3-32 are plots of the *A(t)*

curve for the 2.5 cm thick center ignition tests and 7.5 cm thick edge ignition specimens, respectively.

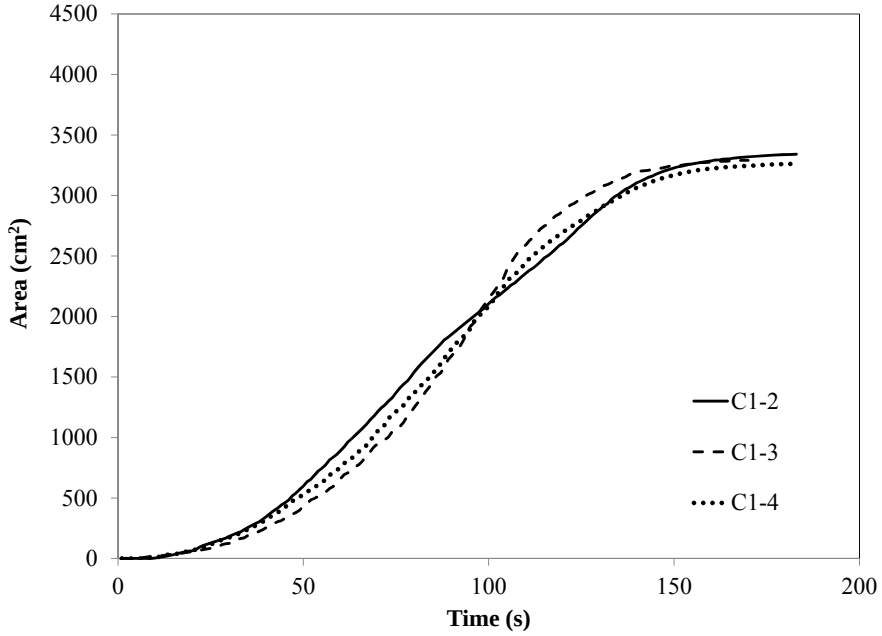

Figure 3-31 Flame spread area in full scale center ignition tests of 2.5 cm thick polyurethane foam.

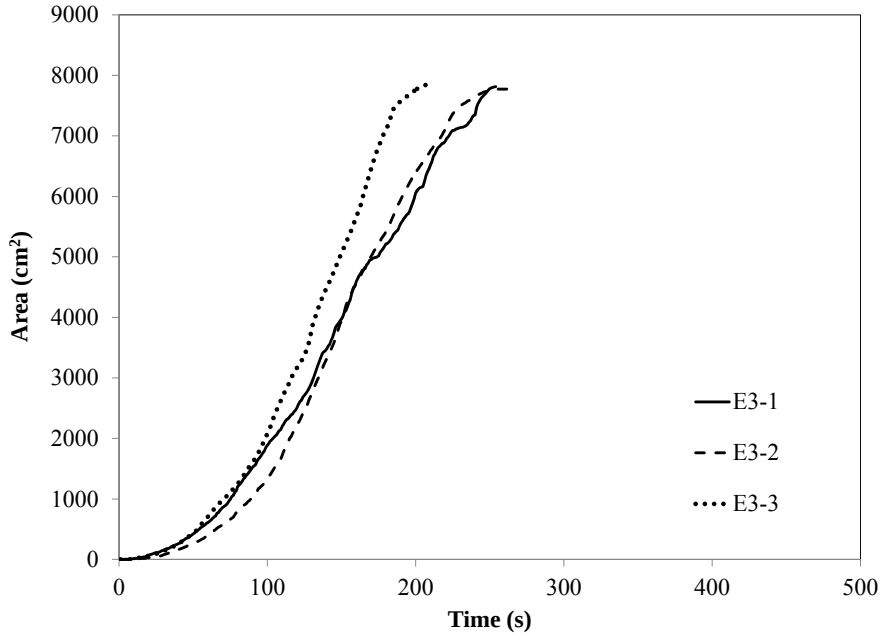

Figure 3-32 Flame spread area in full scale edge ignition tests of 7.5 cm thick polyurethane foam.

Plots of all area spread data from furniture calorimeter tests can be found in Appendix F.

As demonstrated by Figure 3-31 and Figure 3-32, the *A(t)* curves for these tests showed a reasonable degree of repeatability, very similar to the results that were seen for the linear flame spread rate data, and the HRR data for these tests.

Figure 3-33 is a plot showing the *A(t)* curves for a representative cross-section of the center ignited specimens for each of the specimen thicknesses. Similarly, Figure 3-34 shows the *A(t)* curves for a selection of the edge ignited specimens for each of the specimen thicknesses.

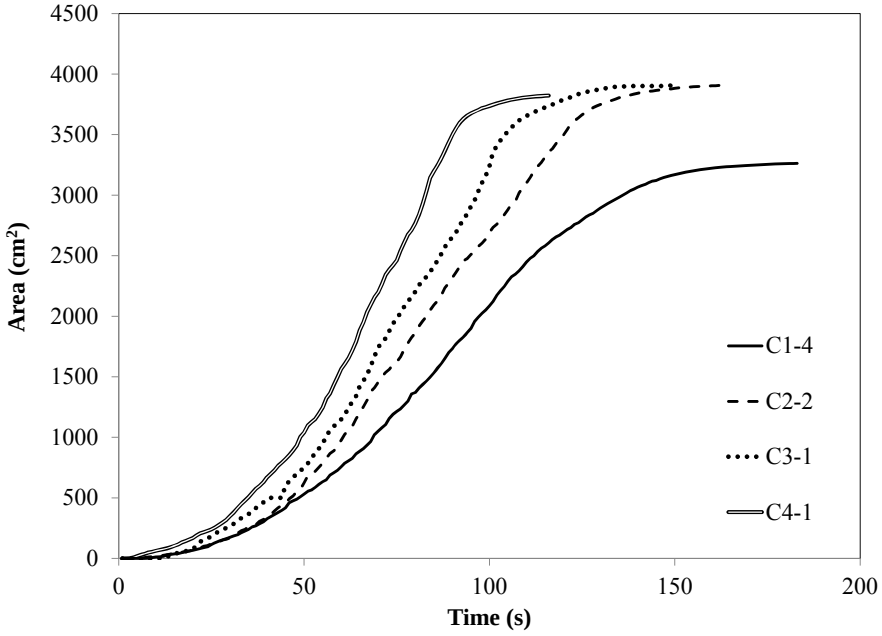

Figure 3-33 Flame spread area in full scale center ignition tests of 2.5 cm (C1), 5 cm, 7.5 cm (C2) and 10 cm thick (C4) polyurethane foam.

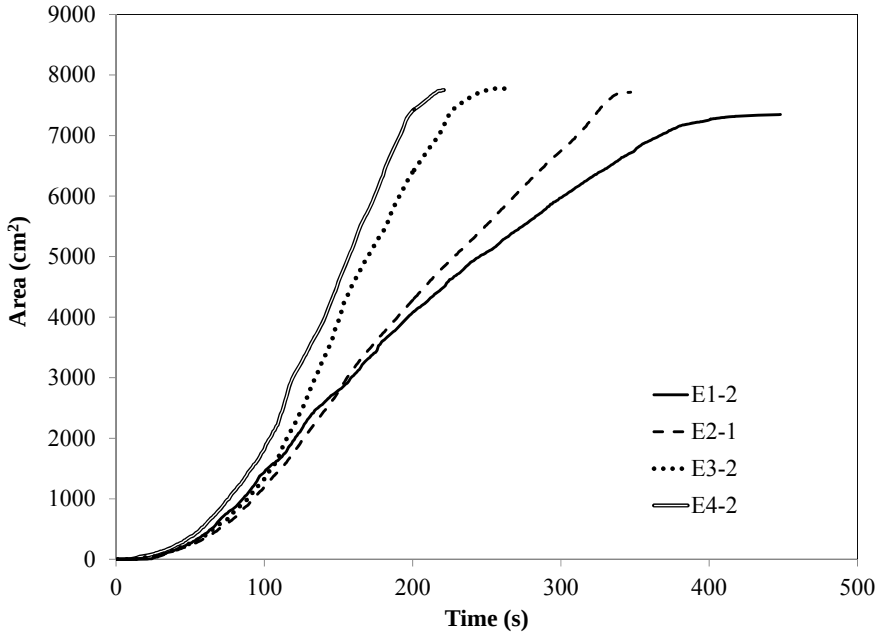

Figure 3-34 Flame spread area in full scale edge ignition tests of 2.5 cm(E1), 5 cm (E2), 7.5 cm (E3) and10 cm thick (E4) polyurethane foam.

In a similar fashion to the linear flame spread rate results, the shape of the *A(t)* curves appear to be influenced by the thickness of the specimen. The trend that appears is that thicker specimens produce more rapidly growing *A(t)* curves than thinner foams. For example, in Figure 3-33 test C4-1 produces the fastest growing *A(t)* curve, followed by the C3-1, C2-2 and C1-4 in descending order of thickness. The same result is seen in Figure 3-34 where the thickest specimens produce the faster *A(t)* curves.

It is apparent that specimen thickness has a significant effect on its fire behavior in a full scale test. In future research, when a flame spread model is being produced to provide *A(t)* input into a convolution model, careful consideration should be taken to account for the effect that specimen thickness has on flame spread rates.

An item that should be noted is that the flame spread technique used in this thesis only took into account the flame spread on the top surface of the specimen, it did not account for flame spread on the sides of the specimen. This area on the sides of the specimen can be significant, particularly for the thicker specimens, for example the exposed area on the sides of specimen E4 are equivalent to 50% of the top surface area. This area was included in the flame spread measurements made by Ezinwa [22], however the flame spread measurements used in this thesis did not include this area. In future research it could prove beneficial to measure the flame spread along the sides of the specimens.

3.4. Summary

Chapter 3 of this thesis has focused on experimental results. This has included bench scale cone calorimeter testing, as well as full scale furniture calorimeter testing. In the bench scale testing conducted in this research, it was found that cone calorimeter HRR density curves showed good repeatability. It was noted that the combustion of the foam took place in two distinct stages, a foam collapse stage and a stage when the foam is in a liquid state. It was found that this behavior was consistent with other research being done in the field. In the cone calorimeter testing it was also found that the incident heat flux setting of the apparatus has a significant effect on the resulting HRR density curves. When the effect of foam age on HRR density curves was investigated, it was found that in the time frame used in this research the burning behavior did not change significantly enough to draw strong conclusions.

In the full scale testing section of this chapter it was found that the HRR curves showed reasonable agreement through the growth and decay phases, however there was some variability in the peak HRR values and the length of time that the peak was sustained. When exploring the effect of foam thickness on the HRR curves, it was noted that for a given ignition location the growth phase of the HRR curve for various thicknesses is very similar. The HRR curves for different foam thicknesses were most distinctly differentiated by the peak HRR that was achieved before the fire began to decay. When looking at the effect of ignition location it was found that specimens that were ignited in the center consistently grew faster than those ignited on the edge. When the CC4 and EE4 test series were compared, which provided the most direct comparison of ignition location, it was seen that the center ignition specimens had a higher peak heat release rate in addition to having a faster growth curve.

The continued analysis of the full scale testing included the flame spread characteristics of the full scale tests. Looking first at the center ignition specimens it was found that specimen

thickness has a strong effect on the flame spread rates, the thicker foams exhibiting a nonlinear flame spread behavior towards the end of the test. The edge ignition specimens on the other hand were not affected to the same degree by specimen thickness. In an evaluation of bench scale flame spread tests, it was found that bench scale flame spread tests produce flame spread rates similar to the thinner full scale specimens.

Finally, the area spread rate curves obtained from the full scale testing were presented. These curves are the area parameter that was used for input into the convolution mode that will be discussed in subsequent chapters. It was found that the area spread rate curves possessed a level of variability similar to that which was seen in the full scale HRR curves. It was noted that in a similar fashion to the full scale HRR curves, the area spread data appears to be heavily influenced by both the ignition location as well as the foam thickness.

CHAPTER 4 : CONVOLUTION MODEL CODING AND VALIDATION METHOD

This section will focus on the coding and validation of the CBUF model that was used in this research. To briefly recap, the underlying assumption of the CBUF model is that a surface does not contribute to heat release rate until it is ignited. Once a given area is ignited, it will contribute the same time dependent heat release rate density as a sample that is burned in the cone calorimeter. Similarly, it is assumed that a given area will stop contributing to heat release rate once it is extinguished, which in this model is the time at which the cone calorimeter specimen is extinguished. This concept is expressed in mathematical terms as

$$\dot{Q}(t) = \int_0^t \dot{q}''(t-\tau)\dot{A}(\tau)d\tau, \qquad (4.1)$$

where $\dot{Q}(t)$ is the predicted full scale heat release rate (kW),

$\dot{q}''(t-\tau)$ is the heat release rate per unit area (heat release rate density) history (kW/m^2) as measured in the cone calorimeter,

$\dot{A}(\tau)$ is the area burning rate at time t (m^2/s) and

τ is a dummy variable (s).

One of the challenges involved with the development of this model is that it requires input from two sub-models: a time-dependent flame spread, and a time-dependent heat release rate density. The time-dependent heat release rate density was experimentally determined using the cone calorimeter. When the CBUF model is fully implemented the flame spread model, on

the other hand, will likely take the form of an empirical relationship that takes geometric information such as surface area, thickness and ignition location and mimics the full scale flame spread rate. If the convolution model were to be assembled, complete with sub-models, and evaluated against experimental data, it would be difficult to discern which part of the convolution model was the cause of a discrepancy. In order to properly develop this model, it is necessary to conduct intermediate evaluations that can isolate the behavior of the sub-models.

The evaluation that was conducted as a part of this research was aimed at isolating the behavior of the time-dependent heat release rate density sub-model. To accomplish this, the flame spread rate sub-model was replaced with the experimentally determined flame spread rate. In practice, this means that to evaluate the model for a given test, the area spread data from that test were convolved with the HRR density data from the cone calorimeter tests of that thickness of foam, and the result was compared to the full scale experimental HRR curve measured by the furniture calorimeter. For example, the area spread data from test CC4-1 were convolved with the average HRR density data from the cone calorimeter tests for 10 cm foam, and the resulting HRR curve was compared to the experimental HRR curve from the furniture calorimeter test of specimen CC4-1. This allowed for the evaluation of the underlying assumption of the CBUF model independent of the uncertainties introduced by the area spread model. This technique of isolating the CBUF model from the area spread model also allowed a more direct examination of the effect that cone calorimeter incident heat flux setting has on the output of the convolution model.

The final item that was examined in the evaluation was the ability of the convolution model to predict the full scale HRRs for specimens with varying thickness and ignition location.

4.1. Coding of the Model

The coding for the CBUF model was performed using Microsoft Excel®. Excel® was well suited for the development of this code due to the small sizes of the data files that are to be processed, and the relative simplicity of the numerical techniques that were implemented in this research.

The specific technique that was employed to perform the convolution process is known as discrete convolution and for this specific application it takes the form of

$$Q^N = \sum_{i=0}^{N} \Delta A^i \dot{q}^{N-i} \tag{4.2}$$

where: Q^N is the predicted full scale heat release at increment N (kW),

ΔA^i is the differential burning area at increment i (m^2) and

$\dot{q}^{N-i}$ is the heat release rate density at time increment $N - i$ (kW/m^2) [22].

Since the input for the $\dot{q}^{N-i}$ term is the experimentally determined heat release rate density, it was discretized at the sampling rate of the data acquisition system used in the experiment, which in this case was 1 Hz. The HRR density data that were used as input for the CBUF model were an average value of the three tests that were conducted for a given configuration. Since the discrete convolution requires a common discretization for both terms being convoluted, the area spread data were also discretized at 1Hz. The area spread data that were used as input into the CBUF model were the data that were collected for the particular test being analyzed, for instance, when the CBUF model was run for test E4-1 with 35 kW/m^2 HRR density data, the inputs were the measured area spread data from test E4-1 and the average HRR density data from cone calorimeter tests 4-35-1, 4-35-2 and 4-35-3.

The spreadsheet used to perform this calculation effectively consisted of three columns: a differential burning area column, a heat release rate density column and a column that calculates the time dependent full scale heat release prediction. A sample of this spreadsheet is shown in Figure 4-1.

	A	B	H	I
4	Time	q"	ΔA	Q
5	[s]	[kW/m^2]	[m]	[kW]
21	14	248.38	5.00E-04	0.014
22	15	251.37	9.88E-04	0.040
23	16	250.52	6.88E-04	0.090
24	17	243.58	6.88E-04	0.169
25	18	239.93	5.88E-04	0.273
26	19	232.22	3.25E-04	0.395
27	20	228.34	1.05E-03	0.536

Figure 4-1 A screen capture of the spreadsheet that is used to calculate the predicted full scale heat release rate.

As seen in Figure 4-1, column A contains the time stamp for the data columns, column B contains the experimental heat release rate density data, column H contains the differential burning area data and column I is where the full scale heat release rate is calculated. The formula in column I performs the discrete convolution and is written for cell I:12 as *SUMPRODUCT ($H$7:H12 , SUBTOTAL (9, OFFSET($B$7:B12 ,LARGE (ROW($B$7:B12)-ROW($B$7),ROW(INDIRECT("1:"&ROWS($B$7:B12)))),0,1)))*.

4.2. Validation of the Convolution Model Code

This section will discuss the validation that was performed to ensure that the discretization of the CBUF model was performed correctly and that there were no errors in coding. This validation was performed in a similar fashion to Ezinwa [22]; input equations were chosen that allowed for a closed form solution to be found.

The area spread relationship that was used for validation was developed by Wickstrom and Goransson [19] through observation of flame spread over room lining materials during room/corner tests. It is expressed as

$$A(t) = A_0 \left[1 + \vartheta \frac{(t - t_x)^2}{t_{ign}}\right], \tag{4.3}$$

where A_0 is the initial burning area due to ignition (m^2),

ϑ is an empirical constant describing the rate of fire growth (s^{-1}),

t_{ign} is the time to ignition for a specimen tested in the cone calorimeter (s) and

t_x is an empirically determined time constant (s).

The values that were chosen to represent the validation flame spread were the same values as were used by Ezinwa [22]. The value of t_{ign} was taken to be 2 s, the initial burning area A_0 was taken to be 0.00321 m^2, and the empirical constants were taken to be ϑ = 0.025 s^{-1} and t_x = 0.2 s. A plot of this flame spread relationship is shown in Figure 4-2.

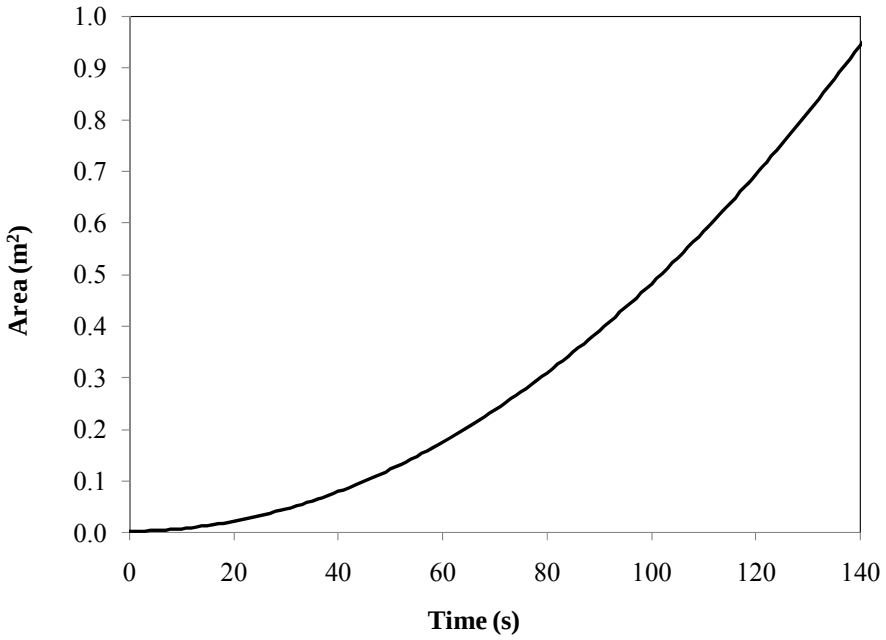

Figure 4-2 Plot of Wickstrom and Goransson's time dependent flame area [19].

To provide a heat release rate density curve for the validation, the same single Gaussian distribution employed by Ezinwa was used. This equation takes the form of

$$q"(t) = a \cdot exp[-b(c-t)^2]\,, \qquad (4.4)$$

where: a is the peak heat release rate measured in the cone calorimeter, during a test of polyurethane foam (kW/m^2),

b is a value that determines the width of the peak value (s^{-2}) and

c controls the time to peak heat release rate density (s).

The values that were used as input for the validation are a = 410 kW/m^2, b = 0.001 s^{-2} and c = 75s. These values were chosen to provide a HRR density curve that is similar to the time duration and amplitude that could be seen in a typical cone calorimeter test of polyurethane foam. A plot if this heat release density curve can be seen below in Figure 4-3.

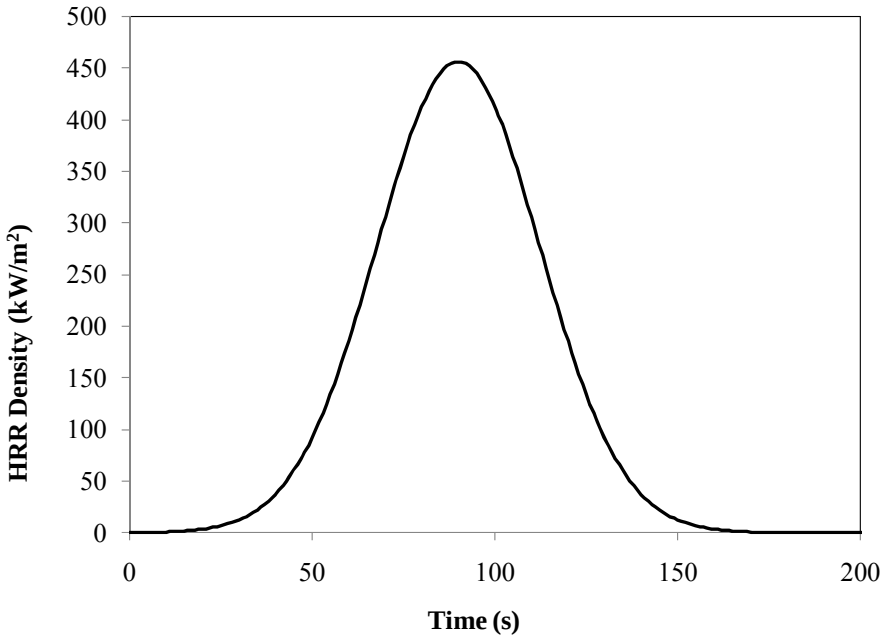

Figure 4-3 Plot of single gaussian distribution used to simulate input HRR density.

When equations (4.3) and (4.4) are substituted into equation (1.5) the convolution of these two expressions becomes

$$Q = \frac{2 \cdot q''_{max} A_0 \cdot a}{t_{ig}} \int_0^t exp(-b(c - t + \tau)^2)\tau \, d\tau \qquad (4.5)$$

The analytical solution for this equation was found using the Maple™ Computer Algebra system and is expressed as

$$Q = -\frac{1}{b^{3/2}} \left[\frac{\dot{q}''_{\max} A_0 \cdot a}{t_{ig}} \begin{pmatrix} -e^{2bct}\sqrt{b} - \sqrt{\pi} erf\left(\sqrt{b}\cdot c - \sqrt{b}\cdot t\right) b \cdot c \cdot e^{bc^2+bt^2} \\ +\sqrt{\pi} erf\left(\sqrt{b}\cdot c - \sqrt{b}\cdot t\right) b \cdot t \cdot e^{bc^2+bt^2} + e^{bt^2}\sqrt{b} \\ +e^{bc^2+bt^2}\sqrt{\pi} erf\left(\sqrt{b}\cdot c\right) c \cdot b - e^{bc^2+bt^2}\sqrt{\pi} erf\left(\sqrt{b}\cdot c\right) tb \end{pmatrix} e^{-bc^2-bt^2} \right] \qquad (4.6)$$

To complete the validation, a numerical convolution was performed using the spreadsheet that employs equation (4.2) and values from the same input equations as were used in the derivation of equation (4.6). To examine the effect of discretization time step, the numerical convolution was performed with time steps of 1s, 3s and 5s.

Figure 4-4 compares the result of the numerical convolutions with the closed form solution of the convolution integral.

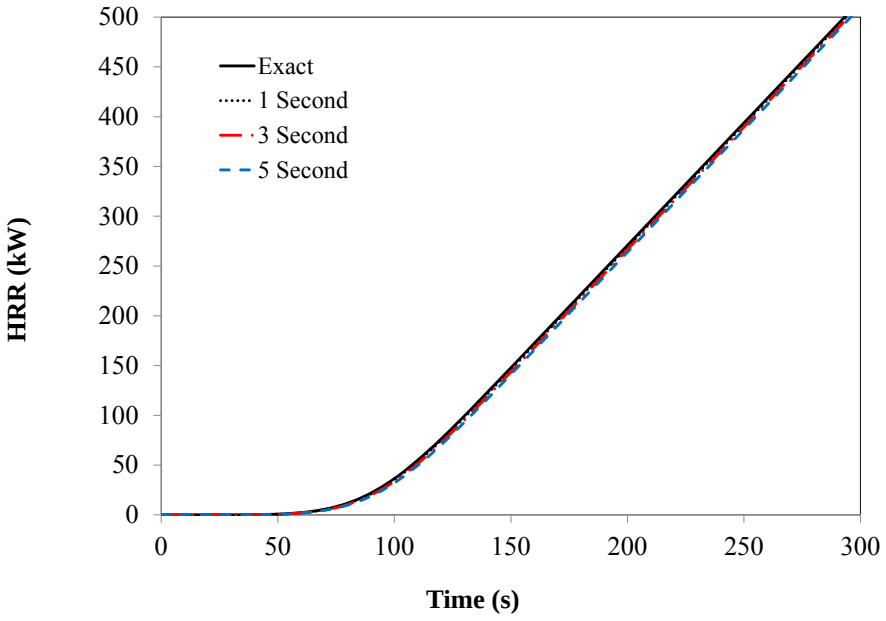

Figure 4-4 Comparison of exact solution and numerical solution for convolution integral.

As seen in Figure 4-4, the numerical convolution does an acceptable job of approximating the closed form solution. As can be expected the time step that is chosen for the discretization has an effect on the numerical result, the best result being obtained with the smallest time step, in this case of 1s. This shows that as the time step of the numerical convolution is refined the result is converging on the closed form solution. Figure 4-5 presents

this result as the magnitude of the error between the numerical convolution and the closed form solution.

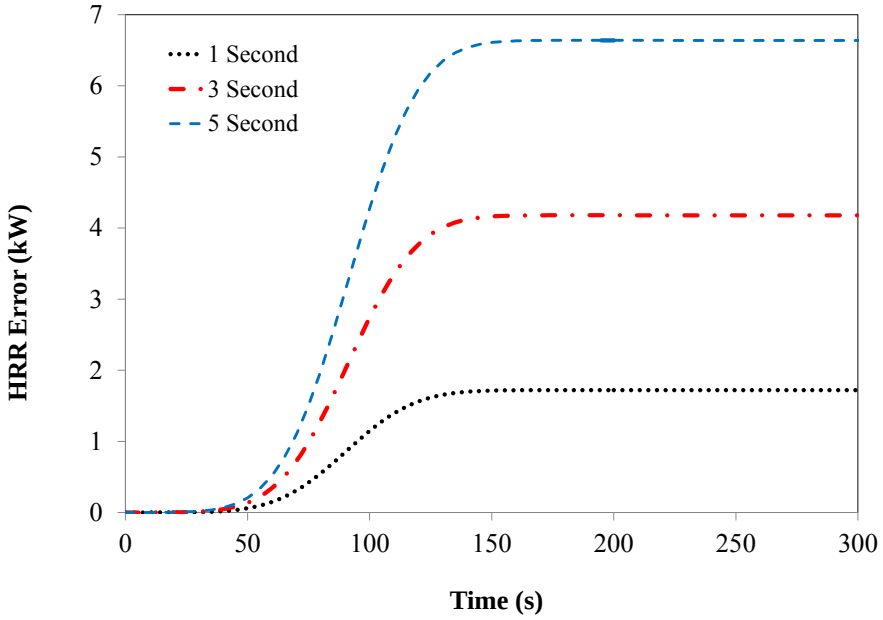

Figure 4-5 Magnitude of error between exact and numerical solutions.

Figure 4-5 once again illustrates the convergence of the numerical solution with the closed form solution as the time step is decreased. In all three cases the error magnitude reaches a nearly steady state error after a time of 150 s. For the 5 s time step the error magnitude approaches 6.6 kW, with a time step of 3 s the error magnitude approaches 4.2 kW, and for the 1 s discretization the error approaches a value of 1.7 kW. By observing this trend it can be seen that each time step refinement produces a significant reduction in error magnitude. A time step reduction of 40% from 5 s to 3 s produces an error reduction of 36%. A time step reduction of 67% from 3 s to 1 s produces an error reduction of 60%.

When the magnitude of numerical error is expressed as a percentage of the exact solution it is seen that at very low HRRs the error appears high. For example at 27 s the error is 10%, however at this time step the HRR is only 0.03 kW. At 80 s, the error drops by half to 5% and

again at 120 s when the heat release rate reaches 75 kW the error had dropped to 2%. Comparing the one second convolution with the peak HRR seen in full scale tests, the C1 test series had an average peak HRR of 36.5 kW. When the one second verification convolution reached 36.9 kW it showed a 3.1% error. Looking at the larger EE4 tests with a peak HRR of 485.9 kW, when the 1 s verification convolution had reached 485.5 kW it had an error of 0.3%

In light of these results, and since the maximum sampling rate of the cone calorimeter is 1 Hz, a time step of 1 s was deemed acceptable for this research.

4.3. Sensitivity Study

The coding of the CBUF model that is used in this thesis functions was similar to the coding used by Ezinwa [24]. Ezinwa found that the when the heat release rate density curve is scaled by ±10% the peak HRR and THR predicted by the CBUF model scales by ±10%. Similarly when the area spread curve is scaled by ±10%, the peak HRR and THR predicted by the CBUF model again scales by ±10%. In this way the output of the CBUF model appears to scale linearly with both the area spread input and the HRR density input.

CHAPTER 5 : EVALUATION OF THE CONVOLUTION MODEL

This section of the thesis will focus on evaluating the convolution model. This evaluation will make use of parameters and statistics that are commonly used in fire protection engineering, such as peak HRR and THR and will make use of the standard t^2 fires as a bench mark. The first part of this section will briefly discuss the effect that incident heat flux setting has on the convolution model results. The incident heat flux setting refers to the heat flux that is emitted from the cone heater to the surface of the cone calorimeter test specimen. Since this parameter has a strong effect on cone calorimeter results, it is worth studying how CBUF model results are affected when various incident heat flux settings are utilized in cone calorimeter tests used for the generation of input data.

The second part of this section will compare results of the convolution model for the different full scale test configurations that were investigated in this research. For each of the test configurations, one test plot will be discussed and compared to convolution model results for that specific test. This section will also compare and contrast common calorimetry measurements for the experimental results and convolution results for the four heat fluxes.

A factor that should be taken into account when evaluating the cone calorimeter incident heat flux setting is that the needs will be different depending on the end user of the convolution model. For instance, a fire protection engineer may want to use the CBUF model to provide input into a computational fluid dynamics (CFD) or zone model to study fire behavior in a building. In this case inputs for the CBUF model should be carefully chosen so that the outputs of the CBUF model predict the full HRR curve from growth through peak and decay phases. It should be

noted that in fire protection engineering a model which produces predictions with an accuracy of 5 to 10% is generally considered to be good.From the perspective of a regulator setting pass/fail criteria for products, the decay phase is less important and more focus should be placed on the ability of the CBUF model to accurately predict the fire growth curve and the peak HRR. Overall the time to peak HRR parameter can be deceiving; however for completeness it is included in this discussion. The importance of time to peak HRR is discussed in more detail later in this chapter.

A quick note should be made regarding the alignment of the CBUF model results with the experimental results. As was noted earlier, the incubation time for large scale experimental fires can be unpredictable. To allow for the comparison of the experimental results with the CBUF model, the plots were aligned at early stages of the fire (between 5 and 10 kW) in a similar fashion to what was discussed in Section 3.2. Further development of this model could take into account an average incubation time that could be used to better predict time based statistical parameters such as time to peak HRR.

5.1. The Effect of Incident Heat Flux on Convolution Model Results

As was seen in the cone calorimeter test results section, the incident heat flux used in the cone calorimeter has a significant effect on the shape of the heat release rate density curve. As would be expected, when these differently shaped curves are used as input to a convolution model, the convolution model results exhibit some of the same characteristics as the cone calorimeter HRR density curves at the different incident heat fluxes.

Figure 5-1 shows cone calorimeter test results for 2.5 cm foam obtained at 25, 35, 50 and 75 kW/m^2 incident heat fluxes and Figure 5-2 is a plot comparing the convolution model results

for test C1-4 when cone data obtained with incident heat fluxes of 25, 35, 50 and 75 kW/m^2 (shown in Figure 5-1) were used as input.

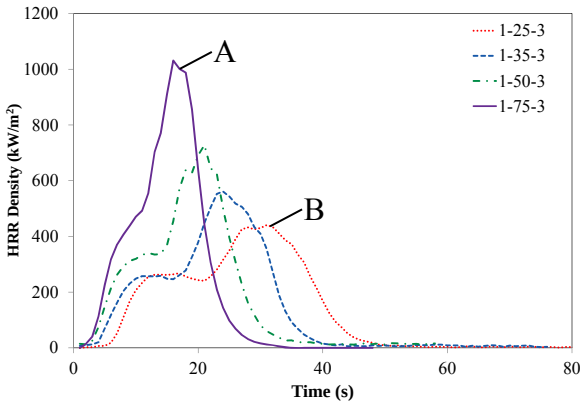

Figure 5-1 Cone calorimeter test results for 2.5 cm foam at 25, 35, 50 and 75 kW/m^2 incident heat flux. A – HRR density curve with highest peak and shortest duration. B – HRR density curve with lowest peak and longest duration.

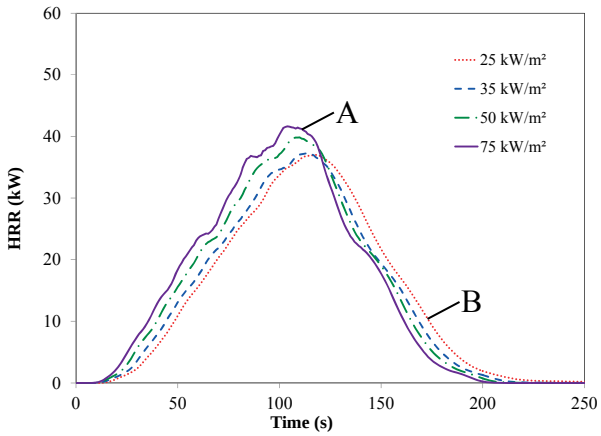

Figure 5-2 Convolution model results for test C1-4 when the cone calorimeter test at each incident heat flux is used as input. A – HRR curve with highest peak and shortest duration. B – HRR curve with lowest peak and longest duration.

Similar to Figure 5-1 and Figure 5-2, Figure 5-3 through Figure 5-8 show this same comparison for 5, 7.5 and 10 cm thick foams.

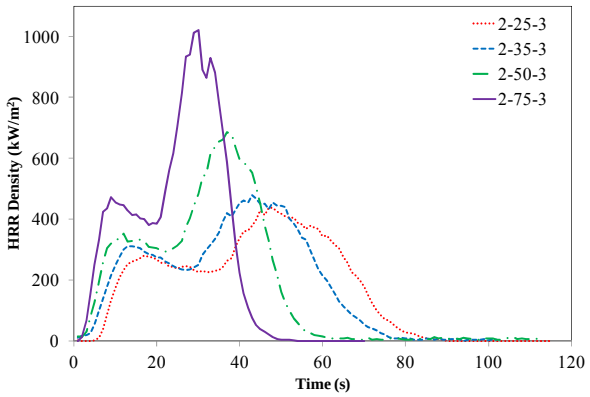

Figure 5-3 Cone calorimeter test results for 5 cm foam at 25, 35, 50 and 75 kW/m^2 incident heat flux.

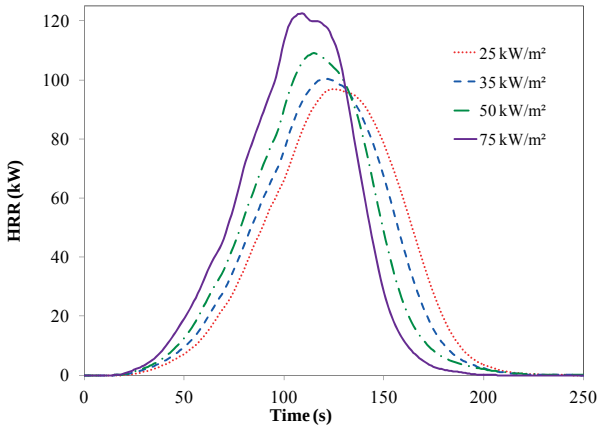

Figure 5-4 Convolution model results for test C2-3 when the cone calorimeter test at each incident heat flux is used as input.

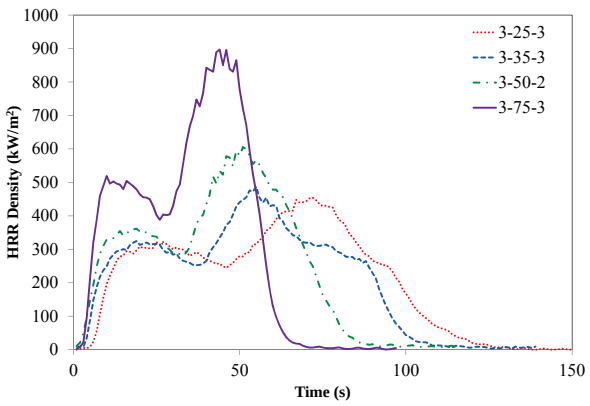

Figure 5-5 Cone calorimeter test results for 7.5 cm foam at 25, 35, 50 and 75 kW/m^2 incident heat flux.

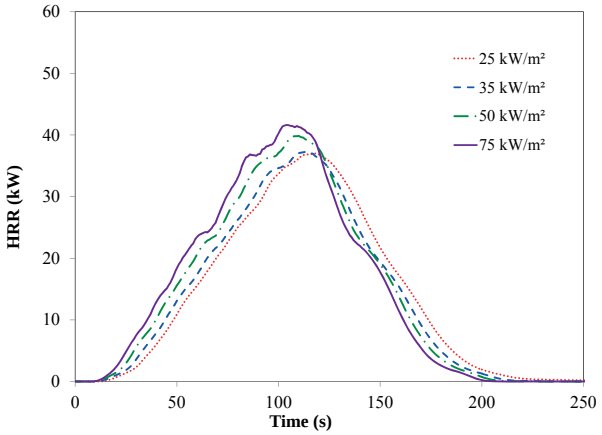

Figure 5-6 Convolution model results for test C3-2 when the cone calorimeter test at each incident heat flux is used as input.

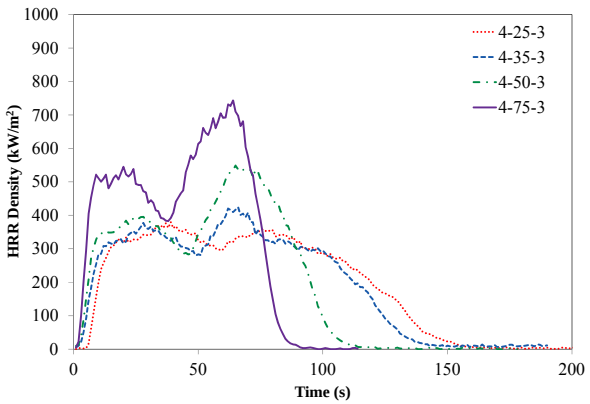

Figure 5-7 Cone calorimeter test results for 10 cm foam at 25, 35, 50 and 75 kW/m^2 incident heat flux.

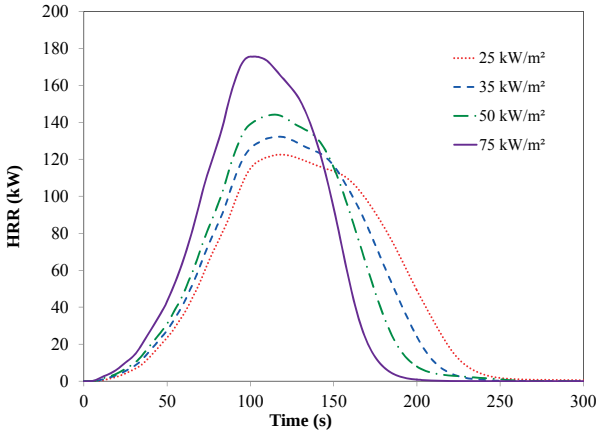

Figure 5-8 Convolution model results for test C4-1 when the cone calorimeter test at each incident heat flux is used as input.

As was discussed in the Experimental Results (Section 3.1.1), when the incident heat flux setting is increased, the resulting peak HRR density increases and the burning duration of the specimen decreases. This effect is shown in Figure 5-1 for 2.5 cm foam. Figure 5-2 shows that these characteristic differences are propagated into the CBUF model predictions when this data is used as input. For example, when the 75 kW/m^2 cone data ("A" in Figure 5-1), which had the highest peak HRR density and shortest burning duration, is used as input into the CBUF model, the resulting prediction has the highest peak HRR and shortest burning duration ("A" in Figure 5-2). Similarly, when the 25 kW/m^2 cone data ("B" in Figure 5-1), which had the lowest peak HRR density and longest burning duration, is used as input into the CBUF model, the resulting prediction has the lowest peak HRR and longest burning duration ("B" in Figure 5-2). As is seen in Figure 5-3 through Figure 5-8 this same phenomena is also seen for the 5, 7.5 and 10 cm thick foams.

These figures illustrate how closely tied the cone calorimeter results are with the CBUF model results. In order to evaluate which incident heat flux should be used for cone calorimeter tests which are to be used to generate input data for the CBUF model, the CBUF model results

from the four incident heat flux results should be compared to the full scale experimental results. That is the aim of the next section.

5.2. Evaluation of the Convolution Model for Center Ignition Test Configurations

The first test configuration that will be discussed is the center ignition. The burning characteristics of the center ignition tests were in general predicted better for the thinner specimens. Figure 5-9 is a plot comparing the experimental results and the convolution model predictions for test C1-4. This plot represents the best fit of the three tests that were run in this configuration. The remaining plots for the 2.5 cm (1 in.) center ignition tests can be found in Appendix G.

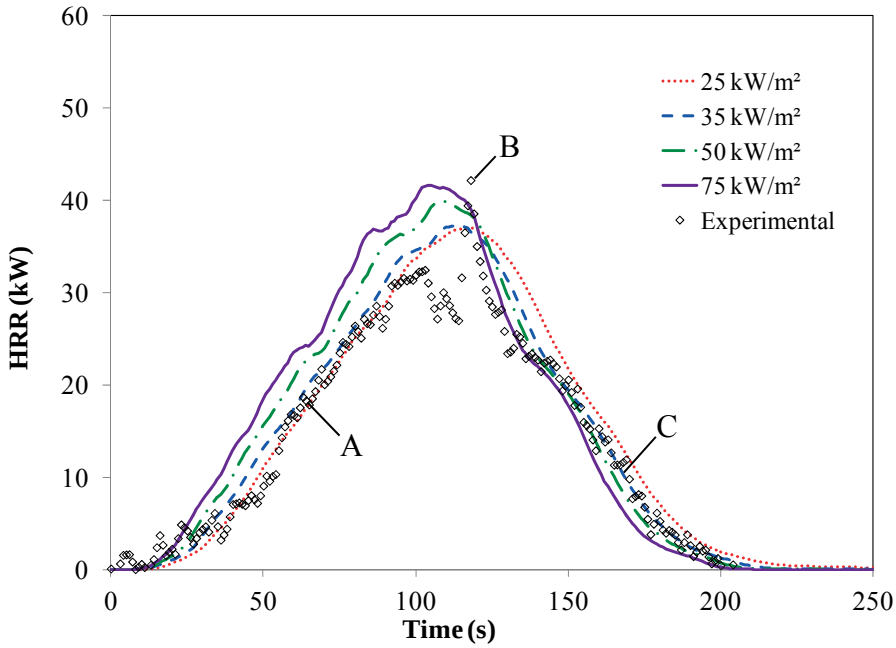

Figure 5-9 Comparison of experimental heat release rate with convolution model results for test C1-4. A – growth phase of fire. B – experimental peak HRR. C – decay phase of fire.

As seen in Figure 5-9, for this test configuration the convolution model does a good job of predicting both the growth and decay phases of this test, and of the four thicknesses the 2.5 cm

(1 in.) thickness was the best predicted using the convolution model. With regard to the comparison of the experimental results with the convolution model results using the four heat fluxes, this test shows the greatest agreement with the 25 kW/m^2 in the growth phase ("A" in Figure 5-9). The peak heat release value however matches closer to the 75 W/m^2 curve ("B" in Figure 5-9) followed by a decay that appears to follow the 35 W/m^2 curve ("C" in Figure 5-9) to extinction.

Table 3-1 shows a comparison of predicted and measured values of commonly used calorimetry measurements, namely peak HRR, time to peak HRR and THR for the center test configurations. These parameters were chosen due to their common usage in the fire protection engineering community. For each of the configurations in Table 5-1, the bolded text indicates the incident heat flux setting for which the convolution result matches most closely the experimental data. Figure 5-10, Figure 5-11 and Figure 5-12 following the table show this data presented graphically.

Table 5-1: Summary of convolution model results for center ignition tests.

Nominal Thickness (cm)	Incident Heat Flux Used in Model (kW/m^2)	Peak HRR (kW)		Time to Peak (s)		THR (MJ)	
		Ave.	(σ)	Ave.	(σ)	Ave.	(σ)
C1	Exp.	40	(6.3)	98	(19.1)	3.0	(0.29)
	25	38	(6.3)	111	(13.6)	3.5	(0.04)
	35	**39**	(6.7)	107	(13.3)	**3.4**	(0.04)
	50	42	(7.7)	105	(11.4)	3.6	(0.04)
	75	44	(8.8)	**102**	(10.7)	3.7	(0.05)
C2	Exp.	86	(8.3)	94	(8.4)	6.9	(0.14)
	25	84	(11.7)	123	(5.3)	**7.7**	(0.07)
	35	**85**	(13.7)	116	(6.4)	**7.7**	(0.07)
	50	89	(17.7)	112	(7.9)	7.8	(0.07)
	75	99	(20.8)	**99**	(9.0)	8.3	(0.07)
C3	Exp.	138	(10.6)	106	(4.5)	10.4	(0.44)
	25	120	(1.2)	134	(13.1)	12.2	(0.02)
	35	127	(2.7)	127	(12.7)	**11.9**	(0.02)
	50	**140**	(4.7)	122	(11.8)	**11.9**	(0.02)
	75	166	(8.3)	**117**	(12.4)	12.3	(0.02)
C4	Exp.	160	(21.6)	97	(10.7)	13.9	(0.94)
	25	122	(3.1)	125	(13.7)	14.8	(0.25)
	35	131	(4.1)	121	(13.1)	14.3	(0.24)
	50	141	(5.6)	119	(13.2)	**14.2**	(0.24)
	75	**172**	(8.7)	**109**	(14.8)	15.0	(0.25)
CC4	Exp.	552	(51.9)	127	(5.7)	55.3	(3.45)
	25	480	(6.9)	157	(3.8)	59.6	(0.76)
	35	509	(4.4)	155	(4.7)	57.8	(0.73)
	50	**551**	(6.0)	168	(14.2)	**57.4**	(0.73)
	75	668	(6.8)	**147**	(3.8)	60.7	(0.77)

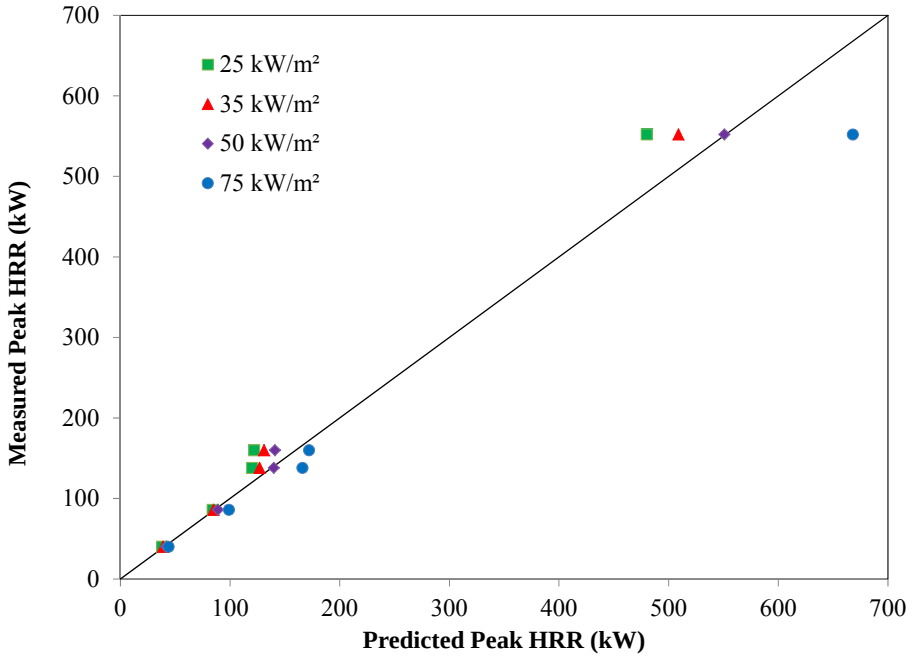

Figure 5-10 Comparison of measured peak HRR values with predicted peak HRR values using various incident heat fluxes for center ignition tests.

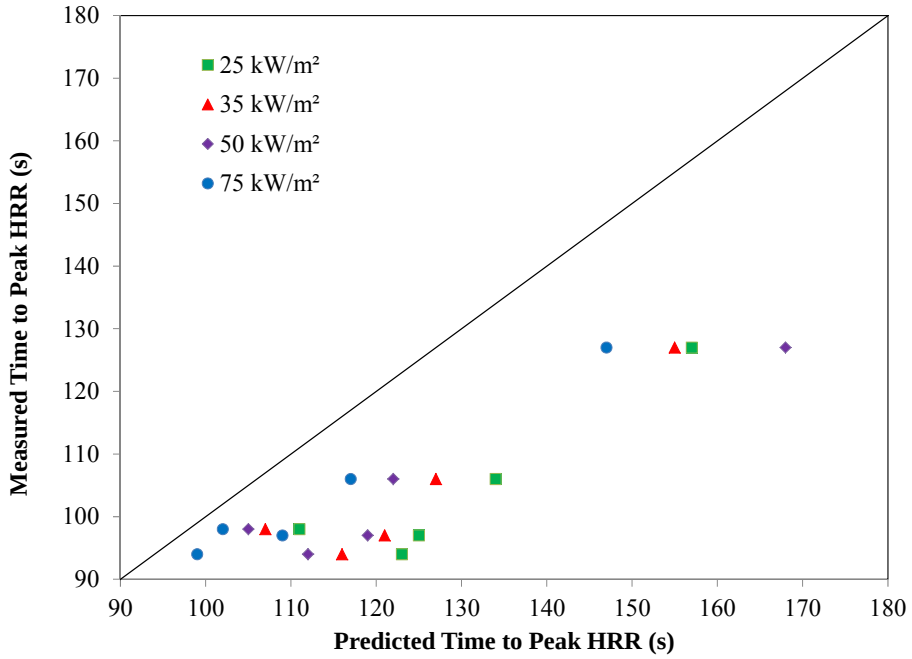

Figure 5-11 Comparison of measured time to peak HRR values with predicted time to peak HRR values using various incident heat fluxes for center ignition tests.

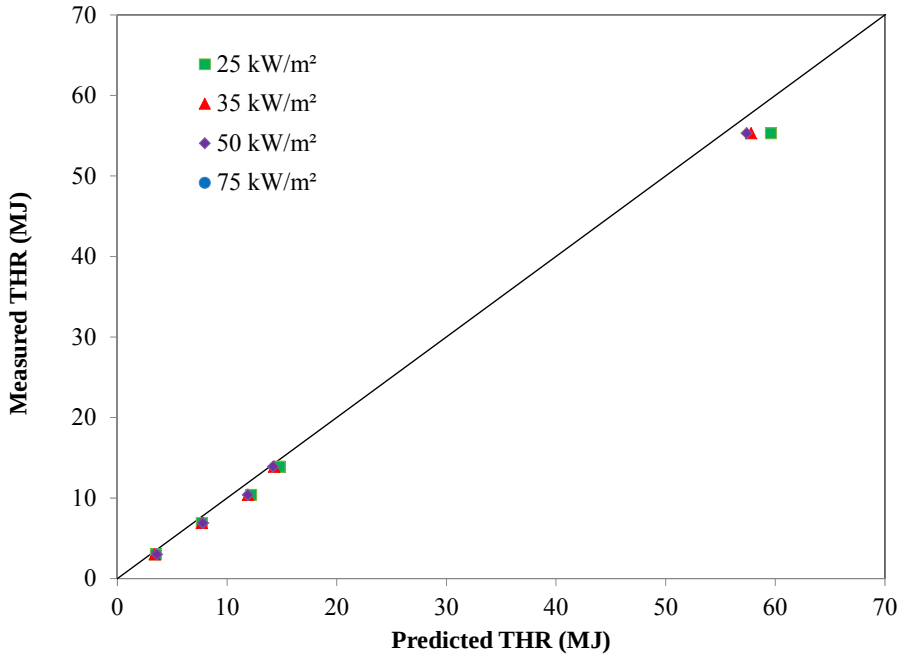

Figure 5-12 Comparison of measured THR values with predicted THR values using various incident heat fluxes for center ignition tests.

One of the characteristics that stands out is that the CBUF model appears to predict the THR values very well for the center ignition specimens (Figure 5-12). Shown in Figure 5-10, the convolution model also appears to predict the peak HRR values relatively well.

As seen in Table 5-1, for the C1 foam configuration, the experimental peak HRR of 40 kW was most closely matched by the 35 kW/m^2 convolution result of 39 kW. Likewise the experimental THR value of the C1 test configuration of 3.6 MJ was most closely modeled by the 35 kW/m^2 convolution result of 3.4 MJ. The time to peak value for the experimental C1 result of 98 s on the other hand was most closely modeled by the 75 kW/m^2 convolution result of 102 s. The trend of the time to peak value being most closely modeled by the 75 kW/m^2 convolution result continues for all test results presented in this research. When comparing average test values, the convolution model consistently over-predicts the time to peak HRR. That said, time

to peak HRR can be a deceptive parameter to analyze and predict. For example, looking at Figure 5-13 below, comparing the experimental results of test C2-2 with the CBUF model predictions, the time to peak HRR is clearly predicted best by the 75 kW/m^2 CBUF prediction; however, the 75 kW/m^2 CBUF prediction does the worst job out of the four predictions of the overall characterization of the HRR curve. Another factor is that, as discussed earlier, incubation times in full scale fire tests can range widely, and can make a significant difference in the experimental time to peak HRR value. In this way, the time to peak HRR parameter may have limited utility when characterizing the ability of a model to make predictions.

The next test configuration that will be discussed is C2 which consisted of 5.0 cm (2 in.) thick specimens ignited in the center. Figure 5-13 is a plot comparing the experimental HRR of test C2-2 with the convolution model predictions of this test.

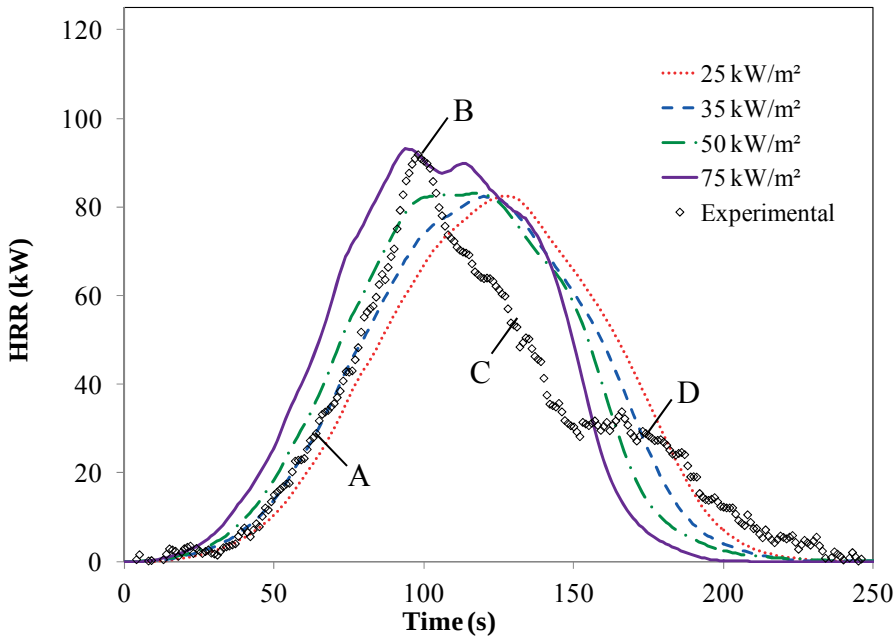

Figure 5-13 Comparison of experimental heat release rate with convolution model results for test C2-2. A – growth phase of fire. B – experimental peak HRR. C – rapid decay phase. D – experimental curve crosses all predictions.

Test C2-2 is indicative of the degree of agreement that was seen between the experimental and convolution results for this test configuration. As seen in Figure 5-13, the 35 kW/m^2 convolution model does a good job of predicting the growth phase of the fire from ignition until 85 s ("A" in Figure 5-13). At this point the heat release rate increases rapidly to 91 kW at a time of 98 s ("B" in Figure 5-13). From reviewing the video footage, the rapid increase coincides with the flame front reaching the edge of the specimen. After the sharp peak, the experimental heat release rate then drops rapidly, far below the heat release rate predicted by any of the convolution results ("C" in Figure 5-13). At 150 s the decay phase slows and a heat release rate of approximately 30 kW is sustained until 180 s when the heat release rate begins to drop until extinction. Between the times of 150 s and 180 s the experimental HRR curve crossed all four of the convolution result curves ("D" in Figure 5-13), and the experimental extinction time is longer than any of the convolution results. In this way the convolution model successfully predicts the experimental results for the growth phase of this fire, however there is some phenomenon in the experiment during the decay phase of the fire that is not adequately modeled using the CBUF model. This could indicate that a model such as this, which relies strictly on the decay of the HRR density curve to model the decay of the full scale fire, is inadequate for the modeling the entire full scale tests.

Comparing the average measurements in Table 3-1 for the C2 test configuration, the experimental peak HRR of 86 kW is most closely modeled by the 35 kW/m^2 convolution result of 85 kW. The experimental THR result of 6.9 MJ is predicted most closely by the 25 kW/m^2 and 35 kW/m^2 convolution results of 7.7 MJ, although the convolution model over predicts the results by 0.8 MJ in both of these cases.

Figure 5-14 shows a comparison of the 7.5 cm (3 in.) C3-2 experimental HRR test results with the CBUF model results.

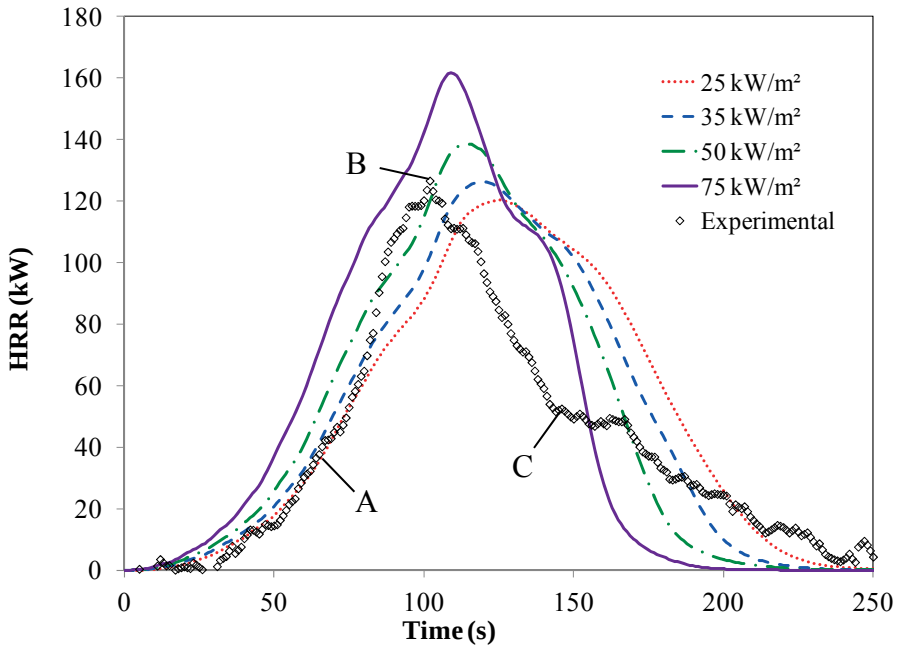

Figure 5-14 Comparison of experimental heat release rate with convolution model results for test C3-2. A – growth phase of fire. B – experimental peak HRR. C – end of rapid decay phase.

Test C3-2 is indicative of the amount of agreement that was seen between the experimental and model results for the C3 test configuration. For plots of this comparison for tests C3-1 and C3-3 see Appendix G. As seen in Figure 5-14 the model successfully predicts most of the growth phase of the fire ("A" in Figure 5-14). For this test the 25 kW/m^2 most closely models the experimental results until 80 s when the model diverges from the experimental results. In a similar fashion to what was seen in test configuration C2, the fire accelerates rapidly to a peak of 127 kW at 102 s ("B" in Figure 5-14). Once again from reviewing the video footage, it appears that the rapid increase in HRR coincides with the flame front reaching the side of the specimen possibly indicating that the flame spread along the edges of the specimen is contributing to this acceleration. The fact that the ΔA curve that was used in

this model does not take into account flame spread along the edges of the specimen could be a reason that the CBUF model fails to reproduce the rapid increase in HRR that occurs when the flame front reaches the specimen edge. Following the rapid acceleration there is a rapid decay to 53 kW at 143 s ("C" in Figure 5-14). Following 143 s, the HRR curve follows a slower decay until the specimen reaches extinction. As was seen in the C2 test configuration, there is some phenomenon during the decay phase of this test configuration that is not adequately modeled by the CBUF model.

The average measurements found in Table 5-1 indicate that for the C3 test configuration the average experimental peak HRR of 138 kW was most closely modeled by the 50 kW/m^2 convolution with a peak HRR of 140 kW. For THR the experimental result of 10.4 MJ was most closely matched by the 35 kW/m^2 and 50 kW/m^2 convolution result of 11.9 MJ.

A possible cause for the over-prediction of THR by the convolution model at higher heat fluxes is that more of the specimen burned in the cone calorimeter tests at the higher heat fluxes than in the furniture calorimeter tests. This was observed in furniture calorimeter tests of thicker specimens where there were pools of a black tarry substance on the foil lining at the end of the test. This is in contrast to cone calorimeter tests at higher incident heat fluxes where very little material was left in the foil lining at the end of the tests.

Figure 5-15 shows a plot of the experimental HRR values versus the CBUF model results for test C4-1 from the C4 test configuration. This test configuration consisted of 10 cm (4 in.) thick foam specimens ignited in the center.

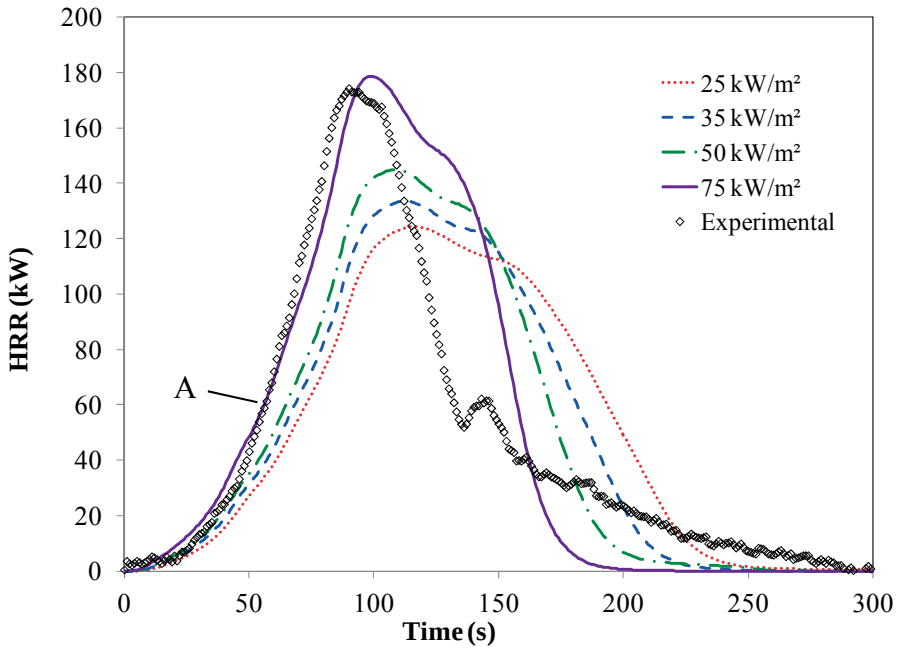

Figure 5-15 Comparison of experimental heat release rate with convolution model results for test C4-2. A – growth phase of fire.

As seen in Figure 5-15, for the C4 test configuration the convolution model once again predicts the growth phase of the fire with greater accuracy than the decay phase. For tests C4-1 and C4-2 the growth phase was most closely modeled by the 75 kW/m^2 convolution result ("A" in Figure 5-15). The C4-3 test on the other hand was most closely modeled by the 50 kW/m^2 convolution result (plots of the remaining C4 tests can be found in Appendix G). A trend that emerges when comparing the convolution results for the various thicknesses of foam is that the ability of the convolution model to predict the decay phase gets worse as the foam thickness increases; this can seen by comparing Figure 5-13 through Figure 5-15.

Comparing the measurements found in Table 3-1, the experimental peak heat release rate of 160 kW is most closely modeled by the 75 kW/m^2 convolution result of 172 kW. Finally, the experimental THR value of 13.9 MJ is most closely modeled by the 50 kW/m^2 convolution result of 14.2 MJ.

The last of the center ignition tests configurations that will be discussed is the CC4 test configuration where a 10 cm thick specimen that is nominally 1.2 m (48 in.) by 1.2 m (48 in.) is ignited in the center. Figure 5-16 shows a comparison of the experimental results from test CC4-2 with the CBUF model predictions of this test.

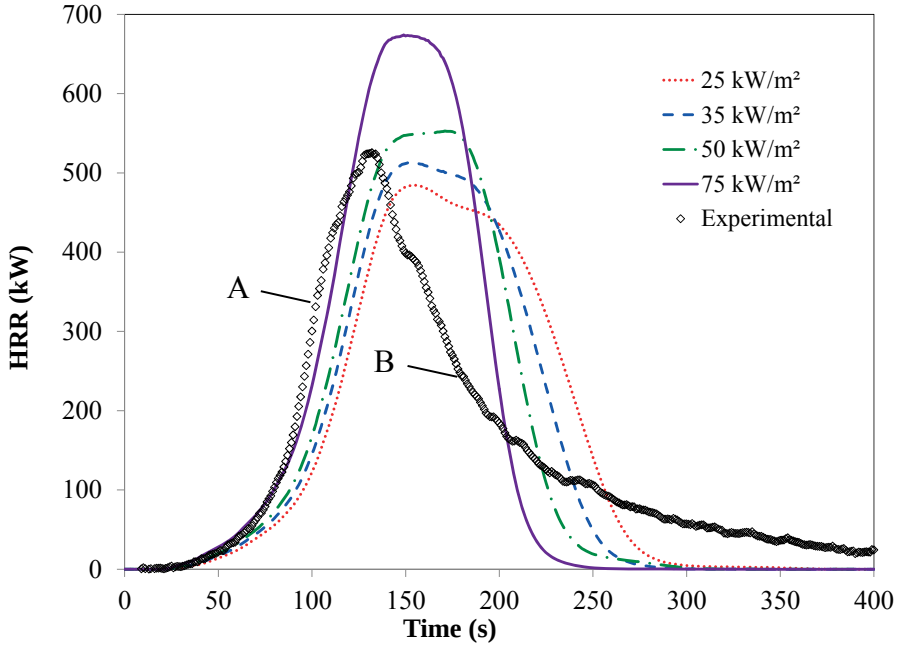

Figure 5-16 Comparison of experimental heat release rate with convolution model results for test CC4-2. A – growth phase of fire under predicted model. B – decay phase of fire.

As seen in Figure 5-16 the convolution model does a reasonable job or predicting the growth phase of the CC4 test configuration. However in all three of the CC4 tests the 75 kW/m^2 convolution test slightly under predicts the growth phase of the experimental result ("A" in Figure 5-16). Once again, as was seen in test configurations C2 through C4 the convolution model over predicts the decay phase of the HRR curve ("B" in Figure 5-16).

Comparing the measurements for the CC4 test configurations, the experimental peak HRR value of 552 kW is most closely modeled by the 50 kW/m^2 convolution result of 551 kW.

The experimental THR value of 57.9 MJ was predicted most closely by the 57.6 MJ result from the 35 kW/m^2 convolution.

5.3. Evaluation of the Convolution Model for Edge Ignition Test Configurations

This section will focus on the ability of the convolution model to predict the full scale fire test results of the foam tested in the edge ignition configuration. The edge test configurations consisted of E1, E2, E3, E4 and EE4.

The first edge ignition test configuration that will be discussed is E1 which consisted of a nominally 50 cm by 142 cm by 2.5 cm thick specimen ignited on the short edge. Figure 5-17 shows a comparison of the E1-1 test with the convolution model result.

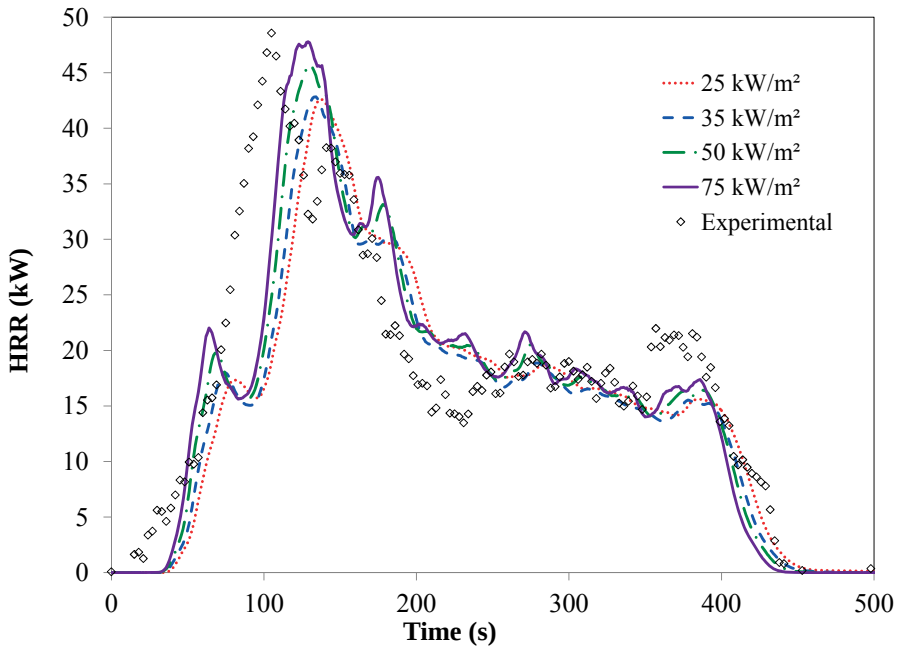

Figure 5-17 Comparison of experimental heat release rate with convolution model results for test E1-1.

As seen in Figure 5-17 for this test configuration the convolution model does a good job of modeling both the growth and decay phases of the fire. This is similar to the behavior that was seen in the C1 test configuration which also used nominally 2.5 cm foam. As was also characteristic of the 2.5 cm (1 in.) foam in the center ignition configuration, the individual tests tended to show a fair degree of variability (Plots of E1-2 and E1-3 can be found in Appendix G). Although there is variation between the individual tests, the convolution model still does a good job of modeling the experimental result.

A phenomenon that can be noted is the presence of extra bumps in the HRR curve produced by the convolution model as was seen in Figure 5-17. The presence of these bumps can be explained largely by the bumps that are present in the area spread data that were used as input in equation 4.2. As was discussed in the experimental results section, these bumps are due to the flickering behavior of the flame front in the test video footage and are stronger in some datasets than others. Figure 5-18 shows a comparison of the area spread data from test E1-1, with the calculated area spread rate for test E1-1, ΔA, which is used as input into the CBUF model.

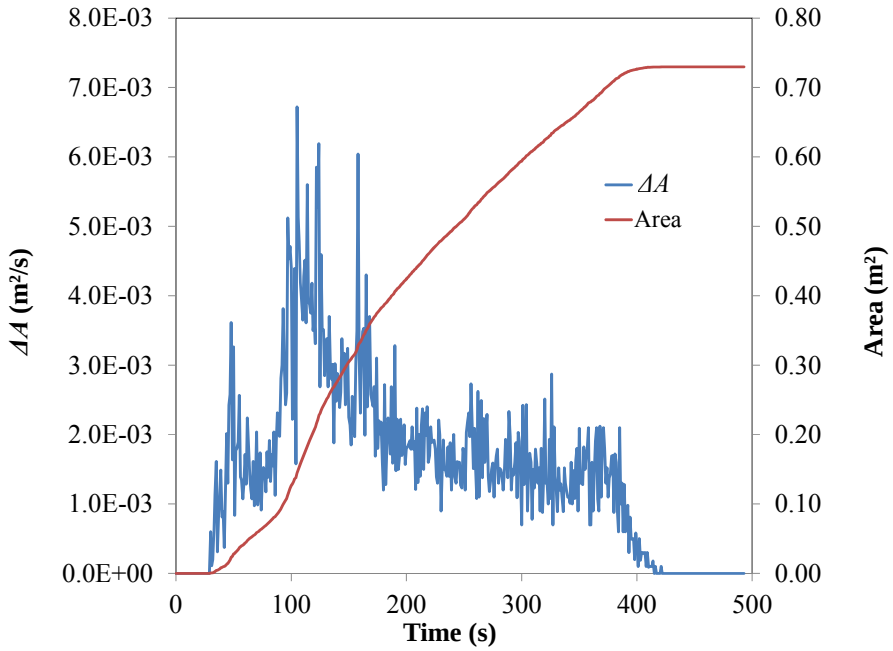

Figure 5-18 Comparison of flame spread area and flame spread rate for test E1-1.

As seen in Figure 5-18 there is a fair bit of noise that is present in the ΔA curve for test E1-1. Comparing Figure 5-17 and Figure 5-18 it can be seen that a bump that is present in the convolution result at approximately 60 s is also present in the ΔA curve at approximately 60 s. Looking further down these curves it can be seen that this is true for other bumps in the ΔA and convolution HRR curves. It is interesting to note that the higher frequency fluctuations appear to have been filtered out in the convolution HRR curves. When comparing the convolution HRR curves from the different incident heat flux settings, it can be seen that as the incident heat flux increases, higher frequency fluctuations begin to appear in the convolution HRR curves. This is likely tied to the duration of the cone calorimeter HRR density curve that is being used as input into the model. When a long HRR density curve, such as a low heat flux or thick foam specimen test, is used as input the convolution process acts as a sort of noise filter damping out high frequency fluctuations present in the input curves. In future research on this model, it may be

useful to implement some simple smoothing filters on the ΔA curves to lessen the impact of fluctuations on the convolution HRR curve.

Table 5-2 shows a comparison of the commonly used calorimetry measurements that are being discussed for the edge test configurations. These data are presented graphically in the three figures following the table, namely Figure 5-19, Figure 5-20 and Figure 5-21.

Table 5-2: Summary of convolution model results for edge ignition tests.

Nominal Thickness (cm)	Incident Heat Flux Used in Model (kW/m^2)	Peak HRR (kW)		Time to Peak (s)		THR (MJ)	
		Ave.	(σ)	Ave.	(σ)	Ave.	(σ)
E1	Exp.	**46**	(10.0)	**99**	(6.0)	**7.4**	(1.01)
	25	39	(5.7)	139	(11.6)	7.8	(0.10)
	35	39	(5.2)	134	(10.0)	**7.7**	(0.10)
	50	42	(5.0)	128	(11.4)	8.1	(0.11)
	75	**45**	(5.0)	**125**	(11.5)	8.3	(0.11)
E2	Exp.	**84**	(12.1)	**143**	(8.5)	**13.7**	(0.29)
	25	74	(13.3)	190	(7.6)	15.0	(0.12)
	35	75	(13.2)	182	(11.1)	**14.9**	(0.11)
	50	79	(14.9)	172	(12.7)	15.2	(0.11)
	75	**87**	(18.4)	**172**	(12.9)	16.1	(0.11)
E3	Exp.	**169**	(13.7)	**188**	(27.2)	**22.7**	(1.23)
	25	163	(24.3)	208	(13.5)	24.4	(0.12)
	35	163	(26.2)	203	(13.5)	**23.8**	(0.12)
	50	**166**	(28.3)	196	(8.0)	**23.8**	(0.12)
	75	179	(31.4)	**182**	(9.3)	24.7	(0.12)
E4	Exp.	**237**	(24.8)	**175**	(10.3)	**28.8**	(3.96)
	25	196	(6.7)	208	(13.5)	30.3	(0.14)
	35	198	(7.4)	203	(12.5)	29.4	(0.14)
	50	202	(8.4)	201	(12.0)	**29.2**	(0.13)
	75	**219**	(10.3)	**196**	(10.0)	30.8	(0.14)
EE4	Exp.	**486**	(34.8)	**173**	(22.4)	**57.9**	(3.67)
	25	449	(8.0)	193	(10.3)	59.4	(0.92)
	35	467	(12.2)	190	(13.2)	**57.6**	(0.89)
	50	**494**	(17.1)	188	(13.6)	57.2	(0.88)
	75	586	(28.8)	**182**	(14.1)	60.4	(0.93)

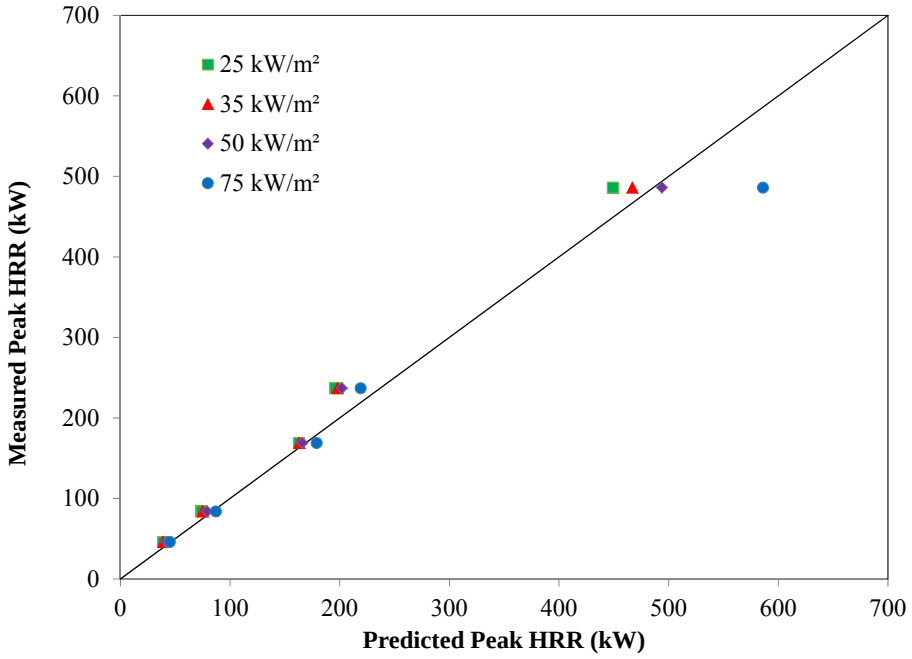

Figure 5-19 Comparison of measured peak HRR values with predicted peak HRR values using various incident heat fluxes for edge ignition tests.

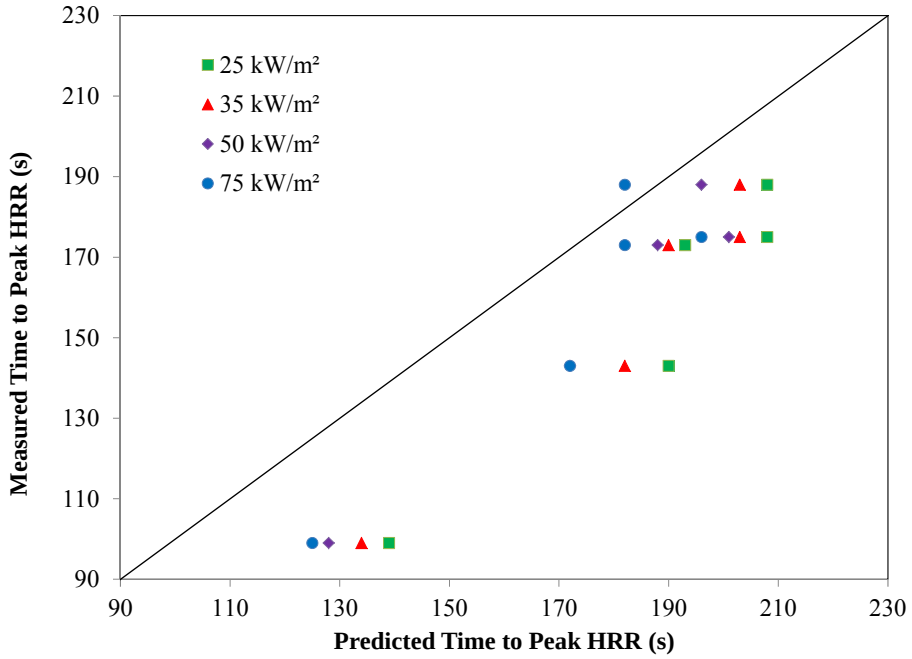

Figure 5-20 Comparison of measured time to peak HRR values with predicted time to peak HRR values using various incident heat fluxes for edge ignition tests.

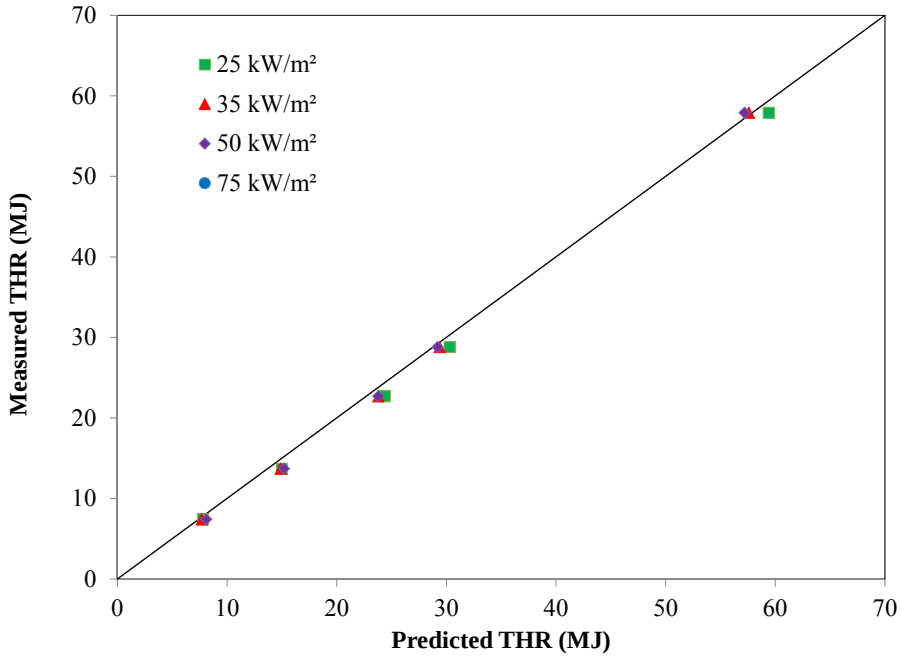

Figure 5-21 Comparison of measured THR values with predicted THR values using various incident heat fluxes for edge ignition tests.

Looking at Figure 5-19, Figure 5-20 and Figure 5-21, it can be seen that the model appears to predict the edge ignition peak HRR, time to peak HRR and THR values in a similar fashion to the center ignition tests. More specifically, the peak HRR values and THR values are modeled relatively well, the time to peak HRR values being consistently over predicted by the CBUF model.

When looking at the calorimetry measurements for test configuration E1 found in Table 5-2, the experimental peak HRR of 46 kW is most closely predicted by the 75 kW/m^2 convolution result of 45 kW. The THR value of 7.4 MJ is predicted most closely by the 35 kW/m^2 at 7.7 MJ.

The next test configuration is E2 which consists of foam specimens with surface dimensions nominally of 0.6 m by 1.2m and thickness of 5.0 cm. Figure 5-22 shows a

comparison of test E2-2 experimental HRR and the result of the convolution model for the various incident heat flux settings.

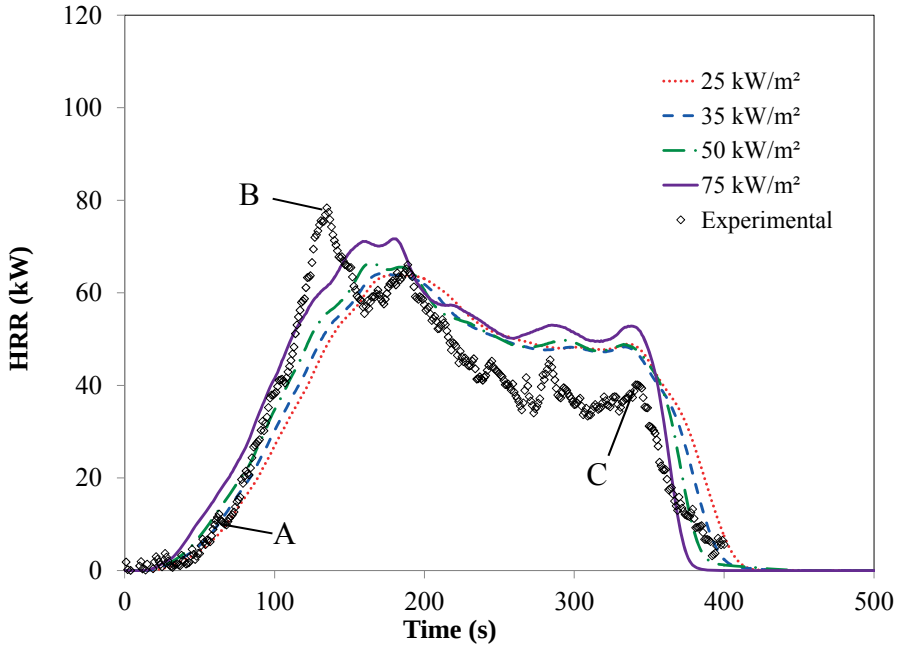

Figure 5-22 Comparison of experimental heat release rate with convolution model results for test E2-1. A – early stages of the fire growth. B – experimental peak HRR. C – beginning of rapid decay phase.

As seen in Figure 5-22, once again the convolution model is doing a reasonable job of predicting the experimental HRR. In this case the growth rate is most closely matched by the 35 kW/m^2 convolution result for the first 80 s ("A" in Figure 5-22). After 80 s the fire accelerates past all four convolution predictions to its peak at 135 s ("B" in Figure 5-22). After the peak there is a long slow decay until 340 s ("C" in Figure 5-22) when the HRR experiences a rapid decay to extinction. During the long decay the convolution model over predicts the HRR, however it does a reasonable job of predicting the time of the rapid decay and the time of extinction. In this way the convolution model appears to capture the burning behavior of this test configuration.

When looking at the measurements found in Table 5-2 the experimental peak HRR of 84 kW is most closely modeled by the 75 kW/m^2 convolution result of 87 kW. The experimental THR for this configuration of 13.7 MJ is most closely modeled by the 35 kW/m^2 convolution model result of 14.9 MJ.

The next test configuration to be discussed is E3 which has the same nominal surface dimensions as the E2 configurations but is 7.5 cm thick. Figure 5-23 shows a comparison of the experimental results from tests E3-2 and the convolution model prediction of this test.

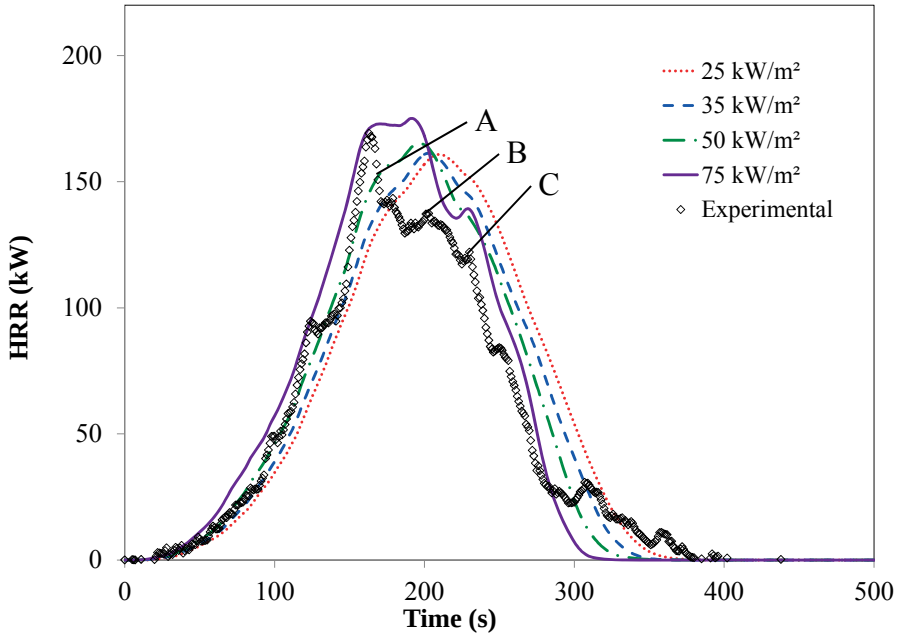

Figure 5-23 Comparison of experimental heat release rate with convolution model results for test E3-1. A – rapid decay in fire not captured by CBUF model. B – brief plateau in HRR curve. C – beginning of rapid decay phase.

As seen in Figure 5-23, the convolution model does a good job of modeling both the growth and decay phases of this test. This is representative of the other tests performed with this configuration. Although the growth and decay phases are modeled well in this instance it can be seen that there is a divergence between the experimental HRR and the convolution model result

at 150 s when the experimental HRR curve has a rapid decrease ("A" in Figure 5-23) to a brief plateau 140 kW decrease ("B" in Figure 5-23) before the sustained decay at 230 s decrease ("C" in Figure 5-23).

Comparing the calorimetry measurements for this test, the average experimental peak HRR of 169 kW was most closely modeled by the 50 kW/m^2 convolution model result of 166 kW. The experimental THR value for this test configuration was 22.7 MJ which was most closely modeled by the 35 and 50 kW/m^2 convolution results of 23.8 MJ.

The next test configuration to be discussed is the E4 test configuration which is the last configuration with nominal surface dimensions of 0.6 m by 1.2m. This configuration consisted of 10 cm thick foam. Figure 5-24 shows a comparison of the experimental HRR from test E4-1 with the convolution results for this test.

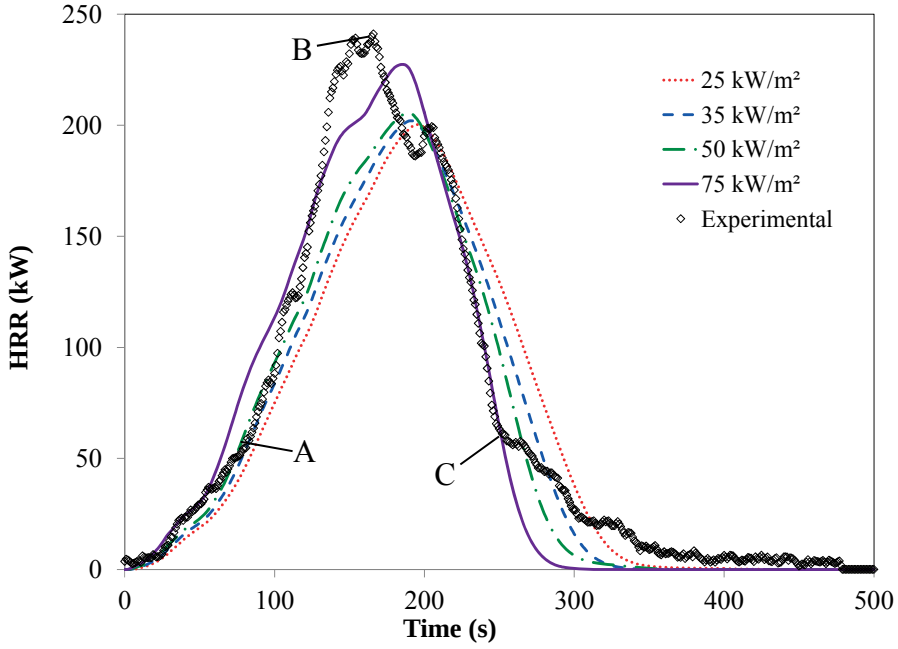

Figure 5-24 Comparison of experimental heat release rate with convolution model results for test E4-1. A – growth phase of fire. B – experimental peak HRR. C – divergence of experimental HRR curve from CBUF model prediction.

As seen in Figure 5-24, both the growth and decay phases of test E4-1 are modeled with reasonable accuracy by the convolution model, the decay phase being modeled more closely than the growth phase. For the first 100 s of the test the experimental HRR follows most closely the 50 kW/m^2 curve ("A" in Figure 5-24) after which it accelerates past the 75 kW/m^2 convolution to its peak of 238 kW at 163 s ("B" in Figure 5-24). In the decay phase the experimental HRR follows the 75 kW/m^2 HRR curve closely until 249 s ("C" in Figure 5-24) when the decay rate decreases. This reduced decay rate can be seen in all three of the E4 tests when the HRR decays to a threshold of approximately 50 kW.

Comparing the measurements for the E4 test configuration found in Table 5-2, the average experimental peak HRR is under predicted by all four of the convolution results. The experimental peak HRR was 237 kW and the closest convolution peak HRR was the 75 kW/m^2 convolution with a peak HRR of 219 kW. Finally, the experimental THR for the E4 test configuration of 28.8 MJ was most closely modeled by the 50 kW/m^2 convolution result of 29.2 MJ.

The final full scale test configuration in this research is EE4 which consisted of 10 cm thick foam with nominal surface dimensions of 1.2 m by 1.2 m which is ignited on the edge. Figure 5-25 shows a comparison of the experimental HRR and the four convolution model predictions for test EE4-1.

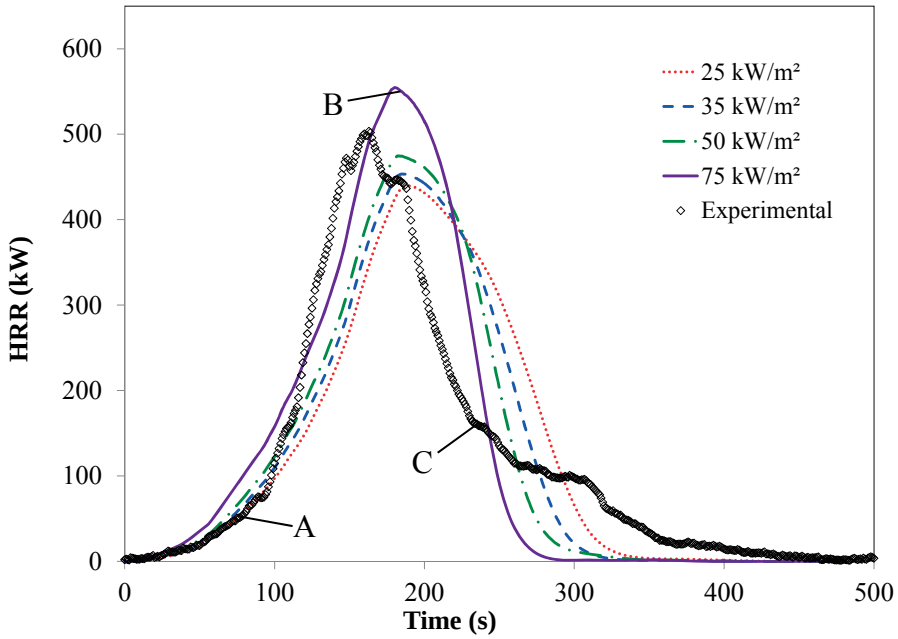

Figure 5-25 Comparison of experimental heat release rate with convolution model results for test EE4-1.

Plots of the remaining tests in the EE4 series can be found in Appendix G. As seen in Figure 5-25 the convolution model does a reasonable job of predicting the early stages of the fire, however the decay phase of the fire is not adequately modeled using the convolution model. For the first 100 seconds of the fire, the HRR curve closely follows the 25 kW/m^2 curve ("A" in Figure 5-25), after 100 s the HRR accelerates past all four convolution model HRR curves to its peak at 161 s ("B" in Figure 5-25). After the peak, the experimental HRR rapidly decays to 163 kW at 230 s ("C" in Figure 5-25) where the decay continues at a decreased rate until extinction. This behavior is close in character to what was seen in the thicker of the center ignition tests, namely configurations C2 through CC4.

Comparing the measurements found in Table 5-2, the average experimental peak HRR for the EE4 test configuration of 486 kW was most closely modeled by the 50 kW/m^2 convolution model result of 494 kW. The time to peak HRR of 173 s was once again lower than

all four of the convolution model results (the closest being the 75 kW/m^2 result of 182 s). Finally, the average experimental THR value for the EE4 test configuration of 57.9 MJ was most closely modeled by the 35 kW/m^2 convolution result of 57.6 MJ.

5.4. Discussion of Convolution Model Evaluation

One of the most significant findings of this evaluation was that for some specific test configurations the convolution model predicted both the growth and decay phases of the experimental HRRs, whereas the convolution model failed to capture the behavior of the decay phase of others. Specifically, the convolution model did a good job of predicting both the growth and decay phases of the following test configurations: C1 (center ignition, 2.5 cm thick), E1 (edge ignition, 2.5 cm thick), E2 (edge ignition, 5.0 cm thick), E3 (edge ignition, 7.5 cm thick) and E4 (edge ignition, 10.0 cm thick). On the other hand, the convolution model only successfully modeled the growth behavior of test configurations C2 (center ignition, 5.0 cm thick), C3 (center ignition, 7.5 cm thick), C4 (center ignition, 10.0 cm thick), CC4 (center ignition large specimen, 10.0 cm thick) and EE4 (edge ignition, large specimen, 10.0 cm thick).

In test configurations C2, C3, C4, CC4 and EE4 the decay phase of the HRR curve exhibits a rapid drop in HRR soon after the peak HRR is reached. Once the decay reaches 1/2 to 1/3 of the peak HRR value, the decay rate moderates into a longer sustained phase until the fire reaches extinction. The convolution model completely misses this behavior predicting instead a more sustained heat release at the peak value followed by a rapid, nearly-linear decay slowing slightly just before extinction.

A possible cause for this discrepancy involves the flame spread geometry of the C2, C3, C4 and CC4 test configurations. When reviewing the video footage from these tests, it is seen

that as the HRR approaches its peak value, the ignition location on the mattress has not yet reached extinction, and a large portion of the mattress is burning (see left panel of Figure 5-26).

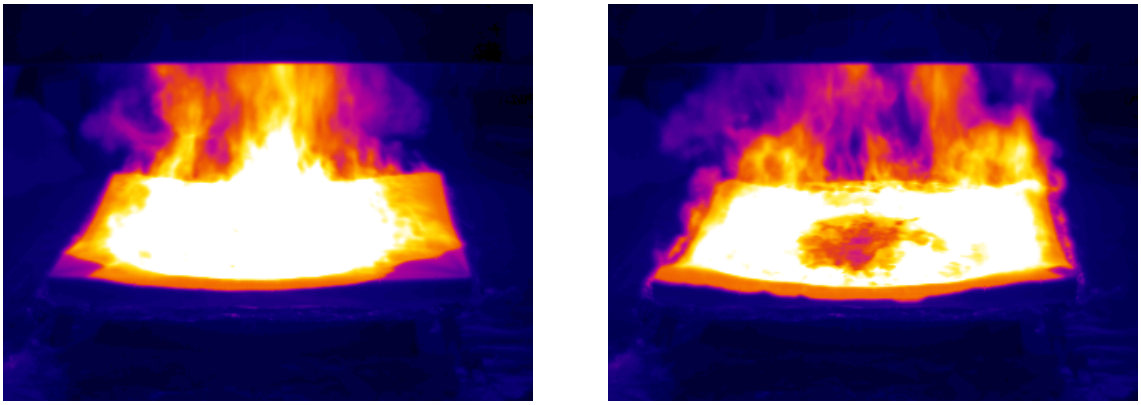

Figure 5-26: IR images taken during center ignition test of 1.2 by 1.2 m by 10 cm polyurethane foam specimen CC4-3 showing extinction of ignition location (left – 143 s, right – 163 s).

The photo shown in the left panel of Figure 5-26 shows specimen CC4-3 near its peak HRR. At this point extinction of the mattress has not begun. Shortly after this a rapid extinction of the center of the mattress occurs (shown in the right panel of Figure 5-26). When comparing this behavior to the experimental HRR curve, it is seen that this extinction behavior is where the sharp drop in HRR occurs. Comparing the predicted HRR curves to this shape it is seen that this behavior is missed completely (see Figure 5-27 below).

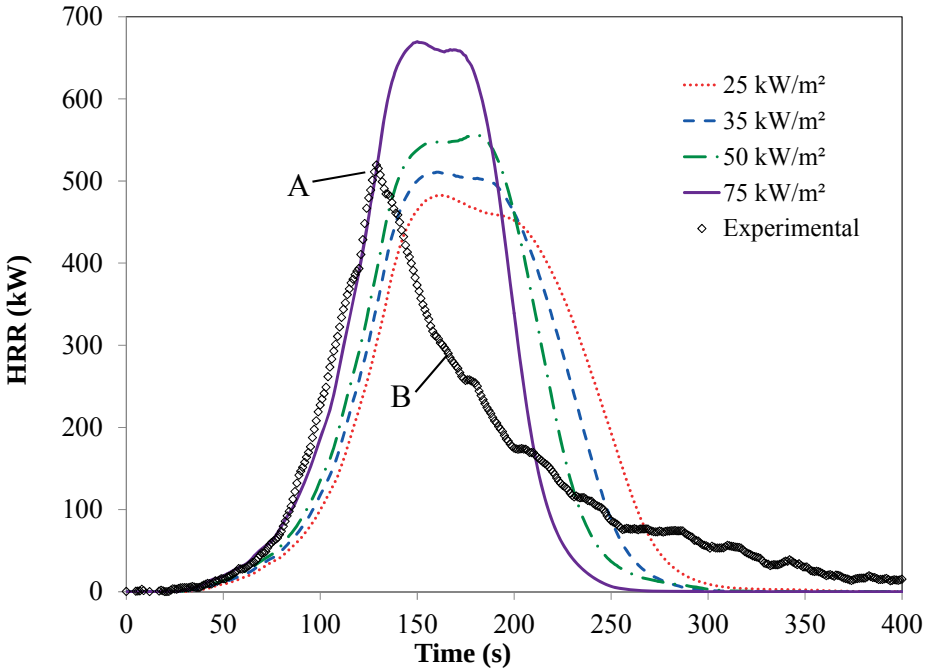

Figure 5-27 Comparison of experimental heat release rate with convolution model results for test CC4-3. A – experimental peak HRR. B – rapid extinction behavior.

As was discussed earlier, the CBUF model assumes that the rate of extinction of the foam in the full scale tests will match the rate of extinction of the cone calorimeter specimen. The result shown in Figure 5-27 suggest that the physics of the extinction on this type of specimen are sufficiently different from the cone calorimeter test that the CBUF model fails to predict the character of the decay phase of the fire. In light of this, future development of a flame spread model may need to incorporate a term which augments the decay of the cone calorimeter specimen to more closely model the behavior of thicker, center ignition specimens.

A similar behavior is seen with the EE4 test configuration. This is likely due to the fact that the EE4 specimen is wider (120 cm rather than 60 cm), and the fire experiences a much more semi-circular growth pattern than the other edge ignition specimens as was discussed in the experimental results section. This is illustrated below in Figure 5-28 and Figure 5-29.

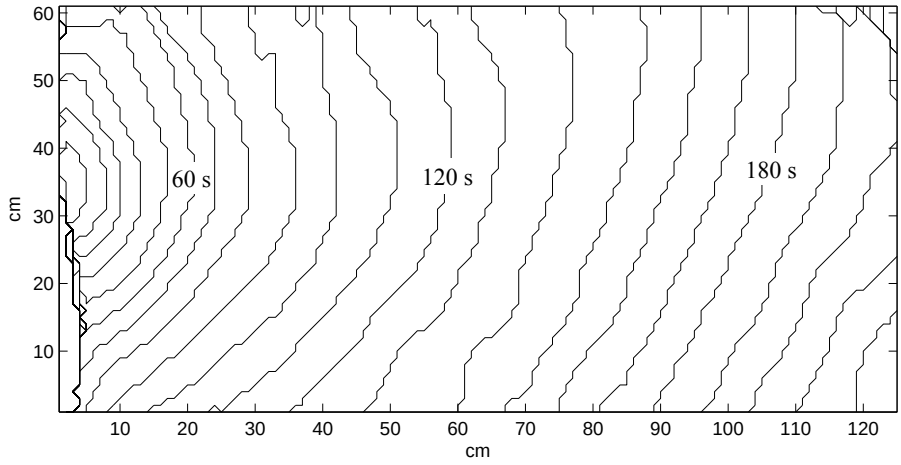

Figure 5-28 Flame spread contours for test E4-3 in 10 s increments.

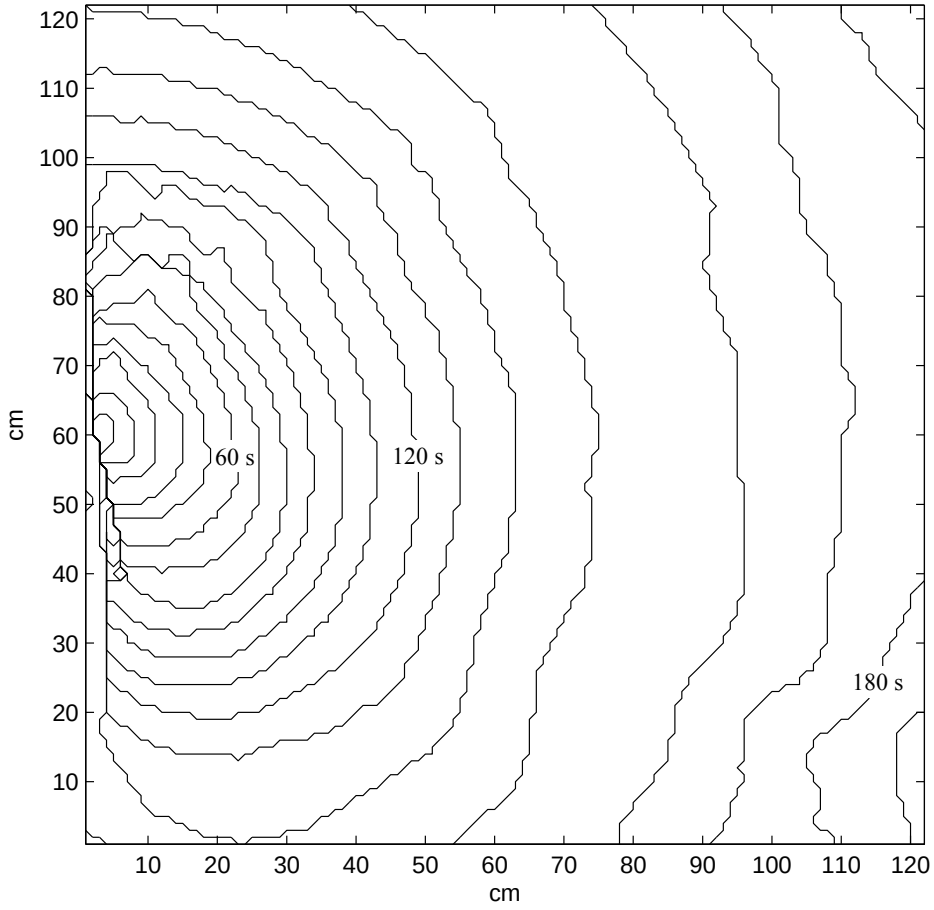

Figure 5-29 Flame spread contours for test EE4-3 in 10 s increments.

Shown in Figure 5-28, the flame front on specimen E4-3 reaches the edge of the specimen after approximately 60 s, subsequently the flame front reaches the end of the specimen at approximately 230 s. For specimen EE4-3 on the other hand, the flame front reaches the edge of the specimen after 130 s and the end of the specimen after 180 s. Put in terms of percentages, in test E4-3 the flame front spread is a semicircle for 26% of the time it took to reach the end of the specimen, whereas in test EE4-3 the flame front spread as a semicircle 72% of the time it took to reach the end of the specimen.

Since the CBUF model uses cone calorimeter data from a single incident heat flux setting, it would make sense that it does not capture the rapid peak and subsequent rapid extinction that is experienced by the C2, C3, C4, CC4 and EE4 test configurations. A possible improvement to the convolution model could involve incorporating cone calorimeter data from several incident heat flux settings. This could allow the model to take into account the rapid acceleration and subsequent rapid decay of these specimens. A possible implementation of this type of model will be discussed in greater detail in the next section.

As was discussed in Section 3.3.2, another factor that may be contributing to the difference in center and edge ignition configuration predictions is that the ignition location and subsequent burning patterns produce different boundary conditions. For the center ignition specimens, for much of the duration of the test, the burning area of the specimen is surrounded by unburned foam, insulating the fire and increasing temperatures. On the other hand, a much larger portion of the edge ignition specimens is exposed to the surroundings. In this way, since the cone calorimeter specimens were burnt without an edge frame, the boundary conditions of the cone calorimeter tests are more similar to those of the edge ignition specimen. This may also be the case when comparing the predictions of thick and thin foams. During much of the test, the

burning portion of thicker edge ignition specimens will be insulated on the bottom by the unburned foam beneath it.

Also discussed in Section 3.3.2 was the fact that thicker specimens appeared to produce larger actively burning areas than thin foams. This was attributed to the fact that a given area in a thick specimen will have a longer burning duration than a thinner specimen. This increased burning area of thicker specimens resulted in a larger fire and as a result higher heat fluxes to the foam ahead of the flame.

One of the major objectives of this research was to examine the effect of cone calorimeter incident heat flux setting on convolution model predictions and to examine which heat flux setting should be used depending on the needs of the end user. The results of this research indicate that the selection of an incident heat flux setting will depend heavily on the geometry and ignition location of the specimen being tested. For instance, in the case of peak HRR for edge ignition specimens, configurations E1, E2 and E4 were most closely modeled by the 75 kW/m^2 convolution results whereas the E3 and EE4 were most closely modeled by the $50kW/m^2$ convolution results. In the case of center ignition tests, the peak HRR was best predicted by the 35 kW/m^2 convolution results for the C1 and C2 configurations, by the 50 kW/m^2 convolution results for the C3 and CC4 configurations, and by the 75 kW/m^2 convolution results for the C4 test configuration

For THR predictions, with the exception of the EE4 test configuration, the convolution model over predicts the THR for all test configurations. It was found that either the 35 kW/m^2 or the 50 kW/m^2 incident heat flux settings would produce an appropriate conservative THR prediction for all of the test configurations. Overall, the results of this thesis show that the specimen thickness and geometry are important to consider when selecting an incident heat flux

for the CBUF model, i.e. there is not a single heat flux setting that will provide a good prediction for all fire scenarios.

In this evaluation of the predictive capability of the convolution model, it was found that the model does a good job of predicting the growth phase of the fire and parameters such as peak HRR and THR, and that in certain configurations (center ignition and thicker specimens) the model does not predict decay as well. This raises the question of what is the relative importance of these fire parameters. In other words, if one can predict the growth phase and peak HRR values, do they need to worry about the decay phase? To understand this one must look at the contexts in which this type of data might be used. As previously mentioned, one context that this type of data might be used is in a regulatory context where a set of criteria are set out such as the American mattress regulation 16 CFR Part 1633 [4] where a maximum HRR of 200 kW is defined and the THR for the first 10 minutes of the test must not exceed 15 MJ. In this context the convolution model could perform adequately since the peak HRR and THR are modeled relatively well using this technique. One caveat in this context is that although the THR for the duration of the test is modeled relatively well, for the center ignition tests it does not characterize all of aspects of the HRR curve. As was previously discussed, in center ignition tests the convolution model incorrectly predicts a period of sustained peak HRR where the experimental result shows a sharp peak followed by a slower decay. This would not be an issue for the specimens used in this research since all tests were extinguished before the 10 minute threshold, however if a mattress design had a tendency to burn for longer durations this could pose a problem. The sustained peak predicted by the convolution model places a portion of heat release earlier in the test than the experimental results. In light of the 10 minute heat release threshold, the convolution model could fail a specimen that otherwise would pass a test of this sort. That

said, in this context the convolution model would provide a conservative estimate of the 10 minute heat release.

Another context in which this type of data might be used is in a computational fire model such as FAST/CFAST or FDS [39] in a single or multiple compartment fire simulation. One of the required inputs for this type of model is a HRR curve that represents the heat released from a fire. Once again in this context, the utility of refining the shape of the decay phase of the convolution model is limited. One of the uses of this type of model is to evaluate the time until a given space is rendered untenable by a fire. In many cases this is considered to be the time to room flashover. There are a number of factors that determine when a room will reach flashover but a heat release of 1000 kW will lead to flashover in a typical residential room [4]. In this context if a burning item in a room reaches its peak HRR below 1000 kW and begins its decay phase, its primary hazard is as an ignition source for other fuels in the vicinity. That said, if a small burning item does not ignite nearby fuel at its peak HRR, it is unlikely that it will act as an ignition source during the extended decay phase that is not captured by the convolution model. A final scenario that can be mentioned is the prediction of activation times for fire detection systems. With this type of test, the detection of the fire should occur early in the fire well before the decay phase of the fire would be encountered. In this case models using the area convolution method may be appropriate.

It seems that the primary utility of refining the CBUF model further would be to better understand the physics of what takes place during the combustion of polyurethane foam. This fuller understanding could prove useful in the context of more complex fire scenarios involving multiple burning items and upholstered furniture.

5.5. Variable Heat Flux Convolution Model

In order to test the hypothesis that a variable heat flux convolution model could predict full scale fire behavior, the convolution model code was modified to use all four of the cone calorimeter HRR density curves in its calculation. To do this, the modeled HRR from previous time steps was used as the selection criteria to determine which HRR density curve was used as input for the CBUF model. For stability reasons the HRR output was averaged over the previous five seconds. Four thresholds were chosen so that this modification to the code could be observed in a variety of test configurations. In this case the thresholds were chosen arbitrarily, however a more thorough implementation should involve the use of correlations which estimate the heat fluxes from pool fires based on fire HRR in order to select the incident heat fluxes at which cone calorimeter data are used for input. For HRRs below 30 kW the convolution model used the 25 kW/m^2 HRR density data as input, for HRRs between 30 kW and 60 kW the convolution model linearly interpolated HRR density data between the 25 kW/m^2 and 35 kW/m^2 HRR for input, for HRRs between 60 kW and 80 kW the convolution model linearly interpolated between the 35 kW/m^2 and 50 kW/m^2 HRR density data, for HRRs between 80 kW and 200 kW the convolution model linearly interpolated between the 50 kW/m^2 and 75 kW/m^2, and for HRRs above 200 kW the convolution model used HRR density data from the 75 kW/m^2 cone tests.

To observe the changes that this modification provided, this model was run using two sets of full scale test data: C4-2 and CC4-2. These tests were selected for demonstration purposes since the differences between predicted and measured results were largest for the thicker center ignition specimens. Figure 5-30 shows a comparison of the variable heat flux convolution model result for test C4-2 and the experimental result as well as the four single-heat flux convolution results.

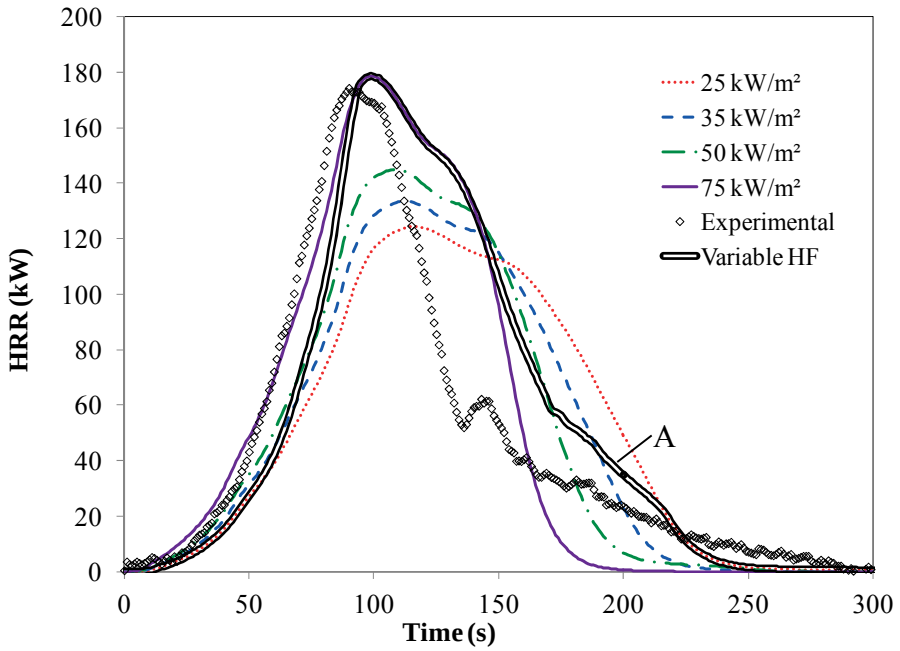

Figure 5-30 Comparison of experimental heat release rate and single heat flux convolution results with variable heat flux convolution model results for test C4-2. A – sustained decay behavior.

The variable heat flux result for test C4-2, as seen in Figure 5-30, stays within the bounds of the single heat flux convolution results. Looking at the growth phase, although this new curve lags behind the experimental curve, it appears to exhibit a more similar shape to the experimental results than the single heat flux convolution results. Another interesting characteristic is that the variable heat flux convolution introduces a sustained decay phase ("A" in Figure 5-30) which more closely mimics the experimental results.

Figure 5-31 shows the same comparison that was made in Figure 5-30 for test CC4-2.

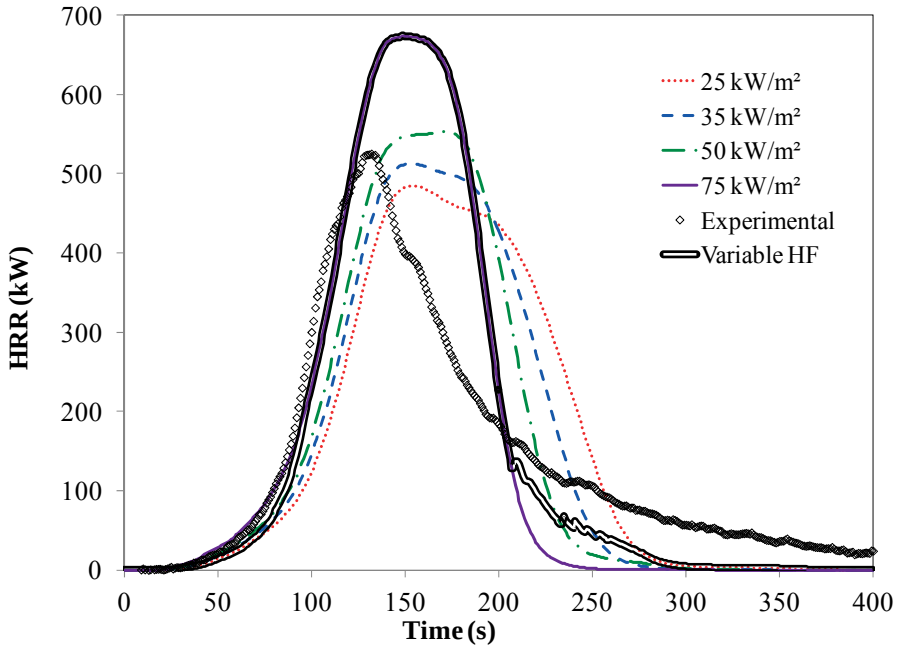

Figure 5-31 Comparison of experimental heat release rate and single heat flux convolution results with variable heat flux convolution model results for test CC4-2.

In a similar fashion to test C4-2, the variable heat flux convolution alters the shape of both the growth and decay phases of the HRR curve. A promising characteristic of the variable heat flux convolution is the late stage of the decay phase of the fire. In the single heat flux convolutions, the decay phase is quite a sharp decline and then just before extinction, a slight leveling out. The variable heat flux convolution on the other hand shows a much more pronounced extended extinction process similar to what is seen in the experimental results.

Unfortunately, the beginning of the decay phase of the fire does not show the same promise. Where the experimental HRR takes a sharp drop shortly after the peak HRR, none of the convolution models are able to mimic this behavior. All of the single heat flux CBUF model results show an extended peak HRR followed by a delayed rapid decay. The variable heat flux convolution shows a very similar characteristic to the single heat flux convolution results since the variable heat flux convolution is unable to produce HRR curves that are outside of the

bounds of the single heat flux convolutions. This is seen in how at no time does the variable heat flux curve rise higher than the highest single heat flux convolution or lower than the lowest single heat flux convolution. This is important to note because if the experimental curve lies outside of the range of HRRs predicted by the single heat flux convolutions, it cannot be predicted better using this style of variable heat flux convolution.

One of the assumptions that the CBUF model makes is that a given area of a full scale specimen will extinguish at the same time as the cone calorimeter test that is used as input. Seeing the difficulty that the convolution model has in predicting the decay phase of thicker center ignition specimens suggests that for these configurations, the decay assumption has limited validity. In light of this it may be beneficial to augment the decay phase assumption with some sort of decay parameter that mimics the decay properties of these tests. A place to begin with this development would be to study the extinction of the full scale specimens. This could be accomplished by examining the infrared footage from the full scale tests and establishing a temperature threshold at which the area would be considered to be extinguished.

When comparing the total heat released for the two tests that were examined using the variable heat flux convolution, it was seen that the variable heat flux convolution tended to over predict the total heat released when compared to the experimental result. For test C4-2 the experimental THR was 14.2 MJ, the highest prediction for the single heat flux convolutions was the 75 kW/m^2 test at 15.2 MJ, and the variable heat flux convolution predicted the THR at 16.4 MJ. Similarly, for test CC4-2 the experimental THR was 57.3 MJ, the highest prediction for the single heat flux convolutions was the 75 kW/m^2 test at 60.7 MJ, and the variable heat flux convolution predicted the THR at 62.9 MJ.

Overall the CBUF model shows promise. Thinner specimens and those ignited at the edge showed particular promise. In these tests the convolution model was able to predict commonly used fire protection engineering parameters well and characterized the shape of the HRR curve from ignition to extinction. For these tests it may be appropriate to move on to the development of a flame spread model for input into the CBUF model. The development of the area spread rate model would allow the CBUF model to stand alone without the need for input from full scale tests.

For the thicker specimens and those ignited at the center, the convolution model had more difficulty particularly in the decay phase where the convolution model missed the sharp decay that occurs immediately after the peak. For these configurations it may be necessary to augment the modeling of the decay phase of the fire. Once it is found that the decay phase of the fire can be modeled satisfactorily the flame spread model could also be tested with the thicker and center ignited specimens.

CHAPTER 6 : CONCLUSIONS AND FUTURE WORK

The focus of this thesis has been to improve the understanding of the relationship between full and small scale testing of mattresses, through the continued study of the fire behavior of flexible polyurethane foam. This was accomplished by contributing to the body of furniture calorimeter and cone calorimeter data that have been collected on this material, and by the continued analysis of the CBUF model which aims to predict full scale fire behavior based on bench scale test results.

6.1. Conclusions

The following list of conclusions corresponds to the objective numbers listed in Section 1.3. The first four objectives were related to the collection and analysis of experimental data.

1. The cone calorimeter tests indicated that incident heat flux setting has a significant effect on the outcome of cone calorimeter tests, higher incident heat fluxes producing higher peak HRR densities and shorter burning durations. These tests also revealed that the polyurethane foam being studied in this research exhibited a distinct two stage burning behavior that has been observed in the burning behavior of polyurethane foam by other researchers in the field.
2. The growth phase of the HRR curves from the furniture calorimeter tests were very similar for a given test configuration, and overall the tests show very good repeatability. It was seen that the foam thickness has a significant effect on the peak HRR for these tests. It was also seen that the ignition location had significant effect

on the character of the HRR curve. The center ignition tests produced a sharper peak and subsequent rapid decay, whereas the edge ignition specimens showed a more sustained peak heat release.

3. It was found that both foam thickness and ignition location had an effect on the flame spread behavior on the foams. The thicker foams tended to show a more rapid flame spread than the thinner foams. The center ignition tests showed a more non-linear flame spread behavior than the edge ignition tests.
4. It was found that the results of the foam aging cone calorimeter tests conducted over a nine month period were not different enough to draw strong conclusions about the effect of foam aging on fire behavior.

The last three objectives of this research focused on the evaluation of the CBUF model.

5. It was found that the CBUF model tended to be more successful at predicting the growth phase of the fires than the decay phase. It was seen that the CBUF model did a better job of predicting the fire behavior of thinner foams than thicker foams. It was also seen that the convolution model predicted the HRR curve more accurately for edge than center ignition tests.
6. The modeling that was done in this research quantified the effect that the cone calorimeter incident heat flux setting has on prediction made by the CBUF model using the cone calorimeter data as input. The results of this research showed that a single heat flux cannot be recommended for a broad range of ignition locations and specimen dimensions, rather these parameters would need to be taken into account when selecting an incident heat flux for the modeling of a particular full scale test.

7. In an attempt to improve the predictions of the CBUF model, the model was modified to take as input multiples sets of cone calorimeter data with varying incident heat flux settings. This variable incident heat flux convolution model showed promise in improving predictions in the later stages of the fire decay, however the model still had difficulty predicting the early stages of decay which occur soon after the peak HRR. It was found that this modification to the CBUF model did not improve predictions of the peak HRR value, however it did produce a growth curve that followed the experimental data more closely.

6.2. Future Work

During the course of this research, a number of items were identified that would be beneficial for the continuation of this research. These items are outlined below.

- The foam aging series of cone calorimeter testing should be continued. The foam aging testing that was conducted for this thesis did not identify any strong characteristic associated with foam aging. Specimens prepared at the time of the original foam aging test series are still available for testing. It is recommended that testing be conducted on these specimens to further characterize the effect of aging on the fire performance of this material. Future testing in this area could involve accelerated aging with techniques such as exposure to concentrated ultraviolet light.
- The remaining furniture calorimeter tests should be modeled using the variable heat flux convolution model. Continued development of the variable heat flux CBUF model could involve collapsing HRR density curves for the various thicknesses and incident heat flux settings into a single curve of normalized HRR

density versus normalized time that could be expanded back into the appropriate HRR density at the current time step. This approach is similar to a model by Dietenberger as cited by Babrauskas [23].

- A procedure for the selection of incident heat flux settings when using cone calorimeter data for input into the furniture calorimeter should be developed. This could involve parameters such as the thickness, ignition location and surface area of the full scale specimen to be modeled.

In this research, some topics were identified that would be interesting areas for future research, and would build well on this research. These topics are outlined below.

- An independent, idealized flame spread model should be developed for use with the CBUF model. The independent flame spread model should function without any input from a full scale test. This would allow the CBUF model to operate as a fully predictive model. This flame spread model will likely need to take into account parameters such as specimen ignition location and thickness. One possible type of model could take a parameter such the HRR at the previous time step and adjust the flame spread rate to mimic the faster flame spread seen in the thicker foams. Another parameter that may be beneficial to study when developing a flame spread model is the effect of pre-heating ahead of the flame front for full scale tests. This could be studied in a number of ways: The existing infrared footage could be analyzed to characterize the foam surface temperature ahead of the flame front. Further full scale furniture calorimeter tests could be conducted and heat flux gauges could be used to measure the radiant heat flux imposed ahead of the flame front. Finally, correlations and models, such as the

CBUF III model could be explored in an attempt to predict the amount of foam preheating that occurs.

- A study of the heat transfer characteristics of this polyurethane foam should be conducted to better understand the multi-dimensional heat transfer that occurs during the burning process and how much of an effect this might have on flame spread behavior. In the same way that surface preheating may accelerate the surface flame spread rate, the heat transfer through the thickness of the foam as the fire intensifies may act to accelerate the collapse and pyrolysis of the foam in a full scale scenario. Future work on a flame spread model could also study the rate of flame spread along the sides of the full scale specimens during the furniture calorimeter tests. It was noted in this research that in thicker specimens, an inflection in the HRR curve appears to occur around the time that the flame reaches the edge of the foam specimen. It was also noted that for thicker specimens, the area of the sides of the full scale specimens accounts for a significant portion of the total foam surface area. To fully characterize the HRR curve for thicker foam specimens using the CBUF model, it may be necessary to incorporate flame spread along the sides of the specimen into the model. It should be noted that special care should be taken when incorporating the burning area of the sides of the specimen. Unlike the surface differential burning areas, the side burning areas are not associated with a unique volume of material. If the specimen side area is incorporated into the CBUF model without adjustment to the model, it will likely result in an over-prediction of the total heat released from the specimen.

- Development of a flame spread model could benefit from a study of the rate at which the foam in the full scale extinguishes. This could be accomplished by studying the infrared video of the full scale fire tests. The assumption of the CBUF model is that a differential burning area of the specimen will stop contributing to the heat release of the fire at the same time as the corresponding cone calorimeter specimen extinguishes. Due to differences in boundary conditions and heat fluxes to the unburned foam, it is expected that this assumption may not be valid for thicker specimens.
- The cone calorimeter test series that were performed in this research were composed of three individual tests. This is the minimum recommended by cone calorimeter test standards. This research could benefit from an extended study of a single test configuration in order to better characterize the repeatability of cone calorimeter tests of this polyurethane foam.

REFERENCES

[1] E. Marotta, *Fire Losses in Canada.* Ottawa, ON.: Canadian Council of Fire Marshals and Fire Commissioners, 2002.

[2] K. Rohr, *Products First Ignited in U.S. Home Fires.* Quincy, MA: National Fire Protection Association, 2005.

[3] Underwriters Laboratories of Canada, *CAN/ULC-S137-07. Standard Method of Test for Fire Growth of Mattresses (Open Flame Test).* Toronto, ON: 2007.

[4] U.S. Consumer Product Safety Commission, *Code of Federal Regulations (CFR) 1633, Standard for the Flammability (Open Flame) of Mattress Sets.* Bethesda, MA: 2006.

[5] American Society for Testing and Materials, *ASTM E 1590 Standard Test Method for Fire Testing of Mattresses.* West Conshohocken, PA: 2007.

[6] U.S. Consumer Product Safety Commission, *Code of Federal Regulations (CFR) 1632, Standard for the Flammability of Mattresses and Mattress Pads.* Bethesda, Maryland: 2006.

[7] Canadian General Standards Board, *CAN/CGSB 4.2 NO.27.7-M89 Textile Test Methods - Combustion Resistance of Mattresses - Cigarette Test.* Ottawa, ON: 2002.

[8] A. J. Peacock, *Polymer Chemistry: Properties and Applications.* Munich: Hanser Gardner Publications, 2006.

[9] American Society for Testing and Materials, *ASTM E 162 Standard Test Method for Surface Flammability of Materials using a Radiant Heat Energy Source.* West Conshohocken, PA: 2002.

[10] American Society for Testing and Materials, *ASTM E 1474 Standard Test Method for Determining the Heat Release Rate of Upholstered Furniture and Mattress Components Or Composites using a Bench Scale Oxygen Consumption Calorimeter.* West Conshohocken, PA: 2004.

[11] D. Lide, Ed., *A Century of Excellence in Measurements, Standards, and Technology A Chronicle of Selected NBS/NIST Publications 1901-2000.* Washington, DC: U.S. Government Printing Office, 2001.

[12] D. Drysdale, *An Introduction to Fire Dynamics.* Second Edition. Chichester, UK: Wiley Interscience, 1999.

[13] International Organization for Standardization, *ISO 9705 Fire Tests - Full Scale Room Test for Surface Products.* Geneva: 1993.

[14] R. Krämer, M. Zammarano, G. Linteris, U. Gedde and J. Gilman, "Heat release and structural collapse of flexible polyurethane foam," *Polymer Degradation and Stability,* 95, 1115-1122, 2010.

[15] K. Prasad, R. Kramer, N. Marsh, M. Nyden, T. Ohlemiller and M. Zammarano, "Numerical simulation of fire spread on polyurethane foam slabs," in *11th International Fire and Materials Conference,* Jan. 26-28, San Francisco, CA, 2009, 697-708.

[16] K. Butler, "A model of melting and dripping thermoplastic objects in fire," in *11th International Fire and Materials Conference,* Jan. 26-28, San Francisco, CA, 2009, 341-352.

[17] H. Saber, A. Kashef, A. Bwalya and G. Lougheed, "Numerical and experimental investigations of fire behaviour due to polyurethane foam and wood cribs in a medium-sized residential room," National Research Council of Canada, Ottawa, ON, Tech. Rep. 291, 2010.

[18] B. Sundström, *CBUF: Fire Safety of Upholstered Furniture: The Final Report on the CBUF Research Programme.* London: European Commission Measurements and Testing, 1996.

[19] Wickstrom, U., Goransson, U., "Full-Scale/Bench-Scale Correlations of Wall and Ceiling Linings," *Fire and Materials,* 16, 15-22, 1992.

[20] T. Threlfall and D. Torvi, "Temperature measurements in full-scale fire tests of mattresses," in *Combustion Institute Canadian Section, Spring Technical Meeting,* May 15-18, Halifax, NS, 2005, 66-71.

[21] M. Hurd, D. Torvi, E. Weckman and E. Enninful, "Small and full scale fire testing of polyurethane foams for mattresses," in *Combustion Institute Canadian Section, Spring Technical Meeting,* May 14-16, Banff, AB, 2007, (Paper No. F1, 6 pages).

[22] J. Ezinwa, *Modeling Full-Scale Fire Test Behavior of Polyurethane Foams using Cone Calorimeter Data.* Saskatoon, SK.: MSc Thesis, University of Saskatchewan, 2009.

[23] V. Babrauskas, "Specimen heat fluxes for bench-scale heat release rate testing," in *Interflam '93,* Mar. 30 – Apr. 1, Oxford, 1993, 57-74.

[24] J. Ezinwa, J. Rigg, D. Torvi and E. Weckman, "Effects of ignition location on flame spread and heat release rates in furniture calorimeter tests of polyurethane foams," in *11th International Fire and Materials Conference,* Jan. 26-28, San Francisco, CA, 2009, 645-656.

[25] L. D. Robson, M. R. Obach, J. Riggs, J. U. Ezinwa, D. A. Torvi and E. J. Weckman, "The effect of polyurethane foam thickness on flame spread and heat release rates measured in cone and furniture calorimeter tests," in *12th International Fire and Materials Conference,* Jan. 31 – Feb. 2, San Francisco, 2011, 309-320.

[26] V. Babrauskas and S. J. Grayson, *Heat Release in Fires.* London: E & FN Spon, 1996.

[27] M. Rezazadeh, *Evaluation of Performance of in-use Firefighters' Protective Clothing using Non-Destructive Tests.* Saskatoon, SK: Ph.D Thesis, University of Saskatchewan, 2014.

[28] American Society for Testing and Materials, *ASTM E 104 Standard Practice for Maintaining Constant Relative Humidity by Means of Aqueous Solutions.* West Conshohocken, PA: 2007.

[29] J. Ezinwa, D. Torvi and E. Weckman, "Full-scale fire modeling of polyurethane foams using cone calorimeter data," in *Combustion Institute Canadian Section Spring Technical Meeting,* May 11-13, Montreal, QC, 2009, 43-48.

[30] L. Robson, M. Obach, J. Ezinwa, D. Torvi and E. Weckman, "Fire modeling of polyurethane foams using convolution integral formulation," in *Combustion Institute Canadian Section Spring Technical Meeting,* May 9-12, Ottawa, ON, 2010, 196-201.

[31] M. DiDomizio and E. Weckman, "Ignition source heat release rates," *Personal E-Mail,* July 7, 2011.

[32] E. Pastor, A. Àgueda, J. Andrade-Cetto, M. Muñoz, Y. Pérez and E. Planas, "Computing the rate of spread of linear flame fronts by thermal image processing," *Fire Safety Journal,* 41, 569-579, 2006.

[33] R. Hartley and A. Zisserman, *Multiple View Geometry in Compute Vision.* Cambridge: Cambridge University Press, 2003.

[34] The MathWorks Inc. (April 27, 2011). *R2011a MathWorks Documentation - MathWorks - matlab and Simulink for Technical Computing*. Available: http://www.mathworks.com/help, last accessed July 13, 2014.

[35] C. A. Wilkie and A. B. Morgan, *Fire Retardancy of Polymeric Materials.* Second Edition, Boca Raton, FL: CRC Press, 2010.

[36] J. Krasny, W. J. Parker and V. Babrauskas, *Fire Behavior of Upholstered Furniture and Mattresses.* Park Ridge, N.J.: Noyes Publications, 2001.

[37] L. Robson, M. Obach, D. Torvi and E. Weckman, "Effects of Variations in Incident Heat Flux When Using Cone Calorimeter Test Data for Prediction of Full-Scale Heat Release Rates of Polyurethane Foam," *Fire and Materials* (in press).

[38] M. Hurd, D. Torvi, E. Weckman and E. Enninful, "Effects of polyurethane mattress foam properties and geometry on small and large-scale fire test results," in *10th International Fire and Materials Conference,* Jan. 29-31, San Francisco, CA, 2007, CD-Rom (13 pages).

[39] The National Institute of Standards and Technology. (March 24, 2014). *Fire modeling programs*. Available: http://www.nist.gov/el/fire_protection/buildings/fire-modeling-programs.cfm, last accessed July 13, 2014.

APPENDIX A: MANUAL AREA SPREAD RATE VERIFICATIONS

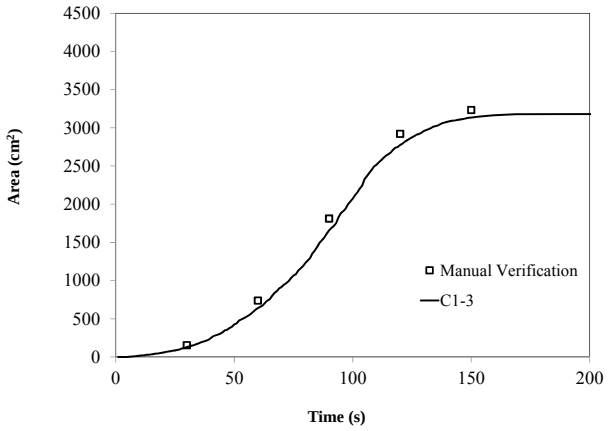

Figure A-1 Comparison of flame area measurements recorded using the automated code and measurements recorded manually for test C1-3.

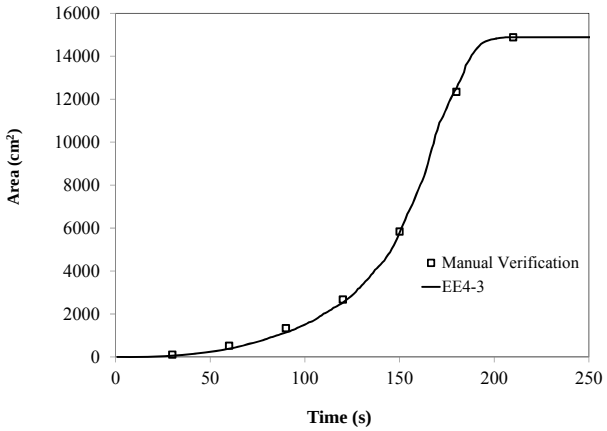

Figure A-2 Comparison of flame area measurements recorded using the automated code and measurements recorded manually for test C2-2.

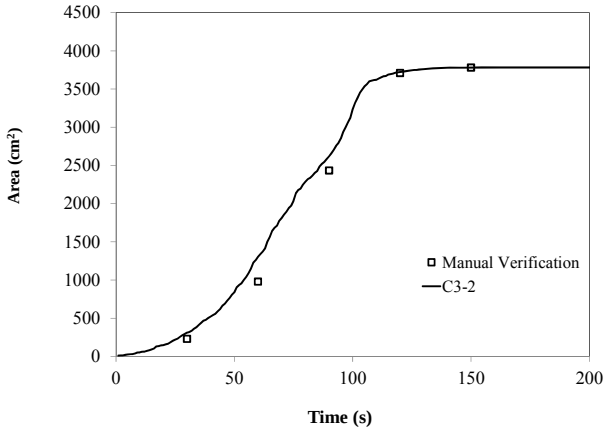

Figure A-3 Comparison of flame area measurements recorded using the automated code and measurements recorded manually for test C3-2.

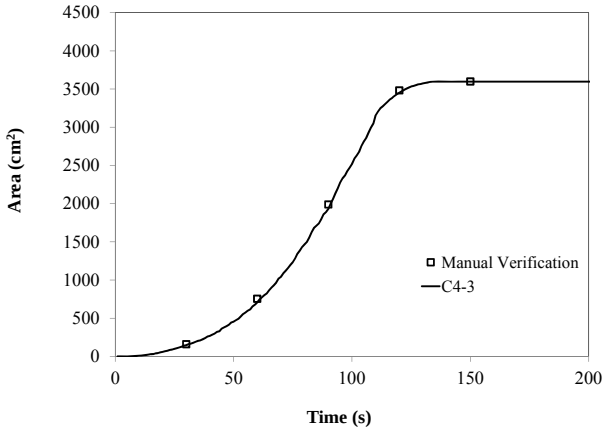

Figure A-4 Comparison of flame area measurements recorded using the automated code and measurements recorded manually for test C4-3.

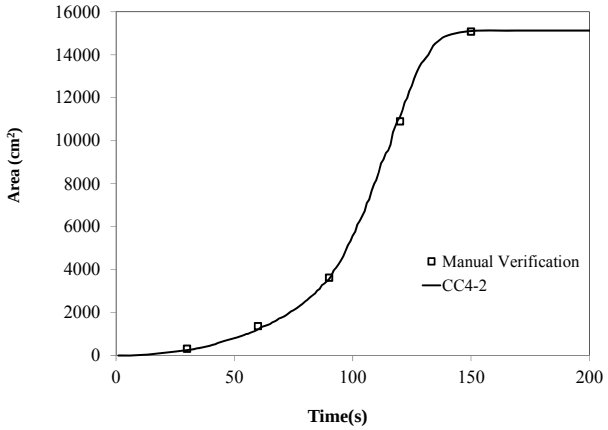

Figure A-5 Comparison of flame area measurements recorded using the automated code and measurements recorded manually for test CC4-2.

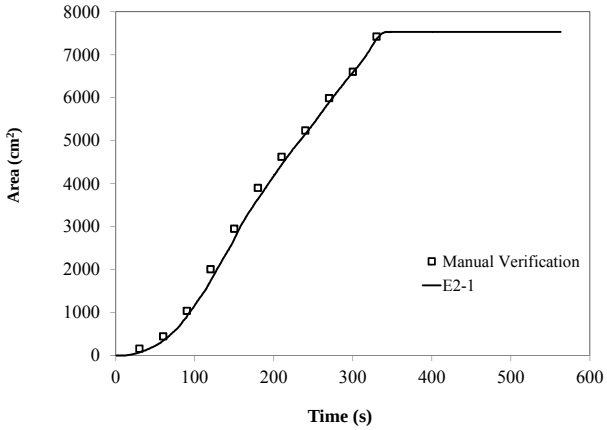

Figure A-6 Comparison of flame area measurements recorded using the automated code and measurements recorded manually for test E2-1.

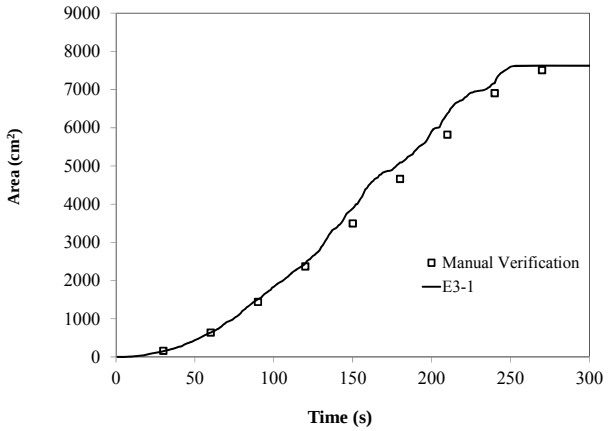

Figure A-7 Comparison of flame area measurements recorded using the automated code and measurements recorded manually for test E3-1.

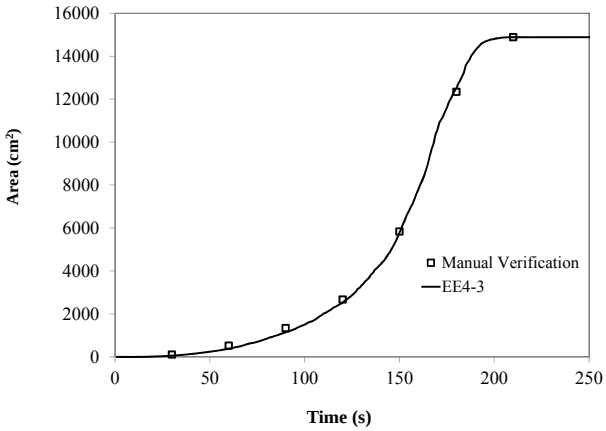

Figure A-8 comparison of flame area measurements recorded using the automated code and measurements recorded manually for test EE4-3.

APPENDIX B: CONE CALORIMETER HRR DENSITY DATA

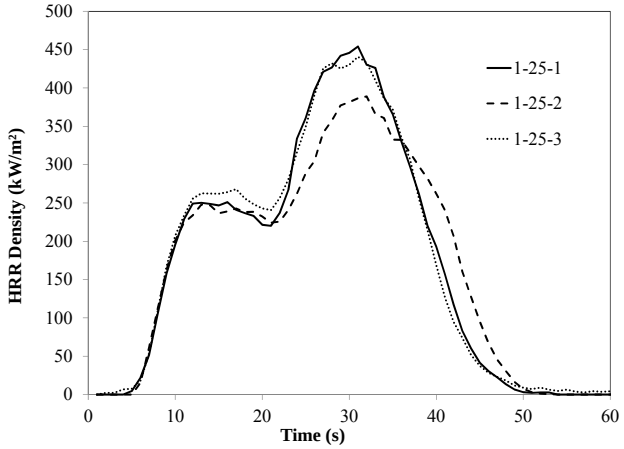

Figure B-1 Heat release rate density measurements in tests of 2.5 cm thick foam specimens exposed to incident heat flux of 25 kW/m^2.

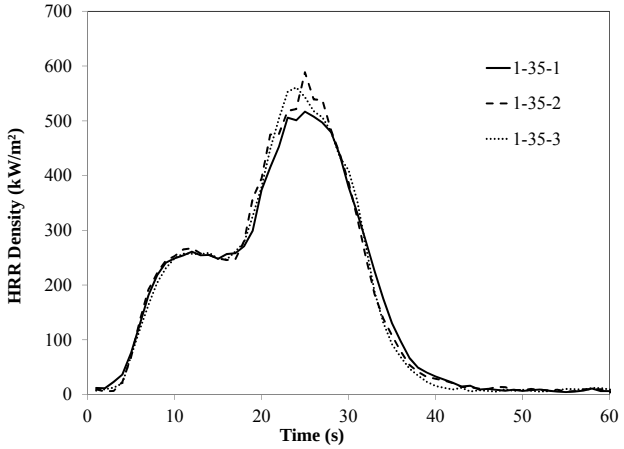

Figure B-2 Heat release rate density measurements in tests of 2.5 cm thick foam specimens exposed to incident heat flux of 35 kW/m^2.

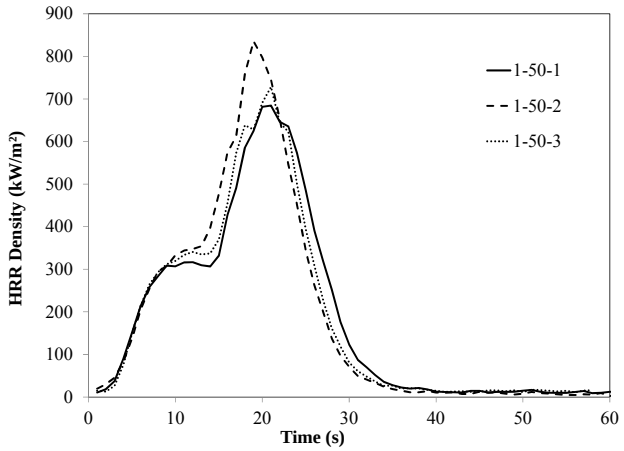

Figure B-3 Heat release rate density measurements in tests of 2.5 cm thick foam specimens exposed to incident heat flux of 50 kW/m^2.

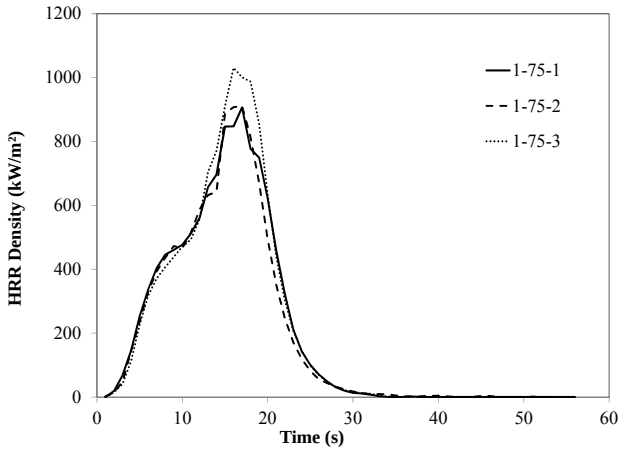

Figure B-4 Heat release rate density measurements in tests of 2.5 cm thick foam specimens exposed to incident heat flux of 75 kW/m^2.

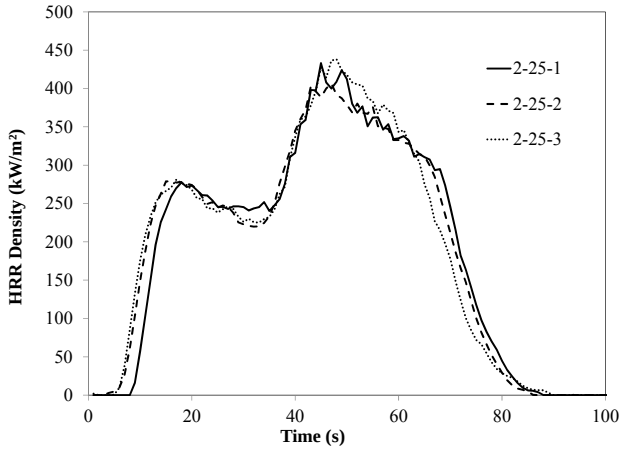

Figure B-5 Heat release rate density measurements in tests of 5.0 cm thick foam specimens exposed to incident heat flux of 25 kW/m^2.

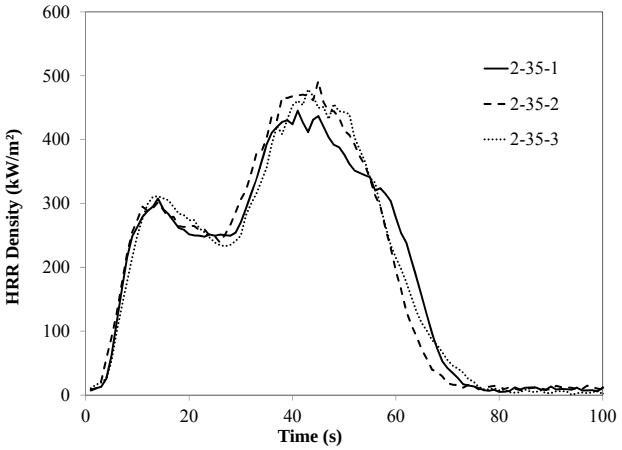

Figure B-6 Heat release rate density measurements in tests of 5.0 cm thick foam specimens exposed to incident heat flux of 35 kW/m^2.

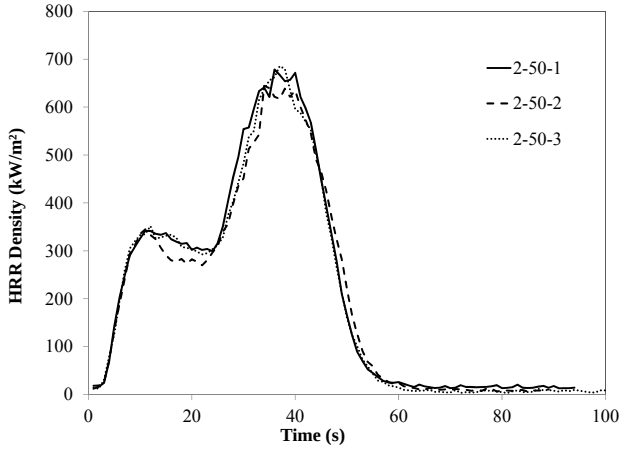

Figure B-7 Heat release rate density measurements in tests of 5.0 cm thick foam specimens exposed to incident heat flux of 50 kW/m^2.

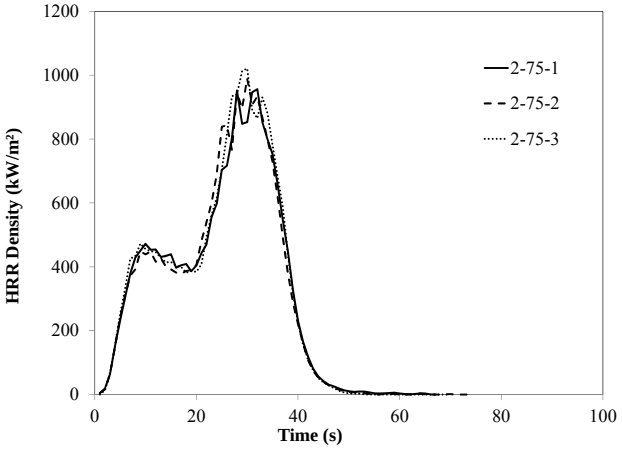

Figure B-8 Heat release rate density measurements in tests of 5.0 cm thick foam specimens exposed to incident heat flux of 75 kW/m^2.

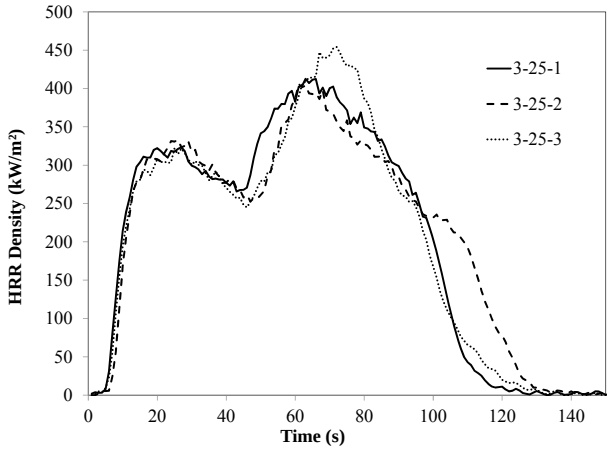

Figure B-9 Heat release rate density measurements in tests of 7.5 cm thick foam specimens exposed to incident heat flux of 25 kW/m^2.

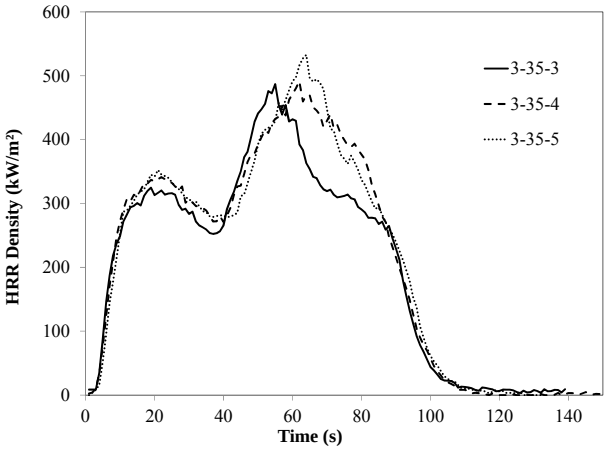

Figure B-10 Heat release rate density measurements in tests of 7.5 cm thick foam specimens exposed to incident heat flux of 35 kW/m^2.

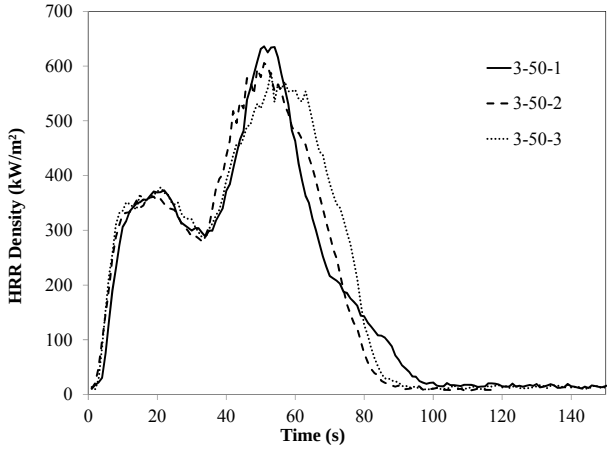

Figure B-11 Heat release rate density measurements in tests of 7.5 cm thick foam specimens exposed to incident heat flux of 50 kW/m^2.

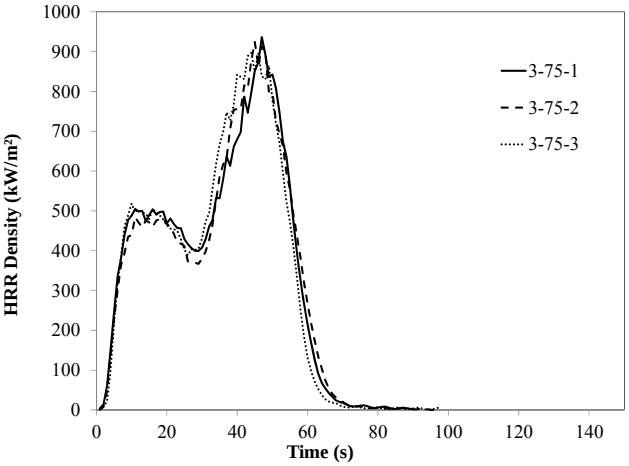

Figure B-12 Heat release rate density measurements in tests of 7.5 cm thick foam specimens exposed to incident heat flux of 75 kW/m^2.

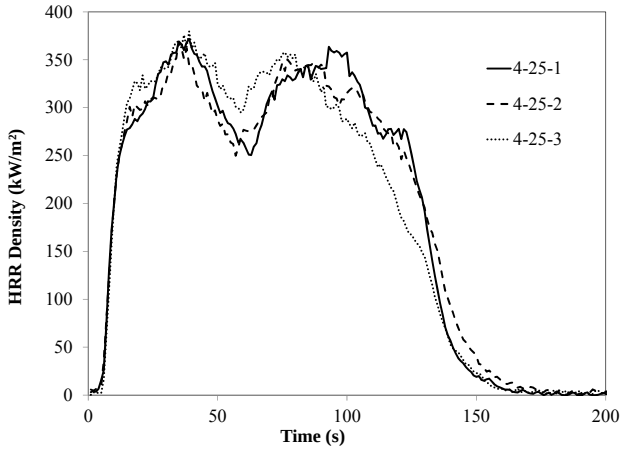

Figure B-13 Heat release rate density measurements in tests of 10.0 cm thick foam specimens exposed to incident heat flux of 25 kW/m^2.

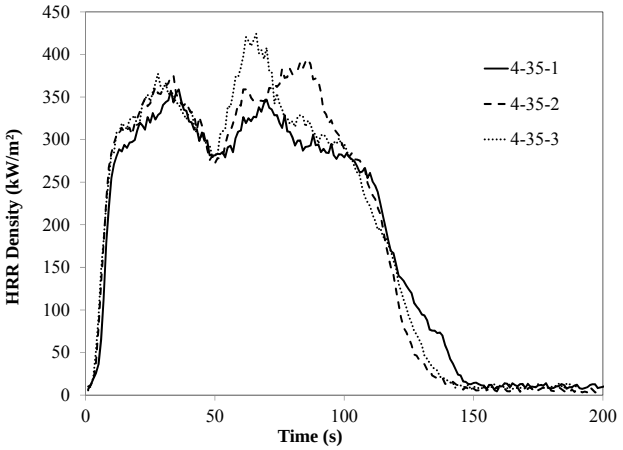

Figure B-14 Heat release rate density measurements in tests of 10.0 cm thick foam specimens exposed to incident heat flux of 35 kW/m^2.

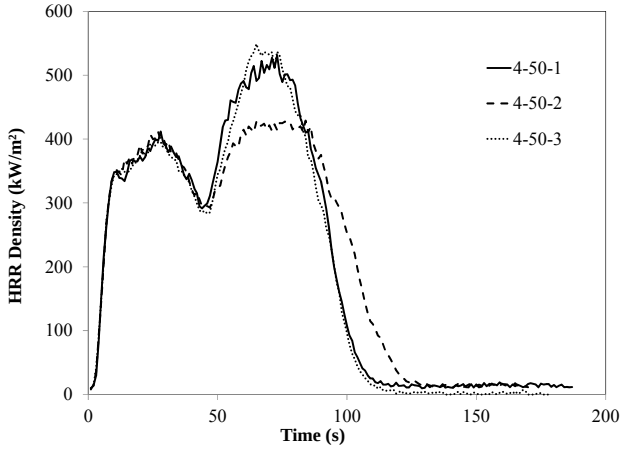

Figure B-15 Heat release rate density measurements in tests of 10.0 cm thick foam specimens exposed to incident heat flux of 50 kW/m^2.

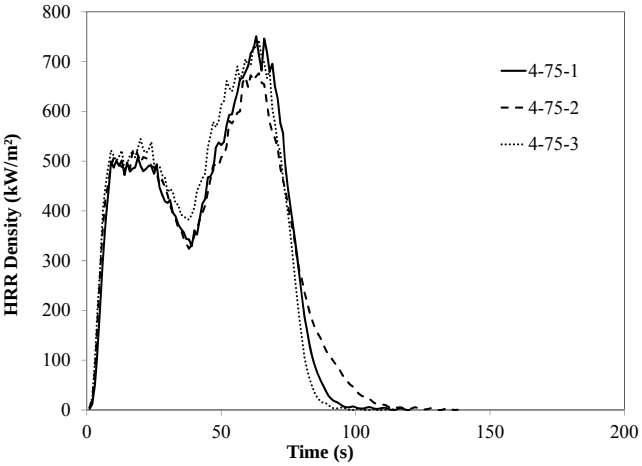

Figure B-16 Heat release rate density measurements in tests of 10.0 cm thick foam specimens exposed to incident heat flux of 75 kW/m^2.

APPENDIX C: FURNITURE CALORIMETER HRR DATA

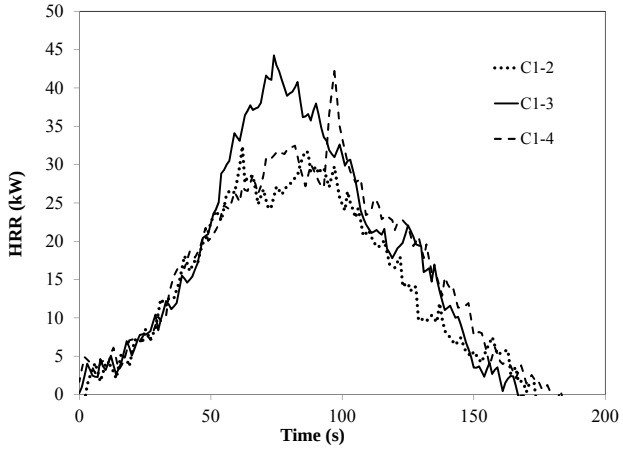

Figure C-1 Heat release rate measurements in center ignition tests of 60 cm x 50cm x 2.5 cm thick foam specimens.

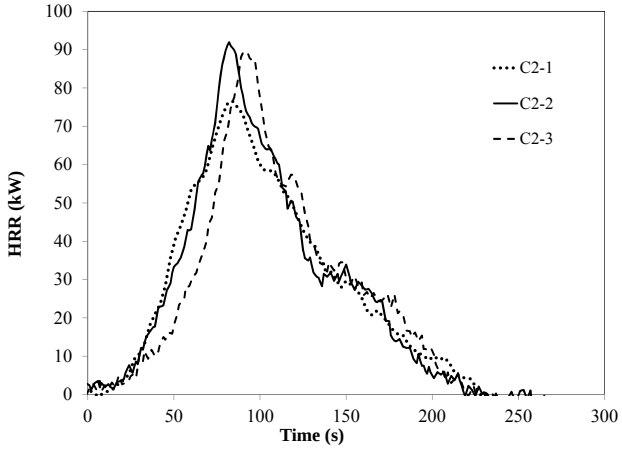

Figure C-2 Heat release rate measurements in center ignition tests of 60 cm x 60cm x 5.0 cm thick foam specimens.

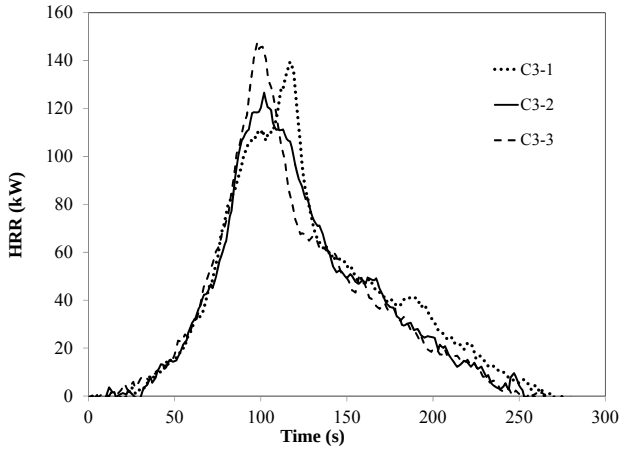

Figure C-3 Heat release rate measurements in center ignition tests of 60 cm x 60 cm x 7.5 cm thick foam specimens.

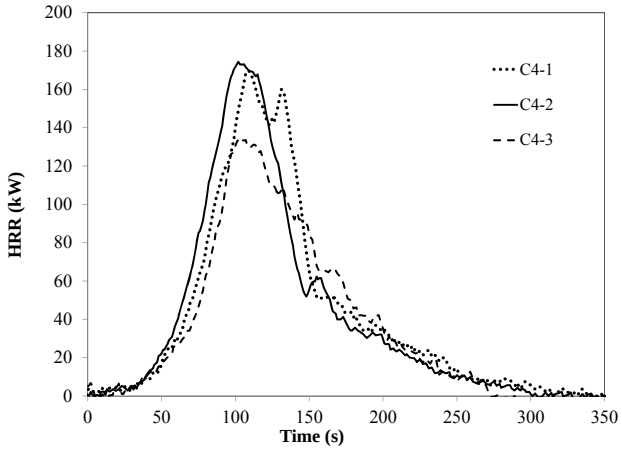

Figure C-4 Heat release rate measurements in center ignition tests of 60 cm x 60 cm x 10.0 cm thick foam specimens.

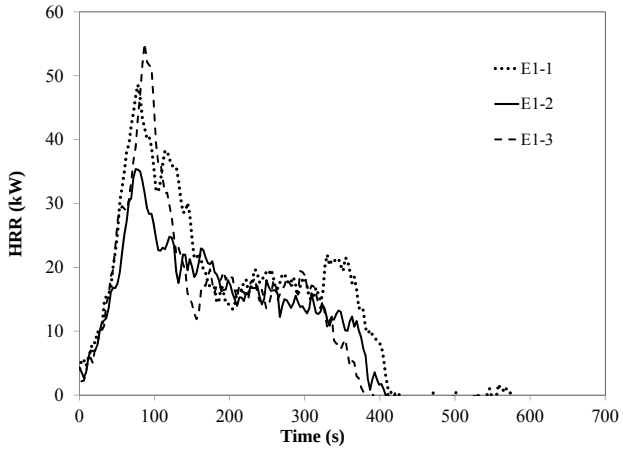

Figure C-5 Heat release rate measurements in edge ignition tests of 50 cm x 140 cm x 2.5 cm thick foam specimens.

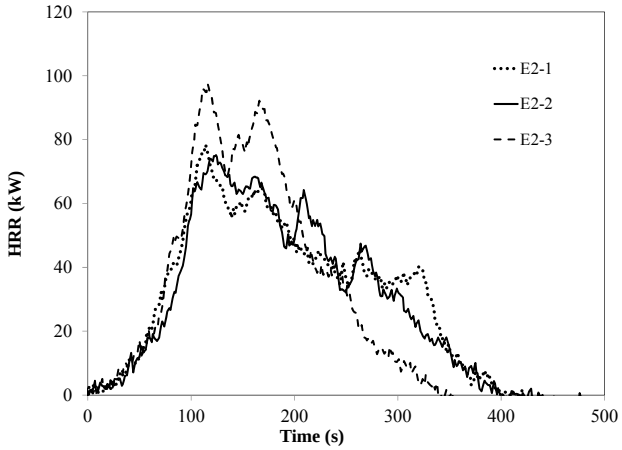

Figure C-6 Heat release rate measurements in edge ignition tests of 60 cm x 120 cm x 5.0 cm thick foam specimens.

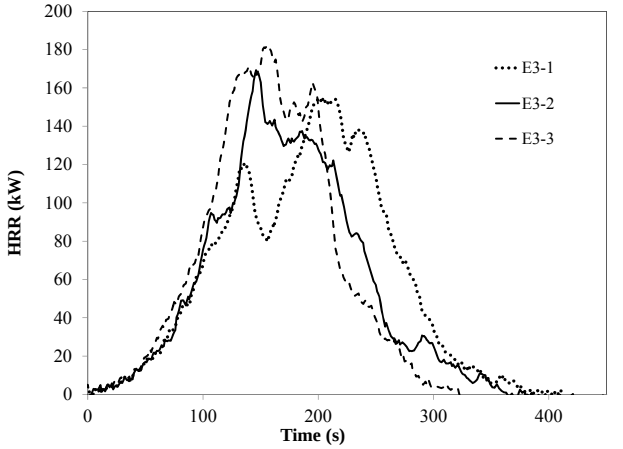

Figure C-7 Heat release rate measurements in edge ignition tests of 60 cm x 120 cm x 7.5 cm thick foam specimens.

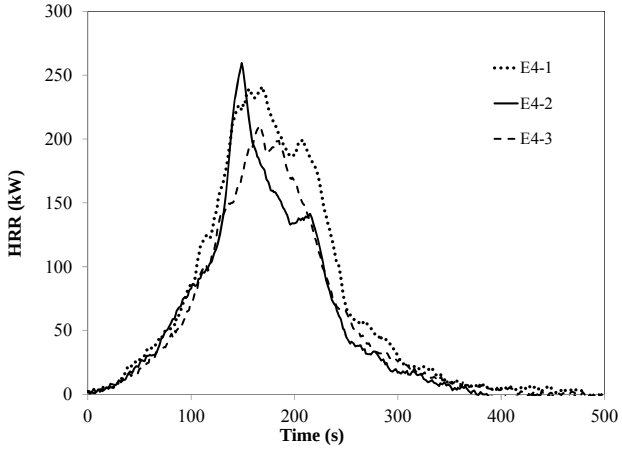

Figure C-8 Heat release rate measurements in edge ignition tests of 60 cm x 120 cm x 10.0 cm thick foam specimens.

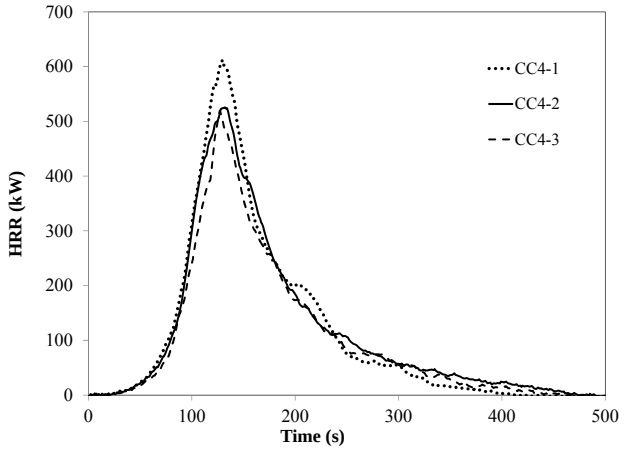

Figure C-9 Heat release rate measurements in center ignition tests of 120 cm x 120 cm x 10.0 cm thick foam specimens.

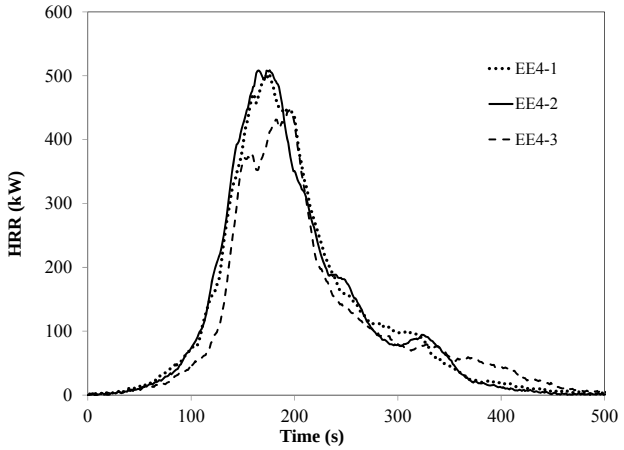

Figure C-10 Heat release rate measurements in edge ignition tests of 120 cm x 120cm x 10.0 cm thick foam specimens.

APPENDIX D: LINEAR FLAME SPREAD IN FULL SCALE TESTS

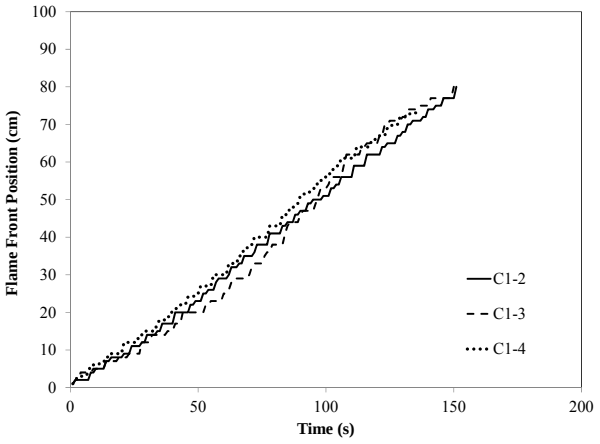

Figure D-1 Flame front position in full scale center ignition tests of 2.5 cm thick polyurethane foam specimens.

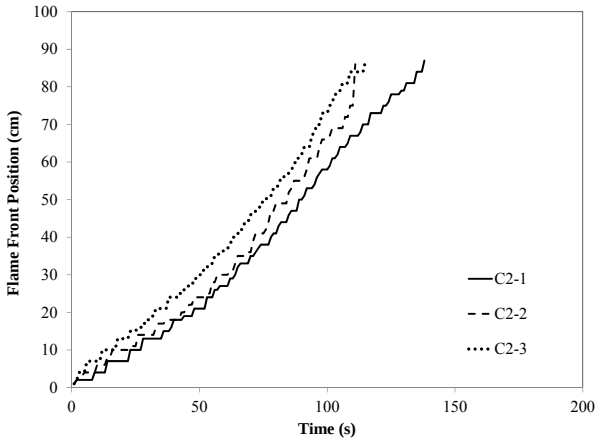

Figure D-2 Flame front position in full scale center ignition tests of 5.0 cm thick polyurethane foam. specimens.

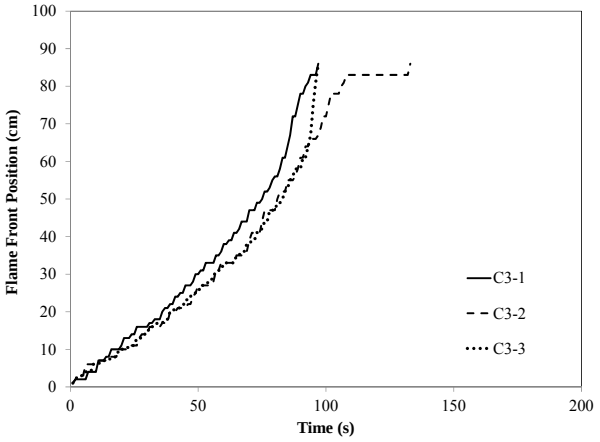

Figure D-3 Flame front position in full scale center ignition tests of 7.5 cm thick polyurethane foam specimens.

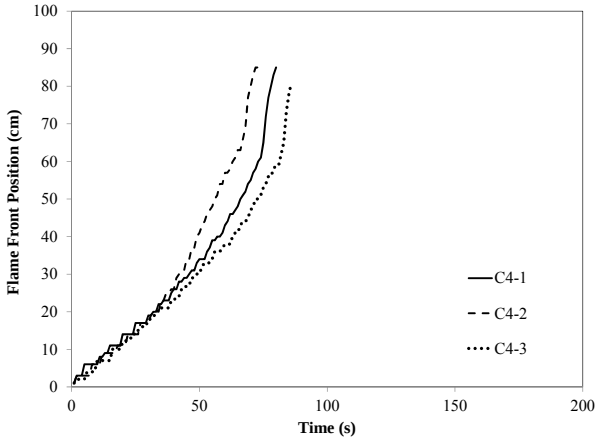

Figure D-4 Flame front position in full scale center ignition tests of 10.0 cm thick polyurethane foam specimens.

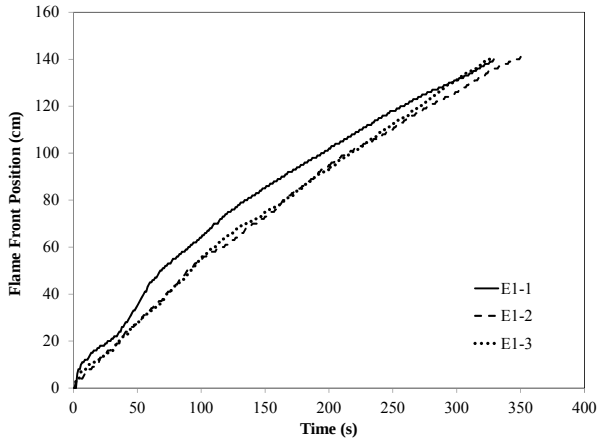

Figure D-5 Flame front position in full scale edge ignition tests of 2.5 cm thick polyurethane foam specimen.

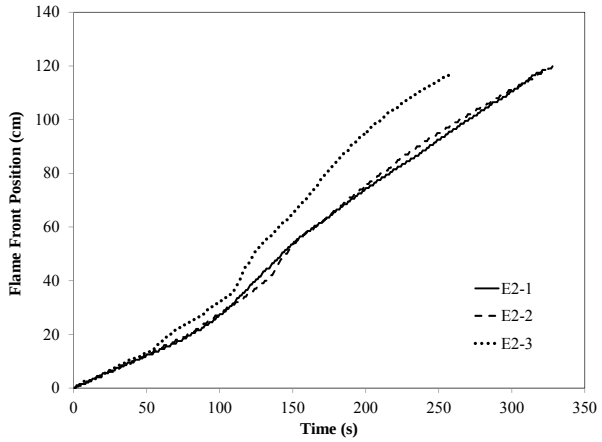

Figure D-6 Flame front position in full scale edge ignition tests of 5.0 cm thick polyurethane foam specimens.

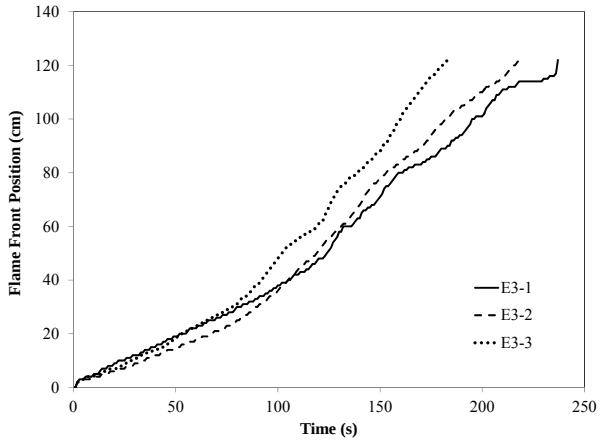

Figure D-7 Flame front position in full scale edge ignition tests of 7.5 cm thick polyurethane foam specimens.

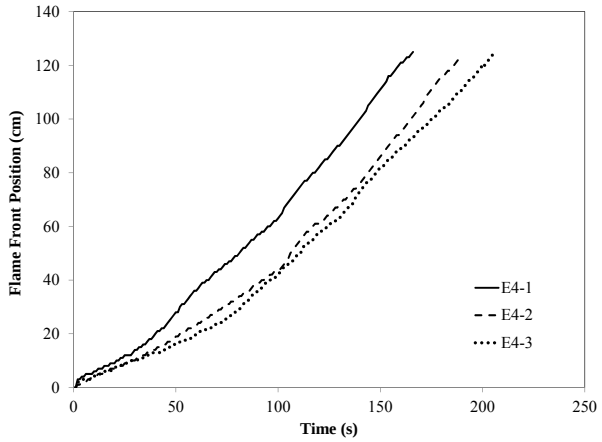

Figure D-8 Flame front position in full scale edge ignition tests of 10 cm thick polyurethane foam specimens.

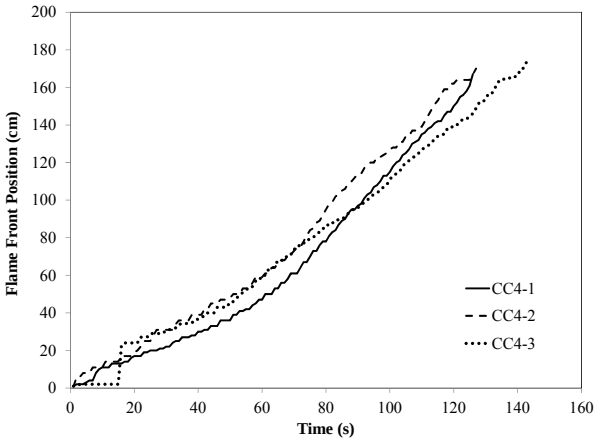

Figure D-9 Flame front position in full scale center ignition tests of 10.0 cm thick polyurethane foam specimens.

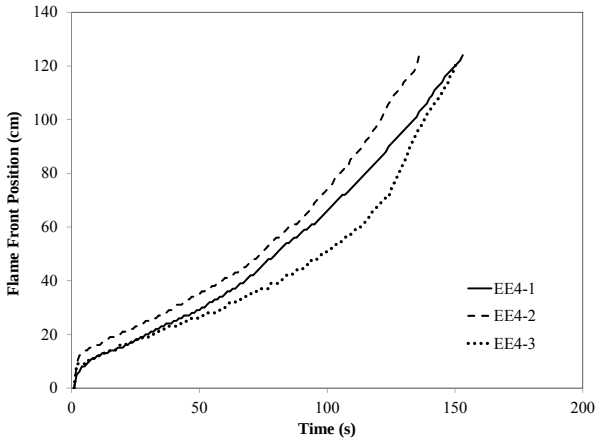

Figure D-10 Flame front position in full scale edge ignition tests of 10 cm thick polyurethane foam specimens.

APPENDIX E: CONTOUR PLOTS OF FLAME SPREAD ON FULL SCALE TESTS

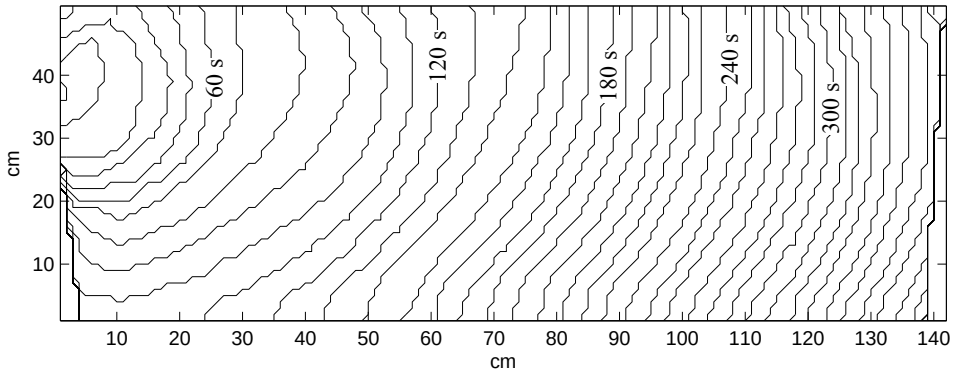

Figure E-1 flame spread contours for test E1-1 in 10 s increments.

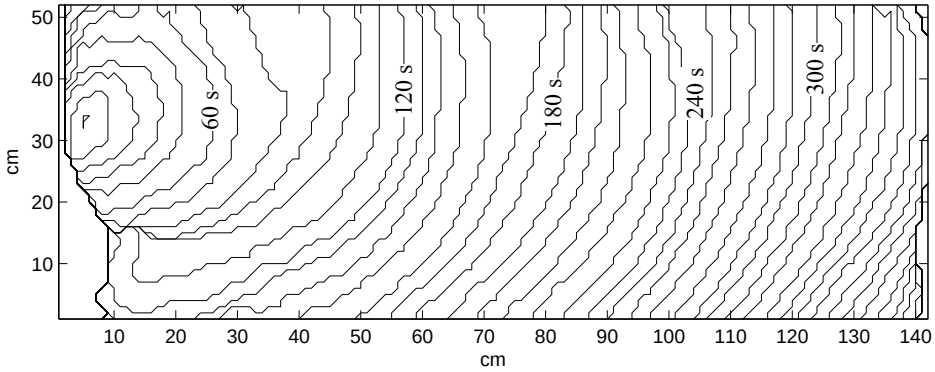

Figure E-2 Flame spread contours for test E1-2 in 10 s increments.

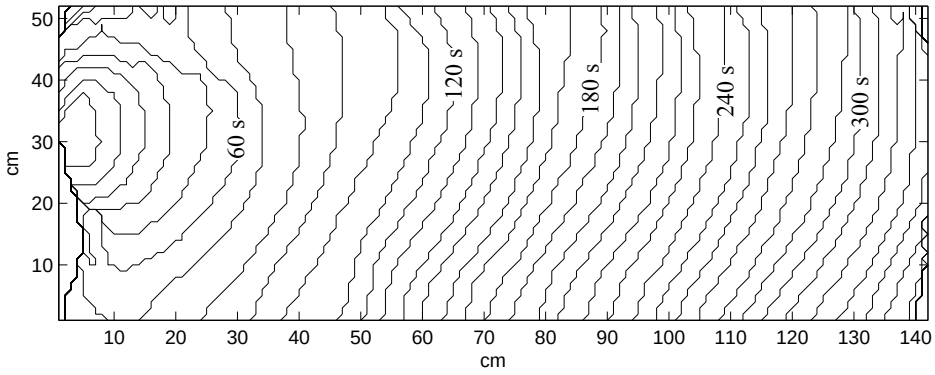

Figure E-3 Flame spread contours for test E1-3 in 10 s increments.

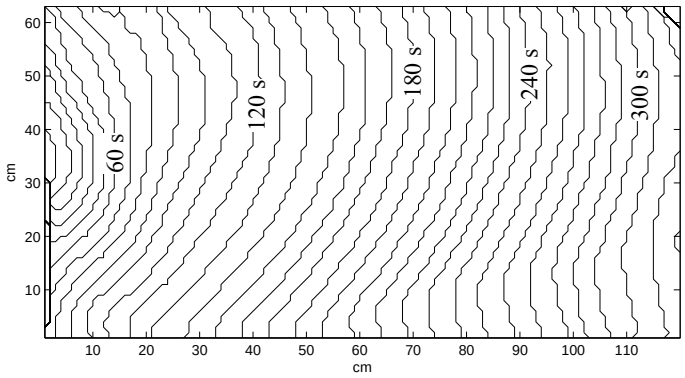

Figure E-4 Flame spread contours for test E2-1 in 10 s increments.

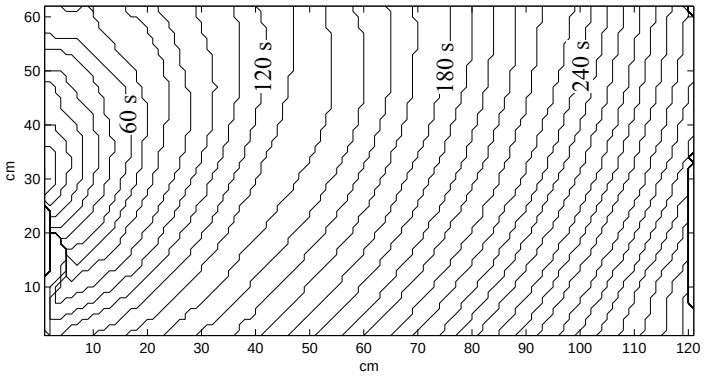

Figure E-5 Flame spread contours for test E2-2 in 10 s increments.

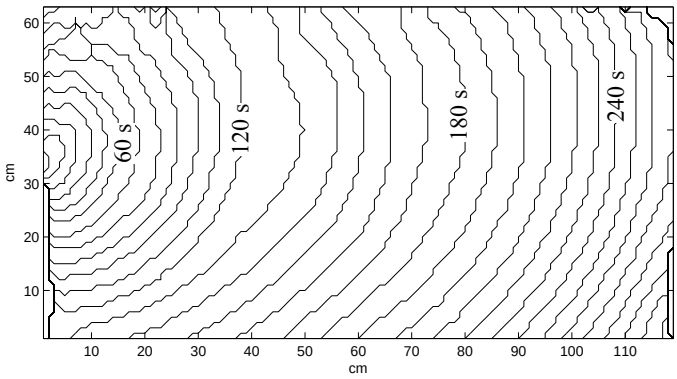

Figure E-6 Flame spread contours for test E2-3 in 10 s increments.

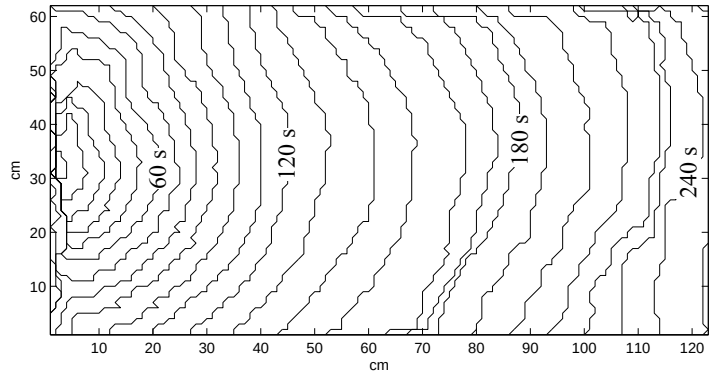

Figure E-7 Flame spread contours for test E3-1 in 10 s increments.

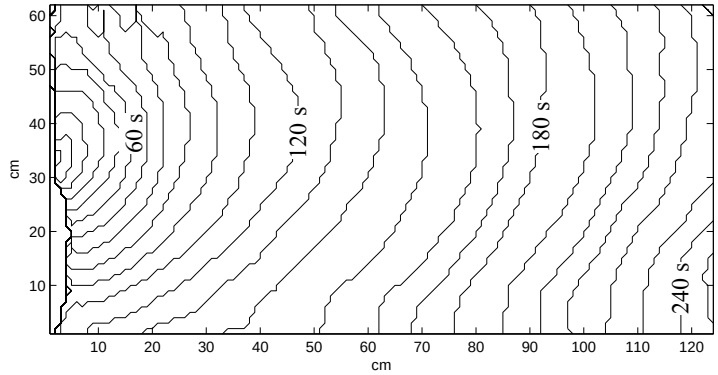

Figure E-8 Flame spread contours for test E3-2 in 10 s increments.

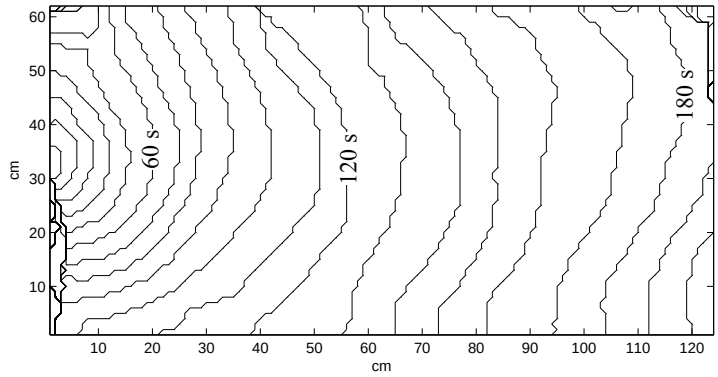

Figure E-9 Flame spread contours for test E3-3 in 10 s increments.

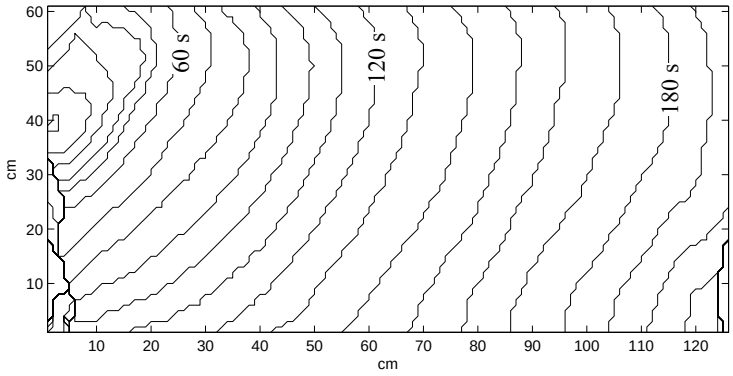

Figure E-10 Flame spread contours for test E4-1 in 10 s increments.

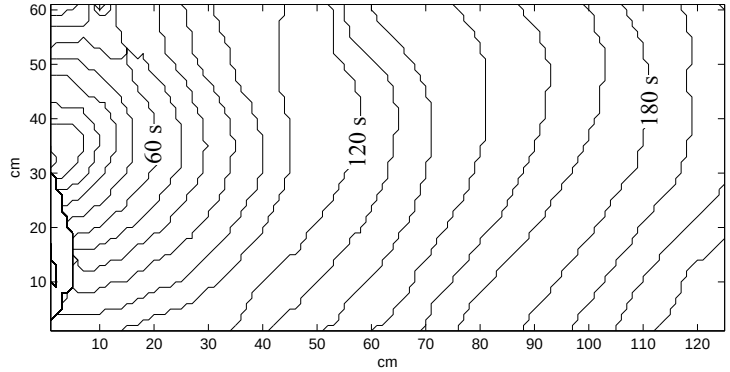

Figure E-11 Flame spread contours for test E4-2 in 10 s increments.

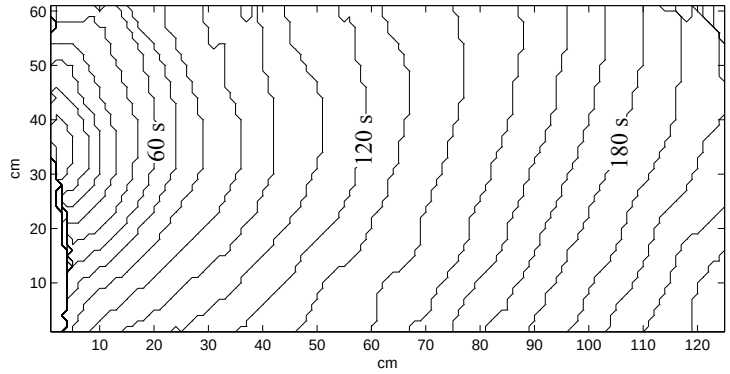

Figure E-12 Flame spread contours for test E4-3 in 10 s increments.

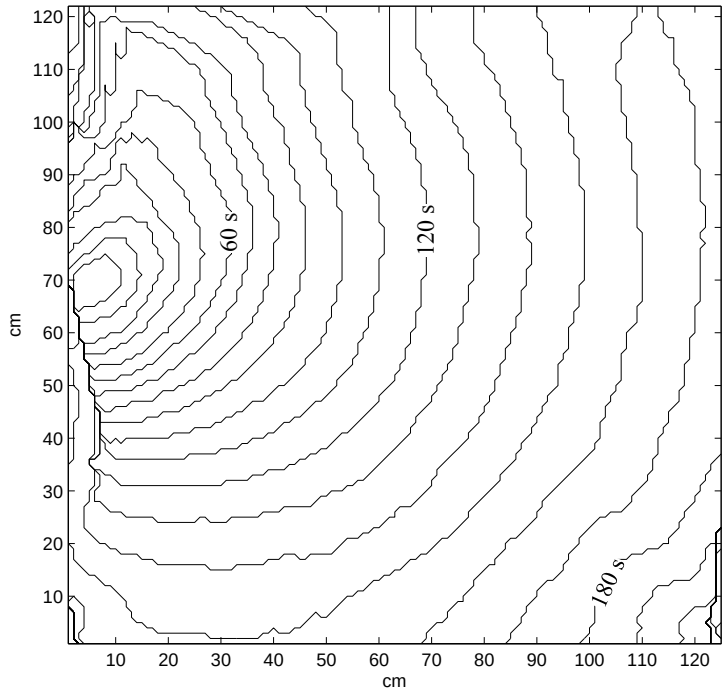

Figure E-13 Flame spread contours for test EE4-1 in 10 s increments.

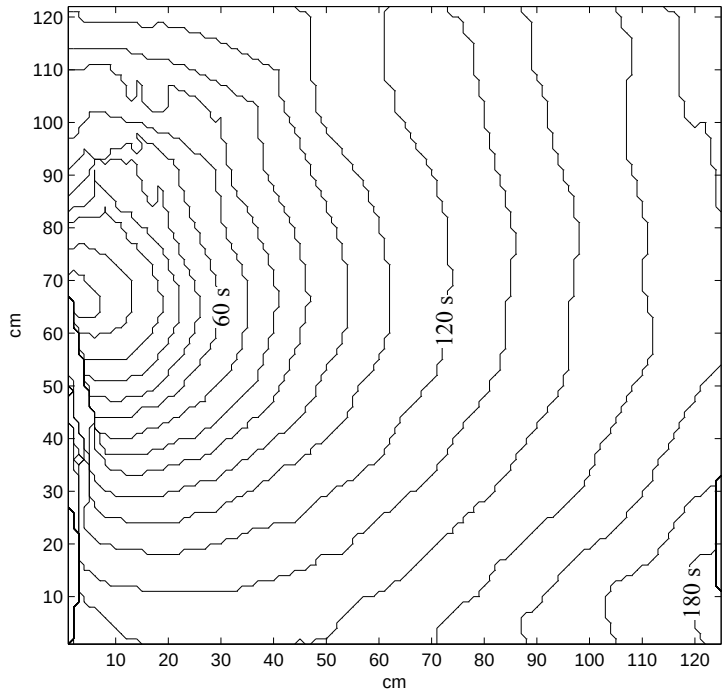

Figure E-14 Flame spread contours for test EE4-2 in 10 s increments.

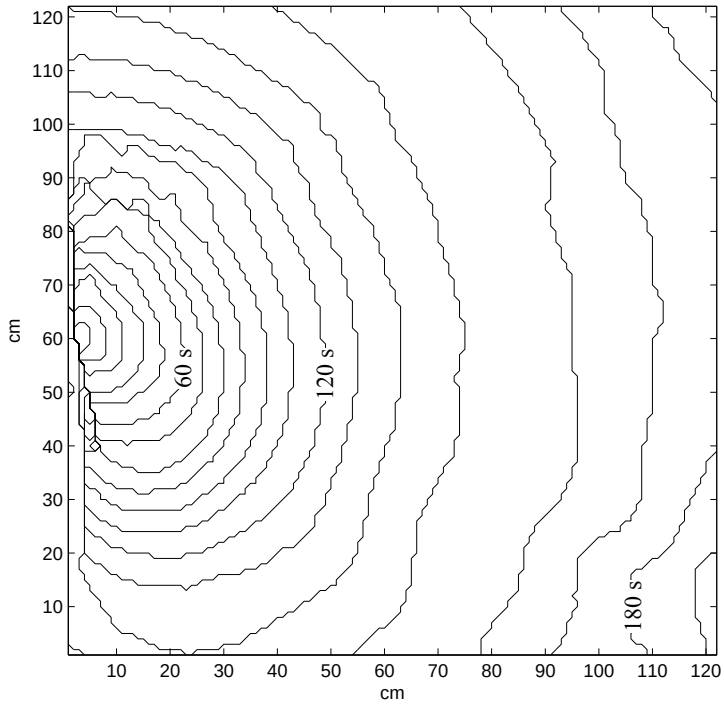

Figure E-15 Flame spread contours for test EE4-3 in 10 s increments.

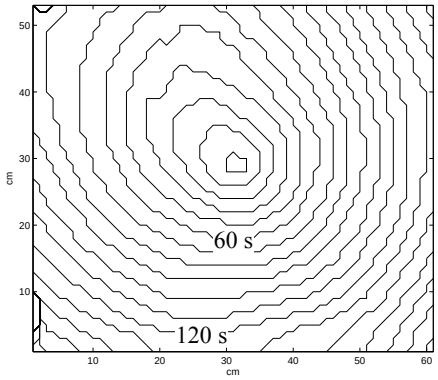

Figure E-16 Flame spread contours for test C1-2 in 10 s increments.

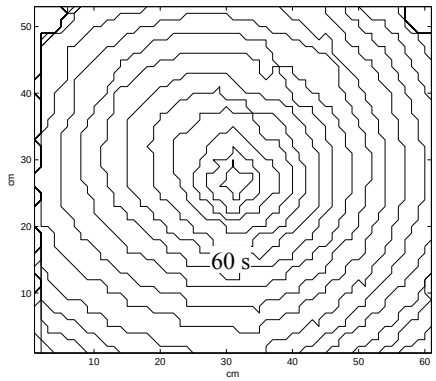

Figure E-17 Flame spread contours for test C1-3 in 10 s increments.

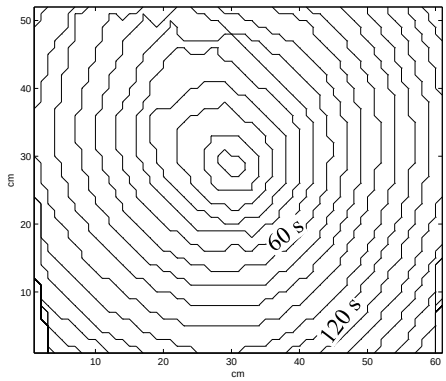

Figure E-18 Flame spread contours for test C1-4 in 10 s increments.

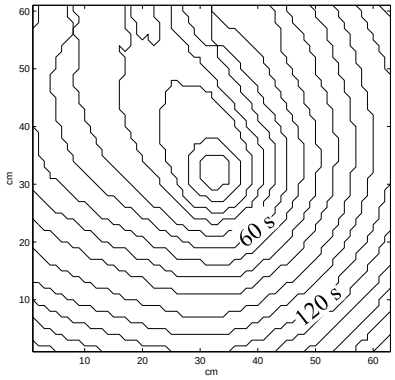

Figure E-19 Flame spread contours for test C2-1 in 10 s increments.

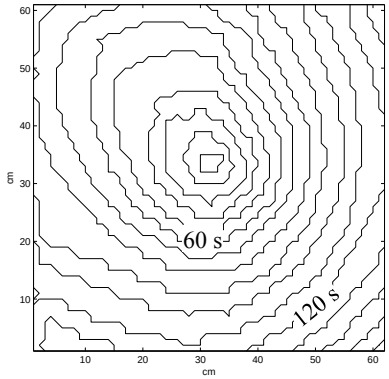

Figure E-20 Flame spread contours for test C2-2 in 10 s increments.

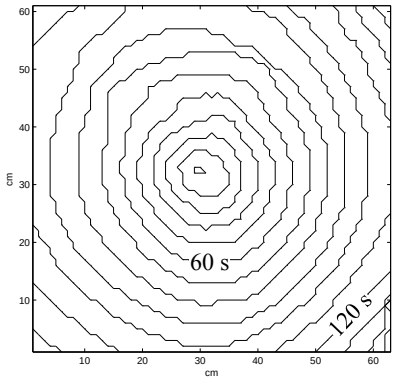

Figure E-21 Flame spread contours for test C2-3 in 10 s increments.

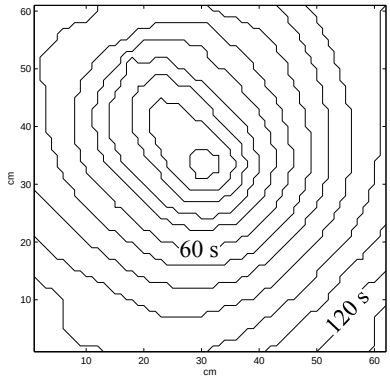

Figure E-22 Flame spread contours for test C3-1 in 10 s increments.

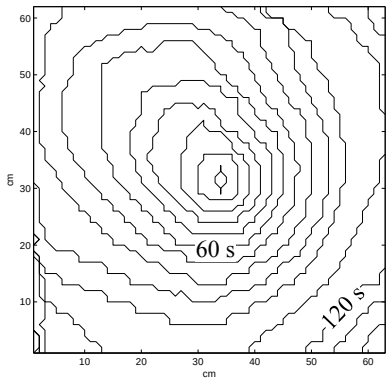

Figure E-23 Flame spread contours for test C3-2 in 10 s increments.

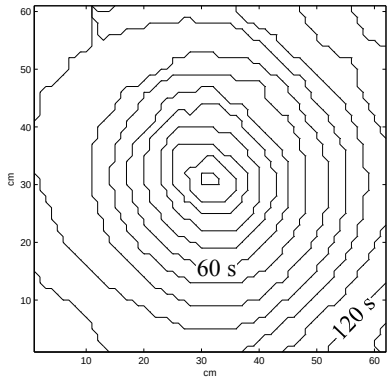

Figure E-24 Flame spread contours for test C3-3 in 10 s increments.

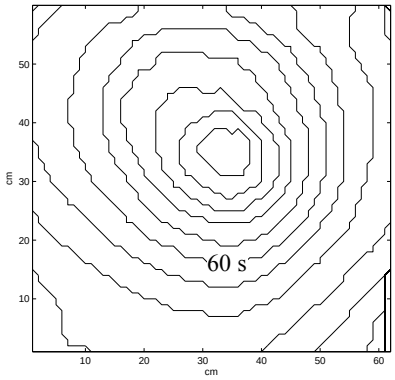

Figure E-25 Flame spread contours for test C4-1 in 10 s increments.

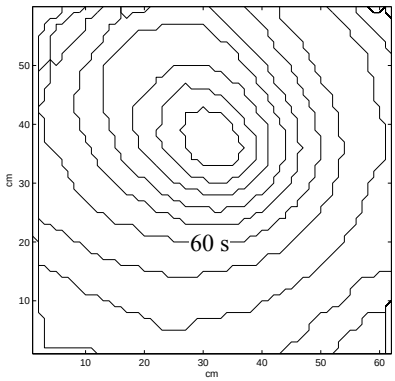

Figure E-26 Flame spread contours for test C4-2 in 10 s increments.

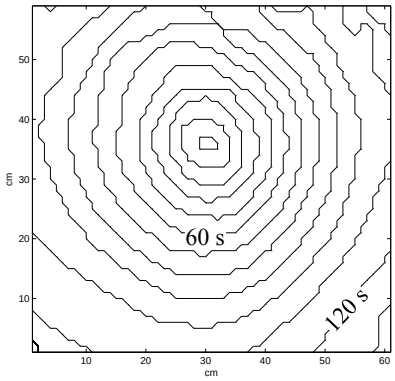

Figure E-27 Flame spread contours for test C4-3 in 10 s increments.

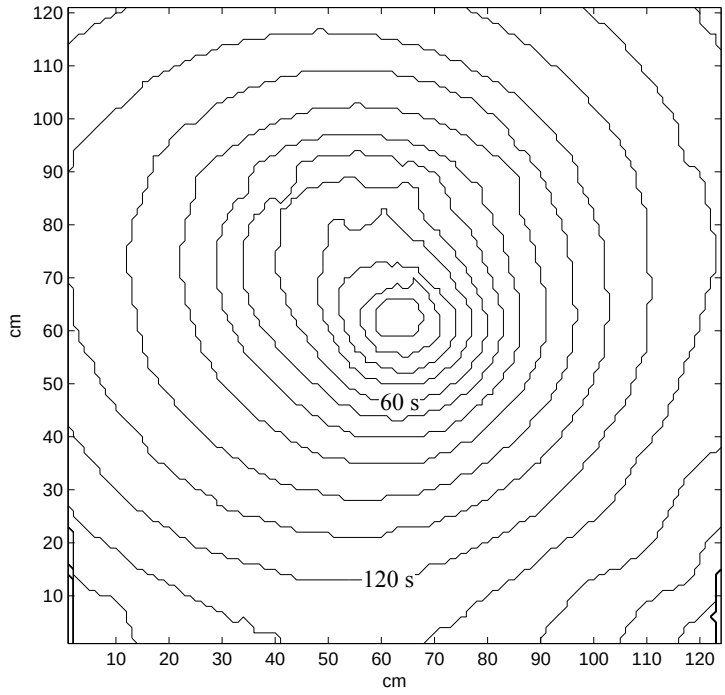

Figure E-28 Flame spread contours for test CC4-1 in 10 s increments.

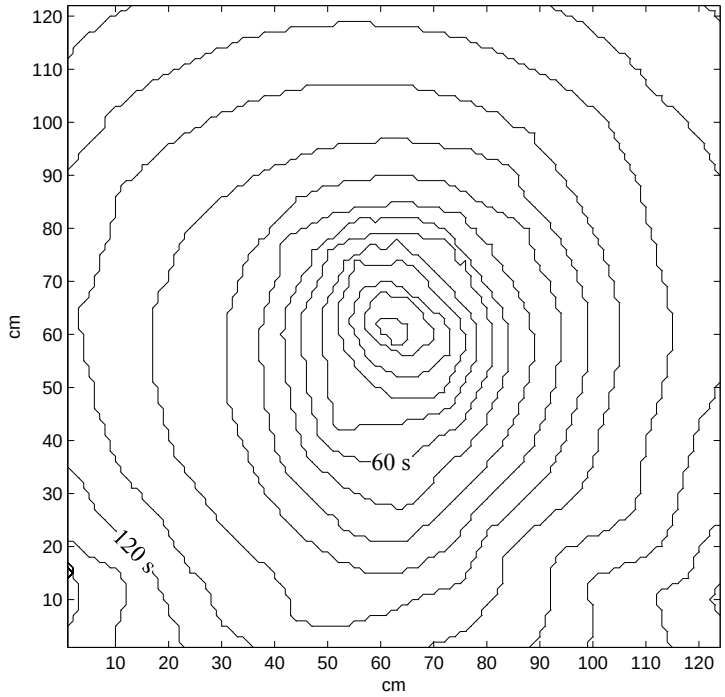

Figure E-29 Flame spread contours for test CC4-2 in 10 s increments.

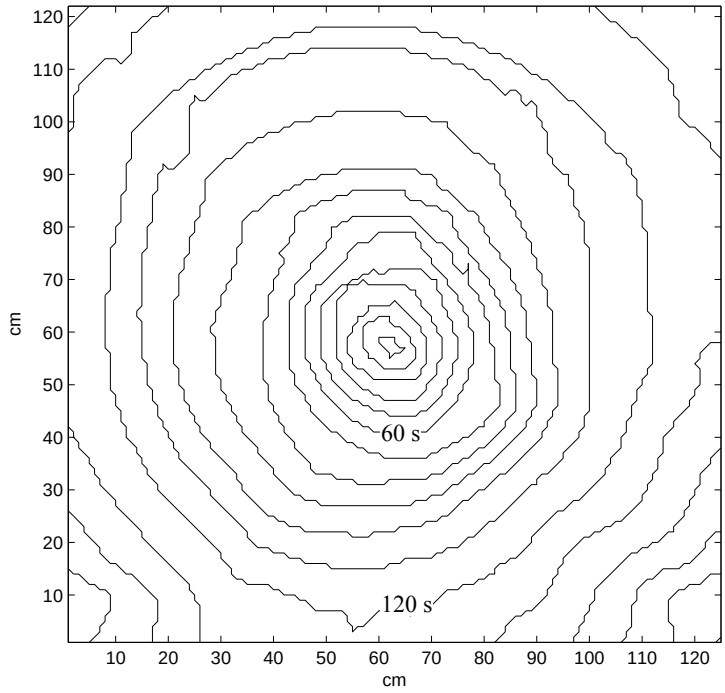

Figure E-30 Flame spread contours for test CC4-3 in 10 s increments.

APPENDIX F: AREA FLAME SPREAD IN FULL SCALE TESTS

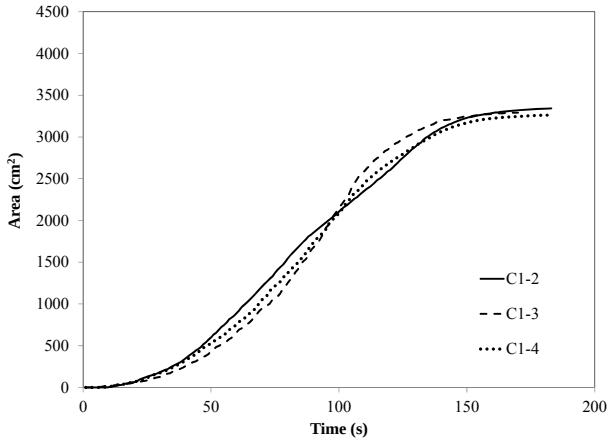

Figure F-1 flame spread area in full scale center ignition tests of 2.5 cm thick polyurethane foam specimens.

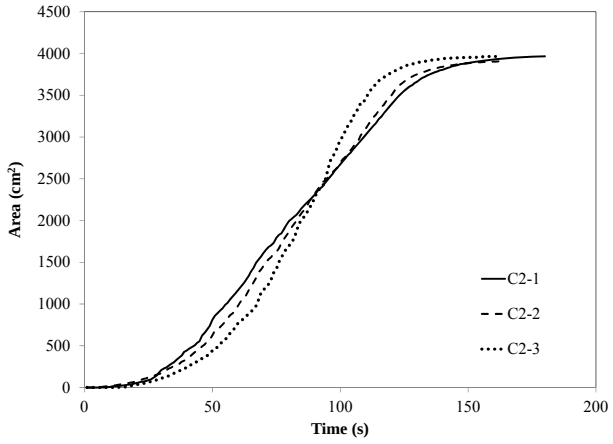

Figure F-2 Flame spread area in full scale center ignition tests of 5.0 cm thick polyurethane foam specimens.

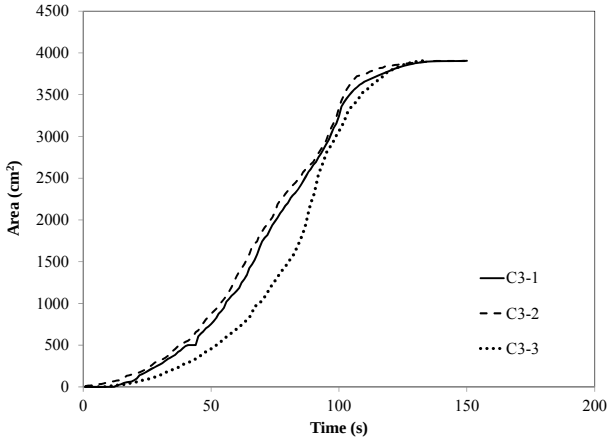

Figure F-3 Flame spread area in full scale center ignition tests of 7.5 cm thick polyurethane foam specimens.

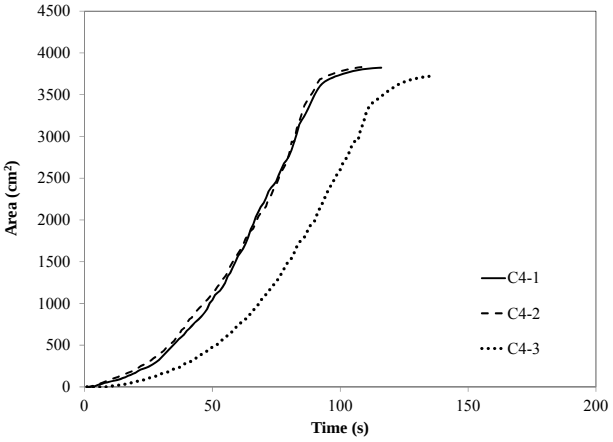

Figure F-4 flame spread area in full scale center ignition tests of 10.0 cm thick polyurethane foam specimen.

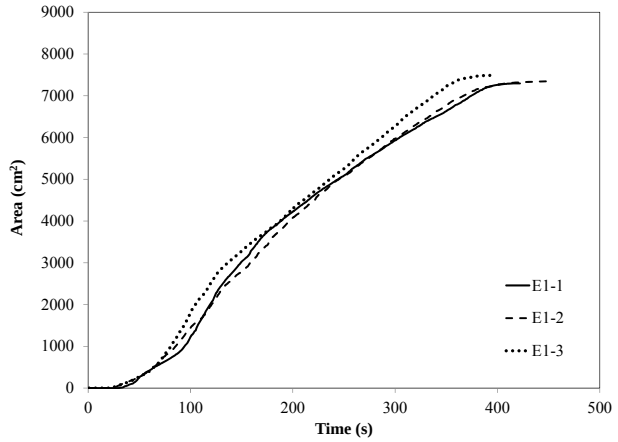

Figure F-5 Flame spread area in full scale edge ignition tests of 2.5 cm thick polyurethane foam specimens.

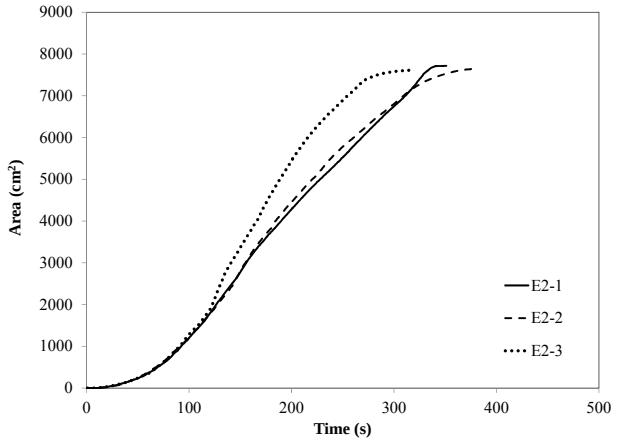

Figure F-6 Flame spread area in full scale edge ignition tests of 5.0 cm thick polyurethane foam specimens.

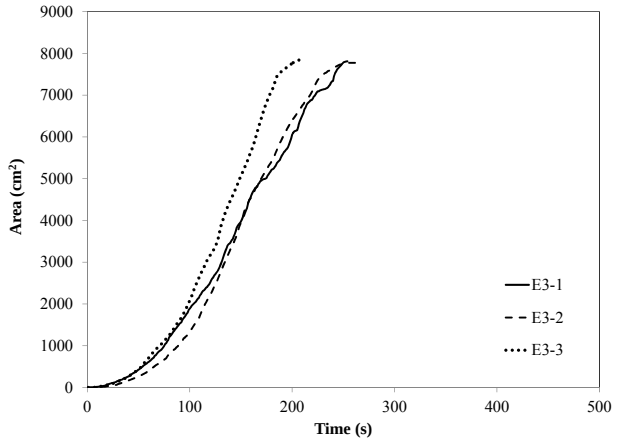

Figure F-7 Flame spread area in full scale edge ignition tests of 7.5 cm thick polyurethane foam specimens.

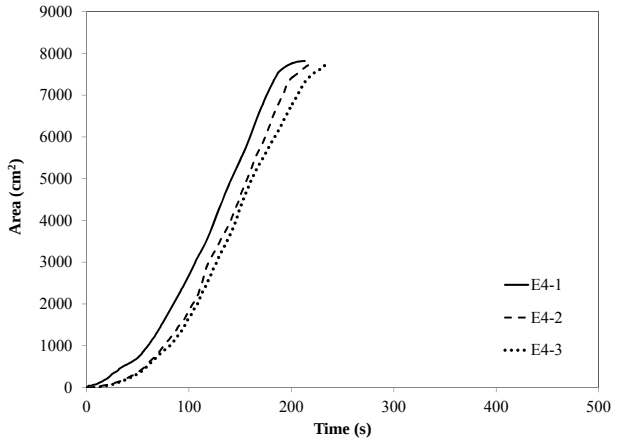

Figure F-8 Flame spread area in full scale edge ignition tests of 10.0 cm thick polyurethane foam specimens.

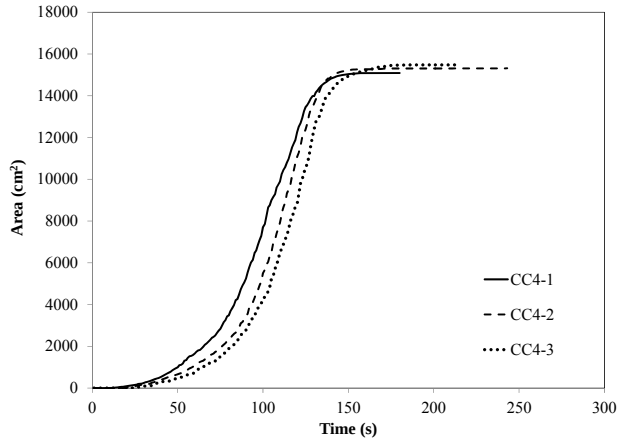

Figure F-9 Flame spread area in full scale edge ignition tests of 7.5 cm thick polyurethane foam specimens.

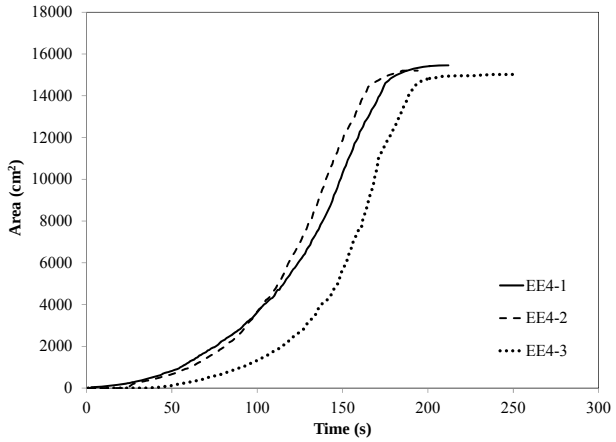

Figure F-10 Flame spread area in full scale edge ignition tests of 10.0 cm thick polyurethane foam specimens.

APPENDIX G: CBUF MODEL RESULTS

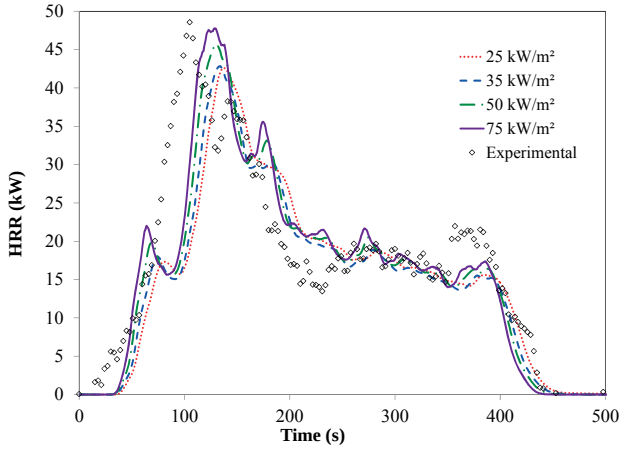

Figure G-1 Comparison of experimental heat release rate with convolution model results for test E1-1.

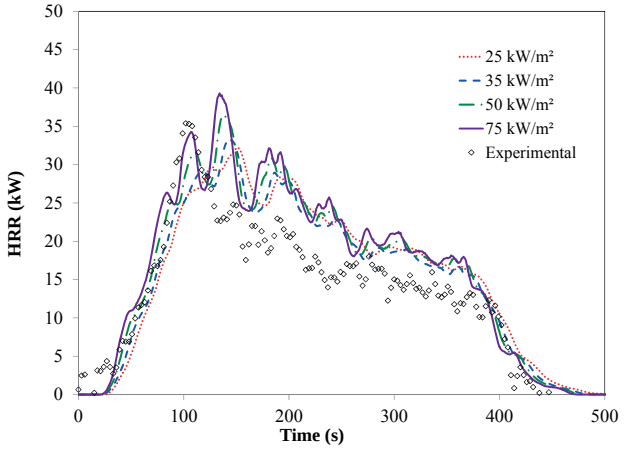

Figure G-2 Comparison of experimental heat release rate with convolution model results for test E1-2.

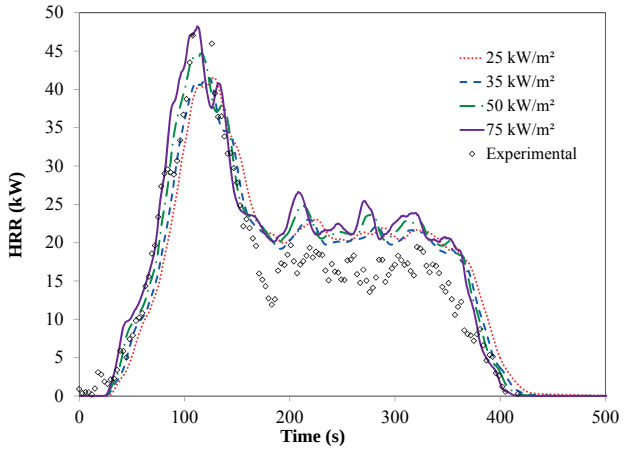

Figure G-3 Comparison of experimental heat release rate with convolution model results for test E1-3.

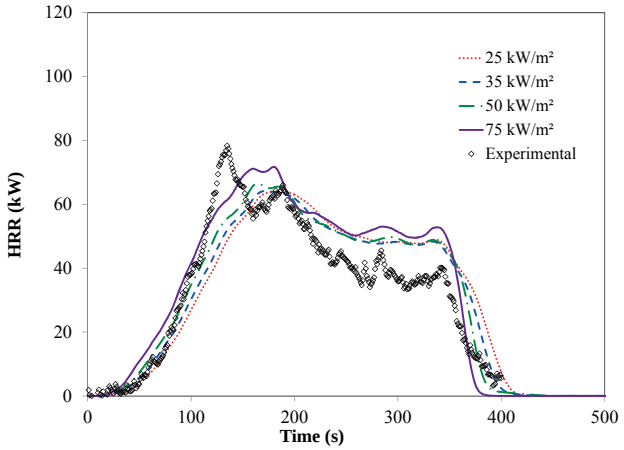

Figure G-4 Comparison of experimental heat release rate with convolution model results for test E2-1.

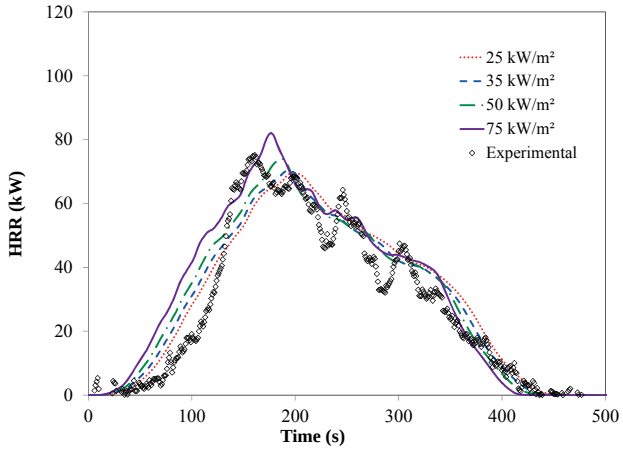

Figure G-5 Comparison of experimental heat release rate with convolution model results for test E2-2.

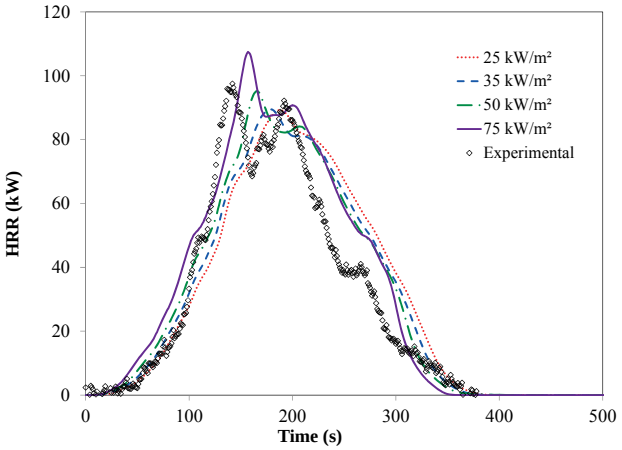

Figure G-6 Comparison of experimental heat release rate with convolution model results for test E2-3.

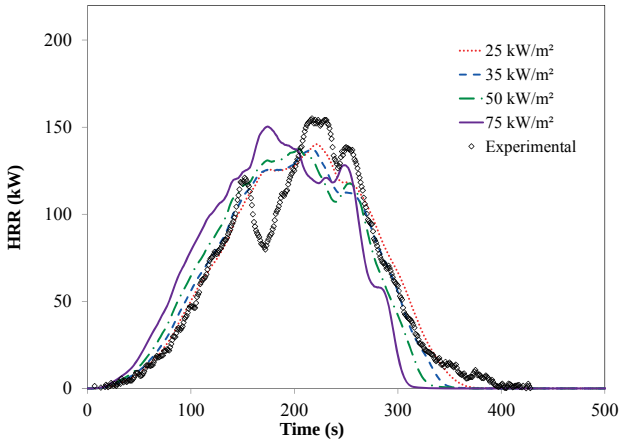

Figure G-7 Comparison of experimental heat release rate with convolution model results for test E3-1.

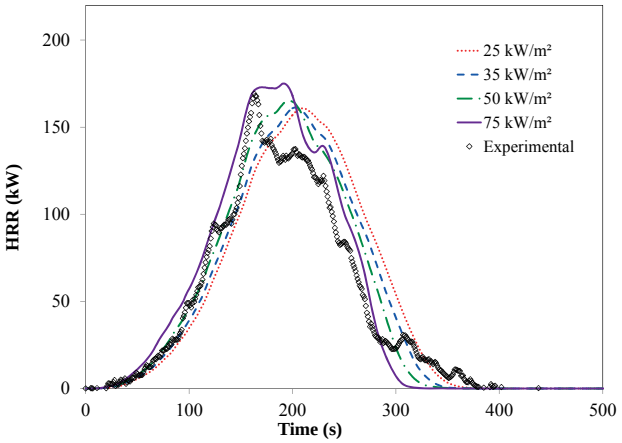

Figure G-8 Comparison of experimental heat release rate with convolution model results for test E3-2.

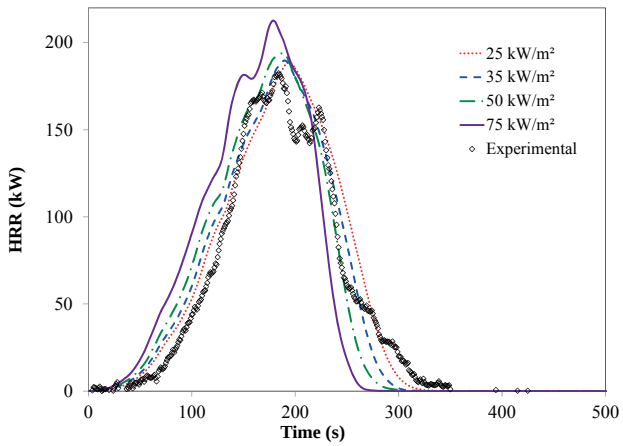

Figure G-9 Comparison of experimental heat release rate with convolution model results for test E3-3.

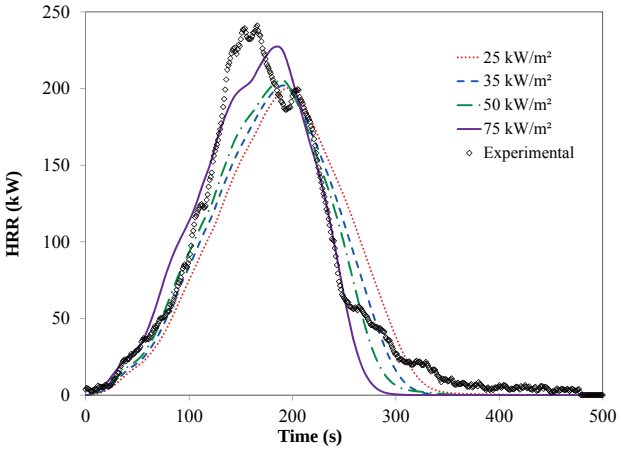

Figure G-10 Comparison of experimental heat release rate with convolution model results for test E4-1.

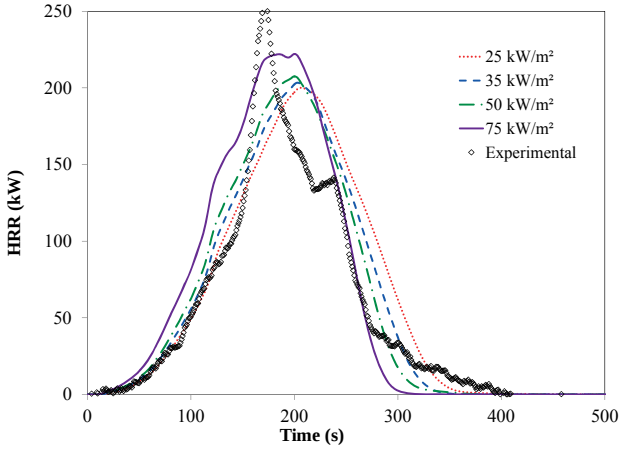

Figure G-11 Comparison of experimental heat release rate with convolution model results for test E4-2.

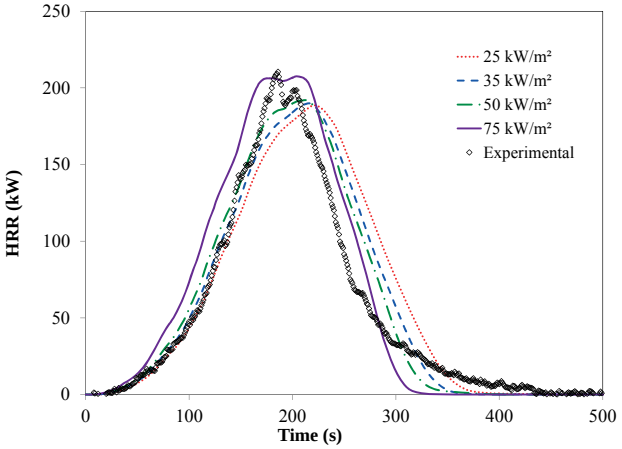

Figure G-12 Comparison of experimental heat release rate with convolution model results for test E4-3.

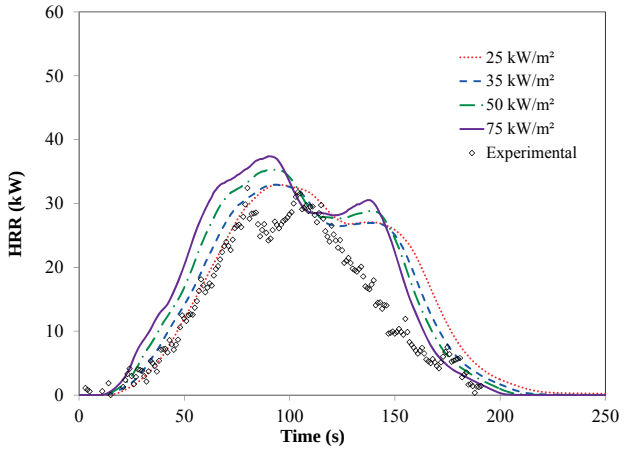

Figure G-13 Comparison of experimental heat release rate with convolution model results for test C1-2.

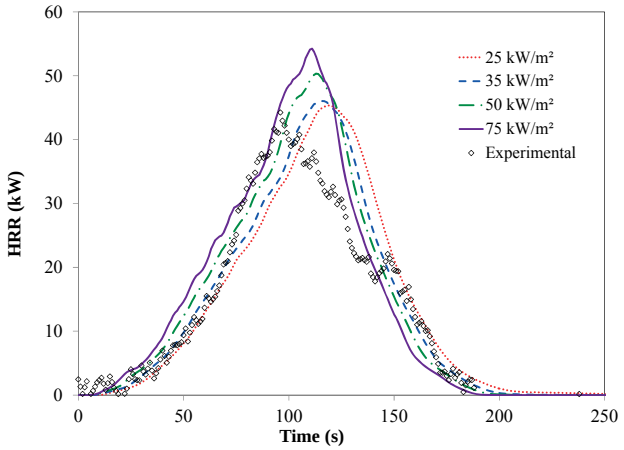

Figure G-14 Comparison of experimental heat release rate with convolution model results for test C1-3.

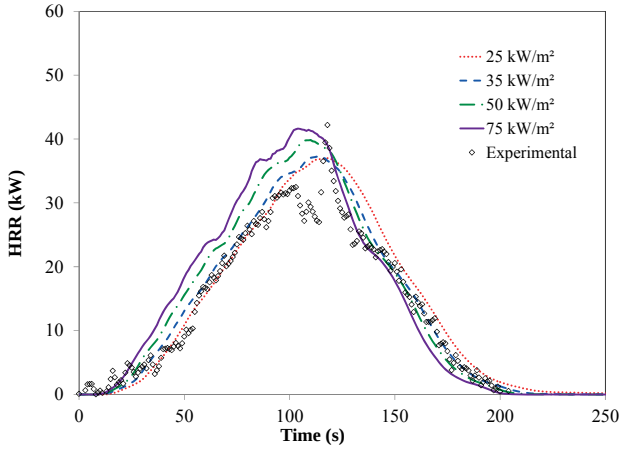

Figure G-15 Comparison of experimental heat release rate with convolution model results for test C1-4.

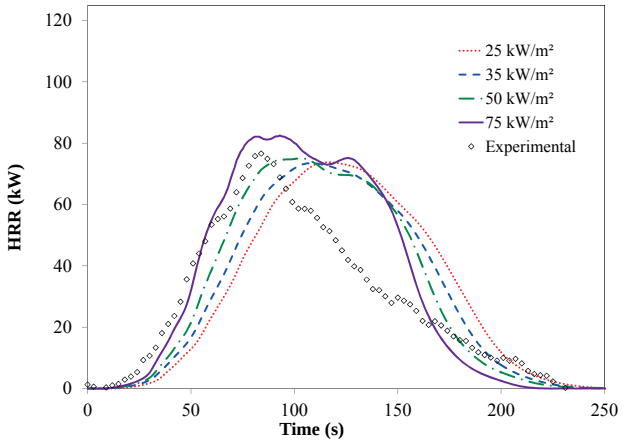

Figure G-16 Comparison of experimental heat release rate with convolution model results for test C2-1.

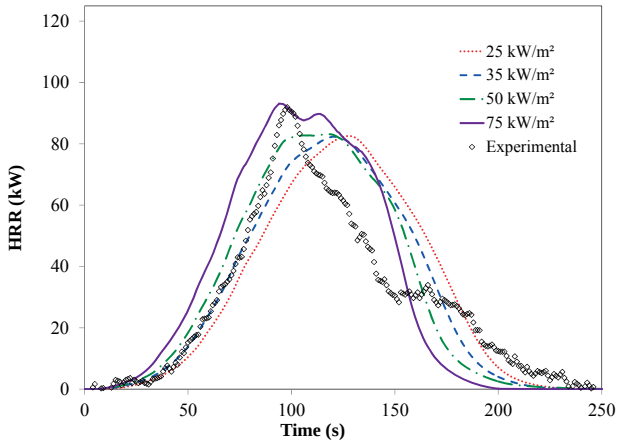

Figure G-17 Comparison of experimental heat release rate with convolution model results for test C2-2.

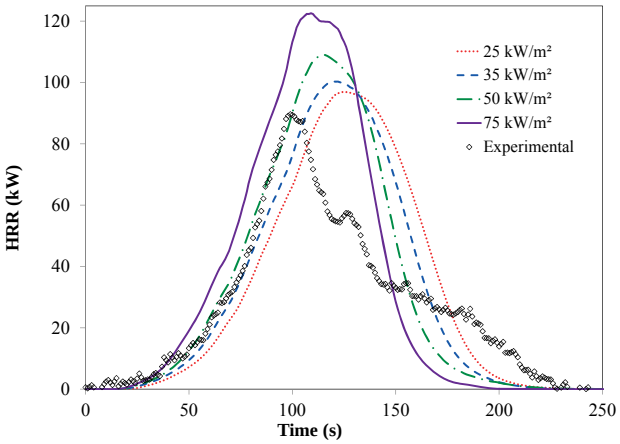

Figure G-18 Comparison of experimental heat release rate with convolution model results for test C2-3.

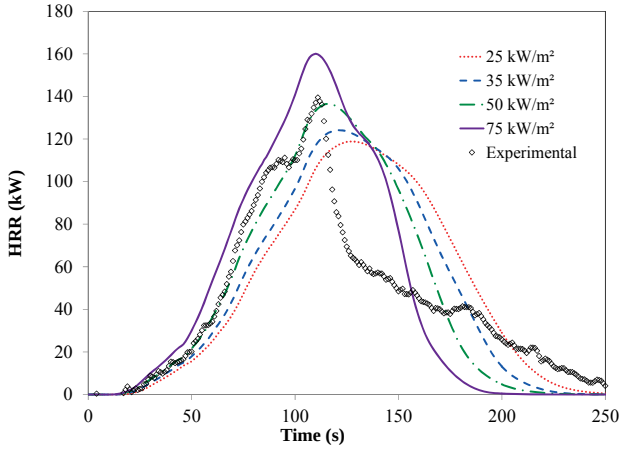

Figure G-19 Comparison of experimental heat release rate with convolution model results for test C3-1.

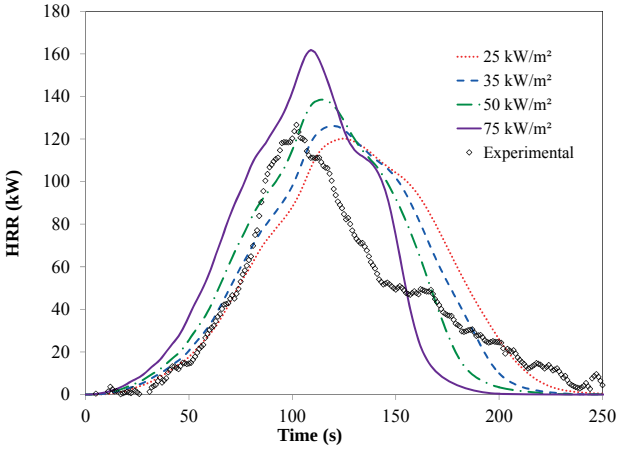

Figure G-20 Comparison of experimental heat release rate with convolution model results for test C3-2.

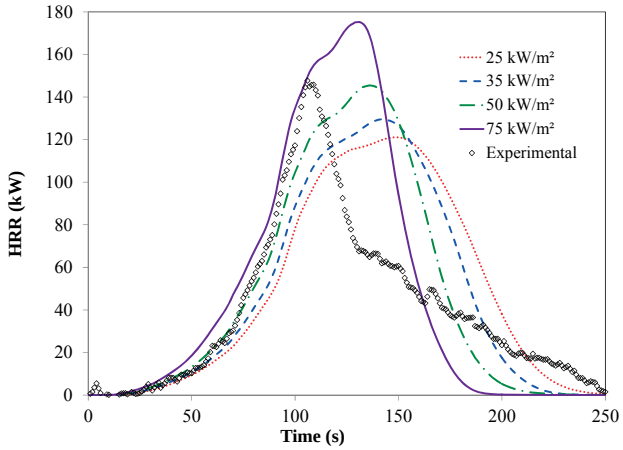

Figure G-21 Comparison of experimental heat release rate with convolution model results for test C3-3.

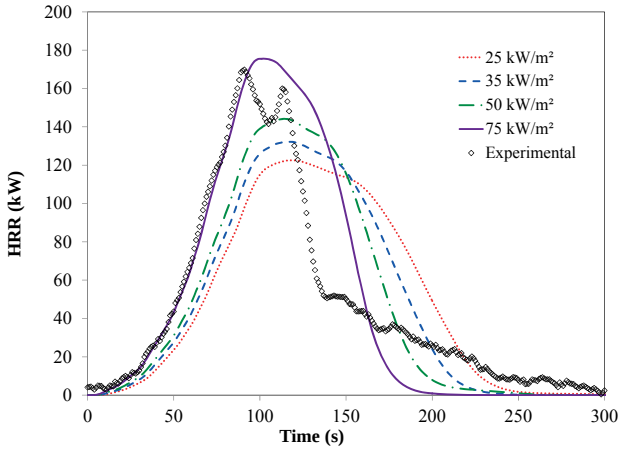

Figure G-22 Comparison of experimental heat release rate with convolution model results for test C4-1.

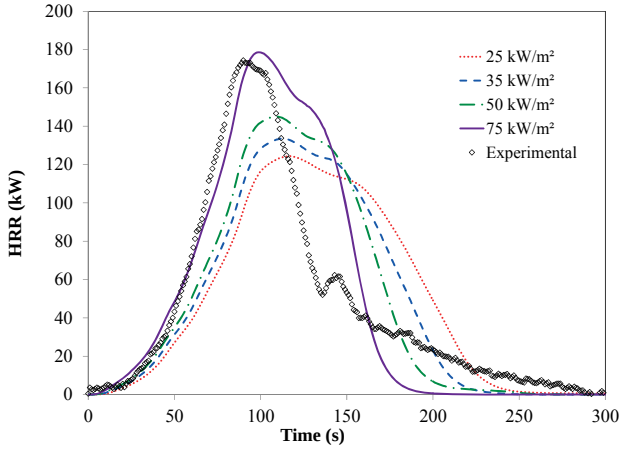

Figure G-23 Comparison of experimental heat release rate with convolution model results for test C4-2.

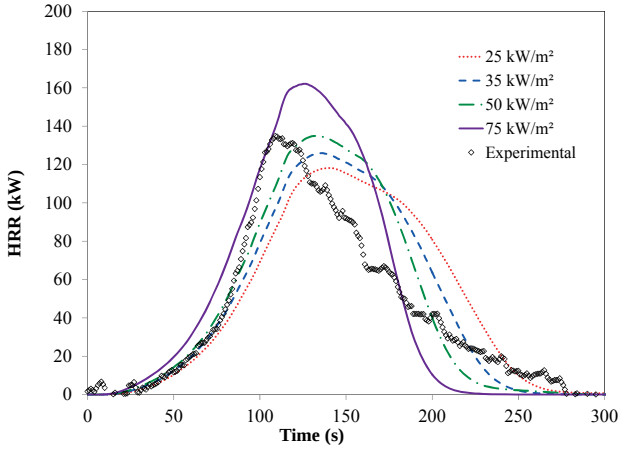

Figure G-24 Comparison of experimental heat release rate with convolution model results for test C4-3.

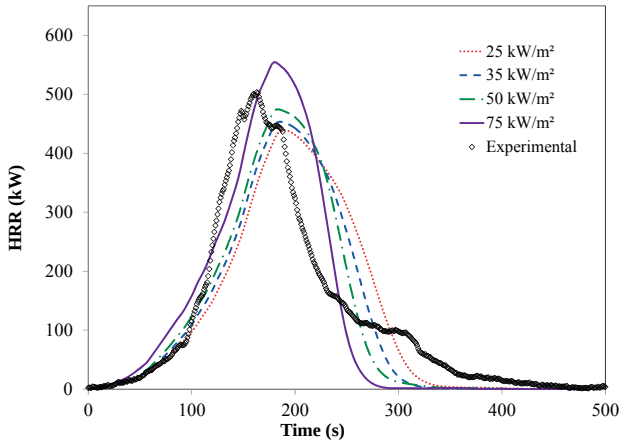

Figure G-25 Comparison of experimental heat release rate with convolution model results for test EE4-1.

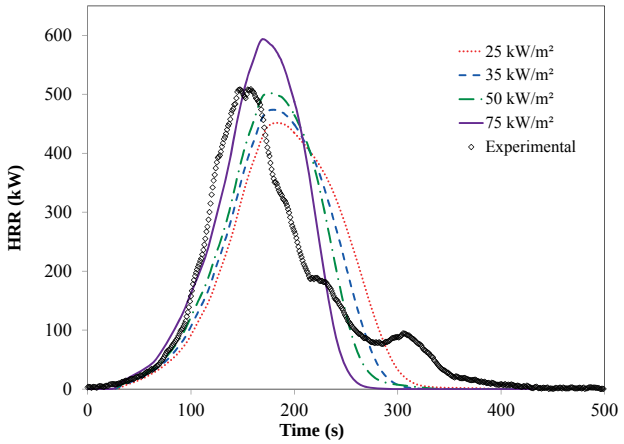

Figure G-26 Comparison of experimental heat release rate with convolution model results for test EE4-2.

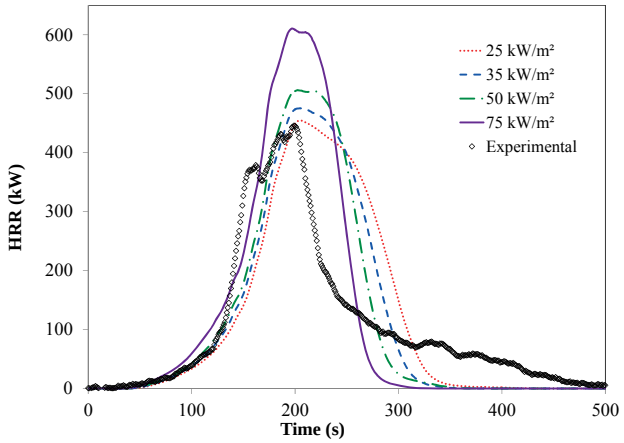

Figure G-27 Comparison of experimental heat release rate with convolution model results for test EE4-3.

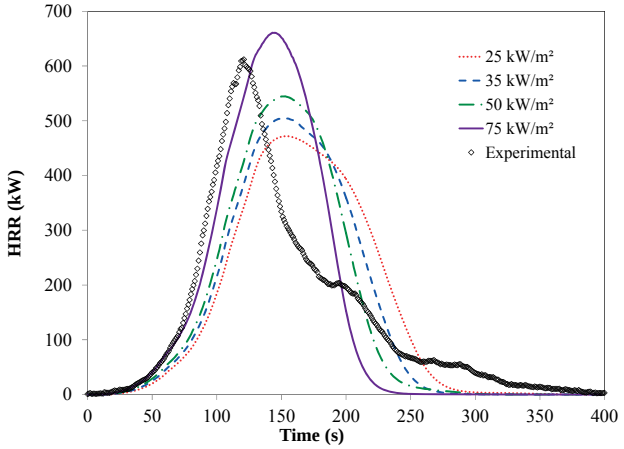

Figure G-28 Comparison of experimental heat release rate with convolution model results for test CC4-1.

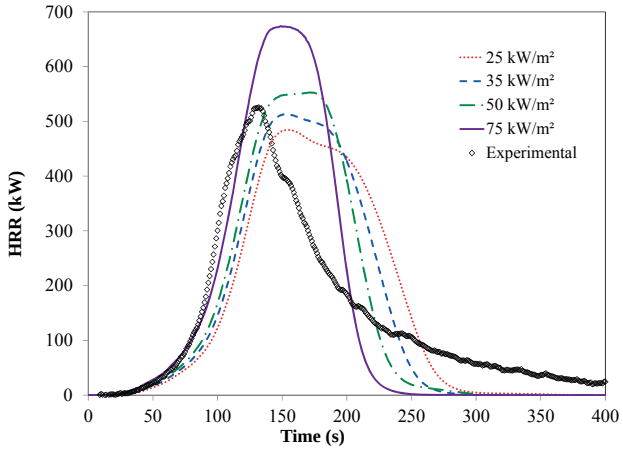

Figure G-29 Comparison of experimental heat release rate with convolution model results for test CC4-2.

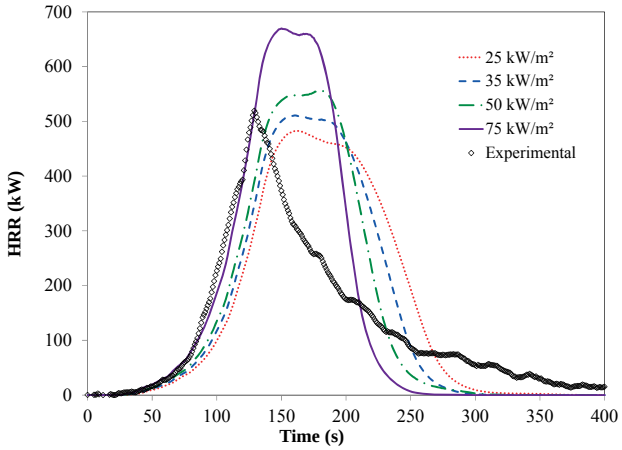

Figure G-30 Comparison of experimental heat release rate with convolution model results for test CC4-3.